Geographia Technica

Technical Geography
an International Journal for the Progress of Scientific Geography

Volume 16, Geographia Technica No. 1/2021

www.technicalgeography.org

Cluj University Press

Geographia Technica

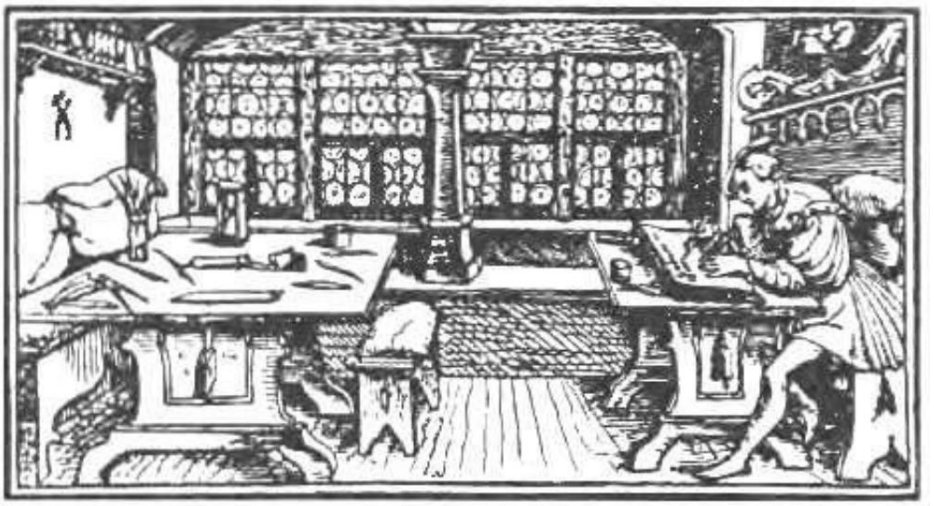

Technical Geography

an International Journal for the Progress of Scientific Geography

2021 – No. 1

Cluj University Press

ISSN: 1842 - 5135 (Printed version)
ISSN: 2065 - 4421 (Online version)

Babeș-Bolyai University
Cluj University Press
Director: Codruța Săcelean
Str. Hașdeu nr. 51
400371 Cluj-Napoca, România
Tel./fax: (+40)-264-597.401
E-mail: editura@editura.ubbcluj.ro
http://www.editura.ubbcluj.ro/

Asociatia Geographia Technica
2, Prunilor Street
400334 Cluj-Napoca, România
Tel. +40 744 238093
editorial-secretary@technicalgeography.org
http://technicalgeography.org/

C o n t e n t s

Geographia Technica

Volume 16, Issue 1, spring 2021

An International Journal of Technical Geography

ISSN 2065-4421 (Online); ISSN 1842-5135 (printed)

APPLICATION OF GIS TECHNOLOGY FOR TOURISM FLOW MODELLING IN THE UNITED KINGDOM

Mărgărit-Mircea NISTOR[1*], Alexandru-Sabin NICULA[2,3*]

DOI: 10.21163/GT_2021.161.01

ABSTRACT:
The fluctuation of tourism flow and its cartographic representation are crucial for transport companies, accommodation and regional tourism, but also for the future modelling of international tourism flow. The origin of tourists and their number represent the most important aspect in tourism flow mapping, which are recorded in statistical databases. One of the most popular and easiest way to obtain tourism flow maps is the Kernel Density function, available on ArcGIS, which uses the vector lines data and density mathematical function to represent the objects' characteristics at spatial scale. Spatial distribution of the tourist flow is a tool to observe and assess the origin and destination countries at spatial scale. In this paper, the modelling of tourist flow from their countries of origin to the United Kingdom (UK) was completed through Geographical Information Systems (GIS) considering four types of visitors. The analysis is based on flow lines and Kernel Density using 48 countries of tourists' source related to 2015. The high and very high densities were found in European countries, US, Australia, China, and Canada. Considering the types of visits, the higher number of tourists during 2015 is in respect with holiday visits (> 1.8 million). The model proposed in this paper and the original maps contribute to future strategies and plans for the international tourism over UK.

Key-words: *Spatiality, Flow models, International visits, GIS technology, United Kingdom.*

1. INTRODUCTION

For a better management of tourist arrivals and visits, mainly at spatial scale, the flow models contribute to the understanding of the relationship between tourists' origin and their destination. Once tourist flow and intensity for each direction are known, additional decisions can be taken (e.g. special tourism packages for that countries, improve the flights and transports, political agreement for visas etc.). In this study, the flow model of the holiday visits, business visits, friend's visits, miscellaneous visits, and total visits in UK during 2015 was used to generate the tourism flow modelling.

The study of tourist flow study has a significant role in policy-making decisions and further improvements regarding transports, hotel infrastructure, and touristic sight preparation taking into account the type of tourists, their country of origin, and type of visits. In UK, the main visits are focused on the holiday purpose, followed by business visits, friends visit, and others or/and mixed of these types, therefore defined as miscellaneous visits. In order to have an exhaustive idea about tourism phenomena and to easier analyse tourism data, various software and statistical programs are used. In addition, scientists process such data and contribute to different kind of models, such as gravity models, spatial clustering, econometric regression etc. Thus, several statistical and regression models were implemented and applied in tourism up to present.

Divisekera (2003) developed a demand model for international tourism based on the consumer theory in the US, UK, Japan, and New Zealand demands in Australia. He used the class of preferences called 'Price Independent Generalized Log-Linear' for market demands and including the preferences as minimum expenditure necessary to attain a specific utility at given prices.

[1] *Earthresearch Company, Department of GIS and Cartography, Cluj-Napoca, Romania: renddel@yahoo.com*
[2]*National Institute for Economic Research "Costin C. Kiritescu" of the Romanian Academy/Centre for Mountain Economy (CE-MONT): sabin.nicula@gmail.com*
[3]*Faculty of Geography, University of Babeş-Bolyai, Cluj-Napoca, Romania*
**Corresponding author: Mărgărit-Mircea Nistor: rendddel@yahoo.com, Alexandru-Sabin Nicula : sabin.nicula@gmail.com*

Peng et al. (2014) conducted a meta-analysis of international tourism demand elasticities, by reviewing 195 studies published between 1961-2011. The authors examined the relationship between estimated international tourism demand elasticities and the data characteristics and study features that may affect empirical estimates. The findings of meta-analysis will be useful wherever an understanding of the drivers of tourism demand is critically important. Assaf et al. (2019) studied the multi-co linearity by Bayesian inference in conjugate and non-conjugate ridge regression models for tourism data set. They found that the Bayesian ridge regression generates better results than a Bayesian regression with diffused prior (Assaf et al., 2019). By downscaling global tourism simulation model, Hamilton and Tol (2007) studied the impact of climate change on tourism in Germany, Ireland, and the UK. Instead of many studies, they have provided the temporal and spatial scale results for the analysed countries. La Rocca (2014) figured out the mechanisms of cities and tourism phenomena. In his view, the city represents the "physical place where tourist desires and inhabitants needs intersect" (La Rocca, 2014). Otoo & Kim (2018) analysed the senior travel motivations by paper frequency ranking.

Through an analysis of cause–effect relationship between sustainable tourism variables, Roxas et al. (2018) found that ecotourism creates profitable businesses and local jobs. In their analysis, the systems thinking tools and causal loop diagram were applied to determine sustainable tourism development including the tourism participants. Song et al. (2000) proposed a tourism destination preference index for UK demand. They have found that the overseas holidays influence the high amount of income elastic. In the same time, the own price elasticities also indicate that the costs of overseas holidays are a significant factor for international tourism demand. Song & Li (2008) evaluated the tourism models demand and the forecasting methods in the literature and they have found that most of the studies had used quantitative approaches.

In the last decade, the gravity models were often used for tourism flow (Fourie & Santana-Gallego, 2011; Santeramo & Morelli, 2016). Through quintile regression, the estimation of the tourism demand segmentation could be achieved (Koenker, 2005; Santeramo & Morelli, 2016). The econometric modelling is used to derive data from the obtained findings (Hall, 2012). Thus, Carey et al. (2013) studied the tourism growth in Wellington used time series analysis and econometrical regression for the cultural attraction and visitors on tourism data (e.g. number of guest arrivals, overnights, occupancy rates). The scientific literature contains several methods for environmental modelling and various elements flow by using GIS, statistics methods or artificial neural network (Ighile & Shirakawa, 2020; Moldovan, 2020). Using statistical data (e.g. domestic trips and foreign trips, income per resident, seats on offer etc.) at NUTS2 and NUTS3 level, Zieba (2016) assessed the impact of tourism flow on demand for city theatres in Austria, between 1972 to 2011. The analysis of domestic tourism flows to 341 cities in China based on space-time analysis and spatial econometric approach was done by Yang & Wong (2012).

Since the 1990s, Butler (1992) and Hall & Page (2009) have argued about the importance GIS technology in Applied Geography, problem-solving, planning and decisions in tourism. Hall & Page (2009) mentioned about the data analysis in the geographical studies on tourism at spatial scale using Geographical Information Systems (GIS) development in the geographical departments.The theory of nonparametric density estimation and bandwidth selectors for Kernel Density estimation were recently explained by Artur (2018). Correa-Quezada et al. (2020) applied the non-parametric method of Kernel density functions in order to analyze the regional growth and convergence processes in the service sector, in Ecuador, through productivity as the reference variable. Xu et al. (2017) analyzed the essential relationship established between e-commerce and tourist flow by appealing to kernel density estimation. In their enterprises they took as a model the ecommerce data of Huangshan tourism cloud platform. The research of Kokonendji & Somé (2017, p.113) emphasized the introduction of "multivariate associated kernels with the most general bandwidth matrix". Zhu et al. (2017) based their research on the Kernel Optimization Function for sentiment word embedding in tourism domain. Asmelash & Kumar (2019) proposed sustainability indicators for the tourism development including unidimensionality, multivariate normality, multicolinearity, construct reliability, convergent validity, discriminant validity. They underline the importance of the tourism

indicators for the decision in tourism industry. The impacts of short-term climate variability on the touristic demand in the UK was studied by Agnew and Palutikof (2006). They analysed the climate variability on intra- and inter-annual scales using mean monthly and annual temperature, rainfall and sunshine in comparison with the domestic monthly numbers of tourist nights and international annual numbers of trips abroad. In their study, the warmer and drier conditions of 1995 contributed to benefits from tourism of up to £309 million. The total number of international visits to the UK was 4.1 million in 2015, from 48 countries. A higher amount of visits was recorded for France, US, and Germany.

One of the most used analyses in tourism and data exchanges refers to gravity models. Ciuriak et al. (2017) used gravity models to study the potential for enhancement post-Brexit of the UK's non-EU trading relationships. De Mello et al. (2002) used the equations models to investigate the tourism demand in UK and neighbour countries. In their study, Portugal, Spain, and France were highly examined through expenditure elasticities, uncompensated own-price elasticities, and uncompensated cross-price elasticities, compensated own-price elasticities, and compensated cross-price elasticities. Xing-zhu & Qun (2013) come up with a spatial data analysis of the international tourist arrivals over 1978–2009 in China using the spatial clustering of inbound tourism flows by the "Global Moran's I" were analysed. However, the spatial scale analysis and flow models visualization are not developed enough in tourism studies. Furthermore, the UK is listed in the first five countries with tourists' source and also as one of the most visited country in the world. A study about international tourism analyses at spatial scale in UK is missing. This study aims to model tourism visits in UK using the flow lines from tourist's source to the UK and to determine the spatial scale of the tourism models through the Kernel Density function in GIS. The methodology is new and contributes to the spatial scale overview of the international visits in UK.

2. MATERIALS AND METHODS

2.1. Tourism data and type of visitors in UK

UK is mainly located on the British Islands, with exception of Republic of Ireland. The tourism statistics in UK indicate most of the visitors as holiday purpose, followed by business and friends visits. The data of holiday's visits, business visits, friend's visits, miscellaneous visits, and total visits related to 2015 in UK international arrivals belong to Office for National Statistics (ONS, 2015). The total visits per origin source, about 48 countries were analysed in this paper considering the spatial scale.

2.2. GIS datasets

The tourism data of visitors' source was assigned to the country of origin. Thus, ArcGIS files with vector country data were employed to process the information at a spatial scale. The centroids of each country source for tourism in UK were extracted. Four types of visits (holiday, business, friends' visits, and miscellaneous visits) were inserted into GIS database and were used to model the flow over UK. Two steps of pre-processing data have been used: (i) row tourism data analysis for each type of visitors and (ii) assign these data to the countries' centroids into ArcGIS. Furthermore, tourism flow lines and density models were generated for UK.

2.3. Tourism flow lines

The international visits and tourism flow directions for UK in 2015 were modelled based on 48 countries using 'XY To Line' function in ArcGIS. This function allows us to obtain the convergence lines from the tourists' sources countries over UK. To perform this operation, the centroids of the countries were extracted and geographical coordinates (latitude and longitude) were assigned to each centroid. Furthermore, the density model of the flow lines, for each type of visits was generated using Kernel Density function. This function is part of the Spatial Analyst Tools from ArcGIS, which allows a smooth surface to each polyline in base of the values of each polyline. Where the density and values of the polyline are higher, the resulted raster will have higher values in that parcels and where the polylines are missing, no data is assigned in the respective parcels. Here, we used Kernel Density for the visit types in UK. The Kernel Density function could also be used for the analysis of point data with population or information to generate the raster map (Silverman, 1986).

The Kernel Density tool calculates the density of flow lines taking into consideration the neighbourhood around those lines. The method is based on search radius algorithm (bandwidth), which has the following formula (Eq.(1)):

$$Search\ radius = 0.9\ \times \min\left(SD, \sqrt{\frac{1}{\ln(2)}}\ \times\ D_m\right) \times n^{-2} \quad (1)$$

where SD is the standard distance; D_m-is the median distance; n is the sum of the visits field values.

2.4. Kernel Density

Considering the vector data of tourism flow lines, the Kernel Density was calculated for each dataset. In this function (Eq.(2)), the distance and number of tourists for that particular line are taken into account for the cartographical representation. Kernel Density represents a non-parametric approach to estimate the probability density function of random data. Being a mathematical function, Kernel Density illustrates mainly the values of the vector data. Through this tool available on ArcGIS, the classification of overlap areas could be completed. This method of Kernel Density includes the statistics for the spatial representation of the travel lines, which were represented in this study through the 'XY To Line' function. The algorithm of Kernel Density return the maximum values and the minimum values are neglected. The calculation of Kernel Density implies the normal low in statistics and the mean square deviation, where the limit of the upper bond and lower bond was fixed at 67% that is standard limit imposed by software. The calculations have been done in kilometres units and the output spatial reference is km^2.

$$f_h(x) = \frac{1}{n}\sum_{i=1}^{n}\binom{n}{k}K_h\ (x - x_i) \quad (2)$$

where f is density *f;* K is the kernel — a non-negative function; h > 0 is a smoothing parameter called the bandwidth; x_1, $x_{2,\ldots,}$ x_n is univariate independent and identically distributed sample.

3. RESULTS AND DISCUSSION

In 2015, the number of tourists visiting the UK for holiday purposes reached 12.93 million, 1.89 million visits originating in France. Business visits registered 8.48 million in 2015, with a maximum amount of 856,457 visits for France. For friendly visits, there were 9.83 million tourists in UK related to 2015 and 1.12 million belong to France. The miscellaneous visits accounted for 2.72 million, 356,443 of which from the Republic of Ireland. The total number of visits in 2015 reached33.98 million, 4.17 million from France. The countries from which most visitors originate are mainly located in continental Europe: France (4.17 million), Germany (3.24 million), Netherlands (1.89 million), Italy (1.79 million) Republic of Ireland (1.63 million), Belgium (1.17 million), as well as the US (3.26 million) (ONS, 2015). Looking at the types of visitors, holiday visits have the tourists originating from Europe, North and South America, Australia, and Asia (**Fig.1**). About four countries from Africa contribute to the international holiday visits in UK. The business visits recorded higher values (over 600,000 visits) for the European countries and the US (**Fig.2**), while the lower values (below 10,000 visits) were recorded for Mexico, Pakistan, Thailand, and some countries from Africa. Friendly visits amount aremuch more diversified in the UK, including higher values (above 400, 000 visits) from the US, Western Europe, and Australia. Five countries from Africa (Morocco, Tunisia, South Africa, Nigeria, and Egypt) and only Brazil and a French colonial state from South America contributed during 2015 at the international friends' visits in UK (**Fig.3**). Kernel Density tool was used to generate the density of the converged flow lines of the international visits to the UK. For holiday visits, a very high density was obtained for European countries (France, Italy, Germany) and for US (**Fig.6a**), while high values could be observed from Australia, Canada, China, Western and Central Europe as well.

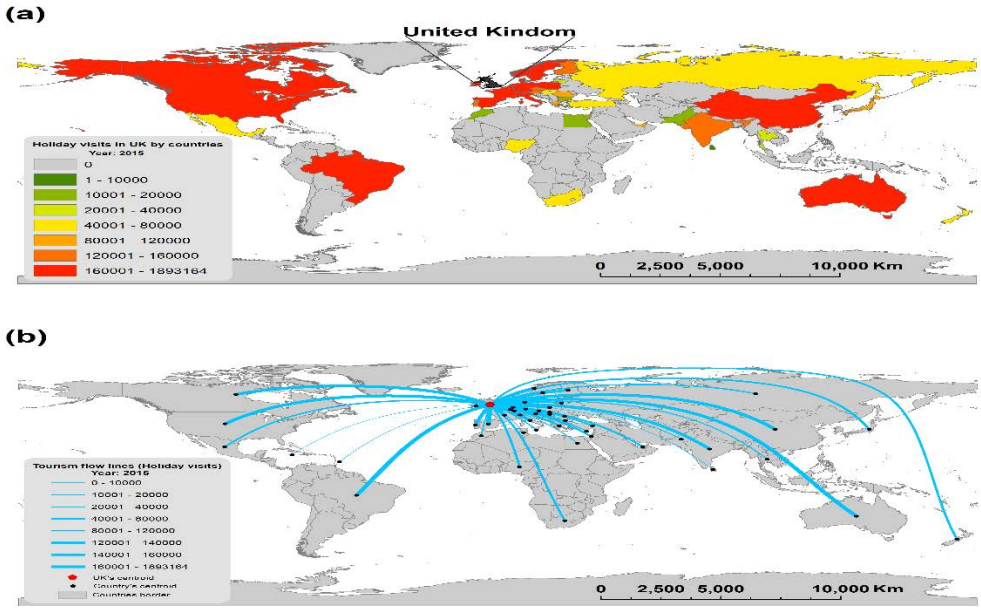

Fig. 1. (a) Holidays visits (2015) in UK by country origin. (b) Tourism flow lines (2015) from the origin countries to UK for the holidays visits.

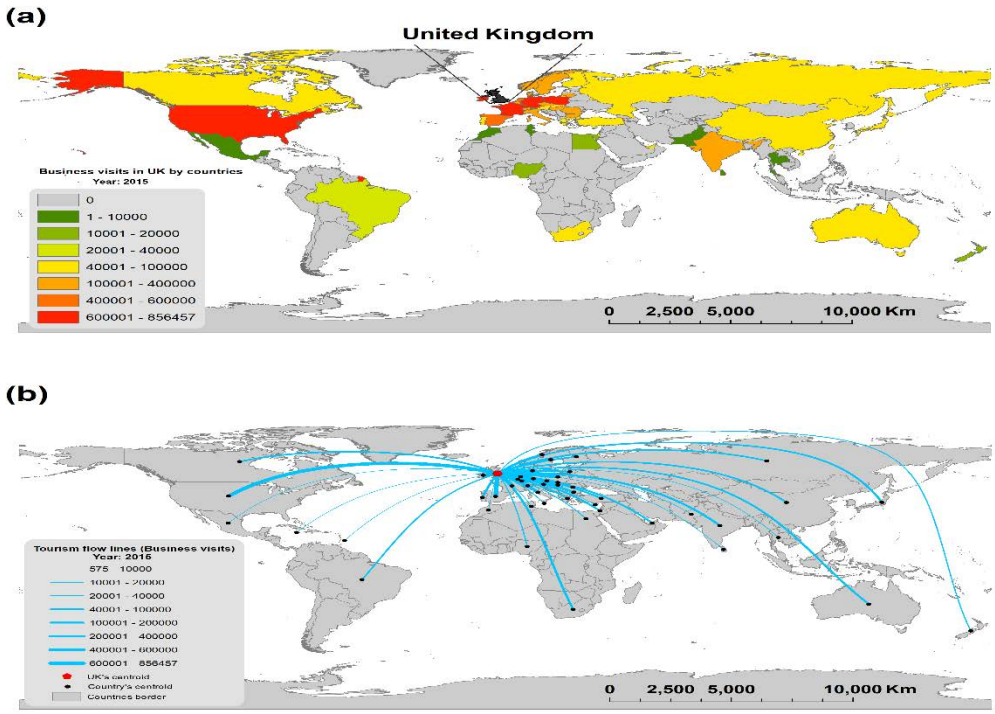

Fig. 2. (a) Business visits (2015) in UK by country origin. (b) Tourism flow lines (2015) from the origin countries to UK for the business visits.

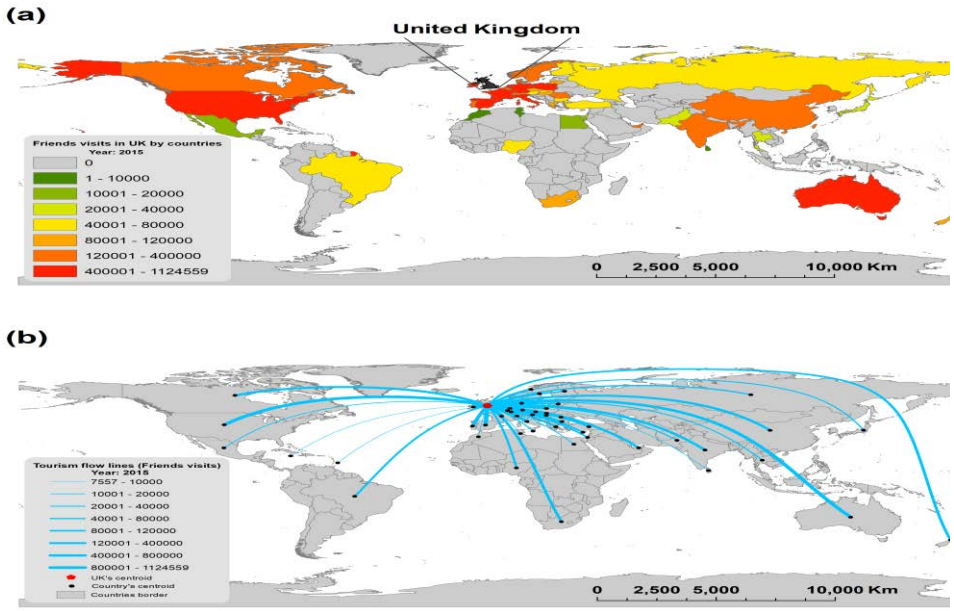

Fig.3. (a) Friends visits (2015) in UK by country origin. (b) Tourism flow lines (2015) from countries of origin to the UK for friends visits.

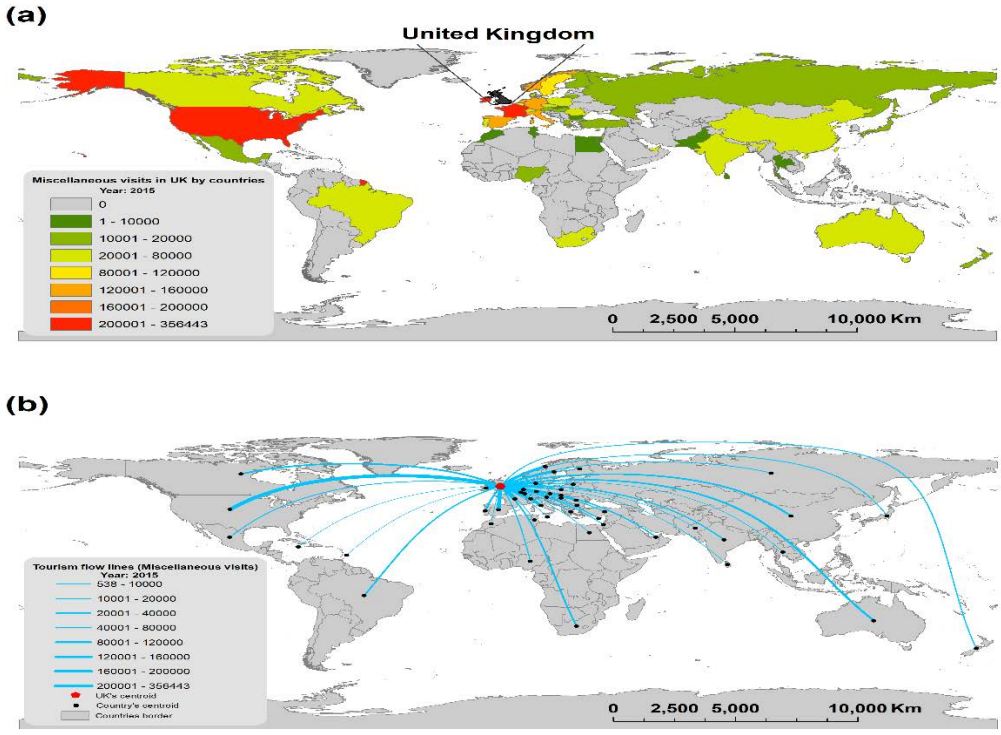

Fig.4. (a) Miscellaneous visits (2015) to the UK by country origin. (b) Tourism flow lines (2015) from the origin countries to the UK for miscellaneous visits.

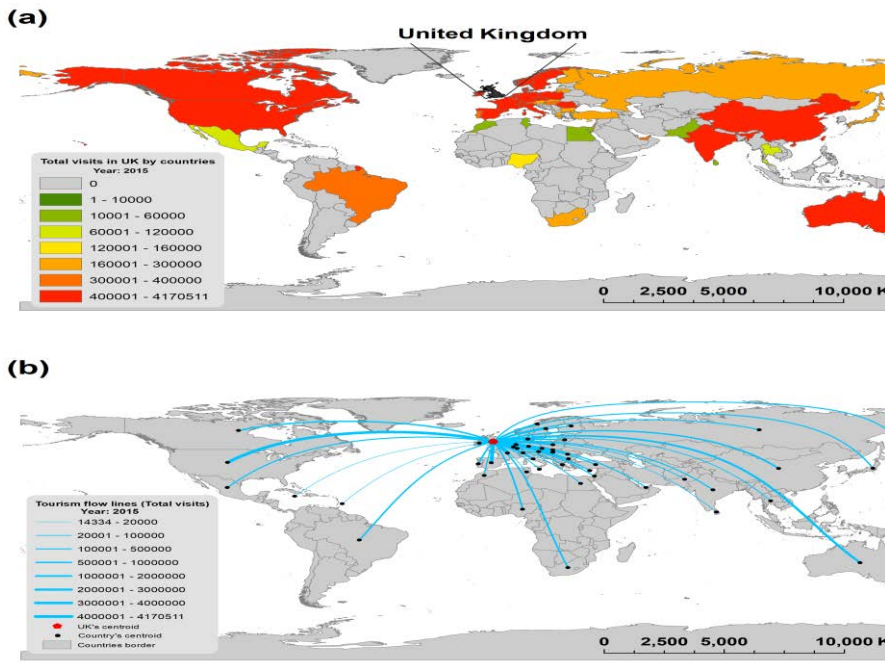

Fig.5. (a) Total visits (2015) to the UK by country of origin. (b) Tourism flow lines (2015) from the countries of origin to the UK for total visits.

Miscellaneous visits had higher values (more than 200,000 visits) for France and the US. **Fig.4** indicates low values around the world, with much implication for the European countries. At a global level, the total visits to the UK in 2015 are significant for France, Italy, US, Australia, China, India, and other European countries (**Fig. 5**). The density model for business visits had extremely high values in the proximity of UK, in Belgium and Netherlands, while high values are from the US, Romania, Italy, and Central European countries (**Fig.6b**). The friendly visits flow model indicates a surprisingly high density from Belgium and France, while the high density is shown from US, Australia, and Central Europe (**Fig.6c**). Miscellaneous visits have high densities from the Republic of Ireland, and from the proximity of the UK border. High density values for the miscellaneous visits were calculated from US, Canada, China, Australia, Central, Southern, and Northern Europe (**Fig.6d**). Medium, low, and very low densities were mainly found for all types of visits from Mexico, Central America, Brazil, African countries, India, New Zealand, Japan, the Middle East, and Russia.

Table 1.

Tourism flow models density.

Density classes	Holiday visits (area %)	Business visits (area %)	Friendly visits (area %)	Miscellaneous visits (area %)	Total visits (area %)
Very low	19.57	27.46	17.60	35.77	10.34
Low	23.86	36.33	34.89	48.02	19.37
Medium	43.93	30.92	38.98	16.10	44.88
High	10.68	5.11	8.42	0.11	20.51
Very High	1.95	0.17	0.11	0.00	4.91

Source: GIS statistics. Note: the values consider only the model density for the UK, without nil values.

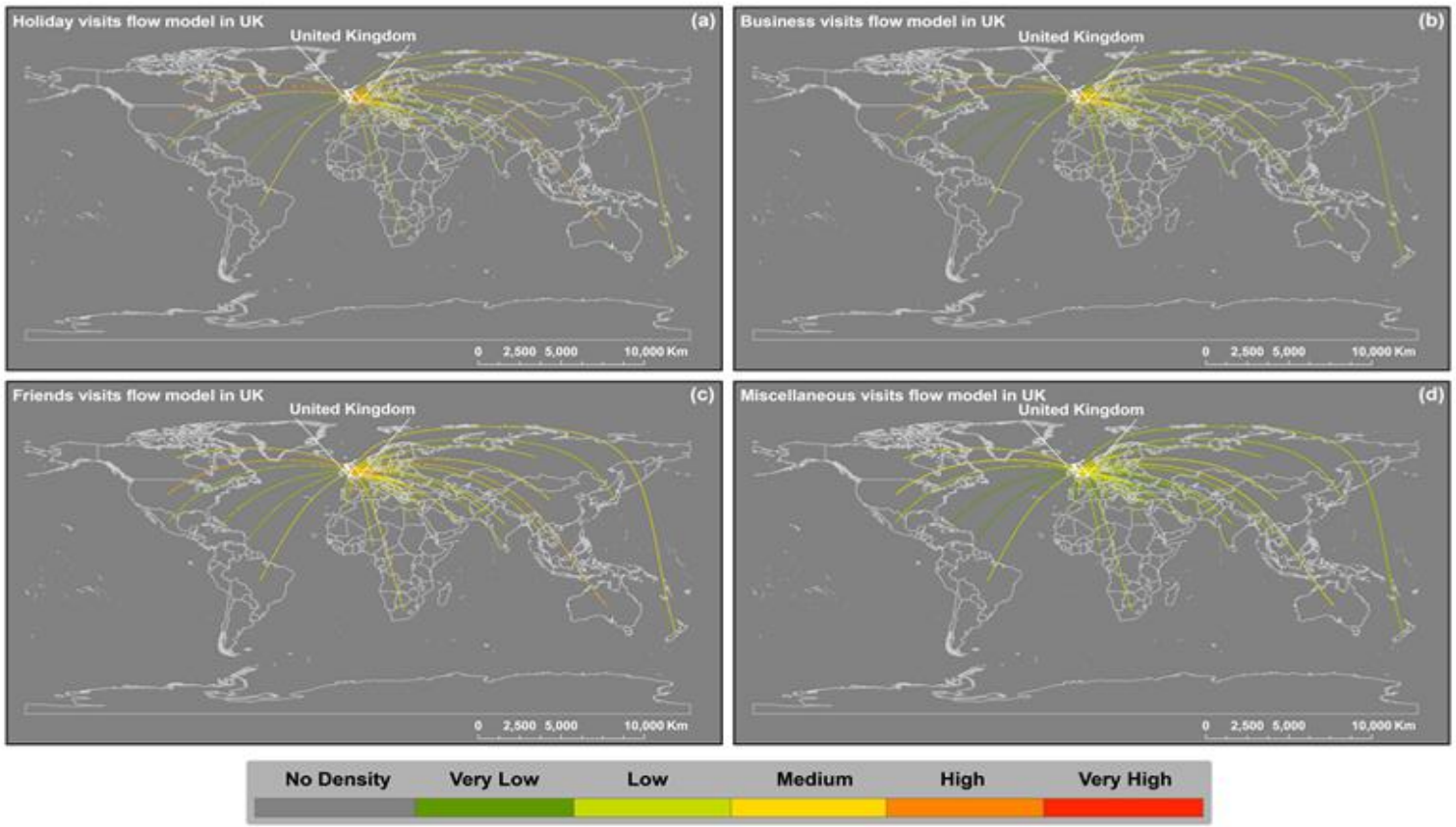

Fig.6. Tourism flow over UK considering the four types of visits in 2015. (a) Kernel model of holidays' visits flow. (b) Kernel model of businesses' visits flow. (c) Kernel model of friends' visits flow. (d) Kernel model of miscellaneous' visits flow. The classes of density are referring to: 0 for No Density, 1 – 10,000 for Very Low, 10,001-100,000 for Low, 100,001 – 1,000,000 for Medium, 1,000,001 – 5,000,000 for High, > 5,000,000 for Very High. Note: the units are km^2.

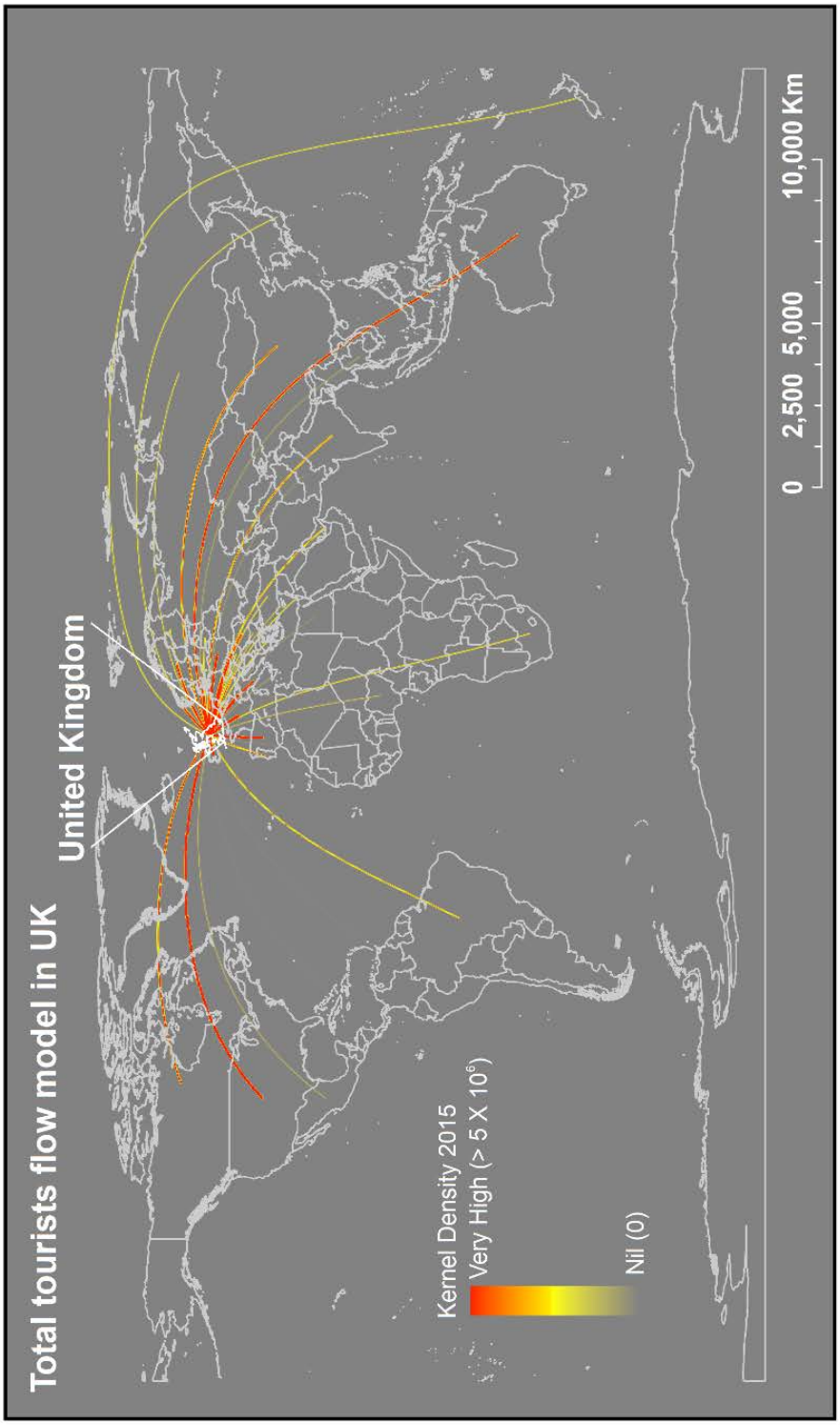

Fig. 7. Kernel model of totals' visits flow in UK considering in 2015. Note: the units are km^2.

The total UK visits in 2015 contributed to very high density in western Europe and the US, while high densities were mainly found in Central European countries, Canada, Brazil, China, the Middle East (United Arab Emirates), India, and Australia. The medium density was depicted over central Europe, Mexico, Nigeria, Russia, New Zealand, Egypt, Israel, Turkey, and Japan. Low and very low densities were found in Central America, Sri Lanka, and North African countries. **Fig.7** illustrates the density model of the total UK visits. The statistical analysis of the density models indicates 1.95% of very high density in area for the holiday visits, while the very high density area for business visits, friendly visits, and miscellaneous visits, the values are 0.17%, 0.11%, respective 0%. The medium density has higher values for holiday visits (43.93%) and friends' visits (38.98%). business visits (36.33%) and miscellaneous visits (48.02%) have higher values in the low density class. The higher area of the density model for the total visits is representative for medium density class, with 44.88%, followed by high density class (20.51%) and low density class (19.37%). **Tab.1** reports the statistical values of the density models for each type of visit to the UK in 2015.

Overall, the proposed methodology depicts visit flow lines and density model in this study reflects the GIS technology implication for the spatial distribution of tourists flow. The applied GIS functions utilized to generate the flow lines and Kernel Density for UK visits contributed to obtain areas with different classes of density global scale. The importance of our model impacts not only the current study, but may also contribute to tourism data analysis at a spatial scale, analytics, and statistics in the field of tourism, considering that the topic of tourism could be also developed in this direction. Number of visitors and proximity of tourists' source influence the model proposed by us. Thusly, the pattern of Kernel Density indicates the flow from European countries to the UK as high and very high density. Countries located at further away (e.g. US, China, Australia) have high and very high density of visits flow due to the higher population and availability to travel for extra-continental visits. As resulted from the models, the holiday visits recorded in 2015 higher values for both European tourists' source and other continents. The usefulness of these models is that they can help policy-makers develop new services for such tourists, improve transport infrastructure during various periods of year and plan the strategies to attract tourist from other countries.

This survey demonstrates how international visits could be represented at a spatial scale, considering flow lines and density models. The methodology was applied on UK data and it combines tourist information with spatial statistics of source countries. Thusly, the geospatial analysis was developed in this study to observe the convergences, density and intensity of the flow lines models. The improvement and continuity of our approach could be focused on future predictions and density calculations. As a limitation, the proposed model does not take into consideration worldwide touring, as the flow lines are directly connected to the tourists' source. This procedure contains the analysis of data in the attributes tables of layers into ArcGIS. The dynamic tourism flow, including visits in other countries before UK, could be considered a desired model, but such as model is currently difficult to implement for a high number of countries (e.g. 48 for this study). The exploration of tourism flows, through multiple countries before the final destination, by oriented programming and GIS technology, may represent a significant improvement for both data analysis and spatial displacement.

The advantages of the proposed model in this study refers to the ease of identifying direct connections between origin and destination countries of tourists, highlighting the countries with higher amount of visitors source, and evaluating the density of tourist flow at spatial scale. For this reason, the integration of tourism data into a GIS database and further analyses might provide the required models based on automatic and validated tools.

4. CONCLUSIONS

Tourism visits in UK during 2015were analysed in this paper. The origin of visitors and their purpose (holiday, business, friendly visits, miscellaneous) were analysed at spatial scale in order to generate a tourism flow model. Using the GIS technology, the flow lines and Kernel Density models of the international visits to the UK served to represent the tourism fluxes. The flow models indicate higher concentration for Europe density, while in the case of more distant countries, such as Australia,

New Zealand, Japan, Brazil, and Canada, the distance factor influences the total visits flows to the UK. Consequently, the Kernel Density is higher in Western Europe and in the US.

The present study is a way to represent the touristic data and international flow visits on the world map. In fact, the proposed model is a contribution at spatial scale using UK data for 2015. The exploration of tourism flows using GIS software with specific functions such as XY To Line' and 'Kernel Density' contributes with advantages for tourism strategies and future tourism planning. For instance, the general movement of tourists and tourism flow lines indicate the main route travel and further travel infrastructure and journey could be planned. In addition, the high demand for tourism is reflected into the transport systems and the social-economic development. In this context, the tourism flow models may help to develop new transports infrastructure or new journey programs in a certain period of year. Thus, the Kernel Density function applied in this study contributes to the better management of big tourism data, future strategies and development plans, both for countries close to the UK and worldwide.

Acknowledgments

The authors would like to extend their gratitude to the UK Office for National Statistics for tourism data. This paper was devised by the authors as an independent initiative and did not receive any grants or funds from any university or agency whatsoever.

REFERENCES

Agnew, M. D. & Palutikof, J.P. (2006) Impacts of short-term climate variability in the UK on demand for domestic and international tourism. *Climate Research*, 31, 109–120.

Artur, G. (2018) Nonparametric Kernel Density Estimation and Its Computational Aspects. Springer Studies in Big Data, ISBN 978-3-319-71688-6.

Asmelash, A.G. &Kumar, S. (2019) Assessing progress of tourism sustainability: Developing and validating sustainability indicators. *Tourism Management*, 71, 67–83.

Assaf, A.G., Tsionas, M. &Tasiopoulos, A. (2019) Diagnosing and correcting the effects of multicollinearity: Bayesian implications of ridge regression. *Tourism Management* 71, 1–8.

Butler, R.W. (1992) Alternative tourism: the thin edge of the wedge. In V. L. Smith, & W. R. Eadington (Eds.), Tourism alternatives: potentials and problems in the development of tourism (pp. 302–321). Philadelphia: University of Pennsylvania Press.

Carey, S., Davidson, L. &Sahli, M. (2013) Capital City Museums and Tourism Flows: an Empirical Study of the Museum of New Zealand Te Papa Tongarewa. *International Journal of Tourism Research*, 15(6), 554–569.

Ciuriak, D., Siauw-Soegiarto, F.& SUN, S.Z. (2017) Quantifying the UK's Post-Brexit Export Potential: A Gravity Model Analysis. Research Report.

Correa-Quezada, R., Cueva-Rodríguez, L., Álvarez-García, J. & del Río-Rama, M.D.L.C. (2020) Application of the Kernel Density Function for the Analysis of Regional Growth and Convergence in the Service Sector through Productivity. *Mathematics*, 8(1234), 1-20.

De Mello, M., Pack, A. & Sinclair, M.T. (2002) A system of equations model of UK tourism demand in neighbouring countries.*Applied Economics*, 34(4), 509–521, DOI: 10.1080/00036840110049310

Divisekera, S. (2003) A model of demand for international tourism. *Annals of Tourism Research,* 30(1), 31–49.

Fourie, J. & Santana-Gallego, M. (2011) The impact of mega-sport events on tourist arrivals. *Tourism Management*, 32(6), 1364–1370.

Hall, C. M. & Page, S.J. (2009) Progress in Tourism Management: From the geography of tourism to geographies of tourism – A review. *Tourism Management*, 30, 3–16.

Hall, C.M. (2012) Spatial analysis: A critical tool for tourism geographies. In J. Wilson (Ed.), The Routledge handbook of tourism geographies (pp. 163–173). London: Routledge.

Hamilton, J.M. & Tol, R.S.J. (2007) The impact of climate change on tourism in Germany, the UK and Ireland: a simulation study. *Reg. Environ. Change,* 7, 161–172.

Ighile, E.H. & Shirakawa, H. (2020) A study on the effects of land use change on flooding risks in Nigeria. Geographia Technica, 15(1), 91-101.

Koenker, R. (2005) Quantile Regression. Cambridge University Press, New York, NY 10011-4211, USA. ISBN 0-521-84573-4

Kokonendji, C.C. & Somé, S.M. (2018) On multivariate associated kernels to estimate general density functions. *Journal of the Korean Statistical Society*, 47(1), 112-126.

La Rocca, R.A. (2014) The Role of Tourism in Planning the Smart City. Tema. *Journal of Land Use, Mobility and Environment*, 7(3), 269-283. DOI: http://dx.doi.org/10.6092/1970-9870/2814

Moldovan, I.F. (2020) Calculation of the river flow with different probabilities of occurrence using artificial neural network. *Geographia Technica,*15(1), 162-172.

Office For National Statistics (ONS). (2015) Visits, nights and spending in UK: by purpose of visit and country of residence 2015.

Otoo, F.E. & Kim, S.S. (2018) Analysis of studies on the travel motivations of senior tourists from 1980 to 2017: progress and future directions. *Current Issues in Tourism*, DOI: 10.1080/13683500.2018.1540560.

Peng, B., Song, H., Crouch, G.I. & Witt, S.F. (2014) A Meta-Analysis of International Tourism Demand Elasticities. *Journal of Travel Research*, 54(5), 611–633. Doi:10.1177/0047287514528283.

Roxas, F.M.Y., Rivera, J.P.R. & Gutierrez, E.L.M. (2018) Framework for creating sustainable tourism using systems thinking. *Current Issues in Tourism*, DOI: 10.1080/13683500.2018.1534805.

Santeramo, F.G. & Morelli, A. (2016) Modelling tourism flows through gravity models: a quantile regression approach. *Current Issues in Tourism*, 19(11), 1077–1083.

Silverman, B.W. (1986) Density Estimation for Statistics and Data Analysis. New York: Chapman and Hall.

Song, H. & Li, G. (2008) Tourism demand modelling and forecasting–A review of recent research. *Tourism Management,*29, 203–220.

Xing-Zhu, Y.& Qun, W. (2013) Exploratory Space–time Analysis of Inbound Tourism Flows to China Cities. International Journal of Tourism Research, 16 (3), 303-312. DOI: 10.1002/jtr.1932.

Xu, J., Liang, C., Lu, W., Zhao, S. & Zhang, H. (2017) Analysis of e-commerce based on data flow kernel density estimation in the Huangshan tourism cloud platform. In 2017 IEEE 2nd International Conference on Big Data Analysis (ICBDA)((pp. 63-67). IEEE.

Yang, Y. & Wong, K.K.F. (2012) A Spatial Econometric Approach to Model Spillover Effects in Tourism Flows. *Journal of Travel Research*, 51(6), 768–778.

Zieba, M. (2016) Tourism flows and the demand for regional and city theatres in Austria. *Journal of Cultural Economics*, 40(2), 191–221.

Zhu, L., Li, W., Guo, K., Shi, Y. & Zheng, Y. (2017) The tourism-specific sentiment vector construction based on kernel optimization function. *Procedia computer science*, 122, pp.1162-1167.

FLOOD DISASTER STUDIES: A REVIEW OF REMOTE SENSING PERSPECTIVE IN CAMBODIA

Chhuonvuoch KOEM[1], Sarintip TANTANEE[1]*

DOI: 10.21163/GT_2021.161.02

ABSTRACT:
Flood is the most critical natural disaster in Asia. It is also the most affected disaster in Cambodia. The solution must be made to manage the disaster from being interrupting people. The purposes of the study are to identify the 2011 flood impact spatial distribution, evaluate how RS has been applied to flood analysis, and assess the gaps of RS for flood analysis over Cambodia. The flood impact can be calculated by using a weighted arithmetic mean (WAM). The flood studies can be accessed through several literary databases. The 2011 flood impacts commonly located in the regions of Tonle Sap and Mekong River. Furthermore, other regions were affected. Fourteen articles have been found, which are six flood hazard mappings, seven flood risk assessments, and one flood damage assessment. Most of the study covered the Mekong River and Tonle Sap Lake catchments; however, there are still lacking studies over other affected areas. Besides, flood forecasting and flood early warning were not paid attention. Due to the limitation of rain gauge stations, RS is very important to apply for flood studies. Likewise, the radar composite with the neighboring countries is useful since some parts of the borders were blocked by the mountains. In brief, this review could generate greater ideas and solutions for further flood studies efficiency.

Key-words: *Flood, Remote Sensing, GIS, TRMM, Cambodia*

1. INTRODUCTION

Flood is a common hazard of all-natural hazards in the world. River flood results from the water level overtop of the riverbank both natural and artificial that interrupt human life and properties. River flood typically unfolds several days or even months due to its occurrence in the large basin (Smith & Petley, 2009). The flood occurs when the water level increases due to the failure of technical infrastructures or heavy rainfall over the capacity of the storage (Ranke, 2016). Flash flood occurs when the water rises during or within a few hours of rainfall (Doswell, 2003). Floods cause negative effects both direct and indirect to human lives, environment, ecosystem, transportation, infrastructure, agriculture, cultural heritage, economic, etc. (Yu et al., 2012). Conversely, the annual monsoon flood plays a significant role in providing nutrients and enriching soil (Manh et al., 2014).

Cambodia is located in one part of the Asia continent with the land of 181,035 km^2. It consists of mountains, plains, and a great river and lake. The climate is monsoon, which consists of a couple of seasons including the rainy season (May-Oct) and the dry season (Nov-Apr). The rainy season is recognized by a strong wind, high humidity, and heavy rainfall (about 85% of annual rainfall). The dry season is categorized by wind and low humidity. According to Thoeun (2015), the average annual rainfall is 1,400mm in the flat region and 4,000mm in the coastal and high regions. The mean temperature, additionally, is 28 °C. The temperature in January is 17 °C then it increases to 38 °C in April. The total population is 16.2 million. The country is internationally known as one of the most susceptibility nations to climate change (Kreft et al., 2017). The country is listed in the rank of 19, high risk, to climate risk index and 54, medium risk, to risk index. The most common hazard in Cambodia is associated with floods (UNDRR, 2019). In 2017, the score of hazard and explorer risk, vulnerability, and lack of capacity are 4.8, 3.0, and 6.5 respectively. The economic loss due to climate change was US$1.5 billion or 10% of GDP in 2015. It was estimated to decrease by at least 2.5% by 2030 and 10% by 2050 (CFE-DM, 2017).

[1]*Naresuan University, Faculty of Engineering, Center of Excellence on Energy Technology and Environment, Phitsanulok 6500, Thailand, chhuonvuochk62@email.nu.ac.th , sarintipt@nu.ac.th*

Flood is a natural disaster that threatens sustainable development (CamDi, 2013), and it the most frequent hazard occurring in Cambodia (72%). The floods cause the most death (97.4%) and the largest economic destruction (91.1%) among disasters. During the rainy season, the Mekong River and Tonle Sap create unique river floods and flash floods, especially during the post-season. The country is affected by the overspill of Tonle Sap and Mekong River, which courses flooding in several provinces. Cambodia faced serious floods in 2000, 2011, and 2013. The 2011 major flood caused 250 people died and 23 people sustained injuries. It affected 18 provinces. There were 350,000 families (over 1.5 million individuals) affected, and 52,000 families were evacuated. Approximately 431,000ha of rice field transplanting were affected, and paddy fields 267,000ha were damaged. Moreover, the national road around 925km and urban roads 360km were damaged. The estimation of the total loss of the 2011 flood to the economy was US$ 630 million (CFE-DM, 2017). Therefore, the flood is the main problem, and it is a significant issue for research in Cambodia. In the existing advancing of Remote Sensing (RS), the specific flood events are more easily determine. Much research on flood has been studied depend on RS. Several researchers put more attempts to support flood disaster management such as Manzul Kumar Hazarika and Bormudoi (2007), Arias et al. (2012), Chung et al. (2019), and Kim et al. (2020). The aims of this paper are to (1) identify the spatial distribution of the 2011 flood impact, (2) evaluate how RS has been applied to flood analysis, and (3) find the gaps of RS for flood analysis over Cambodia. The main contribution of this review is the identification of broad and distinct patterns in terms of data source, method, spatial coverage, and result. Precisely, this paper can serve as a good foundation to develop the method of flood analysis with the help of RS that will lead to greater improvements in the field.

2. METHODOLOGY

According to the study's objectives, the methodology is separated into three different parts including spatial distribution of the 2011 flood impact, literature review of flood analysis using RS, and gaps of RS for flood analysis over Cambodia. **Fig. 1** shows the methodology flowchart of the study. The review put efforts to evaluate flood analysis and find gaps of each study under the Remote Sensing perspective in Cambodia, the study intended to illustrate the 2011 flood impacts, the biggest flood as an example since it had the large extent and impact. Then the gaps could be found more precisely.

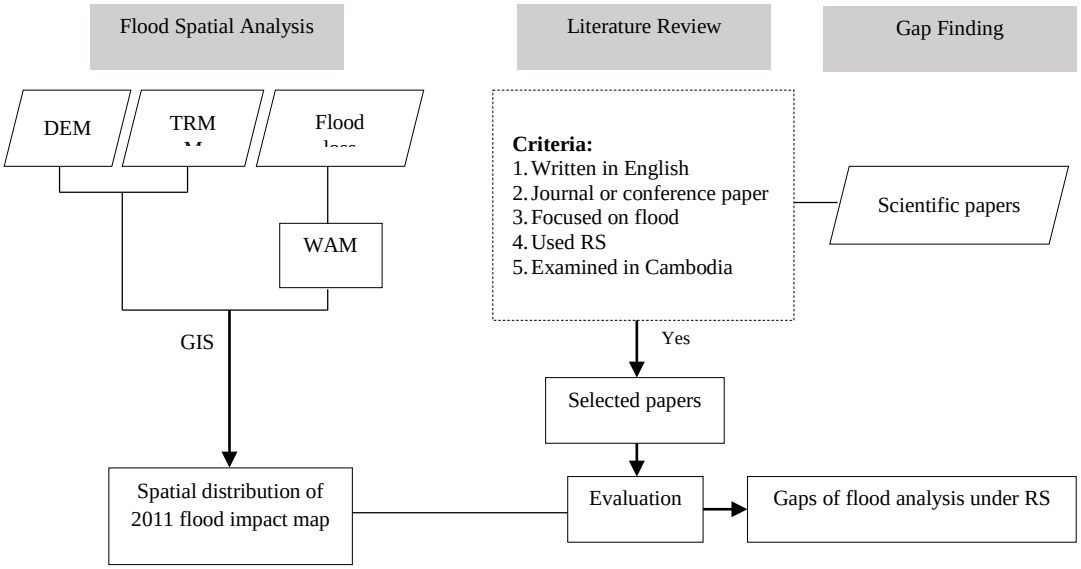

Fig. 1. Methodology flowchart.

The spatial distribution of the flood impact was assessed with the help of GIS and Weight Arithmetic Mean (WAM) by using **Eq. 1**. The weights of different disaster impact are assigned based on the Jenks Natural Break Classification in GIS (Sharma et al., 2019). The weights are assigned 10 to death, 3 to injured, 3 to house destroyed, 1 to house damaged, 0.5 to cattle loss, and 0.5 to crop damaged. The higher value or score means a higher flood disaster loss.

$$\mathrm{WAM} = \sum W_i X_i / \sum W_i \quad (1)$$

where:

W_i is the given weight of each parameter i, based on the study of Sharma et al. (2019).

X_i is the type of flood impacts i, which are the number of death, injured, house destroyed, house damaged, crop damaged, and cattle lost.

Flood impact data were obtained from the National Committee for Disaster Management in Cambodia (NCDM) and UNDP through the website http://www.ncdm.gov.kh/. Rainfall trends and distribution analysis are essential when deliberating flood analysis. Due to the spatial distribution of rain gauge stations in Cambodia is very few, and exited stations are not well maintained and monitored. Thus, it can limit the accessibility of rainfall data. The Tropical Rainfall Measuring Mission (TRMM) dataset obtained from NASA was used in this study. Matingo et al. (2018) assessed TRMM for flood assessment. To get the average rainfall data, 197 random points (a point/district) were used.

A literature review is used a systematical approach, which can reduce biases in selection and ensure all relevant articles. This approach is thorough, methodical, and orderly for considering articles for inclusion. The method consists of three steps. First, the papers were searched through five literary databases including Science Direct, Geographia Technica, Springer, MDPI, and Taylor & Francis Online. Literature regarding flood disaster studies was searched starting by using "Flood analysis using Remote Sensing" as a keyword. The author searched the articles on 23 May 2020. Altogether, this keyword search yielded 1,657 results from Science Direct (2007-2021), 50 from Geographia Technica, 1,014 from Springer, 15 from MDPI-hydrology and environment, and 407 from Taylor & Francis Online. Papers identified from the search are included in the review if they meet the selection criteria such as (1) written in English, (2) journal or conference paper, (3) focused on floods, (4) used remote sensing, and (5) examined in Cambodia. Then the authors reviewed the title and abstract to determine which articles meet the criteria. Second, the articles that met the criteria were reviewed in detail. In total, 14 articles met the criteria and were included in this review. The papers were noted the spatial coverage, data, method, and finding, which is easier to understand and evaluate. The gaps in each study were emphasized by look through some criteria. Is the study cover all the flood-affected areas in Cambodia? Do the studies cover all the flood assessment? Is there any platform of RS that did not use? These questions are considered to find the gaps in the flood analyses under the RS perspective in Cambodia.

3. RESULT AND DISCUSSION

3.1 Spatial distribution of the 2011 flood impact

Both overflow or river floods and flash floods caused severe damages in 2011. Floods occurred during the post-rainy season (Aug-Oct), and the early dry season (Nov). The flood had numerous impacts on people's lives, properties, agriculture, etc. Based on the calculation of WAM for the 2011 flood impact illustrates that 13 districts severely suffered (very high effect) from the flood among of all 197 districts in Cambodia (**Table 1)**. Besides, there were 100 districts affected with high, moderate, and low effects. By using Jenks Natural Breaks Classification in GIS shows that the areas around Tonle Sap and Mekong River were numerously affected. Other regions in the northeast and upland areas are also affected during that time. Flood is dominant; therefore, it is worthy to discuss the rainfall pattern. **Fig. 2** presents the spatial distribution of the 2011 flood impact and monthly average rainfall.

Table 1.

Highest 2011 flood-affected districts.

Province	District	Death (person/s)	Injured (person/s)	House destroyed (house/s)	House damaged (house/s)	Crop damaged (ha)	WAM
Siem Reap	Chi Kraeng	2	4	2	4	17,727	495
Pursat	Bakan	3	0	6	0	16,611	464
Kratie	Chhloung	3	0	7	0	13,845	387
Kampong Thom	Stoung	9	0	0	0	13,163	371
Pursat	Kandieng	2	0	0	16	13,044	364
Prey Veng	Sithor Kandal	3	0	0	48	12,503	351
Kampong Thom	Stung Sen	7	0	0	0	12,350	347
Battambang	Sangkae	4	0	2	0	11,830	331
Prey Veng	Pea Reang	7	0	0	69	11,613	330
Kampong Cham	Batheay	8	0	3	0	11,265	318
Svay Rieng	Kampong Rou	1	0	5	0	10,938	305

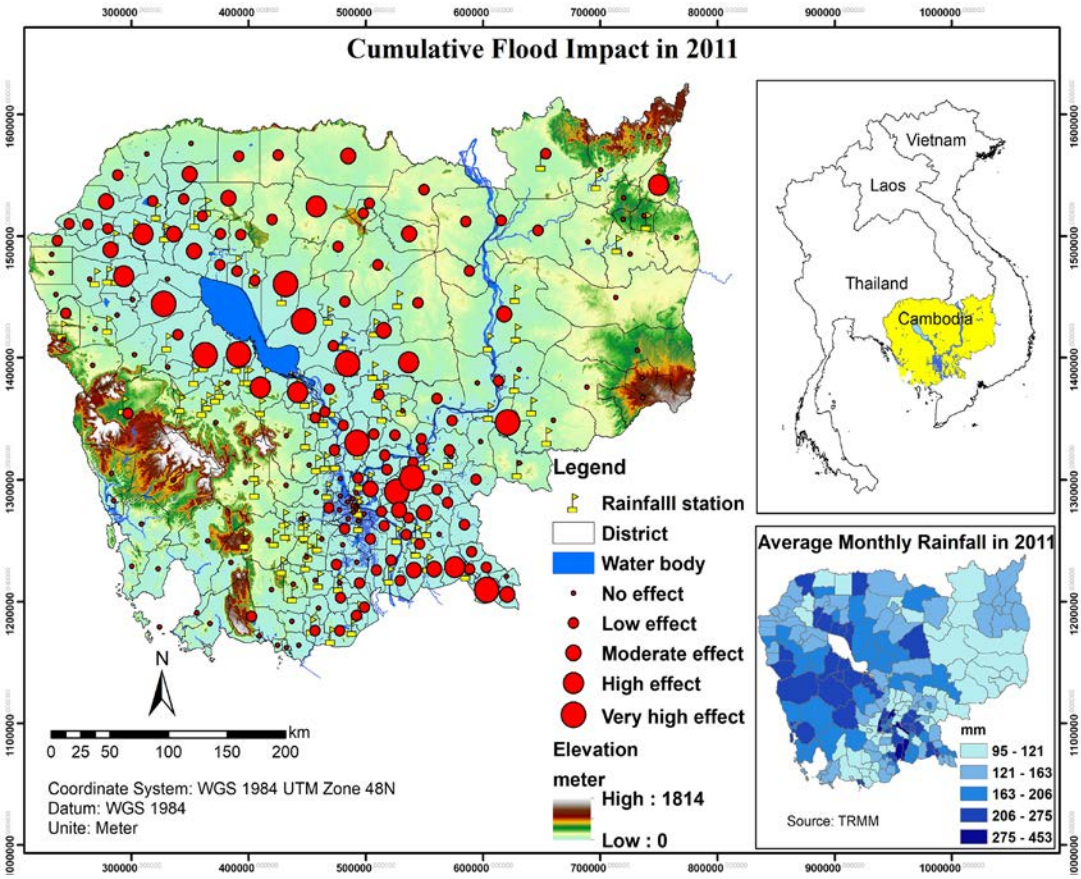

Fig. 2. Spatial distribution of flood impact and average monthly rainfall in 2011.

Annual rainfall intensity and distribution are very vital when discussing the rainfall-induced flooding. **Fig. 3** shows the rainfall with temporal distribution from 2000 to 2019 in Cambodia. TRMM data illustrated that 84% of the entire rainfall was distributed in the rainy season (May-Oct). More than 38% occurred in May, June, and July while 47% occurred in August, September, and October. However, there was only 16% occurring in the rest six months (Nov-Apr). It also shows that the distribution of rainfall in 2000 and 2011 are higher than other years.

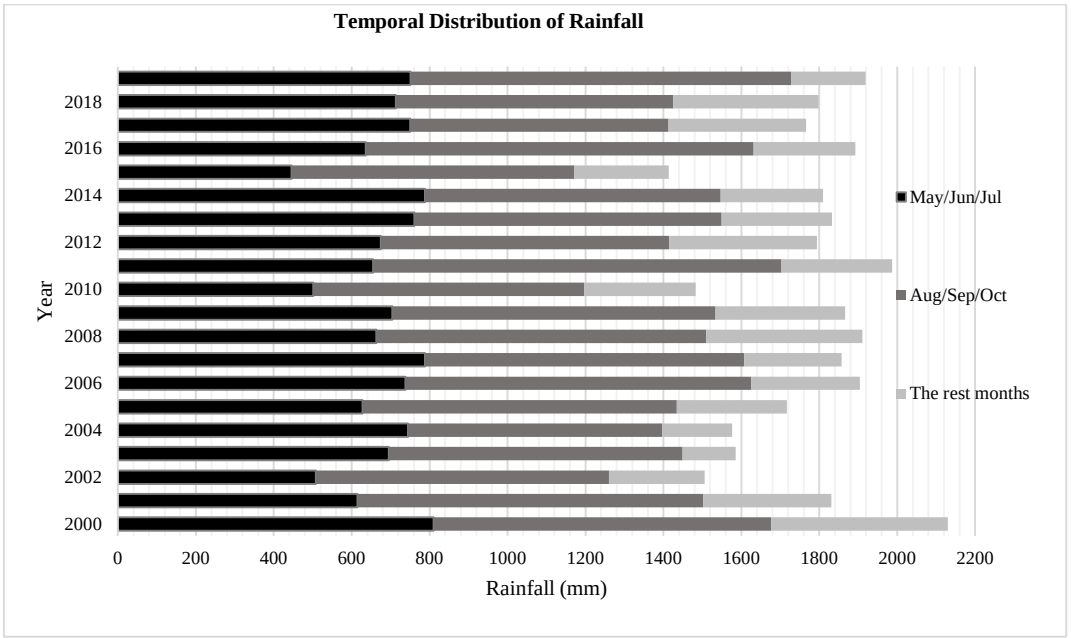

Fig. 3. Temporal distribution of rainfall in Cambodia from 2000-2019 (TRMM).

According to CamDi (2013), flood disasters including the Mekong flood, Tonle Sap flood, and flash floods usually happen during August, September, and October. During this period, the distribution of rainfall is very high if compared to other months. Rainfall 14% occurred in August. About 18% of rainfall occurred in September whereas 13% followed in October. September and October are categorized as the post-rainy season. More notably, August, September, and October are the flooding period and recognized as the peak-flooding period in Cambodia.

3.2 RS application on flood analysis over Cambodia

The development and strengthening of the legal framework for disaster management are prompted by the major occurrence disasters like the 2011 floods. There are several laws, policies, and strategic plans to shape DRR such as disaster management law, which was implemented in June 2015. Moreover, Cambodia joined AADMER, which is the ASEAN agreement on disaster management and emergency response together with Southeast Asian Nations. The national action plan for DRR (NAP-DRR) is practiced along with the national strategic development plan (NSDP). These plans are updated every four years. To address the urgent, immediate needs, and adaptation to climate change, the national adaptation action platform was authorized in 2006. The NCDM is the leader of the DRR action plan, which focuses on the national level to the community level. Moreover, several types of researches including flood hazard mapping, flood risk assessment, and flood damage assessment have been conducted under the effort of DRR. These studies are very valuable for generating the idea and solutions for DRR. Although the limitation of the ground data created the difficulty of researching, RS provides global data cost-effectively. Under the perspective of RS, several types of flood analyses were carried out in various locations over Cambodia (**Table 2**).

Table 2.

List of flood studies in Cambodia.

N	Areas	Data used	Method	Focus	Reference
1	Lower Mekong river	Water level, discharge, RCS GPS survey RADARSAT-1 image Landsat-ETM Population, river, road	HEC-RAS AHP Comparison	Hazard flood mapping	Hazarika et al. (2007)
2	Tonle Sap Lake	DEM TRMM Landsat and MODIS	Regression Monte Carlo simulation	The relationship between flood, precipitation, and deforestation	Kim et al. (2019)
3	Angkor Wat site	PALSAR DEM	AHP	Flood hazard zonation map	Liu et al. (2019)
4	Lower Mekong river	DEM Water level and discharge UNOSAT	HEC-RAS Comparison	Flood map	Ly et al. (2018)
5	Mekong River	MODIS Water level Landsat	EVI or NDVI LSWI WFFI	Temporal change in the extent of annual flooding	Sakamoto et al. (2007)
6	Tonle Sap River and floodplain	MODIS DEM Water level	NDVI MCL	Seasonal changes in inundation area and water volume	Siev et al. (2016)
7	Whole Cambodia	MODIS DEM Radarsat-2 image Population	NDVI Comparison Probability of flood	Multi-temporal flood mapping	Son et al. (2019)
8	Stung Sen River basin	DEM Landsat image Observe rainfall Crop data UNOSAT	RRI Relative damage curves for paddy rice crop Comparison	Rice crop damage	Chung et al. (2019)
9	Tonle Sap basin	GRACE CSR-Release05 MODIS TRMM	GLDAS-NOAH ERA PCR-GLOBWB	Water storage and flood identification	Tangdamrongsub et al. (2016)
10	Mekong river	DEM Landsat-7	Linear binary classifier ROC	Flood hazard mapping	Try et al. (2019)
11	Southern Cambodia, along Mekong	MODIS Landsat-7 ETM+ Landsat-8 OLI Daily water level	WFFI MNDWI	Spatiotemporal flood inundation and land cover change	Vichet et al. (2019)
12	Tonle Sap lake	MODIS DEM Observed rainfall	RRI using CAESAR-LISFLOOD	Hydrological impacts on Tonle Sap lake	Yu et al. (2019)
13	Lower Mekong river basin	DEM MODIS GPM and TRMM Temperature from GLDAS	SWAT Global reanalysis weather data from NCEP and CFSR	Streamflow variability	Mohammed et al. (2018)
14	Lower Mekong river	Peak discharge DEM	Flood frequency analysis HEC-RAS	Hazard flood map and its return period	Kim et al. (2020)

3.2.1 Flood hazard mapping

The flood disaster is the mixture of human susceptibility and physical exposure toward the geophysical process. The importance of flood damage is related to landuse, flood characteristics, and

the capacity of people to cope with it (Smith & Ward, 1998). Flood hazard mapping is significant for mitigation and prevention approaches (Radwan et al., 2018). It can be done by using flood modeling and RS data with the help of GIS. The hydraulic model is used to simulate the floods while the GIS environment can visualize the flood simulation result and hazard analysis. HEC-RAS is one of the popular opened source software with a Graphical User Interface (GUI) that can do hydraulic simulations and develop the flood maps for a river system of steady flow, unsteady flow, and sediment transport (Ly et al., 2018). Kim et al. (2020) used HEC-RAS combined with RS for flood hazard mapping in the Lower Mekong River. The study showed that 2011 and 2013 historical floods influenced most of the flood depth considering return periods. Additionally, Ly et al. (2018) applied HEC-RAS and RS to map hazard areas prone to flood in the Lower Mekong River. It illustrated that extent of the simulation flood was greater than the observed flood. It could be the result of model computation and insufficient data. The depth of the simulation flood was less than the observed overall. Regarding the comparison for verification of the simulated result, RS images can be used to compare the extent of floods. Moreover, microwave RS images can proceed as a base map for inundation areas since it can be obtained in all-weather conditions and all times. UNOSAT image was used to assess the capacity of HEC-RAS such as flood depth and flood extend. Most of the studies have used DEM of 30m resolution; however, the errors have occurred as it cannot detail every elevation changing. Since the extraction and floodplain delineation is based on DEM, the higher resolution of DEM should be taken into account. Moreover, SWAT (Soil and Water Assessment) is a semi-distributed model interfaced with GIS that can identify surface runoff. SWAT can also use observed hydrological data to simulate the discharge, which is compatible with the actual data (Prasanchum et al., 2020) should be used. Still, HEC-RAS and RS combined with GIS provides an ability for flood mapping successfully. Hazarika et al. (2007) also used HEC-RAS and RS to map hazard areas prone to flood in four provinces in the Mekong River catchment. The RS data were used to validate simulated flood and generate the Manning's roughness coefficients. The studies found that most of the flood areas were agricultural areas with a maximum depth between 3.5m to 6.5m. The combination of HEC-RAS and RS with the help of the GIS is effectively used for flood hazard mapping. Flood prevention and management are very crucial for sustainable development. The flood hazard mapping obtained by using SAR images from different years and flood hazard index (FHI) was developed to analyze the flood in the Angkor area. The area around Angkor Wat monuments must be monitored, and flood control measures should be taken into account to protect the site from flooding (Liu et al., 2019). MODIS and DEM were used to investigate the seasonal change of inundation areas and water volume and floodplain of Tonle Sap (Siev et al., 2016).

RS is cost-effective, and it is a suitable source to measure and monitor the floods while the number of hydrological stations is narrow. However, the resampling of the resolution of satellite data might have caused an error. Hence, the high resolution of the digital terrain model obtained from topographical maps should be taken into account. Try et al. (2019) used a Landsat-7 image to generate a flood map. Besides, satellite flood maps were needed to validate the result. The inundation modeling should be taken into account to enhance the predicted accuracy since the flood might be caused by other factors such as topographic condition, landuse change, climate change, etc. To analyze the spatiotemporal distribution of flood in the Southern, MODIS, Landsat-8 OLI, and Landsat-7 ETM+ were used. WWF algorithm for flood inundation detection was applied. The study concluded that the MODIS flood map can be applied to characterize the flooding (Vichet et al., 2019).

3.2.2 Flood risk assessment

The application of RS is very significant in disaster management, particularly in flood analysis from the perspective of Cambodia. It has obviously shown in **Table 2** that most of the RS data have been used in flood risk assessment. Several researchers including Tangdamrongsub et al. (2016), Kim et al. (2019), and Yu et al. (2019) attempted to explore the different tools and techniques for flood risk in Tonle Sap. Tangdamrongsub et al. (2016) use the satellite observation including GRACE, MODIS, and TRMM to identify the flood and water storage by applying the PCR-CLOBWB hydrological model. The results demonstrate that it is a good agreement between the 8-day averaged

over monthly intervals of MODIS-derived TWS variations and the GRACE TWS variations. Therefore, GRACE data can be recognized as a sufficient tool for observing the small-scale hydrological basin. However, the high resolution of satellite images is still encouraged. Furthermore, Yu et al. (2019) has been used Rainfall Runoff Inundation (RRI) model to study hydrological impacts by using MODIS, DEM, and observed rainfall data. The use of the RRI model combined with DEM provides acceptable flooding areas by comparing with the MODIS observed flood map. It can solve the complex hydrological interaction between the Mekong River and Tonle Sap Lake. Regression analysis and Monte Carto simulation, which can predict future flood risk, were applied in Tonle Sap by using DEM, TRMM, Landsat, and MODIS. It concluded that both rainfall and deforestation deteriorated for flood risk. The flash flood frequency occurs in Tonle Sap during the heavy rainfall. Hence, the satellite information, especially TRMM, used in this study can provide a significant result to the analysis of flood severity, and it can be used to predict how the rainfall impacts the flood severity in the study area (Kim et al., 2019).

The recent hydrological circumstance and climate prediction can predict the temporal change of flooding. Sakamoto et al. (2007) studied the transformation of floods by using a wavelet-based filter (WFFI) and land surface water index (LSWI). They adopted MODIS, flood map, DEM, RADARSAT image, and observed water level. The simulated result has a margin of error related to resolution, but it correlates with the surface water obtained from the Landsat, RASARSAT, and hydrological data in terms of spatiotemporal changes. Flood assessment was prepared by Son et al. (2019) using MODIS, DEM, Radarsat-2, and population data. They applied the NDVI and comparison probability to map the multi-temporal flood. It showed that 32 districts were inundated. Besides, MODIS obtained in the rainy season was mostly covered by the cloud even they used the reconstruct cloud-affected value. It still has inappropriate artificial value for the analysis. Other factors also contributed to the error including mixed-pixel and low-resolution.

3.2.3. Flood damage assessment

The flood damage assessment is identical significant in providing potential risk information to support decision-makers and flood managers to reduce the diverse impacts. The general strategy to estimate the direct impact of the flood was using a relative flood damage curve. This curve discusses the relationship between flood characteristics such as depth, duration, and potential damage for objects. RS is one of the most effective tools to observe that provides flood and damage assessment information within cost-effectiveness. DEM, Landsat, Satellite flood map, boundary condition, observed rainfall, and paddy field data were used in flood damage assessment in Stung Sen catchment (Chung et al., 2019). RRI was applied to estimate the flood characteristics including flood level, length, and range. The satellite flood maps were compared with the simulated flood inundation areas. The result suggested that it is possible to use RRI and RS to identify the flood damage assessment. However, there were still some limitations concerning the absence of observed cross-section. The observed rainfall stations are limited, so rainfall-based satellites such as TRMM and GPM should be considered.

3.3 Gaps of flood analysis under RS perspective

Although several flood analyses have used RS combine with GIS effectively, the gaps still exist. Most of the flood analysis in Cambodia was focusing on overflow floods in the Tonle Sap catchment and along the Mekong River. However, the floods are not only occurring in those areas, but overflow floods and flash floods happen in other areas (**Fig. 2**). For example, the area located in the Northeast near the Lao border were classified as high flood impacts. Hence, these areas should have more researches on floods and flash floods. Furthermore, the flood analysis using RS over Cambodia frequently focused on flood risk assessment following by flood hazard mapping while flood damage assessment was only one study. Likewise, trustworthy and timely flood forecasting is a primary phase to disaster management whereas the early warning systems are very essential for mitigation measures. Flood forecasting and flood early warning, however, seem to be not interested in the researcher. Thus, further study should be focusing on flood forecasting and flood early warning.

RS has been commonly used for mapping flood hazards, assessing flood risk, and assessing flood damage were DEM, MODIS, and Landsat. Most of the observed satellite flood map adopted in both flood risk assessment and flood hazard mapping is MODIS. PALSAR image, which is applicable while has a real-time flood monitoring; however, is rarely used because the frequent and open access to PALSAR is limited.

Moreover, several studies have claimed the error of flood extent due to the low resolution of DEM (30m). The low resolution of DEM cannot point each elevation changing; moreover, less cross-section creates inaccurate river bathymetric including extension and contraction. The high resolution of DEM, therefore, is needed to get more precise simulated results as the elevation extraction and floodplain delineation are established based on the DEM. Besides, the application of flood monitoring mainly depends on the availability and reliability of real-time precipitation. The data quality has to be strong.

Rain gauge stations over Cambodia are very few (98 stations) whereas its density is 54 x 10^{-5} per km^2 or 13.5 x 10^{-4} per 25 km^2. The rain gauges provide a spot sample of the rain dropping over a catchment; therefore, the number of gauges is essential to provide a consistent estimation of a catchment rainfall where rainfall slopes are marked. According to Ratnayaka et al. (2009), the minimum rain gauge density should be 1 per 25 km^2 while the significant thunderstorm systems require 1 per 20 km^2. Furthermore, Ground radar precipitation can be used for estimating a practical option for flood monitoring and forecasting. S-Band Doppler weather radar meteor 650C, which has a range of 450 km located in Phnom Penh was not used in any flood analysis over Cambodia.

Table 3.

Satellite data used in flood analysis over Cambodia.

Focusing	Data	Method	Reference
Flood hazard mapping	Radarsat-1 * Landsat-7 ** PALSAR * DEM ***** UNOSAT * MODIS * Radarsat-2 *	HEC-RAS, AHP, NDVI	(Hazarika et al., 2007; Kim et al., 2020; Liu et al., 2019; Ly et al., 2018; Son et al., 2019; Try et al., 2019)
Flood risk assessment	Envisat RA-2 * DEM **** TRMM *** Landsat ** MODIS ******* GRACE CSR-Release05 * Landsat-7/ETM+ * Landsat-8 OLI * GPM *	Monte Carlo, EVI or NDVI, RRI, SWAT	(Kim et al., 2019; Mohammed et al., 2018; Sakamoto et al., 2007; Siev et al., 2016; Tangdamrongsub et al., 2016; Vichet et al., 2019; Yu et al., 2019)
Flood damage assessment	DEM * Landsat-8 * UNOSAT *	RRI	(Chung et al., 2019)

***** is number of studies have been used

3.4 Discussion

The 2011 flood caused numerous losses to the country. Most of the affected areas were located in the Tonle Sap and Mekong River. Other areas located far from these two main water sources are also affected. According to CFE-DM (2017), Cambodia experiences flash floods once there is heavy rainfall through the rainy season, especially in August, September, and October. Moreover, it is affected by the slower but prolonged flooding from the overflow of Tonle Sap and Mekong River. However, several spatial coverages to floods were not paid attention; thus, there should be more studies concerning those areas.

RS provides a powerful technique for object detection in inundation areas. The application of RS is weighty in DRR, particularly in flood disaster studies. Currently, RS has been extensively used in flood studies in Cambodia. Different satellite data have been used such as DEM, MODIS, TRMM, and Landsat images. However, the error related to image resolution is still the problem. The study of Arnesen et al. (2013) in the Amazon River adopted ALOS PALSAR with 12.5m resolution for flood observation. One national radar station can observe covering the whole country with the range of 450km, but some parts may be blocked by the high mountains especially in the Southwest, border to Thailand. The radar composite approach can be applied since several radars in Thailand cover some parts of Cambodia. However, the radar data in the country have not been used in any studies due to the limitation of data access.

Moreover, the distribution of rain gauge stations over the country is very few, and some of them are not well maintained (**Fig. 2**); therefore, data from satellites including TRMM, GPM, and TMPA are essential in flood studies. TRMM was used to validate the ground-based rainfall and replace the areas without or less observed rainfall stations. Iqbal and Athar (2018) used TMPA and TRMM to verify the observed rainfall over Pakistan by using different methods including RMSE, ME, MAE, and correlation coefficients. The result shows a strong correlation between the observed rainfall and satellite rainfall. TRMM and TMPA are very suitable for the areas without or not enough observed rainfall stations. Thus, satellite-based rainfall can be used to replace the areas without rain gauge stations.

Since the map is the most common geographical representation of reality, the flood map is presently being used in various disaster management practices. The accuracy and verification can be found by using the hydraulic model (Horritt, 2006) or satellite flood maps from different sources such as MODIS (Sakamoto et al., 2007) and satellite flood images from UNOSAT along with the verification equations (Ly et al., 2018). The random forest (RF) model was used in the flood vulnerability mapping in mountainous areas in China. It can hold great datasets through factor contribution examination. It also Supports Vector Machine methods (SVM) (Zhao et al., 2018). Furthermore, the AHP model combined with GIS and RS was used for mapping the area prone to flash flood. This method can be applied in the concept of Cambodia since data are finable (Mohamed, 2019). Besides, the SWAT and GUMBEL distribution method used for simulating flood risk areas and creating the river route based on DEM was carried out in Yang catchment, Thailand (Prasanchum et al., 2020). SWAT model can simulate the watershed delineation to distinct the entire areas into sub-catchments, which allows users to distinguish the discharge of each catchment.

4. CONCLUSION

The purposes of this paper are to identify the spatial distribution of the 2011 flood impact, evaluate how RS has been applied in flood studies, and find the gaps of each study under RS perspective over Cambodia. It is found that several gaps are identified such as the lack of studies on the other flood-affected areas, the error due to the satellite image resolution, the focused parts of flood analysis, and the limitation of rain gauges stations. The 2011 floods caused numerous impacts. Many studies have been focusing on Tonle Sap and Mekong River regions; however, floods do not only occur in those areas. There should be more research in other flood-prone areas.

The models such as HEC-RAS and RRI with RS data have been used in most studies due to its efficiency in simulating and providing satisfying results. However, it is suggested that sufficient data and field surveying such as cross-section and floodplain should be taken into account to run this model in future studies. Moreover, the low resolution of DEM caused the error to the results since it cannot detail all elevation changes. The high-resolution DEM, therefore, is needed for a better result. Additionally, flood forecasting and flood early warning, which are very essential for disaster management, was not carried out in the studies. Furthermore, the satellite-based rainfall like TRMM is very important since the distribution of rain gauge stations over Cambodia is limited. Moreover, the radar composite should be considered since it can provide more accuracy of data.

REFERENCES

Arias, M. E., Cochrane, T. A., Piman, T., Kummu, M., Caruso, B. S., & Killeen, T. J. (2012). Quantifying changes in flooding and habitats in the Tonle Sap Lake (Cambodia) caused by water infrastructure development and climate change in the Mekong Basin. *J Environ Manage, 112*, 53-66. https://doi.org/10.1016/j.jenvman.2012.07.003

Arnesen, A. S., Silva, T. S. F., Hess, L. L., Novo, E. M. L. M., Rudorff, C. M., Chapman, B. D., & McDonald, K. C. (2013). Monitoring flood extent in the lower Amazon River floodplain using ALOS/PALSAR ScanSAR images. *Remote Sensing of Environment, 130*, 51-61. https://doi.org/10.1016/j.rse.2012.10.035

CamDi. (2013). *Cambodia disaster loss and damage analysis report 1999-2013*. Phnom Penh: National Committee for Disaster Management and United Nation Development Programme.

CFE-DM. (2017). *Cambodia Disaster Management Handbook*. Phnom Penh: Center for Excellence in Disaster Management & Humanitarian Assistance.

Chung, S., Takeuchi, J., Fujihara, M., & Oeurng, C. (2019). Flood damage assessment on rice crop in the Stung Sen River Basin of Cambodia. *Paddy and Water Environment, 17*(2), 255-263. https://doi.org/10.1007/s10333-019-00718-1

Doswell, C. A. (2003). *Flooding*. the United States of America: Elsevier Science

Hazarika, M. K., & Bormudoi, A. (2007). Flood Hazard Mapping in Four Provinces of Cambodia Under the Mekong River Basin. *5th AMFF - Improving Inputs towards Medium Term Flood Forecasting and Warning in the Mekong Basin*. https://www.researchgate.net/publication/262270027

Hazarika, M. K., Bormudoi, A., Kafle, T. P., Samarkoon, L., Nuon, K., Savuth, Y., & Narith, R. (2007). *Flood Hazard Mapping in Four Provinces of Cambodia Under the Mekong River Basin*. Paper presented at the 5th AMFF - Improving Inputs towards Medium Term Flood Forecasting and Warning in the Mekong Basin.

Horritt, M. S. (2006). A methodology for the validation of uncertain flood inundation models. *Journal of Hydrology, 326*(1-4), 153-165. https://doi.org/10.1016/j.jhydrol.2005.10.027

Iqbal, M. F., & Athar, H. (2018). Validation of satellite based precipitation over diverse topography of Pakistan. *Atmospheric Research, 201*, 247-260. https://doi.org/10.1016/j.atmosres.2017.10.026

Kim, S., Sohn, H.-G., Kim, M.-K., & Lee, H. (2019). Analysis of the Relationship among Flood Severity, Precipitation, and Deforestation in the Tonle Sap Lake Area, Cambodia Using Multi-Sensor Approach. *KSCE Journal of Civil Engineering, 23*(3), 1330-1340. https://doi.org/10.1007/s12205-019-1061-7

Kim, V., Tantanee, S., & Suparta, W. (2020). Gis-Based Flood Hazard Mapping Using Hec-Ras Model: A Case Study of Lower Mekong River, Cambodia. *Geographia Technica, 15*(1), 16-26. https://doi.org/10.21163/gt_2020.151.02

Kreft, S., Eckstein, D., & Melchior, I. (2017). *Who suffers most from extreme weather events? Weather-related loss events in 2015 and 1996 to 2015*. Berlin: Germanwatch.

Liu, J., Xu, Z., Chen, F., Chen, F., & Zhang, L. (2019). Flood Hazard Mapping and Assessment on the Angkor World Heritage Site, Cambodia. *Remote Sensing, 11*(1), 98. https://doi.org/10.3390/rs11010098

Ly, S., Kim, L., Demerre, S., & Heng, S. (2018). Flood Mapping along the Lower Mekong River in Cambodia. *Engineering Journal, 22*(1), 269-278. https://doi.org/10.4186/ej.2018.22.1.269

Manh, N. V., Dung, N. V., Hung, N. N., Merz, B., & Apel, H. (2014). Large-scale suspended sediment transport and sediment deposition in the Mekong Delta. *Hydrology and Earth System Sciences, 18*(8), 3033-3053. https://doi.org/10.5194/hess-18-3033-2014

Matingo, T., Gumindoga, W., & Makurira, H. (2018). Evaluation of sub daily satellite rainfall estimates through flash flood modeling in the Lower Middle Zambezi Basin. *Proceedings of the International Association of Hydrological Sciences, 378*, 59-65. https://doi.org/10.5194/piahs-378-59-2018

Mohamed, S. A. (2019). Application of satellite image processing and GIS-Spatial modeling for mapping urban areas prone to flash floods in Qena governorate, Egypt. *Journal of African Earth Sciences, 158*, 103507. https://doi.org/10.1016/j.jafrearsci.2019.05.015

Mohammed, I. N., Bolten, J. D., Srinivasan, R., & Lakshmi, V. (2018). Satellite observations and modeling to understand the Lower Mekong River basin streamflow variability. *J Hydrol (Amst), 564*, 559-573. https://doi.org/10.1016/j.jhydrol.2018.07.030

Prasanchum, H., Sirisook, P., & Lohpaisankrit, W. (2020). Flood Risk Areas Simulation Using Swat and Gumbel Distribution Method in Yang Catchment, Northeast Thailand. *Geographia Technica*, 29-39. https://doi.org/10.21163/gt_2020.152.04

Radwan, F., Alazba, A. A., & Mossad, A. (2018). Flood risk assessment and mapping using AHP in arid and semiarid regions. *Acta Geophysica*, *67*(1), 215-229. https://doi.org/10.1007/s11600-018-0233-z

Ranke, U. (2016). *Natural Disaster Risk Management: Geosciences and Social Responsibility*. New York: Springer.

Ratnayaka, D. D., Brandt, M. J., & Johnson, K. M. (2009). Hydrology and Surface Supplies *Water Supply* (pp. 63-107): ScienceDirect.

Sakamoto, T., Van Nguyen, N., Kotera, A., Ohno, H., Ishitsuka, N., & Yokozawa, M. (2007). Detecting temporal changes in the extent of annual flooding within Cambodia and the Vietnamese Mekong Delta from MODIS time-series imagery. *Remote Sensing of Environment, 109*(3), 295-313. https://doi.org/10.1016/j.rse.2007.01.011

Sharma, T. P. P., Zhang, J., Koju, U. A., Zhang, S., Baia, Y., & Suwal, M. K. (2019). Review of flood disaster studies in Nepal: A remote sensing perspective. *International Journal of Disaster Risk Reduction, 34*, 18-27. https://doi.org/10.1016/j.ijdrr.2018.11.022

Siev, S., Paringit, E., Yoshimura, C., & Hul, S. (2016). Seasonal Changes in the Inundation Area and Water Volume of the Tonle Sap River and Its Floodplain. *Hydrology, 3*(4), 33. https://doi.org/10.3390/hydrology3040033

Smith, K., & Petley, D. N. (2009). *Environmental Hazards: Assessing Risk and Reducing Disaster* (fifth ed.). Great Britain: Routledge.

Smith, K., & Ward, R. (1998). *Floods: Physical Processes and Human Impacts*: Wiley.

Son, N.-T., Chen, C.-F., & Chen, C.-R. (2019). Flood assessment using multi-temporal remotely sensed data in Cambodia. *Geocarto International*, 1-16. https://doi.org/10.1080/10106049.2019.1633420

Tangdamrongsub, N., Ditmar, P. G., Steele-Dunne, S. C., Gunter, B. C., & Sutanudjaja, E. H. (2016). Assessing total water storage and identifying flood events over Tonlé Sap basin in Cambodia using GRACE and MODIS satellite observations combined with hydrological models. *Remote Sensing of Environment, 181*, 162-173. https://doi.org/10.1016/j.rse.2016.03.030

Thoeun, H. C. (2015). Observed and projected changes in temperature and rainfall in Cambodia. *Weather and Climate Extremes, 7*, 61-71. https://doi.org/10.1016/j.wace.2015.02.001

Try, S., Lee, G., Yu, W., & Oeurng, C. (2019). Delineation of flood-prone areas using geomorphological approach in the Mekong River Basin. *Quaternary International, 503*, 79-86. https://doi.org/10.1016/j.quaint.2018.06.026

UNDRR. (2019). *Disaster Risk Reduction in Cambodia: Status Report 2019*. Retrieved from Bangkok, Thailand:

Vichet, N., Kawamura, K., Trong, D. P., On, N. V., Gong, Z., Lim, J., . . . Bunly, C. (2019). MODIS-Based Investigation of Flood Areas in Southern Cambodia from 2002–2013. *Environments, 6*(5), 57. https://doi.org/10.3390/environments6050057

Yu, Qin, X. S., & Larsen, O. (2012). Joint Monte Carlo and possibilistic simulation for flood damage assessment. *Stochastic Environmental Research and Risk Assessment, 27*(3), 725-735. https://doi.org/10.1007/s00477-012-0635-4

Yu, W., Kim, Y., Lee, D., & Lee, G. (2019). Hydrological assessment of basin development scenarios: Impacts on the Tonle Sap Lake in Cambodia. *Quaternary International, 503*, 115-127. https://doi.org/10.1016/j.quaint.2018.09.023

Zhao, G., Pang, B., Xu, Z., Yue, J., & Tu, T. (2018). Mapping flood susceptibility in mountainous areas on a national scale in China. *Sci Total Environ, 615*, 1133-1142. https://doi.org/10.1016/j.scitotenv.2017.10.037

10 YEARS EROSION-SEDIMENTATION MONITORING: SYSTEM BASED AUTOMATIC INTERPRETATION IN COASTAL AREA OF BREBES REGENCY, CENTRAL JAVA PROVINCE, INDONESIA

Muhammad DIMYATI [1], ***Edy TRIHATMOKO*** [2], ***Muh Aris MARFAI*** [3*]

DOI: 10.21163/GT_2021.161.03

ABSTRACT:
Nowadays, coastal dynamics are mostly viewed in relation to erosion-sedimentation process. It is important to monitor the erosion-sedimentation in the coastal area in order to reduce its negative impact. This paper aims to identify the erosion-sedimentation process in the coastal area of Brebes Regency, Indonesia, using the automatic interpretation of a geographic information system (GIS) for ten years of analysis. Brebes Regency was chosen as the research area due to its high intensity of sedimentation occurrence. It is also traversed by the Jalan Pantai Utara as the most heavily used road in Indonesia. The automatic interpretation is demonstrated through the utilization of band ratio and the Digital Shoreline Analysis System (DSAS). Neither this type of analysis nor the study area in question has ever been examined before. As novelty, the result shows that sedimentation occurrences of up to 3.9 km were recorded in the most significant case in 2007-2016. This sedimentation is obviously as accumulation of the sediment load and sediment material, at least during last ten years. The total length of the shoreline change is the initial research in history, which precisely measures the shoreline change in Brebes Coastal Area. This research result is considered as a valuable data in coastal management for local authority, especially to handle the problem on coastal erosion and to identify the appropriate location for mitigation action due to erosion process.

Key-words: *Band ratio, Coastal dynamics, erosion-sedimentation process, GIS, Brebes Indonesia.*

1. INTRODUCTION

The surface of the Earth features three main systems, i.e. land, atmosphere, and ocean. These three systems directly influence coastal areas (Davidson and Arnott 2010), thus making coastal areas the most dynamic areas on the Earth surface (Marfai et al. 2008; Bush and Young 2009, in Young and Norby 2009; Davidson and Arnott 2010; Marfai et al. 2018; Marfai et al. 2019). Brahzt (1972, in Supriharyono 2000) defined a coastal area as one that stretches from the breakwater zone toward the land to the farthest coastal aspect measured. Based on this definition, a coastal area is directly exposed to the threat of complex natural hazards, including storms, waves, tsunamis, and tides (Obert et al. 2017). The complexity of coastal dynamics makes them an important area for study in an effort to maintain the function of the coastal area in terms of both its ecological functions and in order to better anticipate the threat of natural disasters (Marfai, et al. 2007; Marfai and King 2008a; Cozzoli et al. 2017). The complexity of the threats in coastal areas is closely related to the intensive geomorphic dynamics that characterize such areas, with two main processes at play, namely erosion and sedimentation (Marfai 2011; Mutaqin et al. 2013).

Coastal areas are characterized by their complex geomorphological dynamics (Marfai 2011; Obert et al. 2017). This complexity increases linearly with shallow water conditions and sloping coastal areas in terms of energy modification (Bird 2008). Sedimentation, as one of the main processes of geomorphological dynamics (Marfai 2011; Mutaqin et al. 2013; Dewi et al. 2016), occurs more intensely in shallow water environments. This is due to the weakening of wave and current energy as

[1]*Department of Geography, Faculty of Mathematics and Natural Sciences, University of Indonesia, Pondok Cina, Beji, Pd. Cina, Beji, Depok, West Java, Indonesia 16424, muh.dimyati@ristekbrin.go.id;*
[2]*Department of Geography, Faculty of Social Science, Universitas Negeri Semarang, 50229, Semarang, Indonesia, edytrihatmoko@mail.unnes.ac.id;.*
[3]*Department of Environmental Geography, Faculty of Geography, Universitas Gadjah Mada, 55281, Yogyakarta, Indonesia, arismarfai@gmail.com , corresponding author.*

it approaches the shore, which in turn means that the terrestrial process will be stronger in the nearshore zone. With erosion and sedimentation as the main processes within coastal areas, they also reflect their dynamics (Ritter, et al. 1995; Marfai 2011). Coastal dynamics are aggravated by intensive human activities, e.g., transportation, construction activities, and other land modifications (Morton 2003; Sakijege et al. 2014). There are some GIS techniques for shoreline change monitoring, such as using GIS histogram analysis (Marfai et al. 2008; Aedla et al. 2015), or using masking operation (Randazzo et al., 2020). In the development of the mathematical models nowadays is also applied on the shoreline monitoring such as beach nourishment as part of the strategy to mitigate the erosion (Parkinson and Ogurcak 2018). By using adequate GIS Technique monitoring, the stakeholders can evaluate and take the proper action for handling erosion-sedimentation in precise and detailed measurements so that the miss-implementation of the shoreline protection will no longer occur. The miss-implementation is always followed by environmental degradation and lost, whether inside or outside the location. The environmental degradation as a result of the miss-implementation shoreline protection as reported by Jakobsen et al. (2007).

The GIS computerized methods using vector and raster format is nowadays have been implementing in various fields, including environmental monitoring for avoiding the degradation (Huang and Wu 2010; Shrestha et al. 2016), disaster mitigation (Marfai 2004; Sakijege et al. 2014), spatial planning (Marfai 2007; Buser and Farthing 2011), and many more. In the area of erosion-sedimentation assessment, some reports such as by (Van and Binh 2009; Dewi et al. 2015; Dewi 2018) explained the function and advantages of GIS operation to support the spatial analysis on the erosion-sedimentation study. DSAS is one of the prominent approaches to do the analysis of erosion-sedimentation, especially take into account the role of the catchment area or behavior of the river. In Asia (Zhao et al. 2011; Thinh and Hens, 2017) are using DSAS to do the erosion and sedimentation analysis, especially along the coastline. In addition, DSAS is also use widely in Indonesia for example by Mutaqin (2017) and Dewi (2018), especially dealing with the coastal management.

The northern part of Central Java Province is a coastal area with sloping coastal conditions (Marfai 2012) and shallow water up to the nearshore zone (Department of Marine and Fisheries of Central Java Province 2016). This combination of existing characteristics suggests that special attention must be paid by the government of Central Java Province to managing the coastal area. Brebes Regency in the northern part of Central Java Province has a high rate of sedimentation that is influenced by its large population, commodities, and tourism (Trihatmoko 2017; Central Bureau of Statistic (CBS) of Central Java Province 2016). Establishing Brebes Regency as an area affected by a significant level of sedimentation will help to support the management of planning in preventing loss attributable to coastal dynamics, particularly in the context of sedimentation occurrences.

Sedimentation monitoring can be divided into two types, namely the terrestrial method (Lagomasino, Corbett, and Walsh, 2013) and computerized methods (Marfai et al., 2016). This study was conducted to identify and monitor the erosion-sedimentation process in Brebes Regency by modeling the occurrence of sedimentation and automatically calculating the length of the sedimentation occurrence in 10 years' analysis. This research was conducted as the first erosion-sedimentation monitoring in Brebes that never been done before. The method utilized a geographic information system (GIS): DSAS, as a software extension of ArcGIS. Analysis of sedimentation using the automated ArcGIS tool, namely DSAS, or any other GIS method, has never before been conducted in Brebes Regency; therefore, this study is the first research into sedimentation using the automated ArcGIS tool in Brebes Regency. However, As a preliminary stage on this project, our work did not cover the sedimentation analysis. Since sedimentation processes need a wide study from the transport process ended up to the complex structure of sedimentary rock, it would be considered for the next stage of the project.

2. STUDY AREA AND DATA

According to data from the CBS of Central Java Province, Brebes Regency had the largest population in 2015 among the coastal regencies in the northern part of Central Java Province.

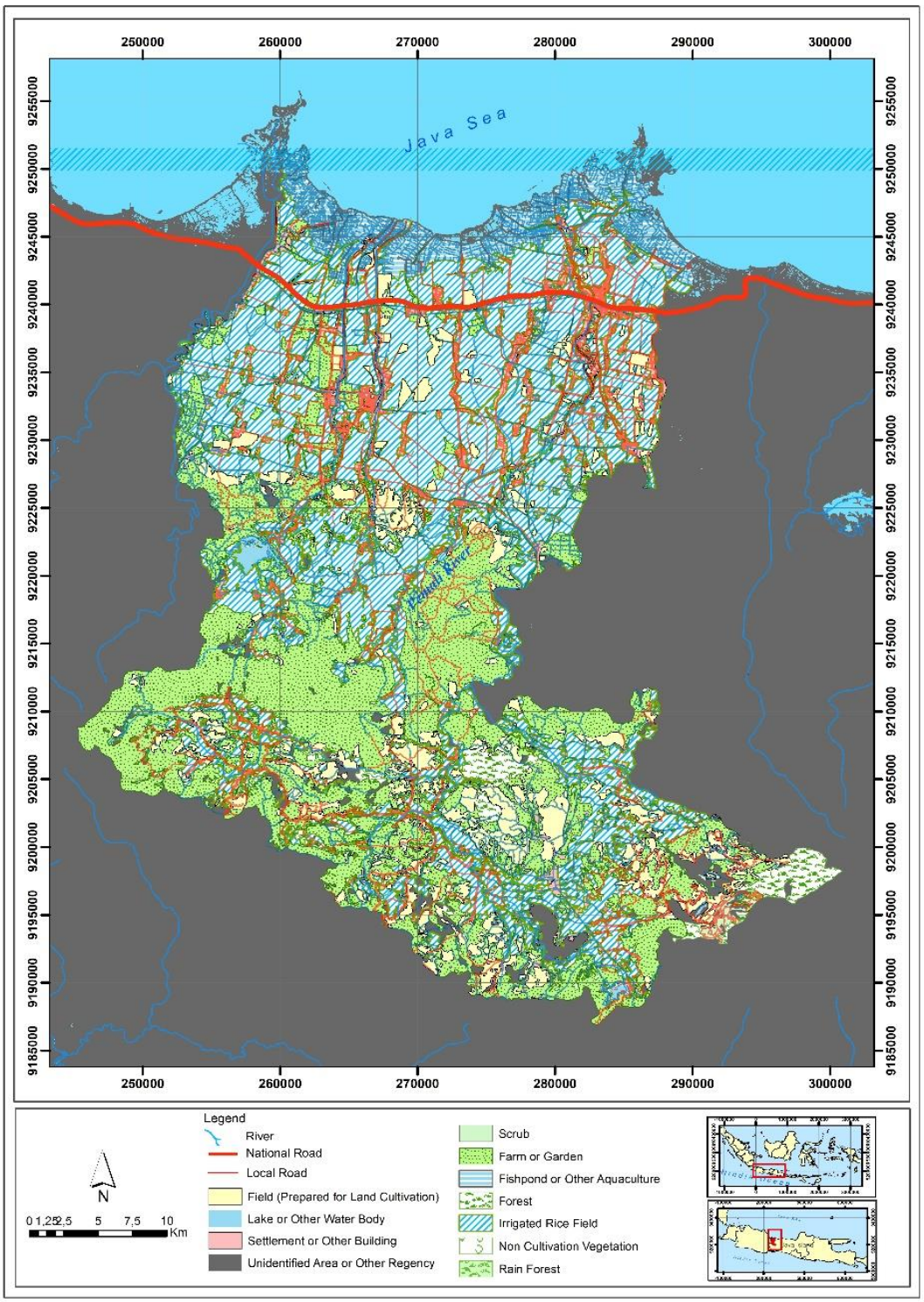

Fig. 1. The land use of Brebes Regency. The image shows that Brebes Regency is dominated by cultivated land. *(Source: Geospatial Information Agency of Indonesia, 2016 and modification)*.

As a regency, it has a population density of 1,075 inhabitants/km2. Based on other data from CBS (2016), Brebes Regency, with its wide fish pond areas, has the highest level of fish production in Central Java Province. Cultivation from fish ponds accounted for 69,853.18 tons, with a total of 4,021 households employed as pond farmers in 2015. The combination of this concentration of fish pond farmers and the high rate of cultivation from fish pond production shows that Brebes Regency has good fish pond potential. According to the Medium-Term Development Plan (MTBP) of Brebes Regency for the period 2017–2022, the area also has good tourism potential. This is shown by the number of visitors to the area compared to other regencies in Central Java Province. Based on tourism data, the most visited site is Randusanga Beach, which recorded 62,582 people in 2015. Such high visitor numbers also have an impact on the total amount of revenue earned from tourism, which was recorded at Rp 494,765,000 in 2015, or equal to USD 37,107.38 (Regional Planning and Development Agency 2016). Tourism in the Brebes coastal area also benefits from mangrove forest tourism. In fact, the mangrove forest has a function not only in supporting tourism, but it also plays an important role in the development of other socioeconomic sectors, including natural resources (Sukarna and Syahid 2015). The report and evaluation from the Pantura rehabilitation of Central Java Province (Fadhilah 2015) highlights the potential of the mangrove forest in the coastal area of the northern part of Central Java Province. Brebes Regency is the second largest mangrove area in the northern part of Central Java Province, with mangrove covering an area of 1,179.02 hectares, while Demak Regency has mangrove covering 2,176.79 hectares (Fadhilah 2015). **Fig. 1** shows the land use of Brebes Regency.

Geomorphologically, Brebes Regency comprises folded geological structures. These structures account for the flat coastal area dominated by small grain materials as an alluvium material (Marfai 2012), which are conditions that are prone to accelerate coastal dynamics (Bird 2008). The coastal dynamic is also worsened considering that Brebes coastal area has an enclosed gulf with big headlands on both sides (Komar, 1976; Bishop, 1984; Coastal Engineering Research Center (CERC), 1984) (**Fig. 1**).

3. METHODOLOGY

In this study conducted in Brebes Regency, the first step in monitoring activity for shoreline extraction study was to identify the sedimentation process (Retnowati et al. 2012). GIS as the computerized technology was utilized as the main process. GIS was clarified as being the best and most reliable technology available nowadays for the purpose of monitoring coastal dynamics (Marfai 2004). **Table 1** contains the GIS data used in this study.

Table 1.

Detailed information on the Landsat images (All images were captured at low tide).

Data	Acquisition Date	Acquisition Time (GMT)	Sensor	Band
Landsat 8	10 August 2016	02.54	OLI-TIRS	5/2
Landsat 5	2 August 2007	02.47	TM	4/1

The GIS data used in the study were obtained from The United States Geological Survey (USGS). Landsat 8 and 5 were chosen since these two images are in the good condition and appropriate to be used for spatial analysis and further image processing in the time span of 2007-2018. Landsat 8 was published on February 2013, and Landsat 5 had been decommissioned on June 2013. Band 5 and band 2 in Landsat 8 were appropriate band to do analysis related to water and land, such as in the coastal environment. Band 5 as the near infrared band has the wave length up to 0.85 - 0.88 μm on the 30 m of spatial resolution. This band is stressing on the biomass content and shoreline. By having a near infrared band, the analysis is easier considering that the wave length is optimally absorbed by the water body, and band 2 is the blue band with emphasizing on bathymetric and soil. By this band combination, distinguishing the land and waterbody will much easier. In the same characteristics, band 4 and band 1 in Landsat 5 are also as the near infrared and blue band, therefore those 2 bands are also suitable to do the shoreline monitoring. Those two types of Landsat images were captured on

the low tide condition and this is considered as the advantages of this data, while those image on the same condition and it will useful for monitoring sensitive area such as shoreline.

The GIS tool has been used to extract the Landsat-5 TM in 2007 and Landsat-8 OLI / TIRS in 2016, paths 120-121 and row 65. The time range of this analysis was classified as a fit time range variation in shoreline change analysis (Rijn 2010). Shoreline data from Landsat-8 OLI/TIRS was obtained using Band 5 and Band 2 or a near-infrared band and blue band. These were the best two combinations for reflecting the boundary of land and water (Khawfany et al. 2017). For more detail, Band 5 on Landsat 8 OLI/TIRS as a near-infrared band has a zero-reflection value for water so that a clear shoreline can be obtained. Furthermore, in terms of wavelength matching, Landsat-5 TM was conducted using Band 4 and Band 1. The band information for Landsat-5 TM and Landsat-8 OLI/TIRS was processed using ENVI (Environment for Visualizing Images) software in order to extract the early shoreline interpretation data, as shown in **Fig. 2**. The band ratio method was selected as the most effective means of manipulation for the pixel values (Van and Binh 2009). Manipulation refers to the use of two binary codes to represent water and land: "1" for land, and "0" for water. However, utilizing the binary code as typical raster data makes it much easier to complete the shoreline determination process. After obtaining the boundary line through band ratio processes using ENVI software (**Fig. 2**), a further process was conducted using ArcGIS software (ENVI software is designed specifically for GIS users and integrates fully with ESRI's ArcGIS software) and the DSAS tool. DSAS is a separate extension of the ArcGIS software that was created in May 2009, which means it is available only for ArcGIS 9.2 and above (Himmelstoss, 2009). The extension works using a vector data format. DSAS processing is based on the principle of determining the length or extent of the dynamic process of the existing coastal areas, whether in the form of erosion or sedimentation. Information on the length or extent of the process of the coastal dynamics in the area is obtained from the data attribute. Use of the DSAS tool enables more accurate and effective measurement of the shoreline changes as mentioned in this research. **Fig. 3** illustrates the workflow of the research.

4. RESULTS AND DISCUSSIONS

Brebes Regency, as one of the regencies in northern Central Java Province, was identified as an area with a high impact of coastal dynamics, especially with regard to the sedimentation effect (Trihatmoko, 2017). **Fig. 4** indicates that the two binary codes were produced by ENVI for the Brebes coastal area in 2016 as raster data. By eliminating the binary code representing the area of water, data for both the land and shoreline are obtained. The later result obtained using the detailed DSAS tool reveals sedimentation to be the dominant process in Brebes Regency compared to erosion. This result is shown in **Fig. 5**.

Zooming is carried out in several parts with significant and clear changes, i.e., on boxes a, b, c, d, and e in Fig 5. In locations marked with the box a, erosion is clearly visible compared to sedimentation, this will certainly bring disadvantages to most of the coastal land in part a, especially agricultural land and residential areas. Meanwhile, box b tends to increase sedimentation. This sedimentation is expected to come from the river above it. Box c is also following the condition in the area of box b. In this area, vegetation protection with mangroves is starting to develop. The existence of the barrier islands in front of box c also contributes to reducing the energy of the sea as the main energy for triggering erosion. So, the sediment that is brought by the stream can spread along the shore. The shape of the delta also verifies it as the main outlet of the Pemali River. The shape is classified as the lobate. That means the stream energy is dominated compare to sea energy. It is also confirmed by the main sedimentation process in the area of box d. This location has been found as the most significant sediment processes compare to other locations, followed by the area of box e. The sedimentation process lead to delta development are appear in the boxes a, b, c, d, and e, we could assume that the sediments transfer from those river plays important role on the development of the sediment formation on the coastal area. Further observation and grand size as well as sediment measurement on rivers are needed in order to get more understanding on the significant contribution of river sediments on the development of the coastal sedimentation process and formation.

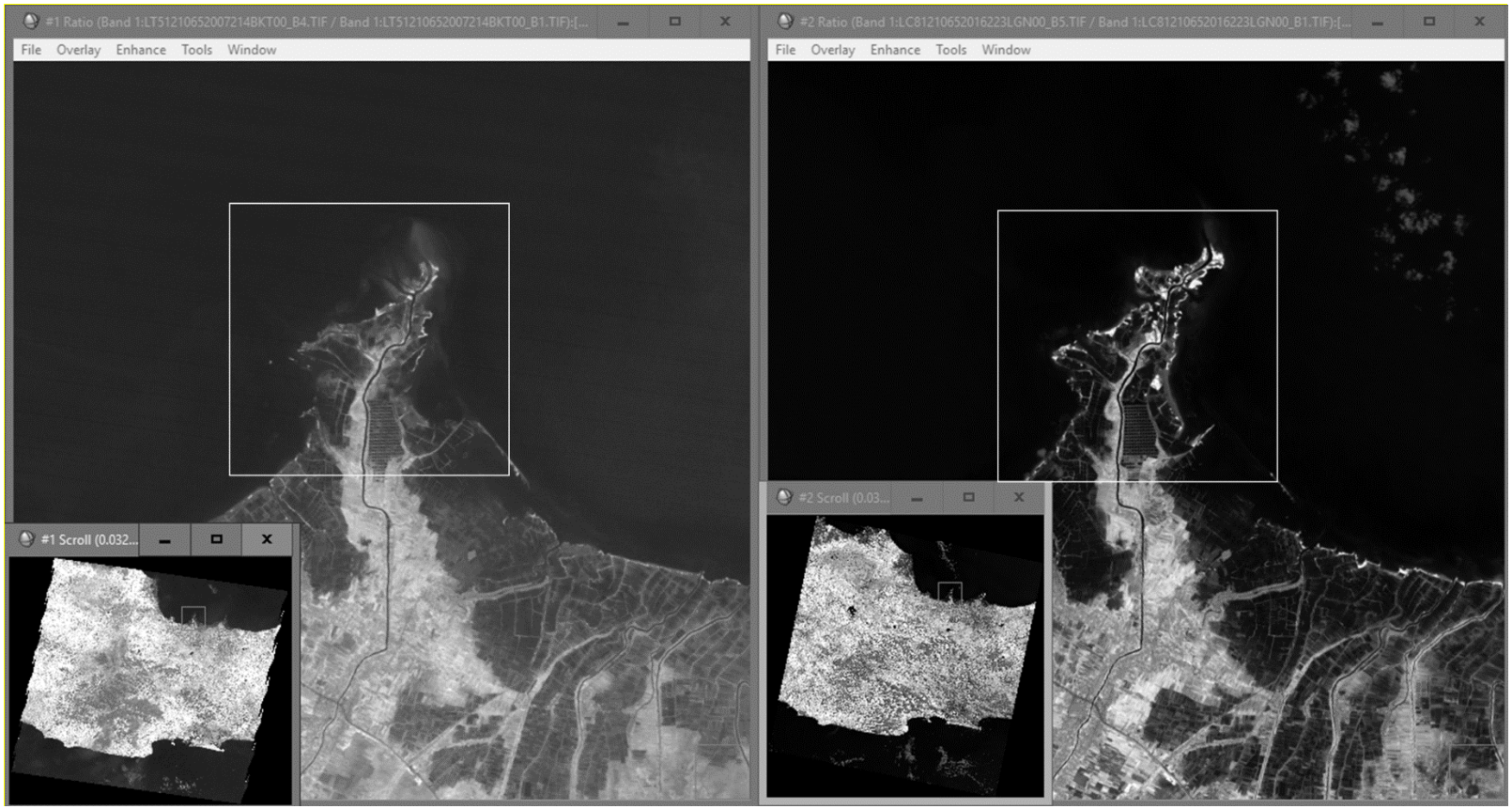

Fig. 2. Northern coastal area of Central Java Province. Brebes Regency is located on the western part of Central Java Province, Landsat 5 band 4/1 in 2006 (left) and Landsat 8 band 5/2 in 2016 (right). The most intensive changes area is highlighted by the boxes on each year. *(Source of data: USGS and modification, 2016).*

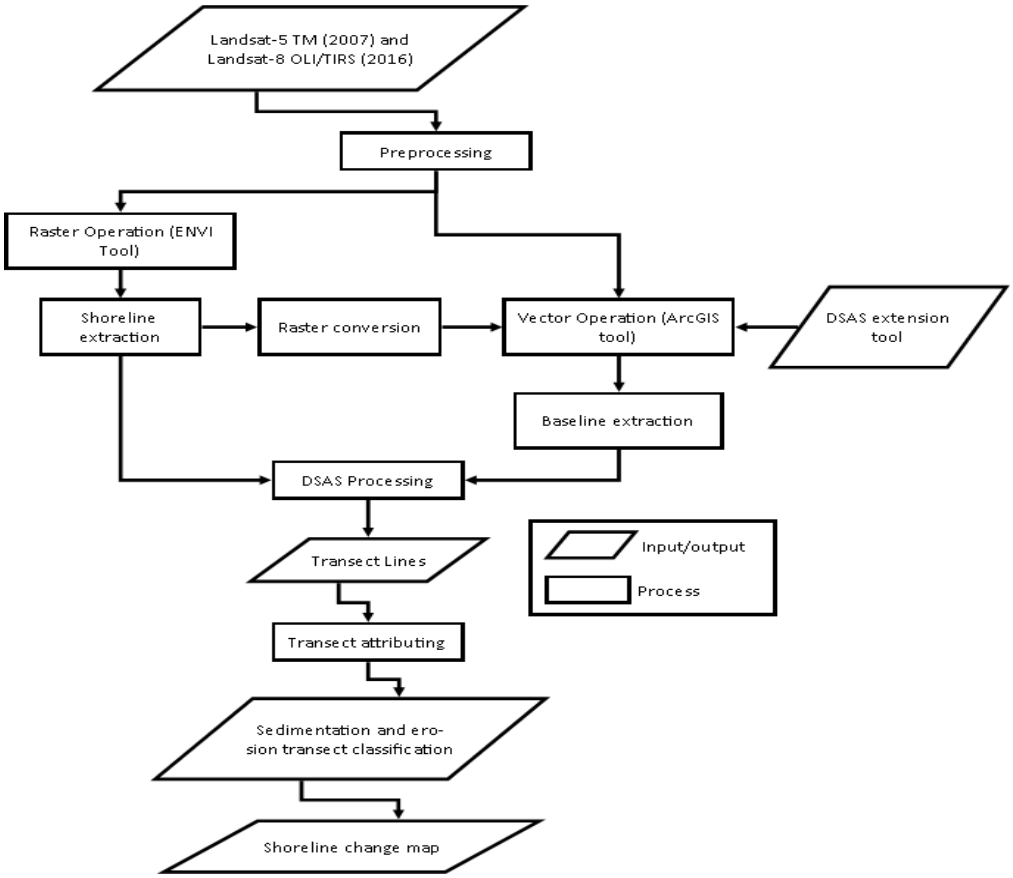

Fig. 3. Research workflow.

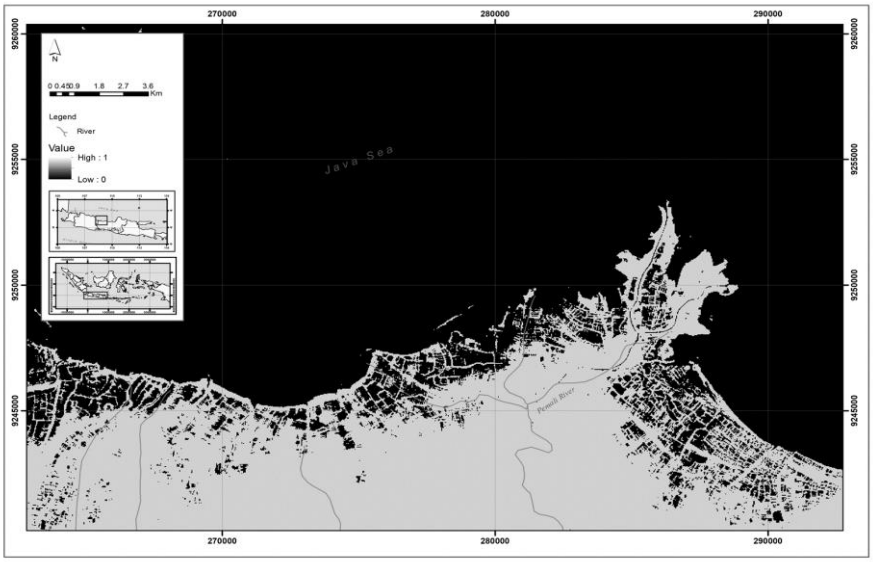

Fig. 4. Map of land and water separation of Brebes coastal area in 2016 using ENVI.

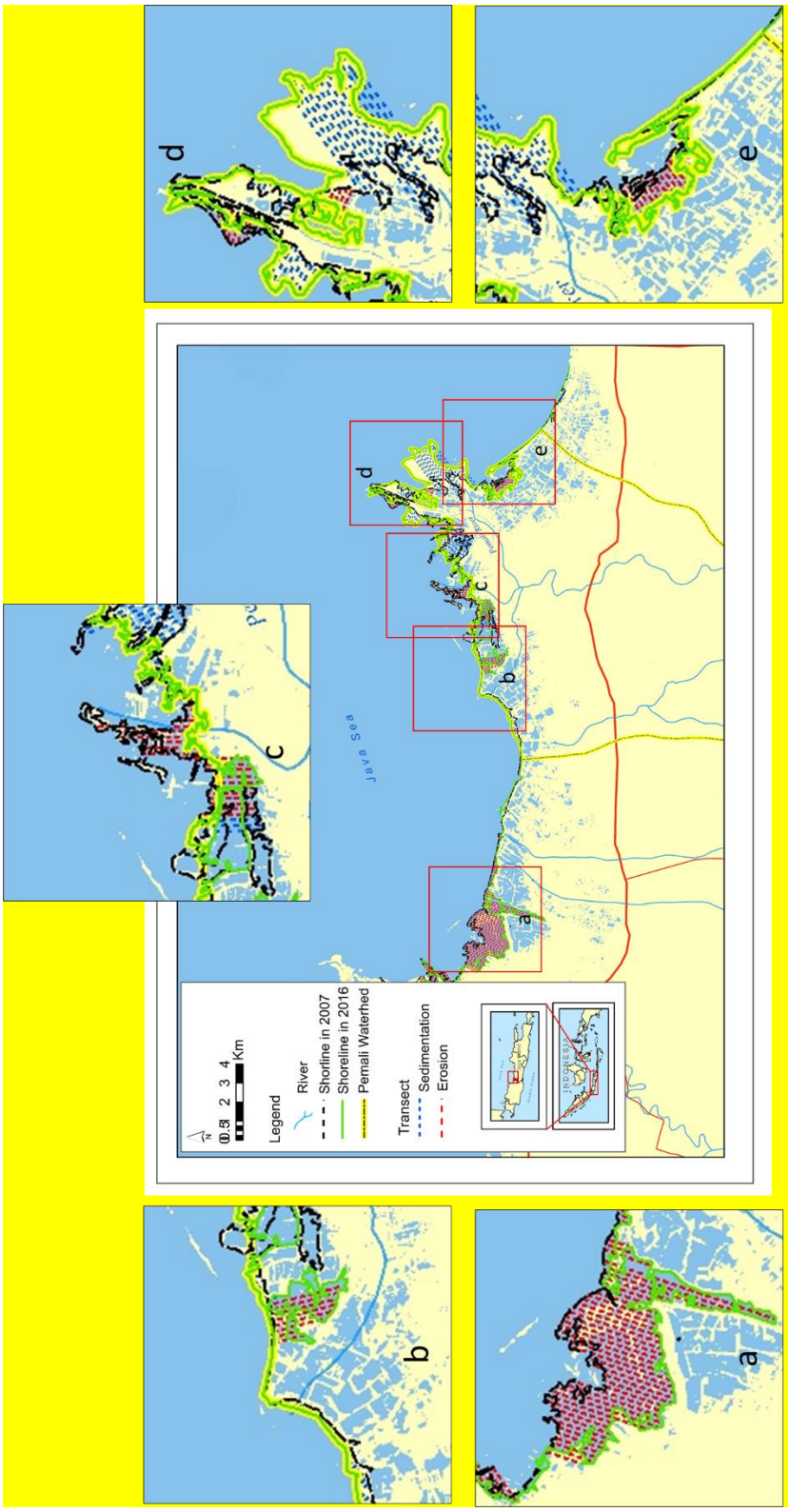

Fig. 5. Map of shoreline change seen during the period 2007–2016 in Brebes Regency, with sedimentation as the main process.

The maximum extent of the sedimentation occurrence was automatically marked using the DSAS method. This gave rise to a particular concern since the existing line of change is based on a point facing open water or sea without any borders; however, it did not always originate from a point on the shoreline but could lead to a curve in a river that when traced to the sea was not blocked by land as a separator. The maximum length of the sedimentation occurrence in this research was found to be 3.9 km over the 10-year period in question. This length of the sedimentation occurrence captured exceeded that of the erosion, which was measured at up to 3.3 km. This data, as obtained from the data attribute in DSAS processing, is shown in **Fig. 6**. Trihatmoko (2017) obtained a measurement of 2.26 km for the maximum shoreline change in the same location. The different result is possible might be due to the different methods were applied. In this research, DSAS is used while Trihatmoko (2017) utilized histogram analysis on the shoreline detection procedure using raster GIS format. The resolution in raster environment may cause the different resolution in result.

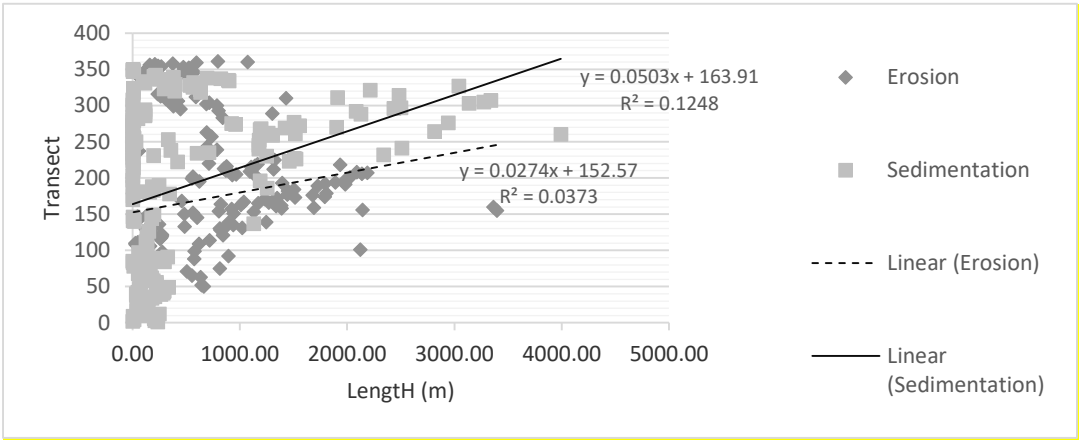

Fig. 6. Graph of erosion and sedimentation occurrences in Brebes coastal area in 2007–2016 using 100 m distance of transect (361 transect multiplied by 100 m equal to 36.1 km).

Fig. 6 shows the trend of erosion-sedimentation occurrences. A more detailed trend analysis can be defined as an attempt to see the movement of an upward or downward trend in the long term which is obtained from the average change over time. An increasing trend is called a positive trend and a downward trend is called a negative trend. The trend can be formulated using a linear function equation. A positive and negative trend can be written, respectively:

$$Y = ax + b \quad (1)$$

$$Y = -ax + b \quad (2)$$

Y is the dependent variable, while *a* is the direction coefficient, *b* is a constant which is the intersection point on the y-axis, and *X* is the independent variable. The two linear equations shown in **Fig. 6** can be analyzed that each of them has a positive trend. It means that there is an increase in both processes. However, the b value for sedimentation ca. of 163.91 while for erosion the value is 152.57. Thus, that sedimentation processes are more dominant than erosion. The trend analysis also shows the coefficient of determination R^2. The value of R^2 is defined as the contribution of the influence given by *X* to *Y*. In other words, the value of R^2 is useful for predicting and seeing the magnitude of the contribution of influence given by X variable simultaneously to Y variable. The value of R^2 generally ca. 0-1. If it shows a negative value, it can be determined that there is inverse influence of X variable on Y variable. Furthermore, the smaller value of R^2 indicates that the effect of X variable on Y variable is getting weaker. On the other hand, if the R^2 value gets closer to 1, then this influence is getting stronger. In the graph shown in **Fig. 6**, the R^2 value for sedimentation is greater than for erosion, although both tend to be small ca. 0.1248 and 0.0373, respectively. However, the R^2 value in

sedimentation means that the closer the transect approaches the estuary, there is a linear relationship with the increase in sedimentation length, since the transect was measured along the shore heading to the east or river mouth of the Pemali River.

The occurrence of sedimentation up to 3.9 km was the result of terrestrial material transported by the river system. It shows that the existing sedimentation linearly follows the flow pattern of the river, which means the deposition originally derived from the mainland. This finding is potentially significant as it contradicts the theory that a build-up of sedimentation in coastal areas results from erosion in other coastal areas (Pethick 1984). Sedimentation processes are indeed controlled by several energies, whether form the inland such as river energy or from the sea such as wave and current energies. In this case, wave characteristics in the study area is considered calm and only sometime a bit strong wave occurs. Domination of the sediment supply from the river are very obvious, as it is indicated in several parts of the shore with the delta developments. However, further research is needed to observe, measure and quantify the sediment supply from the rivers as well as to measure the tide and wave energies. It can be concluded that coastal and watershed management should be integrated (Marfai and King 2008b). This type of integrated management demands the targeted involvement of many aspects and sectors related to both watershed and coastal areas (Buser and Farthing 2011).

As measured, sedimentation in the nearshore zone occurs in the Pemali River mouth (shown in **Fig. 5**), or as riverine sediments (Kao et al. 2008). Guided by data from the Geospatial Information Bureau (GIB), the Pemali Watershed is the widest of the ten watersheds in Brebes Regency. This means that the measurement results obtained using DSAS show a direct correlation with the watershed-wide situation. The main land use in the Pemali Watershed was identified as farm or garden, accounting for up to 35.26%, as shown in **Table 2**. This finding demonstrates that farming activities in Pemali Watershed are the main activity of the community and make a major contribution to sedimentation occurrence. It also reveals that the anomaly in the form of Jalan Pantai Utara has no impact on the urban activities, as is the case in other areas through which it traverses (Marfai et al. 2017). Surface material is transferred to the river system via overland flow as a result of continuous tillage activity (Arsyad 2010). These findings thus reveal that farm and garden activities are the two main activities that trigger sedimentation processes arising from soil erosion. The dynamic of the land cultivation in a farm and garden contribute to the sediment load and material brought to the river. In a certain period of time it would also contribute to the river convection.

Table 2.

Pemali Watershed Characteristics.

Land use	Area (ha)	Percent
Lake	67.91	0.05
Pond	2,813.50	2.13
Building	9.38	0.01
Mangrove	21.28	0.02
Wood	3,472.24	2.63
Grassland	439.92	0.33
Farm/garden	46,573.51	35.26
Settlement	10,360.25	7.84
Rice field	30,474.72	23.07
Rain-fed field	15,030.19	11.38
Moor	14,349.97	10.86
Non-cultivated vegetation	47.12	0.04
Unidentified landuse	8,423.32	6.38
Total	**132,083.32**	**100.00**

Information: W stands for watershed

Source: BIG, 2017 (information: W refers to watershed)

The results displayed in **Fig. 5** show the location of the dominant occurrence of sedimentation in Brebes Regency, precisely in Brebes District. This sedimentation has an adverse impact in terms of making the estuary shallow and difficult for fishermen to either anchor or sail. The sedimentation is potentially harmful as accumulations are potentially toxic due to the previously mentioned farming activities that may employ chemical fertiliziers and are detrimental to the environment, such as by reducing fish catches and compelling fishermen to travel greater distances (Fleischer, Orsi and Richardson 2001).

In addition, evaluating accuracy of the GIS-model is necessary to be done in order to ensure the quality of the developed model. In this project ground checking has been done in 2016 and 2017 on the study area, particularly on the spot of erosion and sedimentation, to confirmed the model result. There are three important spots have been confirmed using ground checking and all the areas confirmed the model results. The ground checking was focused on the location limited on box b, c, d, and e (**Fig. 6**) since the trend analysis was confirmed intensively occurred when the transect getting closer to the river mouth of the Pemali River. Four observed areas are shown in **Fig. 7** with their coordinates. This ground checking is a common method but considered as an appropriate validation procedure. However, advanced validation process for more detail model could be considered and could be proposed for the next agenda of research.

Fig. 7. Location 1, 2, 3, and 4 are respectively show the area of box b, c, d, and 3 in **Fig. 5**. All of the areas are dominated by the process of sedimentation, it is confirmed by the mangrove development in these areas (white arrows). The land and fish ponds are also well developed (white arrows), furthermore people have tried to build new dykes for the fish pond that is showed in location 4, it shows that people may realize that the location is stable.

5. CONCLUSIONS

Bands 4 and 1 of Landsat-5 TM were used to extract the ratio information between land and water bodies, while Landsat-8 OLI/TIRS used Bands 5 and 1. This non-conformity was used to adjust the different wavelengths of the two Landsats. Even if the result shown by DSAS is completely automatic, the line of change was based on a point facing open water or sea without any borders, although it does not always originate from a point on the shoreline but can lead to a curve in a river that when traced to the sea is not blocked by land as a separator. Sedimentation was found to be the dominant process as opposed to erosion, with a maximum sedimentation length of 3.9 km recorded, as triggered by farming activities in the Pemali Watershed. The direct impact of the sedimentary occurrence on the community centered on the reduced ability to anchor or sail.

Both erosion and sedimentation on the coastal area are the most important issue for coastal manager and community. Erosion triggers the environmental problem lead to the loss of land for agriculture, and thread the coastal settlement. In other hands, additional coastal land appears due to the sedimentation process. The coastal manager should aware with this situation, since it might be possible that social conflict occurs due to this "new" land development. Therefore, this research result could contribute to the local authority in the form of spatial data for the decision-making process. A recommendation is thus proposed to conduct an integrated study related to the amalgamation of watershed and coastal management since the river served as the main source of sediment.

Acknowledment

High appreciation and special thanks to Sunarto for the constructive advice on this work. We also thank to Medina Uli Alba Somala and Isbakhul Lail for the field survey.

REFERENCES

Aedla, R., Dwarakish, G. S., & Reddy, D. V. (2015) Automatic Shoreline Detection and Change Detection Analysis of Netravati-GurpurRivermouth Using Histogram Equalization and Adaptive Thresholding Techniques. *Aquatic Procedia*, 4, 563-570.

Arsyad, S. (2010) Land and Water Conservation Second Ed. (in Bahasa: Konservasi Tanah dan Air Edisi Kedua). IPB Press, Bandung.

Bird, E. (2008) *Coastal Geomorphology an Introduction Second Edition*. University of Melbourne, Melbourne.

Buser, M. & Farthing, S. (2011) Spatial Planning as an Integrative Mechanism: A Study of Sub-Regional Planning in South Hampshire, England. *Planning Practice and Research*, 26 (3), 307-324.

Center Bureau of Statistic. (2016) *Province of Central Java Province in Number, 2016 (in Bahasa: Provinsi Jawa Tengah dalam Angka Tahun 2016)*. Statistic Center Bureau, Central Java Province.

Cozzoli, F., Smolders, S., Eelkema, M., Ysebaert, T., Escaravage, V., Temmerman, S., Meire, P., Herman, P. M. J. & Bouma, T. J. (2017) A Modeling Approach to Assess Coastal Management Effects on Benthic Habitat Quality: A Case Study on Coastal Defense and Navigability. *Estuarine, Coastal and Shelf Science*, 184, 67-82.

Davidson, R. & Arnott (2010) Introduction to Coastal Processes and Geomorphology. Cambridge University Press, London.

Dewi, R. S. (2018) Monitoring Long-term Shoreline Changes Along the Coast of Semarang. *IOP Conf. Series: Earth and Environmental Science,* 284 (2019) 012035.

Dewi, R. S., Bijker, W., Stein, A. & Marfai, M. A. (2016) Fuzzy Classification for Shoreline Change Monitoring in a Part of the Northern Coastal Area of Java, Indonesia. *Remote Sensing*, 8, 1-25.

Department of Marine and Fisheries of Central Java Province (2016) Coastal Resources Study for Region Act Revision of Zonation Plan of Coastal and Small Island (RZWP3K) in the Province of Central Java Province

(in Bahasa: Kajian Sumberdaya Pesisir dalam Rangka Revisi Perda RZWP3K Provinsi Jawa Tengah). *Brief Repot*. Department of Marine and Fisheries of Central Java Province, Semarang.

Fadhilah, S. M. (2015) Mangrove Ecosystem Restoration in Kendal Regency (in Bahasa: Restorasi Ekosistem Mangrove di Kabupaten Kendal). *Bachelor Thesis*. Faculty of Economics and Business, Diponegoro University, Semarang.

Fleischer, P., Orsi, T. H. & Richardson, M. D. (2001) Distribution of Free Gas in Marine Sediments: A Global Overview. *Geo-Marine Letters*, 21, 109-122.

Geospatial Information Bureau (2017) Geospatial for Nation (in Bahasa: Geospasial untuk Negeri). http://tanahair.indonesia.go.id/portal/downloadViaZipFile. Accessed 13 January 2017.

Himmelstoss, E. A. (2009) *DSAS 4.0 Installation Instructions and User Guide,* in: Thieler, E. R., Himmelstoss, E. A., Zichichi, J. L. & Ergul, A. (2009) Digital Shoreline Analysis System (DSAS) version 4.0 — An ArcGIS extension for calculating shoreline change: U.S. Geological Survey *Open-File Report,* 2008-1278.

Huang, M. & Wu, Y. (2010) Environmental Monitoring System Based on GIS and Wireless Communications. *Proceeding.* The 4th International Conference on Bioinformatics and Biomedical Engineering.

Jakobsen, F., Hartstein, N., Frachisse, J. & Golingi, T. (2007) Sabah Shoreline Management Plan (Borneo, Malaysia): Ecosystems and Pollution. *Ocean & Coastal Management,* 50 (1), 84-102.

Kao, S. J, Jan, S., Hsu, S. C., Lee, T. Y. & Dai, M. (2008) Sediment Budget in the Taiwan Strait with High Fluvial Sediment Inputs from Mountainous Rivers: New Observations and Synthesis. *Terrestrial, Atmospheric and Oceanic Science*, 19 (5), 525-546.

Khawfany, A., Aref, M. A., Matsah, M. & Taj, R. (2017) Utilizing Landsat-8 Data in Mapping of Sabkha, Mangroves, and Land Covers in Jizan Coastal Plain, Southwestern Saudi Arabia. *Arabian Journal of Geosciences,* 10 (5), 102-120.

Lagomasimo, D., Corbett, D. R. & Walsh, J. P. (2013) Influence of Wind-Driven Inundation and Coastal Geomorphology on Sedimentation in Two Microtidal Marshes, Pamlico River Estuary, NC. *Estuaries and Coasts*, 2013 (36), 1165-1180.

Marfai, M. A. (2004) Tidal Flood Hazard Assessment: Modeling i Raster GIS, Case in Western Part of Semarang Coastal Area*. Indonesian Journal of Geography*, 36 (1), 25-38.

Marfai, M. A. (2007) Coastal Dynamic and Shoreline Mapping: Multi-Sources Spatial Data Analysis in Semarang Indonesia. *Environ Mont Assess*, 142, 297-308.

Marfai, M. A. (2011) The Hazards of Coastal Erosion in Central Java, Indonesia: An Overview. *Malaysian Journal of Society and Space*, 3, 1-9.

Marfai, M. A. (2012) Preliminary Assessment of Coastal Erosion and Local Community Adaptation in Sayung Coastal Area, Central Java – Indonesia. *Quaestiones Geographicae*, 31 (3), 47-55.

Marfai, M. A. & King, L. (2007) Monitoring Land Subsidence in Semarang, Indonesia. *Environmental Geology*, 53, 651-659.

Marfai, M. A. & King, L. (2008a) Coastal Flood Management in Semarang, Indonesia. *Environmental Geology*, 55, 1507-1518.

Marfai, M. A. & King, L. (2008b) Tidal Inundation Mapping under Enhanced Land Subsidence in Semarang, Central Java Indonesia. *Natural Hazards*, 44, 93-109.

Marfai, M. A., Almohammad, H., Dey, S., Susanto, B. & King, L. (2008) Coastal Dynamic and Shoreline Mapping: Multi-Sources Spatial Data Analysis in Semarang Indonesia. *Environ Monit Assess*, 142, 297-308.

Marfai, M. A., Trihatmoko, E., Hizbaron, D. R., Sandholz, S. & Dimyati, M. (2017) Band Ratio Modification for Monitoring the Suspended Sediment Distribution Pattern in the Urban Coastal Area. *Unpublished Manuscript*.

Marfai, M. A., Tyas, D. W., Nugraha, I., Fitriatul'Ulya, A. & Riasasi, W. (2016) The Morphodynamics of Wulan Delta and its Impacts on the Coastal Community in Wedung Subdistrict, Demak Regency, Indonesia. *Journal of Environmental Protection*, 2016(7), 60-71.

Marfai, M. A., Trihatmoko, E., Sunarto, Wulandari, Risanti, A. A. & Kurniawan, I. A. (2018) Preliminary Study of Coastal Circulation Cells in the Coastal Area of Kendal, Indonesia. *IOP Conf. Series: Earth and Environmental Science*, 256 (2019) doi:10.1088/1755-1315/256/1/012030.

Marfai, M. A., Trihatmoko, E., Ervita, K. & Purnama, I. S. (2019) Granulometric Extraction Value to Determine Waves, Currents, and Tides Characteristic of Tangsi Beach (Pink Beach) East Lombok Regency, Indonesia. *IOP Conf. Series: Earth and Environmental Science*, 256 (2019) doi:10.1088/1755-1315/256/1/012030.

Mutaqin, B. W. (2017) Shoreline Changes Analysis in Kuwaru Coastal Area, Yogyakarta, Indonesia: An Application of the Digital Shoreline Analysis System (DSAS). *International Journal of Sustainable Development and Planning*, 12(7), 1203-1214.

Mutaqin, B. W., Trihatmoko, E., Ftriani, A. K. N. & Jumari (2013) Preliminary Study of the Coastal Dynamics in Porong Delta after the Sidoarjo Mud Volcano Eruption in 2006 (in Bahasa: Studi Pendahuluan Dinamika Wilayah Kepesisiran di Muara Delta Porong setelah Erupsi Mud Volcano Sidoarjo Tahun 2006). *Proceeding of Seminar Nasional Pendayagunaan Informasi Geospasial untuk Optimalisasi Otonomi Daerah 2013*, Universitas Muhammadiyah Surakarta, Surakarta.

Morton, R. A. (2003) An Overview of Coastal Land Loss: With Emphasis on the Southeastern United States: U.S. *Geological Survey, Open File Report*, 3(337), 29.

Obert, A. I. (2017) High-Resolution Multi-Scale Modelling of Coastal Flooding due to Tides, Storm Surges and Rivers Inflows. A Cork City Example. *Coastal Engineering*, 121, 278-296.

Parkinsonm R. W., & Ogurcak, D. E. (2018) Beach Nourishment is not a Sustainable Strategy to Mitigate Climate Change. *Estuarine, Coastal and Shelf Science*, 212, 203-209.

Randazzo, G., Barecca, G., Cascio, M., Crupi, A., Fontana, M., Gregorio, F., Lanza, S., & Muzirafuti, A. (2020) Analysis of Very High Spatial Resolution Images for Automatic Shoreline Extraction and Satellite-Derived Bathymetry Mapping. *Geosciences,* 10, 172.

Regional Planning and Development Agency of Brebes Regency (2016) *Technocratic Study of the Initial Draft of Medium Term Regional Development Plan (RPJMD) of Brebes Regency 2017-2022 (in Bahasa: Kajian Teknokratis Draft Rancangan Awal Rencana Pembangunan Jangka Menengah Daerah (RPJMD) Kabupaten Brebes tahun 2017-2022).* Regional Planning and Development Agency of Brebes Regency, Brebes.

Retnowati, A., Marfai, M. A. & Sumantyo, J. T. S. (2012) Rip Currents Signatures Zone Detection on ALOS PALSAR Image at Parangtritis Beach, Indonesia. *Indonesian Journal of Geography*, 44(1): 12-27.

Ritter, D. F., Kochel, R. C. & Miller, Jr. (1995) *Process Geomorphology. Third Edition*. Wm C Brown Company Publishers, USA.

Sakijege, T., Sartohadi, J., Marfai, M. A., Kasenga, G. R. & Kasala, S. E. (2014) Assessment of Adaptation Stategies to Flooding: A Comparative Study between Informal Settlements of Keko Machungwa in Das ed Salaam, Tanzania and Sangkrah in Surakarta, Indonesia. *Jàmbá: Journal of Disaster Risk Studies,* 6 (1), Art. #131, 10 pages. http:// dx.doi.org/10.4102/jamba. v6i1.131.

Shrestha, F., Uddin, K., Maharjan, S. B., & Bajracharya, S. R. (2016) Aplication of Remote Sensing and GIS Environmental Monitoring in the Hindu Kush Himalayan Region. *Environmental Science,* 3(4), 646-662.

Sukarna, R. M. & Syahid, Y. (2015) FCD Application of Landsat for Monitoring Mangrove in Central Kalimantan. *Indonesian Journal of Geography*, 47 (2), 160-170.

Supriharyono. (2000) *Natural Resources Preservation and Management in Tropical Coastal Area (in Bahasa: Pelestarian dan Pengelolaan Sumber Daya Alam di Wilayah Pesisir Tropis)*. PT Gramedia Pustaka Utama, Jakarta.

Thinh, N. A., & Hens, L. (2017) A Digital Shoreline Analysis System (DSAS) Applied on Mangrove Shoreline Changes Along the Giao Thuy Coastal Area (Nam Dinh, Vietnam) during 2005-2014. *Vietnam Journal of Earth Sciences,* 39(1), 87-96.

Trihatmoko, E. (2017) Process and Impact of the Coastal Dynamics in the Central Java and Special Region of Yogyakarta (in Bahasa: Proses dan Dampak Dinamika Wilayah Kepesisiran Jawa Tengah dan Daerah Istimewa Yogyakarta). *Master Thesis*, Faculty of Geography Universitas Gadjah Mada, Yogyakarta.

Van, T. T., & Binh, T. T. (2009) Application of Remote Sensing for Shoreline Change Detection in Cuu Long Estuary. *VNU Journal of Science, Earth Science*, 25, 217-222.

Young, R. & Norby, L. (2009) Geological Monitoring: Boulder. *Geological Society of America*, USA.

Zhao, X., Wang, S., Xu, L., & Feng, Y. (2011) Practice and trend of DSAS in China. *Proceeding in 2011 International Conference on Advanced Power System Automation and Protection, Beijing, 2011, pp. 1762-1766. doi: 10.1109/APAP.2011.6180836.*

APPLICATION OF GIS IN THE DETERMINATION OF VERTICAL RELIEF FRAGMENTATION: A CASE STUDY ON DRENICA RIVER BASIN (KOSOVO)

***Albert BERILA*[1], *Florim ISUFI*[2*]**

DOI: 10.21163/GT_2021.161.04

ABSTRACT:
Advances in Remote Sensing (Digital Elevation Models) products and GIS techniques have made the calculation and analysis of morphometric indices much more accurate, effective, and less time-consuming. The energy of relief is a morphometric parameter that indicates the vertical variety of relief and represents the potential energy of a given terrain. Calculating morphometric parameters by manual methods is inconvenient because it takes a long time, is subject to mistakes that can be made by humans when extracting these parameters and, consequently leads to wrong conclusions. There is currently no fully automated method to calculate this parameter. The purpose of this paper is to define the procedures for extracting this parameter within a GIS environment using data from high resolution (HR) ALOS-PALSAR (Advanced Land Observing Satellite-Phased Array-Type L-band Synthetic Aperture Radar) Radiometrically Terrain Corrected (RTC) DEM with a spatial resolution of 12.5 m with the help of ArcGIS software. To calculate this parameter, a grid with 1x1 km cells with interpolation points in each cell was constructed. IDW was chosen as the most suitable method for the interpolation of points. Based on the obtained results, the maximum value of relief's energy for the Drenica River basin reaches 328 m/km^2. 57.19% of the surface belongs to the low and very low values of relief's energy, 42.72% belongs to the average values while only 0.09% belongs to the high values. The high participation of very small and small values of this parameter for the Drenica River basin indicates that the total area is increasing towards the creation of flat surfaces. The importance of deriving this parameter is reflected in the fact that the data obtained are quantitative (have numerical value), can be verified and applicable in practice for the purposes of the construction sector, tourism, spatial planning, etc.

Key-words: *GIS, energy of relief, ALOS-PALSAR DEM, geoprocessing, Drenica River basin.*

1. INTRODUCTION

GIS techniques are now widely used to calculate and analyze various morphometric parameters of river basins, providing a powerful tool for manipulating, and analyzing spatial information. River basins are presented as ideal units of the river landscape and are considered to be suitable for managing natural resources and subsequent planning, as well as for implementing various development plans. In recent decades, Geographic Information System (GIS) and Digital Elevation Models (DEMs) have become very efficient tools, both in the analysis of river basins and measures for their conservation.

The role of GIS in estimating various terrain parameters and manipulating spatial data related to river basins is very important. The increasing availability of DEM has led to considerable application in environmental, geomorphological, and hydrological investigations (Moore et al., 1991; Hancock et al., 2006; Liu, 2008). DEM is a digital representation of terrain in three dimensions and through existing GIS tools the terrain can be analyzed and accurate information can be obtained directly.

[1]*Department of Geography, Faculty of Mathematical and Natural Sciences, University of Prishtina, Prishtina, Republic of Kosovo, albert.berila@outlook.com.*
[2]*Department of Geography, Faculty of Mathematical and Natural Sciences, University of Prishtina, Republic of Kosovo. *Corresponding author: florim.isufi@uni-pr.edu*

Morphometric parameters represent a significant segment of the natural geographical base of each region. The geomorphological characteristics of a given morphological process, shapes, and relief in general can be given through a variety of quantitative parameters. Defining the morphological characteristics of a given whole through units of measurement determines the size of the forms. The way of researching and assigning these parameters is defined as morphometry.

Relief energy expresses the depth of valleys from ridges or the intensity of erosive cuts formed by surface runoff activity on the one hand, and the intensity of neotectonic uplifts on the other, including epirogenetic and eustatic movements, tectonic, etc (Talani, 1997). It means the parameter of vertical fragmentation of relief and represents the potential energy of a particular terrain defined by the vertical difference between the highest and lowest point within the observed unit surface of terrain (1 km^2). Relief energy, being correlated with the horizontal fragmentation of the relief, the slope of the relief, the average height, etc., express the degree of evolution of the relief and creates a close connection with the intensity of the current morphodynamic processes (Talani, 1997).

In recent decades, undoubtedly, in applied geomorphology, extremely great importance has been given to the development of quantitative physiographic methods to describe the evolution and behavior of surface drainage networks (Dobos et al., 2010). Quantitative geomorphological analysis, simply put, involves the presentation of morphological processes, relief, and its forms by applying or using various quantitative (numerical) parameters. The application of such an analysis is of great importance because such data are dimensioned and, in addition, can be verified having numerous benefits in practice. The results have broadly usable value and are unavoidable in the process of erosion intensity determination, protection, and improvement of area and environment, etc.

Due to its effective functions, such as data management, calculation, and analysis, GIS provides strong support to quantitative research. In many areas of geosciences, GIS has been extensively developed and implemented, with a particular emphasis on resource assessment and the environment and their management. Starting from the earliest works that have been carried out on the application of GIS in geomorphology, their focus or main point was on the digital classification of landforms, especially on digital relief models and their advantages (Moore et al., 1991; Dikau et al., 1991; Wilson and Gallant, 2000). GIS merged with RS data offers the possibility of creating a database for each watershed. This database is very important because it helps to conduct spatial analysis, thus helping decision-makers to formulate appropriate measures for these areas (Thakkar and Dhiman, 2007; Magesh et al., 2010; Mukherjee et al., 2007, 2009).

In the last decades, there were developed GIS technologies that allow quick and effective modeling of many derivations from DEM. The benefit of quantitative analysis of morphometric parameters is extraordinary in the conservation and further development of soils and waters at the catchment level (Kanth and Hassan, 2012). In this context, the use of data obtained from Remote Sensing associated with GIS has proven to be an important and quite efficient and powerful tool for managing and analyzing river basins (Markose et al., 2014; Patel et al., 2012; Oliveira et al., 2010; Tamma Rao et al., 2012). The shared use of GIS, mathematical models, and geomorphological theories radically improves on previous methods of quantitative geomorphic analysis and mapping.

In the present study, an attempt has been made to calculate the relief energy of the Drenica River basin from HR ALOS-PALSAR RTC DEM using GIS tools. The results of the calculation of this parameter will be presented in tabular and on thematic geomorphological maps.

2. STUDY AREA

The Drenica River basin is located in the central part of the Republic of Kosovo (**Fig. 1**). The catchment area is 438.47 km^2. The main river that flows through the basin is Drenica, with an average annual flow of 2.0 m^3/sec. The bed of this stream in the vast majority until its discharge in the river Sitnica lies in the basin of the same name, which has deepened and expanded in the thickness of Neogene and Quaternary deposits. The lithological composition of this basin is dominated by flysch rocks, followed by the Paleozoic schists and the Paleolithic to Quaternary igneous rocks, being distinguished by different degrees of hardness and permeability.

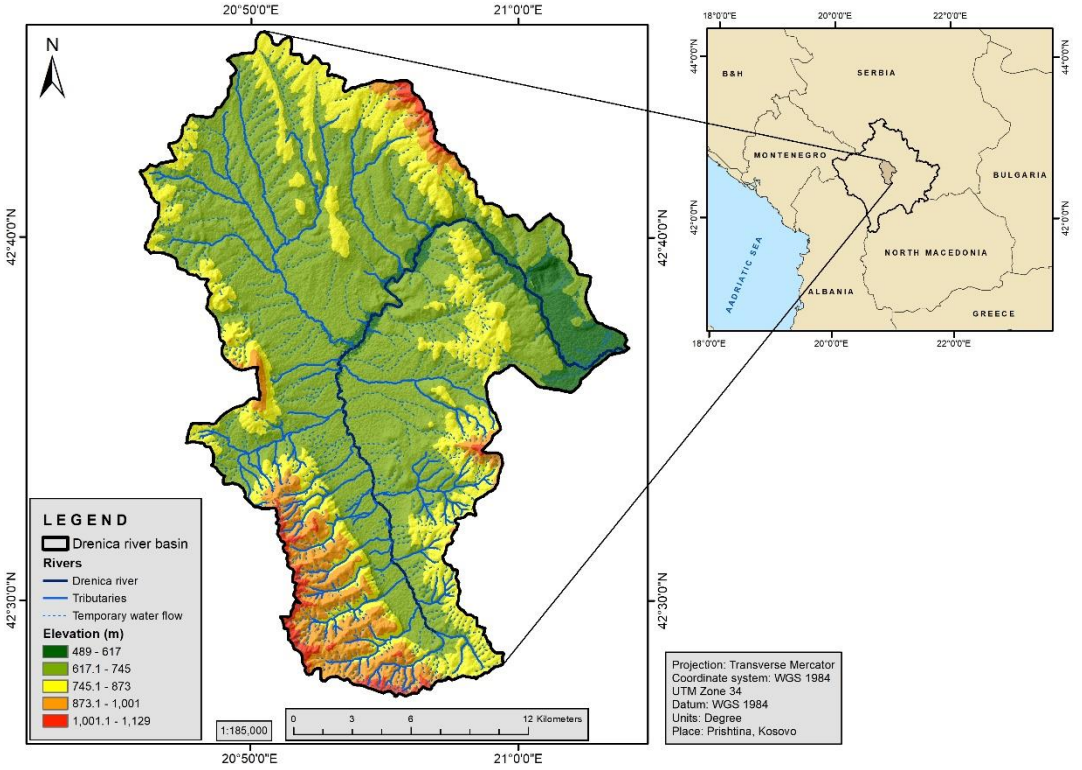

Fig. 1. Geographic position of Drenica River basin.

In the hypsometric aspect, the basin extends from an altitude of 489 m as the lowest point of the Drenica plain, while in the peripheral parts of the monocline ridges, the altitude exceeds 1,129 m, showing an average hypsometric amplitude.

From **Tab. 1** it can be seen that the hypsometric floor with a height of 489 - 745 m has high participation (66.6%). Such a high percentage indicates high extension/insertion of the hypsometric field floor within the Drenica plain. At an altitude of over 745.1 meters is located 33.4% of the basin, which make up the edges of the basin, including the lateral slopes bounded by detachment cliffs and the monocline ridges of the peripheral boundary mountains. The Drenica River basin belongs to the Sitnica river system, whose waters flow in the direction of the Black Sea. The main river that flows through the basin is Drenica. Drenica is the left tributary of Sitnica. From north of Petreshtica to Drenas, Drenica is wider and with a smaller slope with all the features of a plain river. Drenica from Drenas to Bardh i Madh, enters a narrow part, taking the appearance of a gorge. In this part of the river, the slope is greater. It originates in Bretenc on Mount Carraleva, flowing towards the central part of the Drenica valley, then takes a turn towards the east and through the transverse gorge of Dobroshec passes into the Kosovo valley and joins Sitnica.

Table 1.

Values of hypsometrical categories of studied area.

No	Elevation (m)	Area (km^2)	%
1	489 - 617	24.93	5.69
2	617.1 - 745	267.05	60.91
3	745.1 - 873	99.05	22.59
4	873.1 – 1001	38.64	8.81
5	1001.1 - 1129	8.8	2.00
Total		438.47	100%

3. RESEARCH METHODOLOGY

The Drenica River basin was delineated based on the water divide line concept. The next step was the digitalization of the entire river network. This was done based on the 1: 25000 scale topographic maps that we had available. Topographical maps were rectified/referenced geographically and mosaiced and the entire study area was delineated in a GIS environment with the help of ArcGIS 10.3 software.

Calculating morphometric parameters by manual methods is inconvenient because it takes a long time, is subject to mistakes that can be made by humans when extracting these parameters and, consequently leads to wrong conclusions. Although the energy of the relief parameter has great applicability and importance, so far, there is no fully automated way to extract it. Thus, this paper presents a methodology that broadly and clearly shows how this parameter is derived. We did the calculation of the relief's energy using the formula (Talani, 1997):

$$Cv = \frac{Hmax - Hmin}{S} (m/km^2) \quad (1)$$

where:

Cv	-energy of the relief;
$Hmax$	-maximum height in the square;
$Hmin$	-minimum height in the square;
S	-surface of a square (1 km^2);

The general workflow is shown in **Fig. 2**. The HR ALOS-PALSAR RTC DEM from Alaska Satellite Facility is used in this study to determine the energy of relief using GIS tools. ALOS-PALSAR was launched in 2006 by the Japan Aerospace and Exploration Agency (JAXA) and it was operational until May 12, 2011. ALOS was launched in a sun-synchronous orbit and circled around the Earth every 100 minutes, 14 times a day. ALOS-PALSAR returned to the original path (repetition cycle) every 46 days. The inter-orbit distance was about 59.7 km at the equator. ALOS-PALSAR has a spatial resolution of 12.5 m at 23.62 cm (1.27 GHz) wavelength with HV polarization and angle of incidence 38.7° (Khal et al., 2020).

Through GIS techniques, 1x1 km areas are formed together with the interpolation points (**Fig. 3**) in which the relief's energy is defined. The calculation of the energy of the relief was made possible using tools in ArcGIS. More precisely, after the preliminary steps taken, we calculate it using the tool "Zonal Statistics". After clicking on "Zonal Statistics", a dialog box opens in which we set the necessary parameters. A few different parameters appear in the dialog box, but we only need the "Range" parameter. This parameter calculates the difference between the maximum and minimum quota of each cell separately. After this calculation, the next step is the interpolation of points. Considering simplicity and accuracy, this study chooses the Inverse Distance Weighted (IDW) method to interpolate these points in order to extract relief's energy (Cv). The concept of the IDW method is based on the first law of geography (Tobler's first law) from 1970: It was defined as "everything is related to everything else, but near things are more related than distant things" (Johnston et al., 2001; Tobler, 1970).

4. RESULTS AND DISCUSSIONS

Relief energy or vertical fragmentation of relief is an expression of the difference in terms of height between the lowest level (valley bed) and the highest level (peaks of a complex) and represents the potential energy of a given terrain, determined by the vertical difference between the highest and lowest point within the observed unit of terrain surface. The depth of vertical fragmentation of the relief expresses the degree of the relief and creates a close connection with the intensity of the current morphodynamic processes.

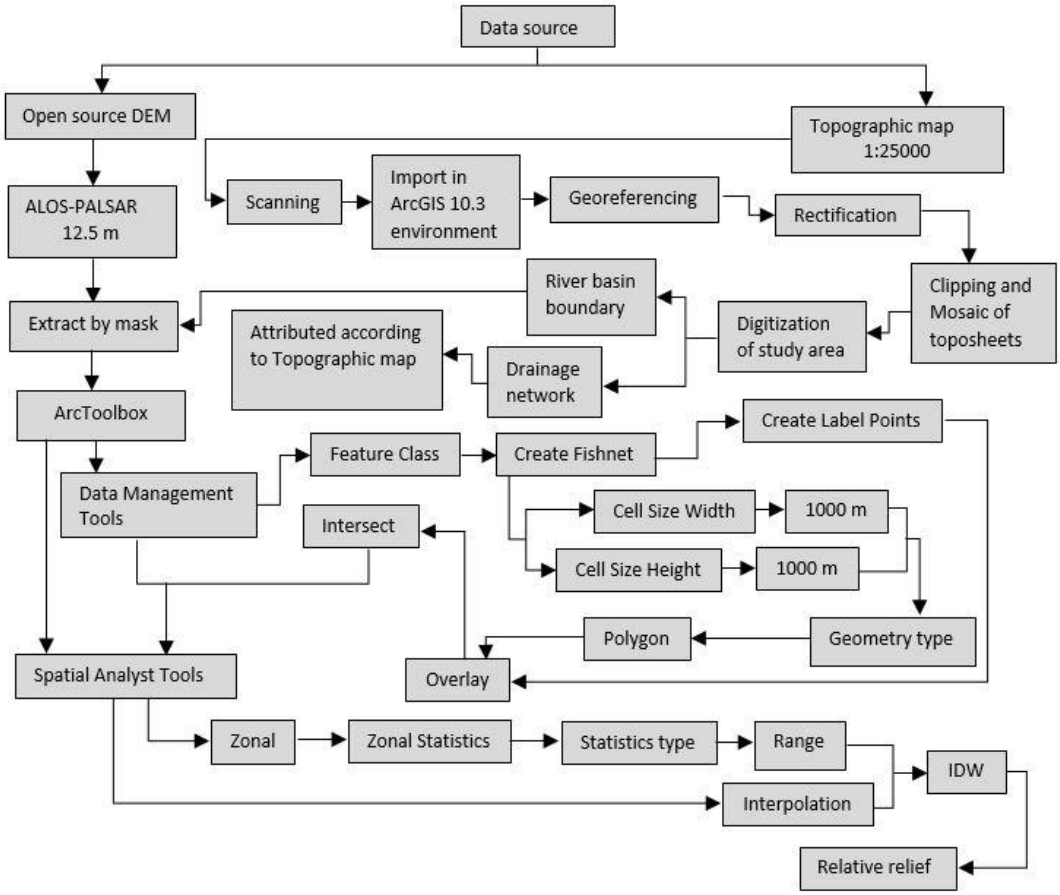

Fig. 2. Flow chart depicting methodology.

The energy of the relief is determined by parameters such as the geological composition, the susceptibility of the substrate to be eroded, the presence of disjunctive structures, and the slope of the terrain, which allows differentiating areas of greater or lesser amplitude (Román and Castillo, 2017).

Through the map of relief energy, the territories with high or low relief energy that are closely related to the detachment deformations are determined. Specifically, in those areas where the relief energy is high, tectonic, longitudinal, or transverse tectonic phenomena are very pronounced, while in areas with low relief energy the deformations are less pronounced (Talani, 1997).

Areas with high relief energy have a stronger or more pronounced erosion, while terrains with lower energy represent areas in which accumulation is expressed, which can affect the cause of flooding in the river basin. Vertical relief fragmentation has a direct effect on soil cover. This is because, in an area with high values of relief fragmentation, a restriction of soil spread and pedogenetic processes is caused.

The spatial distribution of relief energy of the Drenica River basin is shown in **Fig. 4**. Based on the use of the ArcGIS 10.3 program, for the analysis of the Drenica River basin, the classification of relief energy classes is done based on hypsometric levels. The maximum energy values of this parameter reach 328 m/km^2. From the analysis of the spatial distribution of relief energy in the Drenica River basin (**Fig. 4**) and from **Tab. 2**, we notice that in this basin small to moderate values of relief energy prevail. Terrains with very small and small energy, together, occupy about 57.19%. Areas with very low values of relief energy (< 50 m/km^2) are areas of expected deposition. These territories occupy about 17.7% of the total surface of the basin. Terrains with these values are found

mainly along the lower sectors of the Drenica River and they mainly lie along the central part of the Drenica plain. Low energy terrains (50.1 – 150 m/km^2) occupy about 173.13 km^2 or expressed in percentage 39.49%. From the map showing the spatial distribution of relief energy, it is clear that the terrains with low relief energy lie, in the vast majority, around the terrains with very low relief energy. Such terrains are mainly the lower parts of the watershed in which there are no large relief differences. While terrains with high relief energy (300.1 – 328 m/km^2) occupy a very small area (0.09%) of the total area of the basin. In these territories, the erosion process is more intensified. Terrains with these values are found mainly in areas where the valley bed contacts the highest level of a complex. The small action (to a small extent) of exogenous (external) forces in the modeling of the dimensions created in the basin has made the territories with high energy to have a small spread in this basin.

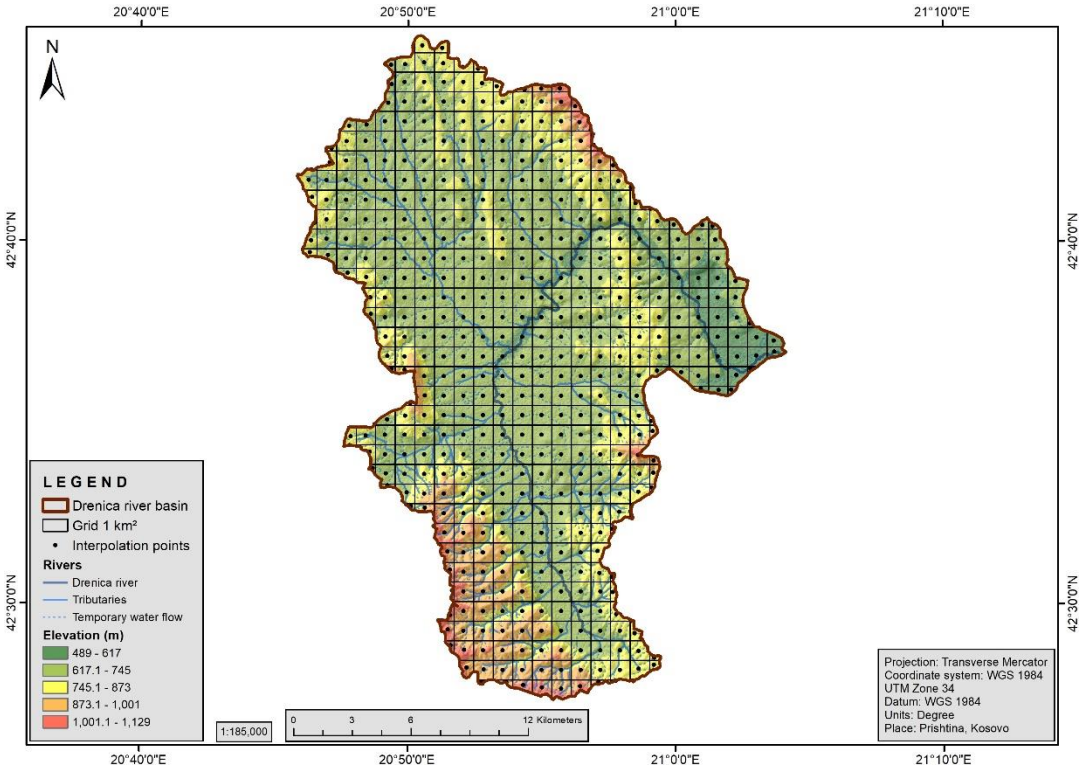

Fig. 3. Grid with interpolation points.

Table 2.

Values of relief energy in Drenica River basin.

No	Relief energy values	Area (km^2)	%
1	<50 m/km^2	77.64	17.7
2	50.1 – 100 m/km^2	173.13	39.49
3	100.1 – 150 m/km^2	98.6	22.49
4	150.1 – 300 m/km^2	88.70	20.23
5	300.1 – 328 m/km^2	0.4	0.09
Total		438.47	100

The terrains with average relief energy in this watershed occupy about 187.3 km^2. These terrains extend mainly along the peripheral parts of the basin and at the same time represent the hilly-mountainous areas, in which the relief differences begin to be highlighted.

5. CONCLUSIONS

In recent decades, DEMs have been the object of increasing use and attention to them. This has come as a result of the convenience they offer in calculating the various morphometric parameters. The objective of our study was to calculate the relief energy from the DEM through GIS techniques. Working in the ArcGIS program, a database system based on the grid system has been created, which provides an opportunity to overlay geospatial data, extract certain parameters, and analyze them.

The reason why it is important to calculate the relief energy of territory lies in the fact that it highlights the rate of relief evolution. So simply put it shows the degree of aging of the territory. Another importance of calculating relief energy through GIS is human socio-economic activity. All this activity is directly affected by the values of this morphometric parameter because the construction and placement of all the necessary infrastructure require that they be placed in full compliance with the width, depth, and slope of the valleys. GIS techniques have been proved to be an effective tool in computing relief energy for a given area

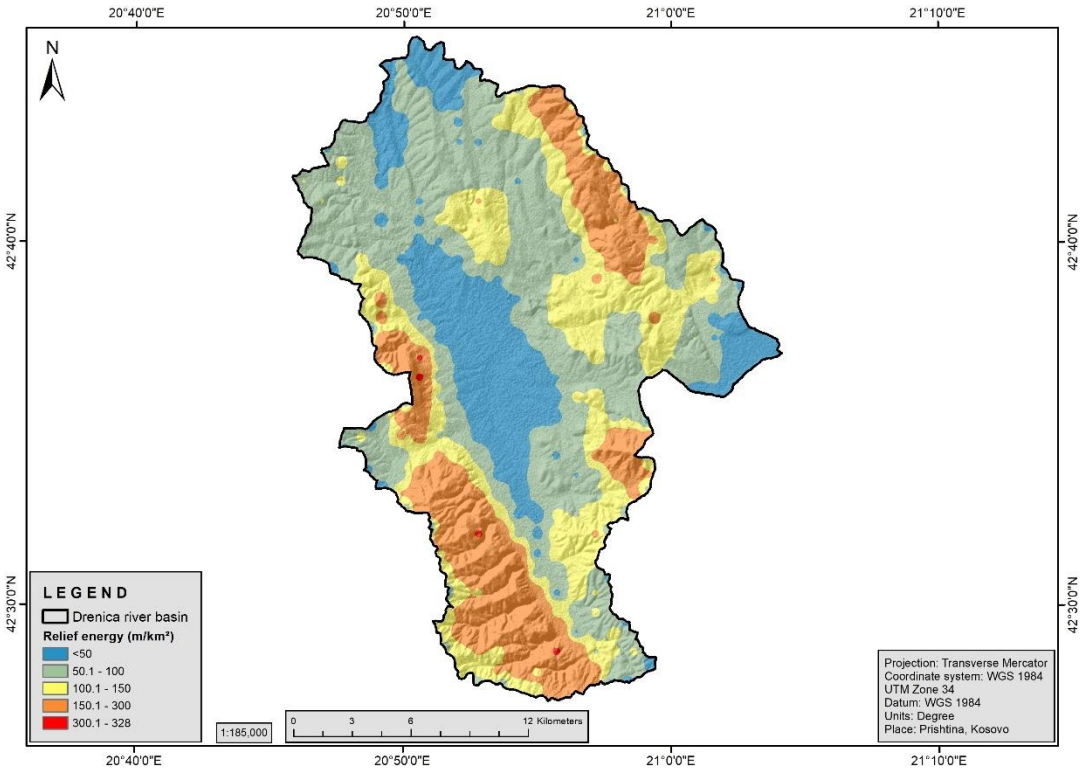

Fig. 4. Relief's energy map of the Drenica River basin.

The use of digital relief models through GIS has been shown to be a powerful tool for analyzing topographic features because it allows different methods to analyze them with operational advantages and high quality.

The relief energy values show the degree of fluvial erosion action in the modeling of the Drenica River basin. Through such an analysis geomorphological maps can be compiled that can have different scales. In our paper, a large-scale map has been compiled, which gives a detailed view of our study area based on 1km^2 cells. Also, given that the database is based on the created grid system, the possibility to overlay data and perform correlative analysis is very wide thus enabling the widespread use and application of geospatial data.

From the analyzes made with GIS, it appears that in the basin of the river Drenica dominates the terrains with small and very small values of energies, which, together, constitute more than half of the whole territory (57.19%) followed by the territories with medium energy (42.72%) and, at the very end, come the territories with high energy which occupy only 0.4 km^2. The low values of relief energy occupy the central part of the Drenica plain and along with the lower sectors of the Drenica River. Such low values are of course related to the soft rocks of this area. While the average and high values extend along with the areas where strong rocks are highlighted.

The value of the results obtained from the determination of the values of the relief energy in the Drenica River basin is very useful and is inevitable, both in determining the intensity of erosive processes, as well as in the protection and improvement of the living environment. In addition, the results obtained can be applied to problem-solving when drafting spatial plans and planning other economic activities.

REFERENCES

Dikau, R., Brabb, E. E., & Mark, R. M. (1991). Landform classification of New Mexico by computer. In Open-File Report. US Geological Survey. https://doi.org/10.3133/ofr91634

Dobos, E., Daroussin, J., & Montanarella, L. (2010). A quantitative procedure for building physiographic units supporting a global SOTER database. *Hungarian Geographical Bulletin*, 59(2), 181-205. Available: https://ojs3.mtak.hu/index.php/hungeobull/article/view/3092 [Accessed March, 2020]

Hancock, G. R., Martinez, C., Evans, K. G., & Moliere, D. R. (2006). A comparison of SRTM and high-resolution digital elevation models and their use in catchment geomorphology and hydrology: Australian examples. *Earth Surface Processes and Landforms*, 31(11), 1394‐1412. https://doi.org/10.1002/esp.1335

Johnston, K., Hoef, J. M. V., Krivoruchko, K., Lucas, N. (2001). Using ArcGIS geostatistical analyst. New York: Environmental systems research institute Inc. Available: https://dusk.geo.orst.edu/gis/geostat_analyst.pdf [Accessed April, 2020]

Kanth, T .A. and ul Hassan, Z. (2012). Morphometric Analysis and Prioritization of Watersheds for Soil and Water Resource Management in Wular Catchment Using Geo-Spatial Tools. *International Journal of Geology, Earth and Environmental Sciences*, 2, 30-41. Available: https://www.cibtech.org/J-GEOLOGY-EARTH-ENVIRONMENT/PUBLICATIONS/2012/Vol%202%20No%201/17%20Zahoor.pdf [Accessed March, 2020]

Khal, M., Algouti, A., Algouti, A., Akdim, N., A. Stankevich, S., & Menenti, M. (2020). Evaluation of open Digital Elevation Models: estimation of topographic indices relevant to erosion risk in the Wadi M' Goun watershed, Morocco. *AIMS Geosciences*, 6(2), 231‐257. https://doi.org/10.3934/geosci.2020014

Liu, Y. (2008). An Evaluation on the Data Quality of SRTM DEM at the Alpine and Plateau Area, North-western of China, The International Archives of the Photogrammetry, Remote Sensing and Spatial Information Sciences 37, 1123‐1127. Available:

https://www.isprs.org/proceedings/XXXVII/congress/1_pdf/191.pdf [Accessed 13 March, 2020]

Magesh, N. S., Chandrasekar, N., & Soundranayagam, J. P. (2010). Morphometric evaluation of Papanasam and Manimuthar watersheds, parts of Western Ghats, Tirunelveli district, Tamil Nadu, India: a GIS approach. *Environmental Earth Sciences*, 64(2), 373‐381. https://doi.org/10.1007/s12665-010-0860-4

Markose, J.V., Dinesh, A. C., & Jayappa, K. S. (2014). Quantitative analysis of morphometric parameters of Kali River basin, southern India, using bearing azimuth and drainage (bAd) calculator and GIS. *Environmental Earth Sciences*, 72(8), 2887‐2903. https://doi.org/10.1007/s12665-014-3193-x

Moore, I. D., Grayson, R. B., & Ladson, A. R. (1991). Digital terrain modelling: A review of hydrological, geomorphological, and biological applications. *Hydrological Processes*, 5(1), 3‐30. https://doi.org/10.1002/hyp.3360050103

Mukherjee, S., Sashtri, S., Gupta, M., Pant, M. K., Singh, C., Singh, S. K., Srivastava, P. K., Sharma, K. K., (2007). Integrated water resource management using remote sensing and geophysical techniques: Aravali quartzite, Delhi, India, *Journal of Environmental Hydrology* 15 (4), 1-10. Available: http://www.hydroweb.com/protect/pubs/jeh/jeh2007/mukh.pdf [Accessed June, 2020]

Mukherjee, S., Shashtri, S., Singh, C. K., Srivastava, P. K., & Gupta, M. (2009). Effect of canal on land use/land cover using remote sensing and GIS. *Journal of the Indian Society of Remote Sensing*, 37(3), 527‑537. https://doi.org/10.1007/s12524-009-0042-6

Oliveira, P. T. S. de, Alves Sobrinho, T., Steffen, J. L., & Rodrigues, D. B. B. (2010). Caracterização morfométrica de bacias hidrográficas através de dados SRTM. *Revista Brasileira de Engenharia Agrícola e Ambiental*, 14(8), 819‑825. https://doi.org/10.1590/s1415-43662010000800005

Patel, D. P., Gajjar, C. A., & Srivastava, P. K. (2012). Prioritization of Malesari mini-watersheds through morphometric analysis: a remote sensing and GIS perspective. *Environmental Earth Sciences*, 69(8), 2643‑2656. https://doi.org/10.1007/s12665-012-2086-0

Quesada Román, A., & Barrantes Castillo, G. (2017). Modelo morfométrico para determinar áreas susceptibles a procesos de ladera. *Investigaciones Geográficas*, 94. https://doi.org/10.14350/rig.57318

Talani, R., 1997: Laboratory manual for cartography and topography, CP, Shkodër. (In Albanian)

Tamma Rao, G., Gurunadha Rao, V. V. S., Dakate, R., Mallikharjuna Rao, S. T., & Raja Rao, B. M. (2012). Remote sensing and GIS based comparative morphometric study of two sub-watershed of different physiographic conditions, West Godavari District, A.P. *Journal of the Geological Society of India*, 79(4), 383‑390. https://doi.org/10.1007/s12594-012-0059-2

Thakkar, A. K., & Dhiman, S. D. (2007). Morphometric analysis and prioritization of miniwatersheds in Mohr watershed, Gujarat using remote sensing and GIS techniques. *Journal of the Indian Society of Remote Sensing*, 35(4), 313‑321. https://doi.org/10.1007/bf02990787

Tobler, W. R. (1970). A Computer Movie Simulating Urban Growth in the Detroit Region. *Economic Geography*, 46, 234. https://doi.org/10.2307/143141

Wilson, P. J., Gallant, C. J., 2000: Digital Terrain Anaysis (eds.): Terrain analysis: principles and applications, John Wiley & Sons, New Jersey, 520. Available: https://johnwilson.usc.edu/wp-content/uploads/2016/05/2000-Wilson-Gallant-Terrain-Anaylsis-Chapter-1.pdf [Accessed July, 2020]

SEASONAL CHARACTERISTICS OF PRECIPITATING CLOUD PROPERTIES AND STRUCTURES IN THE INLAND OF THE INDOCHINA PENINSULA: A LEGACY OF 16 YEARS OF THE TROPICAL RAINFALL MEASURING MISSION (TRMM) SATELLITE

***Nattapon MAHAVIK*[1*], *Sarintip TANTANEE*[2]**

DOI: 10.21163/GT_2021.161.05

ABSTRACT:
Seasonal characteristics of cloud properties and structure based on mesoscale properties of precipitation systems over the inland Indochina Peninsula (IP) and surrounding regions during the years 1998-2013 were investigated in this study. Using daily product from Tropical Rainfall Measuring Mission, the monsoon season, firstly, was demarcated to find onset and withdrawal dates for each year, and then to divide the period into the premonsoon, monsoon and postmonsoon seasons. In the 16-yr "climatology", on average, the variations were found both in physical properties and structures of precipitation features (PFs) for each season. Based on applied definition, the intra-seasonal and the inter-seasonal variation of rainfall intensity and periodical duration length were considered to identify the seasonal period of each year. Mesoscale Convective Systems (MCSs) played a significant role through their contribution of rainfall for all periods. Sub-MCSs were major contributors of rainfall during the postmonsoon season, while the highest percentage of intense MCSs (IMCSs) was found in the premonsoon season. The enhancement of IMCs for the premonsoon season is the largest over the inland IP based on microwave signal and radar reflectivity sensors. Distinct spatial concentration was found over west and north IP for sub-MCSs during monsoon seasons. Convection intensity proxies and vertical radar reflectivity demonstrate intra-seasonal variation over land, were identified through cumulative density function analysis by enhancement of MCSs during the premonsoon season. Spatial distribution of PFs based on maximum height cloud average over the inland IP has shown at height exceeding 8 km over the western inland IP during premonsoon season. Spatial variation of the microphysical structure of cloud is distinctly shown by seasons based on scattering of microwave signals, and lightning flash counts. The most frequent lightning was found during premonsoon season over inland IP, while the most flash count average was also found over inland IP especially over west, north in highland of IP during premonsoon season. Further study should be conducted to analyze on seasonal periods for understanding on the variations of microphysical structure and cloud properties.

Key-words: *TRMM 16 years, Cloud Structure, Indochina Peninsula, Convective Cloud, Precipitation Features*

1. INTRODUCTION

Rainfall characteristics and dynamic-thermodynamic environments vary from regions to regions. Characteristics of convective cloud differ by areas based on topography and atmospheric forcing. For instance, Xu (2013) found that mixed phase process on precipitation play more significant role over the south of China more other regions. Some extreme convective hot spots, observed by three-dimensional precipitation radar retrieved from Tropical Rainfall Measuring Mission (TRMM), are founded on the steep slope and foothill regions in South America. Meanwhile, some intense convective features are located over the southwest foothills of the Himalayas (Zipser et al., 2006; Houze et al., 2007; Medina et al., 2010; Romatschke & Houze, 2010). Understanding these spatial and temporal variations in rainfall characteristics using satellite observation is crucial for building knowledge for disaster prevention in Indochina Peninsula (IP). The IP is the region located within the

[1]*Department of Natural Resources and Environment, Faculty of Agriculture Natural Resources and Environment, Naresuan University, Phitsanulok, 65000, Thailand, nattaponm@nu.ac.th*
[2]*Centre of Excellence on Energy Technology and Environment, Faculty of Engineering, Naresuan University, Phitsanulok, 65000, Thailand, sarintipt@nu.ac.th*

region of the Asian monsoon. The IP is defined as a transitional zone between two Asian monsoon systems (Wang and Ho 2002). TRMM was launched in 1997 and ceased data collection in April, 2015 (Li et al., 2019). The TRMM project was the first space-borne radar observation precipitation radar (PR) with additional sensors, including TRMM Microwave Imager (TMI), the Visible and Infrared Radiometer System (VIRS), the Clouds and Earth's Radiant Energy System (CERES) and the Lightning Imaging System (LIS) (Kummerow et al., 1998). Long-term accumulated data based on TRMM observations can be used to describe the climate features of rainfall and its properties. Vertical profiles and horizontal variations in radar reflectivity have been used to investigate the climatic features at different times (e.g. Petersen & Rutledge, 2001; Petersen et al., 2002; Kodama et al., 2005; Xu et al., 2009).

Understanding microphysical precipitation characteristics over the tropics is one of the keys to elucidating climate change (Kodama et al., 2015; Satoh et al., 2018). The two types of precipitating clouds in the tropics are convective and large stratiform rain areas, which are, in the main part, embedded in mature mesoscale convective systems (MCSs) (Houze, 1989). Both convective precipitation and stratiform precipitation coupled within Tropical Cyclones, resulting a long duration of rainfall can cause the damage and deaths from flooding (Jorgensen, 1984; Yokoyama & Takayabu, 2008). Therefore, it is necessary to understand MCSs embedded in Precipitation Features (PFs) over the tropics. Nesbitt et al. (2000) developed an algorithm to identify PFs using data from TRMM PR and TMI. Based on definition MCSs from (Houze, 1993), precipitation systems can be successfully described from the convective intensity and rainfall distributions over the tropics. The finding has clearly shown that such features which develop over land are much more intense than similar oceanic features. Although the TRMM mission ended in 2015, related studies are still ongoing based on the PR data in storage. The University of Utah Precipitation Measuring Missions (PMM) science group has produced its work using all primary data retrieved from TRMM sensors on PF studies (Nesbitt et al., 2000; Liu et al. 2008; Liu, 2013). The event-based reanalysis database of PFs has collocated TRMM data to generalize precipitation and cloud features as well as study the radar, passive microwave and lightning characteristics of precipitating systems in the tropics. Many studies have been carried out using this database, including rainfall estimates validation, diurnal cycle of precipitation systems, global distribution of storms with LIS-detected lightning, deep convection reaching the tropical tropopause layer rainfall production and convective organization, and the categorization of extreme thunderstorms by their intensity proxies (Nesbitt et al., 2003; Nesbitt et al., 2004; Cecil et al., 2005; Liu & Zipser, 2005; Zipser et al. 2006).

In addition, there have been many studies to describe regional variation on PFs over the tropics using TRMM data. In Asia, for example, studies of the organized convective systems characteristics in eastern Asia, such as Mei-yu seasons, used the TRMM PF database (Xu et al., 2009). Besides, Guy & Rutledge (2012) investigated climatology of MCSs associated with the West African monsoon using TRMM PR and TMI based on 13-year (1998–2010) from the University of Utah TRMM PF database. Convective intensity metrics indicate that land-based systems exhibit stronger characteristics, such as higher storm tops, maximum 30 dBZ heights, and significant 85 GHz brightness temperature depressions. Rapp et al. (2014) investigated the role of storm characteristics on the seasonal and diurnal cycles of precipitation in four distinct regions of Costa Rica by utilizing The University of Utah TRMM PF database. They found that the relative importance of convective precipitation increases on the Caribbean side during wintertime cold air surges. However, there are still gaps on studying of spatial and temporal variability in the convective cloud properties and structure in the Inland IP using the TRMM PF database.

In this study, our aim is to focus on precipitation structure and its properties using a TRMM dataset over the inland of IP and surrounding area. Most of the figures were produced using the Python script. This paper comprises of four sections. Section 1 provides some background and an introduction. Section 2 describes data and methodology: study area, the datasets, and definition of monsoon periods, the PFs database, and interpretation of PF parameters. Section 3 describes the results and discussion: finding monsoon season periods, Classified PFs, and spatial distribution on PFs properties. The conclusion is given in section 4.

2. DATA AND METHODOLOGY

2.1 Study Area

The Indochina Peninsula (IP) and surrounding areas demonstrate spatial variation of annual precipitation (**Fig. 1a**). Less annual rainfall occurs in the middle part of the IP, while large amounts fall over the coastal regions and surrounding seas. Moisture transportation from the Indian and Pacific Oceans contributes to annual rainfall in the IP during monsoon seasons. The rainfall variability over the IP is mainly influenced by the southwesterly monsoon from the Indian ocean during the first half of the summer monsoon and from the Pacific Ocean during the latter half (e.g., Matsumoto 1997, Takahashi &Yasunari 2006). In addition, topography is also a key factor in controlling the amount of rainfall over the IP (**Fig. 1b**). A mountainous region is located across the northern IP, while narrow and steep mountain ranges and basins are found in the middle part of the IP (**Fig. 1b**).

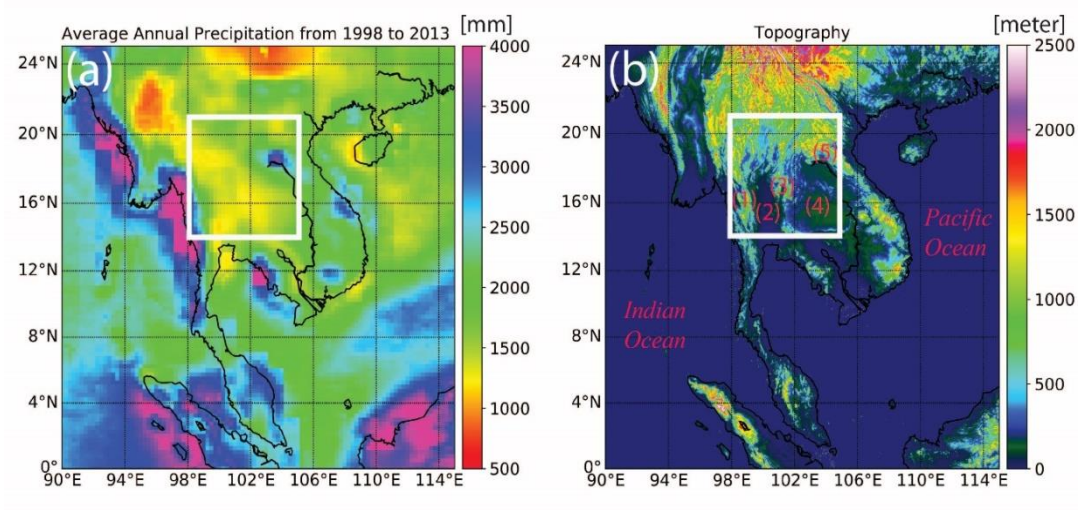

Fig. 1. Study area (a) annual precipitation average from 1998 to 2013 from TRMM3B42. White solid box represents study area for analysis of convective cloud properties and structures (b) Topography of the study area and surrounding area over Indochina. Locations referred in text include 1) Tenasserim mountain range, 2) Chao Phra Ya basin, 3) Phetchabun range, 4) Khorat basin, 5) Annamite mountain Range.

2.2 TRMM Dataset

2.2.1 TRMM Version-7 3B42 Dataset

The primary sources of data are from sensors on board the TRMM satellite namely PR, TMI, and LIS (Kummerow et al., 1998). The TRMM PF database (Nesbitt et al., 2000; Liu et al., 2008) from link http://atmos.tamucc.edu/trmm/data/trmm/level_2/rpf/ is used to assess rainfall characteristics and convective cloud properties over inland IP from 1998 to 2013. In addition, to define seasons, the TRMM version-7 3B42 from link https://disc.gsfc.nasa.gov/mirador-guide is employed (Huffman et al., 2007). TRMM3B42daily Version 7 has spatial resolution of 0.25° x 0.25° located from 50° S to 50° N with the collecting period from 1998 to 2014, and it continues as an ongoing global precipitation measurement (GPM) project. The infrared radiance measurements from geostationary satellites provide the primary source of rain estimates, which are calibrated by passive microwave sensors, including TMI and PR, on board TRMM.

2.2.2 TRMM Precipitation Feature Database

A new version of the PF database that was reprocessed in 2012 based on TRMM product version 7 (Liu, 2013) is used to analyze convective characteristics inland IP for a 16-year period (1998-2013) before starting GPM. The PF database was developed by Liu et al. (2008), based on Nesbitt et al. (2000) algorithm. The PF database was updated to new version in 2008 by including both PFs and cold cloud features (Liu et al., 2007) to account for warm rainfall under clouds without ice. The PR-detected Precipitation Feature (RPF) is used due to the combination level-2 files from monthly statistics are easily built. The PF database incorporates many standard product outputs (e.g., 2A25; TRMM PR3-D reflectivity) along with calculated statistics (e.g., min 85 GHz microwave brightness temperature) (Liu et al., 2008). The PF algorithm is used to define PFs by grouping contiguous rain area originally observed by the TRMM Precipitation Radar (PR) and Microwave Imager (TMI). Therefore, the properties of each PF, such as size, rain volume, and convective intensity proxies (e.g., lightning flash rate, height of radar echoes) can be summarized.

2.3 Methodology

As shown in **Fig. 2**, the TRMM data set was used in the analysis. Firstly, the periods of monsoon seasons were defined and calculated based on TRMM 3B42. Then, the analysis of PFs was done using TRMM PF database to understand precipitation structure and its. Properties based on defined monsoon periods.

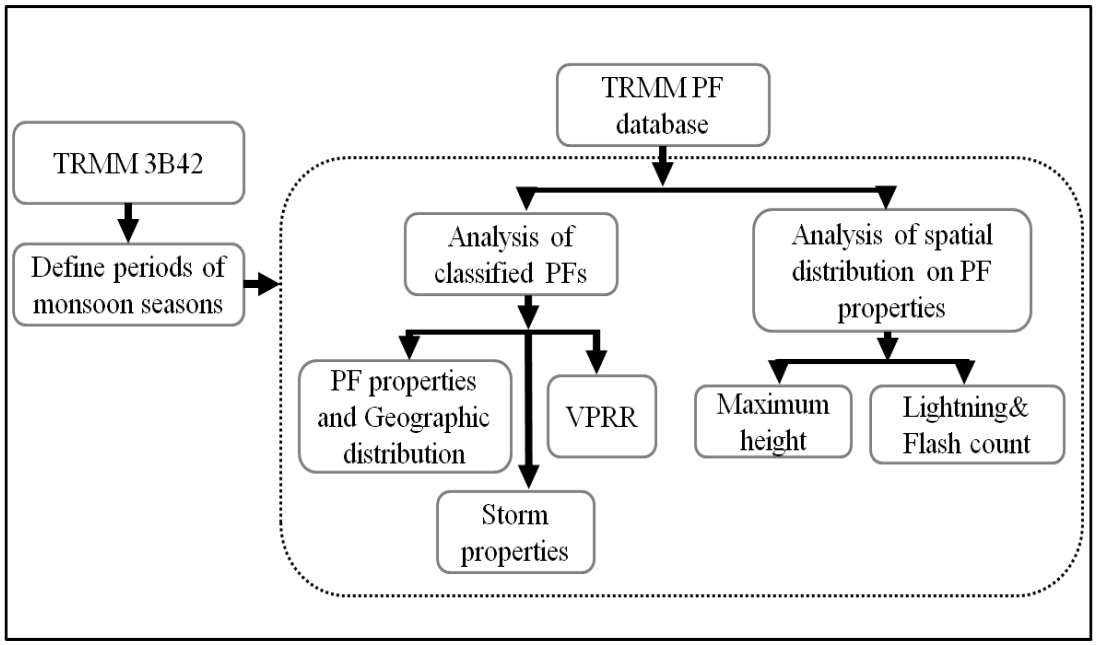

Fig. 2. Flowchart of the study.

2.3.1 Definition of Monsoon periods

To define the periods of monsoon seasons, onset and withdrawal dates, using 5-day mean (pentad), must be defined based on Matsumoto (1997). Specifically, the 5-day mean rainfall computed from daily rainfall TRMM3B42 is considered with annual mean pentad (Pm = (Annual precipitation)/73). Matsumoto (1997) defined onset and withdrawal pentad for each rain gauge

station, while this study, with its specific interest in the inland IP, defines the whole study area (**Fig. 1**). Therefore, the onset and withdrawal pentads are representative for the white box (**Fig. 1a**).

The definition of the onset (withdrawal) of summer rainy season is that the first (last) pentad in which the mean pentad precipitation exceeds Pm in at least three consecutive pentads after (before), dropping it in more than three consecutive pentads. The onset and withdrawal dates are defined as the middle date of the defined pentad. Therefore, the monsoon period for each year can be defined from the onset date to one day prior to the withdrawal date. The premonsoon period can be defined from 1st February to one day prior to the onset date. Finally, the postmonsoon period is defined from withdrawal date to 30th November.

2.3.2 Classification of PF

The PFs are analyzed for two regions based on analysis purposes. The first region (14° -21° N, 98° -105° E) is defined for analysis of convective cloud properties and structures over the inland IP, while the second region (0° -25° N, 90° -115° E) is a subset area used for discussion of spatial distribution of PFs. In this study, the PFs are analyzed in three periods of premonsoon, monsoon and postmonsoon. Areas and the presence of convective pixels are used as condition to classify further the selected PFs into MCSs, intense MCSs, sub-MCSs, or non-convective systems (NCs) (Xu et al., 2009). The area used to define MCSs is based on the definition by Houze (1993) used in Xu et al. (2009). PFs with an area greater than 1000 km^2 containing at least one convective pixel are classified in MCSs. Intense MCSs are classified separately from MCSs when the maximum height of 30 dBZ echo is higher than 8 km. Sub-MCSs are defined as PFs with an area less than 1000 km^2 and occupying at least one convective pixel. Finally, NCs are the systems without any convective pixel, indicating decayed convective systems or stratiform systems.

2.3.3 PF Interpretation Parameters

Radar Reflectivity: Many parameters of PFs derived from PR, TMI and LIS are used in analysis of convective cloud properties and structures. PR parameters used are area coverage of PFs, maximum radar reflectivity, maximum height of 30-dBZ echo, and maximum radar echo at the height of 6 km. The supercooled liquid droplets or large ice particles is presented by high values of radar reflectivity above the freezing level. The maximum height of 30-dBZ echo indicates the updraft level which supercooled liquid raindrops or large ice particles can be lifted (DeMott & Rutledge, 1998). Echo height of 6 km can refer to electrical phenomena when echo exceeds the value of 35-40 dBZ in the mixed-phase region (where $0^\circ C \geq T \geq -40^\circ C$) with temperature lower than -5° C reported by many studies (Dye et al., 1989; Williams et al., 1992; Petersen et al., 1996; Petersen et al., 1999). The convective cores are presented by Vertical profiles of radar reflectivity (VPRR) retrieving from maximum reflectivity factors of precipitation systems as a function of height (Donaldson, 1961; Zipser & Lutz, 1994; Xu et al., 2009).

*Passive Microwave Brightness Temperature:*To prevent mix-up with low brightness temperatures caused by low surface emissivity of ice scattering, Polarization Corrected Temperature at 85 GHz from TMI (85-GHz PCT) is derived from conversion of polarization for both horizontal and vertical signals (Spencer et al. 1989). The 85-GHz PCT responds to upwelling scattered background radiation caused by ice particles lifted by the updraft as a proxy for ice water content integrated over depth (IWP) (Vivekanandan et al., 1991). The lower GHz PCT, the more enhanced IWP responds to strong convective intensity (Mohr & Zipser, 1996; Cecil & Zipser, 1999; Zipser et al., 2006).

Interpretation of PF Parameters Measured from LIS: A strong updraft can produce supercooled cloud liquid water and large heavily rimed graupel particles in the mixed-phase clouds (Williams, 1989). The collision between small size of ice particles with large size of graupel, producing the supercooled liquid water can induce charge separation leading to lightning (Saunders, 1998).

3. RESULTS AND DISCUSSION

In this section, the classification on monsoon seasons from 16 years of TRMM data is described on the results. The concept of rainfall in pentad (5 days) is used to compute in finding the onset and withdrawal dates on summer monsoon season of each year.

3.1. Finding Monsoon Season Periods

Based on method of defining monsoon from Matsumoto (1997), the daily rainfall estimates from 16 years of TRMM data had been done over the white boundary box of the central area of the IP (**Fig. 1a**). The onset and the withdrawal of monsoon pentads had been calculated for each year. The period of premonsoon, monsoon, postmonsoon dates were found for each year, depending on annual variation of rainfall amount. The premonsoon starting date is defined as the 1st of February annually, while last date of the postmonsoon is defined as being the end of November annually. The monsoon onset and withdrawal dates provide information about the wet and dry years. A longer duration of the monsoon season means more rainfall above the annual pentad mean for each pentad. In this study, dry spell periods are not considered during monsoon periods due to few and noncontiguous pentads.

Using 2011 as an example, annual rainfall is relatively larger than average annual rainfall (**Fig. 1b**) over the inland IP (**Fig. 3a**). To find seasonal periods of each year, the pentad mean rainfall is computed over the white solid box (**Fig. 3a**). In **Fig. 3b**, Pentad Numbers 21 and 58 are defined as onset and withdrawal pentads for 2011.

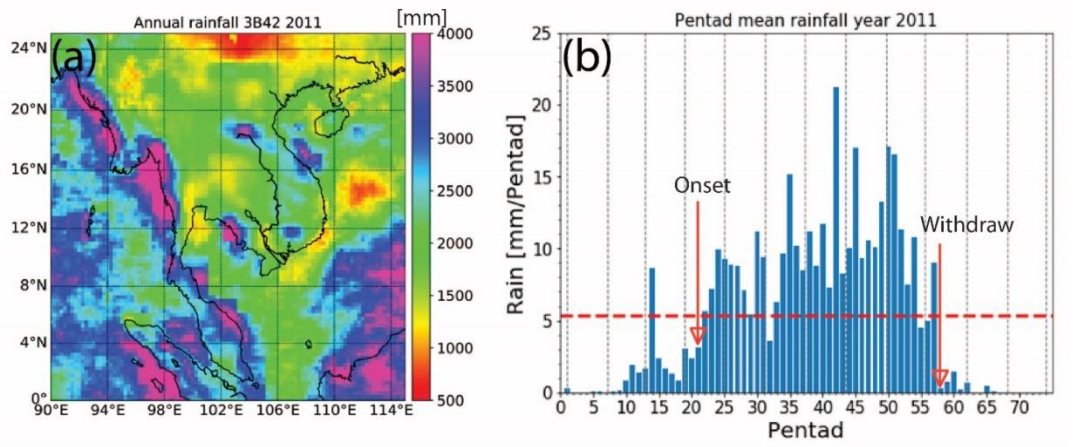

Fig. 3. Seasonal periods defined: (a) annual rainfall in 2011 (b) pentad mean rainfall in 2011. Red-dashed horizontal line indicates annual mean pentad.

Inter-annual variations of rainfall periods are shown in **Table 1**. For example, the early onsets in 1999 and 2006 started on pentad number 19, while the longer monsoon period occurred in 1999. Variation of mean rainfall was also observed. In 2011, the highest mean rainfall caused massive flooding in the Chao Phraya basin, where locates in the middle of the IP.

3.2. Classified PFs

In this section, precipitation feature and geographical distribution is investigated on classified monsoon seasons and analyzed with classified PFs based on criteria mentioned in section 2.2.3. Next, the storm properties over the inland IP were analyzed using mentioned criteria in section 2.2.3. The vertical profile of radar reflectivity (VPRR) for classified seasons is also investigated and compared among classified PFs.

Table 1.
Sixteen years of statistics for seasons defined by TRMM observations from 1998 to 2013.

Year	mean rain (mm)	Onset PT	Withdrawal PT	Num Pre-MS Dates	Num MS Dates	Num Pt-MS Dates
1998	3.7	25	58	97	166	44
1999	4.9	19	61	67	211	29
2000	4.9	21	56	77	176	55
2001	4.7	23	60	87	186	34
2002	5.0	23	61	87	191	29
2003	4.1	24	58	92	171	44
2004	4.3	22	53	82	156	70
2005	4.5	24	56	92	161	54
2006	4.8	19	57	67	191	49
2007	4.4	23	57	87	171	49
2008	5.0	21	56	77	176	55
2009	4.2	24	59	92	176	39
2010	4.4	26	59	102	166	39
2011	5.3	21	58	77	186	44
2012	4.5	22	56	82	171	55
2013	4.7	23	59	87	181	39

3.2.1 PF Population and Geographical Distribution

MCSs made a significant contribution to rainfall over the inland IP in all periods. Based on the white solid box **(Fig. 1a)** the total sample of 21,171 PFs were found over the inland IP during three periods (**Table 2**). About 24% fall into NCs class, while a large number of PFs, about 72% fall in Sub-MCSs class. Only 2.3% of the PFs reach the threshold of MCSs, with only 1.7% of these reaching the threshold definition of intense MCSs. The sample size of monsoon PFs is the largest, followed by the premonsoon and the postmonsoon seasons, respectively, due to the defined periods based on Matsumoto (1997). The premonsoon season has the largest percentage of intense MCSs and NCs compared to other periods. On the other hand, the small convective systems of Sub-MCSs comprise the largest percentage of the classified PFs during the postmonsoon season.

Table 2.

Precipitation Features.

Period/type	Tot PFs No.	NCs		Sub-MCSs		MCSs		Intense MCSs	
		No.	%	No.	%	No.	%	No.	%
Pre-MS		2296	30.6	4838	64.5	154	2.1	205	2.7
Monsoon		17884	26.5	46356	68.8	1954	2.9	1079	1.6
Post-MS		991	13.9	5951	83.4	128	1.8	59	0.8
Tot		21171	23.7	57145	72.2	2236	2.3	1343	1.7

Geographically, MCSs concentrate in the western part of the inland IP, over the Tenasserim mountain range, during monsoon (**Fig. 4b**), while they are found with greater frequency over the southern part of the IP and near the equator for both land and ocean in premonsoon and postmonsoon seasons (**Fig. 4a** and **4d**), respectively. Sub-MCSs is located in the western and northern regions of the inland IP during monsoon (**Fig. 4e**) and they occur with greater frequency over ocean areas during premonsoon and postmonsoon seasons (**Fig. 4d** and **4f**).

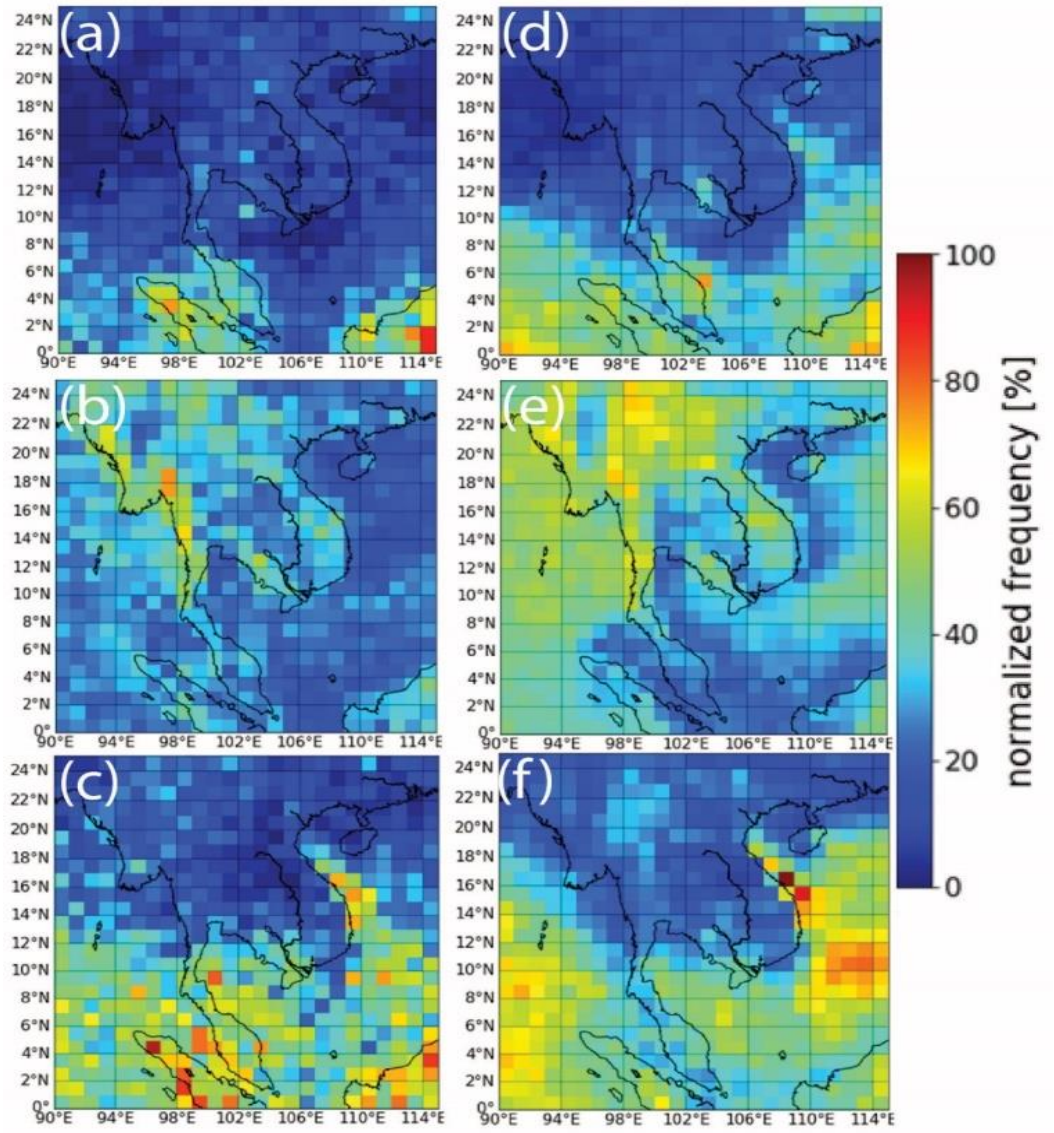

Fig. 4. Frequency occurrence of classified PFs for premonsoon, monsoon, and postmonsoon (a), (b), (c) for MCSs (d), (e), (f) for sub-MCSs.

3.2.2 Storm Properties over the Inland IP

Median values and their cumulative distribution functions (CDFs) are shown in **Table 3** and **Fig. 5**, respectively. The area is calculated from parameters named "NPIXELS_PR" that is the number of pixels observed by PR. The altitude of spacecraft's orbit before and after booting are considered due to the direct effect to horizontal resolution.

Table 3.

Median values of selected parameters.

Period	Type	Area	Min85pct	Maxht30	Maxdbz6
Pre-MS	Tot PFs	26.0	276.6	5.0	22.5
	MCSs	617.4	244.0	6.0	33.3
	IMCSs	1300.5	168.3	11.3	48.0
Monsoon	Tot PFs	26.0	277.7	4.8	22.0
	MCSs	494.2	238.1	6.0	33.6
	IMCSs	1248.5	164.4	10.0	45.0
Post-MS	Tot PFs	26.0	279.6	4.3	21.6
	MCSs	598.2	248.3	5.6	31.7
	IMCSs	1196.5	173.0	10.0	43.2

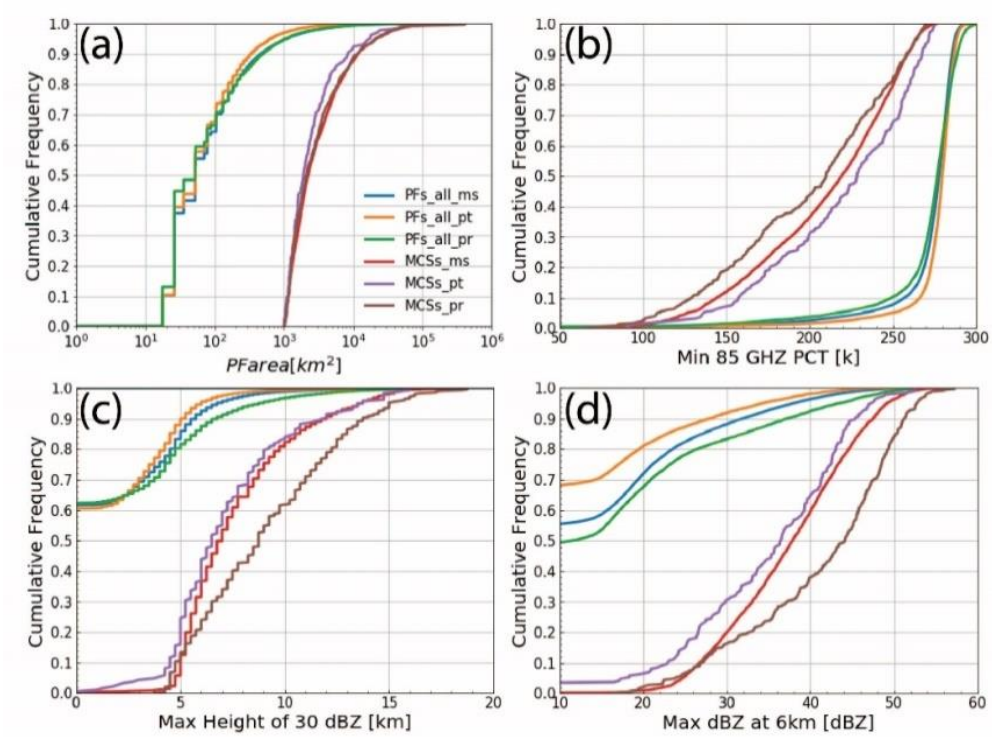

Fig. 5. Cumulative Density Function of statistics extraction from premonsoon, monsoon, and postmonsoon (a) area, (b) min PCT of 85 GHz, (c) max height of 30 dBZ, and (d) max dBZ at 6 km, for all PFs and MCSs over inland Indochina from solid white box, as shown in **Fig. 1a**.

1) Area Structure

PFs of different seasons do not differ in area size when all the PFs are analyzed (**Table 3** and **Fig 5a**). The PFs in small features dominate more than 95% being at area size smaller than 1000 km^2. However, only the more intense systems are considered, differences in area structures are found of PFs by seasons. The largest-area MCSs are found in the premonsoon season, but the frequency of

IMCSs is not very different between premonsoon and monsoon seasons. Relatively smaller IMCSs are found in the postmonsoon season.

2) Statistics for convection intensity proxies

As shown in **Table 3**, median values for IMCSs during postmonsoon are the most severe compared to other periods, except for Min85PCT for monsoon season. Taller and stronger clouds (MaxHT30; MaxdBZ6) derived from PR on board TRMM are enhanced over the inland IP in the case of IMCSs. PFs with very weak intensity dominate in the study area presenting by high PCT values according to CDFs of minimum 85-GHz PCT (Min85pct; **Fig. 5b**). Only about 10% of the total features have values less than 250 K, which is used as the threshold to delineate systems with low rain intensity (Spencer et al., 1989). Only about 5% of all PFs indicate for the deep convection using threshold lower than 225 K following McGaughey et al. (1996).

More than 60% of all PFs does not have sufficiently large hydrometeors concentration to produce a 30-dBZ radar echo (**Fig. 5c**). Besides, the shallow PFs less than 6 km are found about 50% (**Fig. 5d**). In contrast to shallow PFs, more than 90% of MCSs are found to exceed a height of 6 km. A small fraction of MCSs is found with radar echoes at 30 dBZ reaching up to 15 km, and 6 km radar echo exceeding 50 dBZ. The strong MCS intensity during premonsoon is observed through ice scattering signal (Min85pct), vertical radar reflectivity (MaxHT30; **Fig. 5c**), and maximum radar reflectivity at 6 km (MaxDbz6; **Fig. 5d**). The MCS intensity is ordered from stronger to weaker by premonsoon, monsoon and postmonsoon, respectively. About 40% and 60% of features for both maximum height at 30dBZ (**Fig. 5c**) and Max dBZ at 6 km (**Fig. 5d**), which exceed for both height of 10 km and 40 dBZ, are found in premonsoon period. The statistics indicate the presence of larger super-cooled raindrops in the mixed-phase clouds during premonsoon season that are larger than those found in Xu et al. (2009). In addition, Guy & Rutledge (2012) used the same database PFs for 13 years that are shorter period than this study to assess convective characteristics from May to October during period of African Easterly Waves. They found that mean vertical profiles of convective were stronger in the location of continental interior. However, this study shows that MCSs of the premonsoon period over the inland is stronger and higher than other seasons that are different from Guy & Rutledge (2012) found during monsoon period.

3.2.3 Vertical Profile of Radar Reflectivity

The reflectivity profiles as a function of height are based on VPRR from Donaldson (1961), which is used to produce the PF product MaxdBZ (Xu et al. 2009). VPRR is produced from radar echoes observed by TRMM PR at a vertical resolution of 0.25 km, from the TRMM precipitation and cloud feature database (Liu, 2013). VPRR indicates storm intensity respected to radar echo above the mixed-phase region (Szoke & Zipser, 1986; Zipser & Lutz, 1994; Cecil et al., 2005; Xu et al., 2009). However, recent study shows that the extreme rainfall events are mostly associated with less intense convection (Hamada et al., 2015).

Fig. 6 shows the VPRR for MCSs and Sub-MCSs in the inland IP during the defined periods. MCSs with more intense convection according their extending echo top height are found compared to those of sub-MCSs. The maximum radar height for MCSs reaches to a height of more than 18 km for the premonsoon season. The MCSs intensity during premonsoon is the strongest among the three seasons (**Fig. 6a**), while monsoon and postmonsoon periods are in close proximity (**Fig. 6b** and **6c**), indicating no significant difference in the convective structures. Sub-MCSs for both premonsoon and postmonsoon indicate stronger intensity than during the monsoon season, with height exceeding 15 km (**Fig. 6d**, **6e**, and **6f**).

In this study, stronger radar echoes between 2 and 5 km for MCSs are observed during premonsoon than during other periods. This enhanced radar reflectivity may be generated from the mixed-phase region of the premonsoon season. Compared to sub-MCSs over the South China from Xu et al. (2009), the inland IP has a wider range of radar echoes and heights for all periods. Larger liquid drops or precipitation-sized ice particles can be found in the mixed-phase region where a higher potential for charge separation exists (Dye et al., 1989).

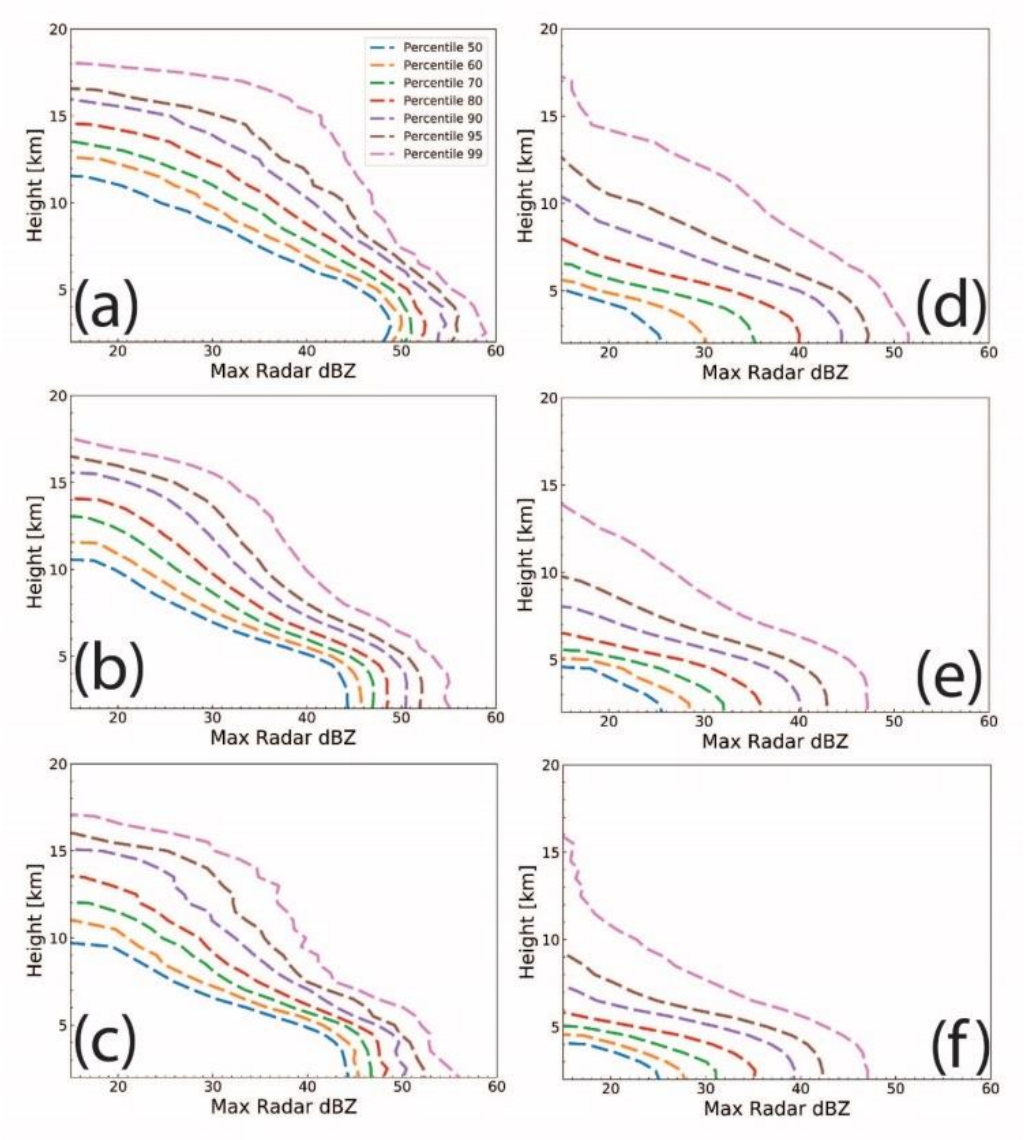

Fig. 6. Vertical profiles of radar reflectivity (from bottom to top in 50th, 60th, 70th, 80th, 90th, 95th, and 99th percentile) over inland IP during premonsoon, monsoon, and postmonsoon: (a),(b),(c) for MCSs; (d),(e), (f) for sub-MCSs. Data used for statistical calculations are from those grids inside the solid white box, as shown in **Fig. 1a**.

Table 4.

Precipitation Features with flashes counted over inland Indochina.

Period/criteria	PFs with flashes		With 1-9 No.	With 10-99 No.	With >=100 No.
	No.	%			
Pre-MS	566	7.5	412	136	18
Monsoon	2093	3.1	1749	338	6
Post-MS	116	1.6	103	13	0

As identified by Xu et al. (2009), lightning activity is one of the proxies used to examine convective activity. The lightning activity before monsoon onset is higher than other periods (Petersen et al., 2002; Xu et al., 2009; Williams et al., 1992; Qie et al., 2003; Yuan & Qie, 2008). In this sub section, the flash rate is analyzed for all three seasons. Not surprisingly, the highest flash rate of 7.5% was recorded during premonsoon over inland IP (**Table 4**). The flash rate decreases only 4 times from class 10-99 to class 1-9 in case of premonsoon seasons, while the monsoon abruptly decreases 5 times. The highest flash rate (>=100) was not observed in the postmonsoon season. In this study, the flash rate found in the inland IP is similar to that observed over the South China by Xu et al. (2009) during the premonsoon season.

Table 5.

Total flash counts.

Period	PFs	NCs	Sub-MCSs	MCSs	IMCSs	Rain area	Conv area
	Flash No.	Flash No.	Flash No.	Flash No.	Flash No.	(km^2 / flash)	(km^2 / flash)
Pre-MS	7638	10	1227	216	6118	205.5	77.8
Monsoon	13669	28	2268	414	10841	653.6	181.9
Post-MS	691	0	107	23	560	366.1	163.0

As shown in **Table 5**, flash rate caused by intense MCSs is larger than 80% in all seasons. Sub-MCSs are the second-ranked contributors for flash rate, followed by MCSs. The smallest rain area per flash occurs in the premonsoon season, followed by postmonsoon and monsoon seasons, which is consistent with the flash rate normalized by the convective area. When compared with pre-meiyu season, the normalized flash count over the inland IP in the premonsoon season is about three times less than that observed over southern China (Xu et al., 2009). This may be due to the fact that their study area including PFs over sea, which produce less lightning (Nesbitt et al., 2000).

3.3. Spatial Distribution on PF Properties

In this section, the spatial distribution of PF properties is analyzed on maximum height of PFs. In addition, the spatial distribution of Lightning and Flash Count is also investigated and disussed on the classified seasons with the classified PFs.

3.3.1 Maximum Height of PFs

Maximum height of PFs (MaxHT) can be used as one of the cloud characteristic proxies to investigate severity of precipitating cloud. Spatial variation in both frequency of occurrence and MaxHT average is clearly shown on the seasonal variation pattern (**Fig. 7**). A relatively low frequency of MaxHT is found during the premonsoon season over the inland IP compared to near equatorial regions (**Fig. 7a**), while the average height of PFs is relatively taller than that found during other periods over the inland IP, with approximate height exceeding 8 km (**Fig. 7d**). The highest frequency MaxHT was found inland of the northern ICP during monsoon (**Fig. 7b**). The frequency of the highest MaxHT over southern SCS, Bay of Bengal and Andaman Sea increases during postmonsoon season (**Fig. 7c**). The tallest average MaxHT were observed in the premonsoon season over the inland IP, compared to PFs over sea and other seasons (**Fig. 7d**). The tallest PFs are located over the middle part of Myanmar. The spatial pattern of average MaxHT shows a similarity of distribution between monsoon and postmonsoon seasons (**Fig. 7e** and **7f**). There were clearly spatial variations of MCSs and Sub-MCSs in the inland IP during premonsoon. In Western and central Africa, Balogun et al. (2020) analyzed TRMM PF database and detected echoes at high altitude much more frequently in the rainforest and savannah zones during March‑May, but the savannahs, Sudano, and Sahel zone convections tend to reach higher altitude more frequently than the rainforest zones during June‑September.

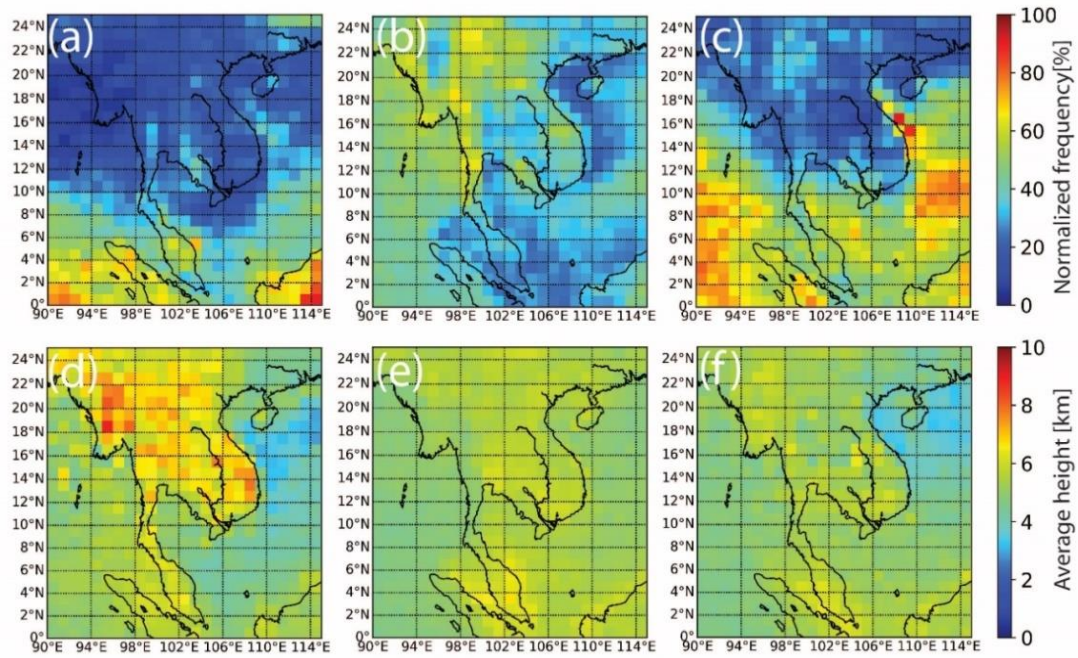

Fig. 7. Spatial distribution of MaxHT over IP and vicinity during premonsoon, monsoon, and postmonsoon. (a), (b), (c) represent frequency occurrences; (d), (e), (f) represent averages. The resolution grid size is at 1° degree.

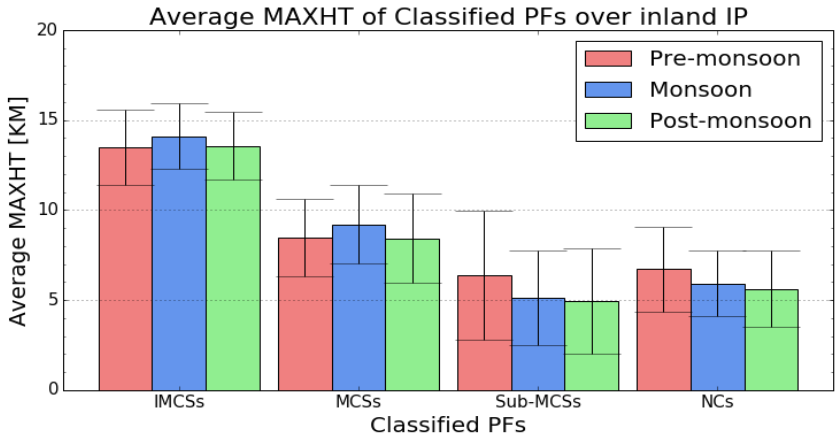

Fig. 8. Average MaxHT and standard deviation of classified PFs over solid white box shown in **Fig. 1a** during premonsoon, monsoon, and postmonsoon. Data used for statistical calculations are from those grids inside the solid white box, as shown in **Fig. 1a**.

As shown in **Fig. 8**, intense MCSs have the tallest average MaxHT, above 13 km. There are no differences observed in the height of MCSs in each season. However, greater variation was observed in sub-MCSs and NCs, with a storm height close to 10 km for premonsoon season. The reason for taller PFs being located over the IP during the premonsoon season is the variety and large population of Sub-MCS and NCs. The contribution of each PF type shows that NCs during post monsoon contribute the largest proportion up to 84% of all PF types. Sub-MCSs and NCs together comprise more than 95% of PF types. Using the three-dimensional structure of TRMM PR, Houze et al. (2007) found intense convective echoes occur just upstream, over the lower elevations of the Himalayas, of which sometimes extending above 17 km, indicating that exceptionally strong updraughts loft graupel

to high altitudes. The south Asian monsoon, supporting warm moisture, provides very warm and highly unstable conditions to produce orographically influenced precipitation. However, IMCSs in this study are not so intense compared to the South Asian Monsoons. Generally, over these hot spots where IMCSs are located, low-level moist air is capped by very dry air aloft to form a capping inversion situation that builds unstable layers (Houze et al., 2007).

3.3.2 Spatial Distribution of Lightning and Flash Count for Three Seasons

Based on ice scattering of convective core criteria using Min85PCT, convective systems are located on both land and sea, but spatial distribution varies among seasons (**Fig. 9**). In the premonsoon season, intense convection is sparse over the IP inland (**Fig. 9a**) and low Min85PCT is shown over the coastal areas in the eastern Gulf of Thailand and over the SCS, east of Hainan and the southern part of the SCS (**Fig. 9d**). In the monsoon season, the frequency of 85PCT is high over the northern IP (**Fig. 9b**), while intense convection occurs in the middle of the IP with relatively low intensity compared to the premonsoon and postmonsoon seasons (**Fig. 9e**). In the postmonsoon season, there is a high frequency of 85PCT located over the southern part the IP, Peninsular Malaysia, Sumatra and Borneo Islands (**Fig. 9c**). However, extremely intense convection is located over the middle and north of the IP, with relatively low 85PCT (**Fig. 9f**).

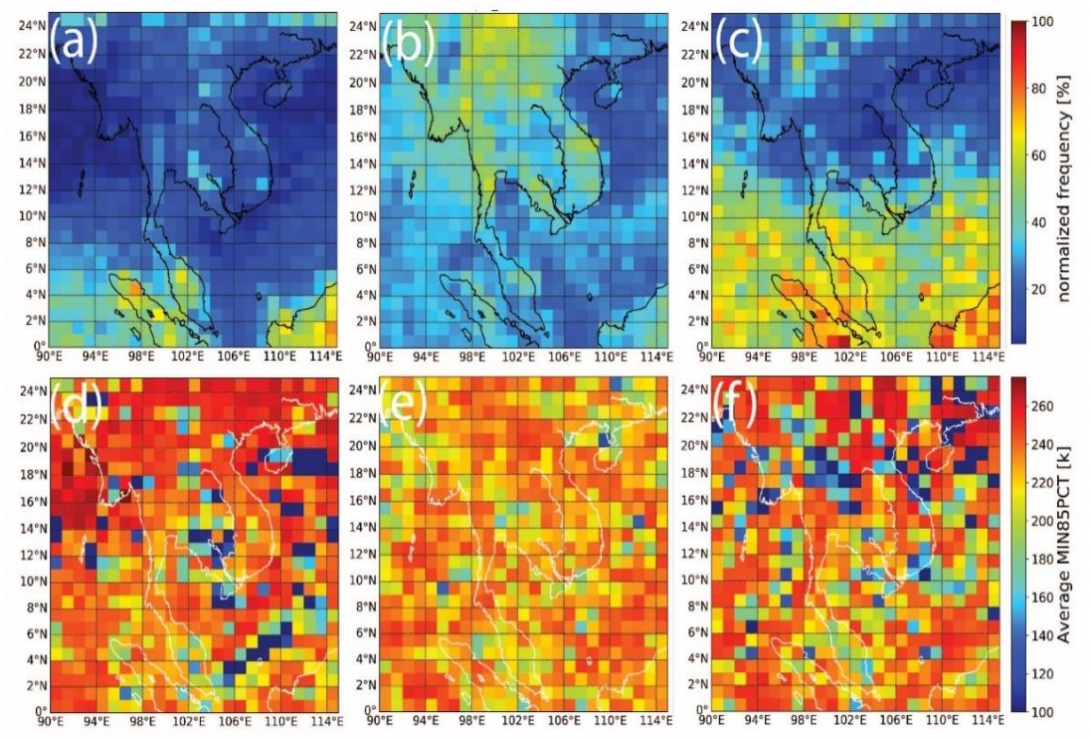

Fig. 9. PFs Locations categorized by min PCT of 85 GHz during premonsoon, monsoon, and postmonsoon (a), (b), (c) frequency of occurrences; (d), (e), (f) average. The resolution grid size is at 1° degree.

Flash count is calculated where the number is greater than zero. Generally, flash frequency over land is much greater than over open water (**Fig. 10**). The average flash count during the premonsoon season is higher than other seasons, with flash numbers exceeding 20 counts per PF over the northern region of the inland IP. Flash numbers are consistent with frequency over the IP during the premonsoon season. While the flash frequency seems high over the Malay Peninsula and north Sumatra, which is low compared to the IP. Liu et al. (2020) found that favorable environments of high flash rate thunderstorms in the tropics are characterized by higher Convective Available Potential

Energy, lower Convection Inhibition, and weaker wind shear, compared to the high flash rate thunderstorms in the subtropical regions. In the monsoon season, flash frequency increases over the IP and offshore areas in the southern region, although the flash number is relatively low compared to the premonsoon season. The finding, in this study, the higher flash rate in the premonsoon season is consistent with findings by Xu et al. (2010) regarding the flash rates before Mei-Yu onset. In the postmonsoon season, the flash frequency dramatically decreases over the IP, but it increases over the Malay Peninsula. Overall, the flash number is relatively high, but it is not consistent across the IP compared to other high frequency areas. Mao and Li (202) found that lightning activity over South China during spring, corresponding to premoonson season of this present study, has shown interannual variations and significantly correlated with El Niño‐Southern Oscillation (ENSO) by having frequent lightning in El Niño events.

There are many studies that have compared the characteristics of MCSs over both land and ocean. The enhanced convective systems over land are larger than those found over ocean regarding to structures and properties (LeMone & Zipser, 1980; Zipser & LeMone, 1980; Xu, 2013; Xu et al., 2009; Yuan & Qie, 2008). Generally, oceanic cloud systems have less intense embedded convection, but can form wide stratiform regions, while continental MCSs often have more intense embedded convection (Nesbitt et al., 2000; Houze et al., 2015; Toracinta et al., 2002). Nesbitt et al. (2000) and Toracinta et al. (2002) identified PFs using criteria of intensity and areal based on TRMM PR data by collocating them with the simultaneous passive microwave sensor measurements on frequencies of ice scattering. They found that convection over tropical landmasses is characterized by more lightning, stronger ice scattering, and more intense radar echo in the upper levels of convective clouds than in precipitating clouds over tropical oceans. Using aircraft to measure vertical draft velocities, deep convection over tropical oceans is typically found to be much lower than over land (LeMone & Zipser, 1980; Zipser & LeMone, 1980). Therefore, the high updraft velocity over land can support the generation of large supercooled water concentrations required for the graupel and hail particle formation associated with charge separation.

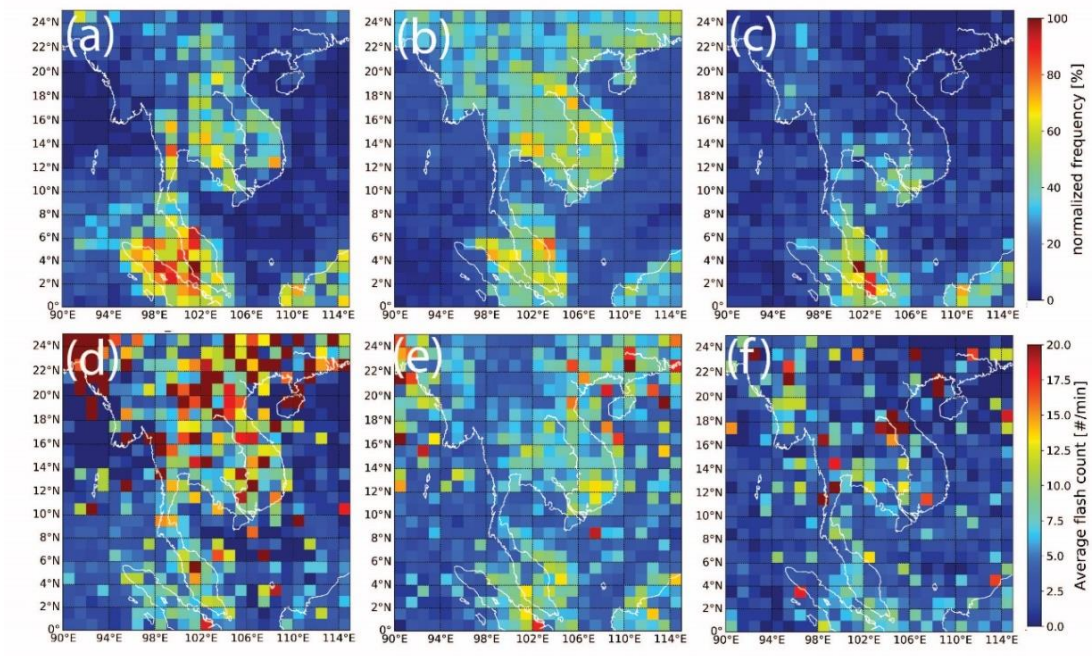

Fig. 10. Locations of PFs categorized by Flash Count during premonsoon, monsoon, and postmonsoon (a), (b), (c) frequency of occurrences; (d), (e), (f) average. The resolution grid size is at 1° degree.

4. CONCLUSIONS

Using the seasonal definitions to define onset and withdrawal dates for monsoon based on the daily TRMM 3B42 dataset, the premonsoon, monsoon and postmonsoon seasons were found for each year over the inland Indochina Peninsula (IP) and surrounding regions. Climatology of cloud properties and structure from 1998 to 2013 (16 years) over the inland and surrounding regions were investigated based on TRMM Precipitation Features (PFs) database constructed by the university of UTAH, derived from original sensors of the TRMM project. The major findings of this analysis are as follows:

Intra-seasonal and inter-seasonal variation of rainfall intensity and periodical duration are clearly found based on the applied definition to identify the seasonal period of each year. Mesoscale Convective Systems (MCSs) play a significant role for all periods. Sub-MCSs are major contributors of rainfall during the postmonsoon season, while the highest percentage of intense MCSs (IMCSs) is found during the premonsoon season. Geographically, western and northern parts of the inland IP show the most frequent occurrence of sub-MCSs and MCSs during the monsoon season, while the frequency of occurrence of MCSs and sub-MCSs during the postmonsoon season is highest over the southern part of the IP, and over sea during, respectively.

In the case of IMCSs, taller and stronger clouds (MaxHT30; MaxdBZ6) identified from PR on board TRMM are found in greater numbers over the inland IP. IMCSs in the premonsoon season are the most numerous over the inland IP, based on microwave signals and radar reflectivity sensors, with distinct spatial concentration over western and northern regions of the IP for sub-MCSs during the monsoon season. Convection intensity proxies and vertical radar reflectivity have shown intra-seasonal variation over land from cumulative density function analysis by enhancement on MCSs during the premonsoon season. The intensity of MCSs during the premonsoon season is observed through ice scattering signal (Min85PCT), MaxHT30, and MaxdBZ6. The MCSs for three periods have shown more intense properties compared to sub-MCSs. The maximum height exceeds 18 km for the premonsoon season as measured by Vertical Profile of Radar Reflectivity (VPRR).

Based on ice scattering of convective core criteria using Min85PCT, convective systems are found on both land and sea, but spatial distribution varies among seasons. Spatial variation on microphysical structure of clouds is distinctly shown by seasons based on scattering of microwave signals and lightning flash counts. Lightning is relatively more frequent over land than over surrounding ocean. The most frequent lightning over the inland IP is found during the premonsoon season, while the highest average flash count over inland IP is also found over the west, north of the IP highlands during premonsoon season. The transitional period between seasons is interesting due to the properties and structure of precipitation systems occurring over both land and oceans because the difference in microphysical clouds involved during the periods. Limitation of this study is that the fine resolution data of ground-based radar is not used to investigate in structure of extreme storm cases. Future research should attempt to elucidate this to be useful information to people to avoid the extreme weather on the transitional period. Satellite products based on TRMM legacy and ground-based radar will be used in the future analysis over the IP and surrounding seas.

5. ACKNOWLEDGEMENTS

We would like to express our gratitude the anonymous reviewers for their helpful comments and discussions. This research was supported by National Research Council of Thailand (NRCT) through the Naresuan University R2561B062 and R2562B031. We are really appreciated to “Advancing Co-design of Integrated Strategies with Adaptation to Climate Change in Thailand (ADAP-T)” supported by the Science and Technology Research Partnership for Sustainable Development (SATREPS), JST-JICA for providing research fund to support the project. Most of the figures were produced using the Python script.

REFERENCES

Balogun R.A., Adeyewa Z.D., Adefisan E.A.&Okogbue E.C. (2020) Vertical structure and frequencies of deep convection during active periods of the West and Central African monsoon season. *Theor. Appl. Climatol*., 141, 615–626

Cecil D.J., Goodman S.J., Boccippio D.J., Zipser E.J. & Nesbitt S.W. (2005) Three Years of TRMM Precipitation Features. Part I: Radar, Radiometric, and Lightning Characteristics. *Mon Wea Rev*., 133, 543–566.

Cecil D.J. & Zipser E.J. (1999) Relationships between Tropical Cyclone Intensity and Satellite-Based Indicators of Inner Core Convection: 85-GHz Ice-Scattering Signature and Lightning. *Mon Wea Rev*., 127, 103–123.

DeMott C.A. & Rutledge S.A. (1998) The Vertical Structure of TOGA COARE Convection. Part I: Radar Echo Distributions. *J Atmos Sci*., 55, 2730–2747.

Donaldson R.J. (1961) Radar Reflectivity Profiles in Thunderstorms. *J Meteorol*., 18, 292–305.

Dye J.E., Winn W.P., Jones J.J. & Breed, D.W. (1989) The Electrification of New Mexico Thunderstorms. 1. Relationship between Precipitation Development and the Onset of Electrification. *JGR*., 94, 8643–8656.

Guy N. & Rutledge S.A. (2012) Regional Comparison of West African Convective Characteristics: A TRMM-based Climatology. *QJR Meteorol Soc*., 138, 1179–1195.

Hamada A., Takayabu Y.N., Liu C. & Zipser E.J. (2015) Weak linkage between the heaviest rainfall and tallest storms. *Nat Commun*., 6, 6213.

Houze Jr. R.A. (1993) *Cloud Dynamics*. Academic Press, 573 pp.

Houze Jr. R.A. (1989) Observed Structure of Mesoscale Convective Systems and Implications for Large-scale Heating. *QJR Meteorol Soc*., 115, 425–461.

Houze Jr. R.A., Wilton D.C. & Smull B.F. (2007) Monsoon Convection in the Himalayan Region as seen by the TRMM Precipitation Radar. *QJR Meteorol Soc*., 133, 1389–1411.

Houze Jr. R.A., Zuluaga M.D. & Brodzik S.R. (2015) The Variable Nature of Convection in the Tropics and Subtropics: A Legacy of 16 years of the Tropical Rainfall Measuring Mission (TRMM) Satellite. *Rev Geophys*, 53, 994–1021.

Huffman G.J. & Coauthors. (2007) The TRMM Multisatellite Precipitation Analysis (TMPA): Quasi-global, Multiyear, Combined-Sensor Precipitation Estimates at Fine Scales. *J. Hydrometeorol*., 8, 38–55.

Jorgensen D.P. (1984) Mesoscale and Convective-scale Characteristics of Mature Hurricanes. Part I: General Observations by Research Aircraft. *J Atmos Sci*., 41, 1268–1285.

Kodama C., Yamada Y., Noda A.T., Kikuchi K., Kajikawa Y., Nasuno T., Tomita T., Yamaura T., Takahashi H.G., Hara M., Kawatani Y., Satoh M. & Sugi M. (2015) A 20-year climatology of a NICAM AMIP-type simulation. *J Meteorol Soc Japan*., 93:393–424.

Kodama Y.-M., Ohta A., Katsumata M., Mori S., Satoh S. & Ueda H. (2005) Seasonal Transition of Predominant Precipitation Type and Lightning Activity over Tropical Monsoon Areas derived from TRMM Observations. *Geophys Res Lett*., 32, L14710.

Kummerow C., Barnes W., Kozu T., Shiue J. & Simpson J. (1998) The Tropical Rainfall Measuring Mission (TRMM) Sensor Package. *J Atmos Ocean Technol*., 15, 809–817.

LeMone M.A. & Zipser E.J. (1980) Cumulonimbus Vertical Velocity Events in GATE. Part I: Diameter, Intensity, and Mass Flux. *J Atmos Sci*., 37, 2444–2457.

Li N., Wang Z., Chen X. & Austin G. (2019) Studies of General Precipitation Features with TRMM PR Data: An Extensive Overview. *Remote Sensing*., 11, 80.

Liu C. (2013) University of Utah TRMM Precipitation and Cloud Feature Database Description Version 2.0, Department of Atmospheric Sciences, University of Utah, 33pp.

Liu C. & Zipser E.J. (2005) Global Distribution of Convection Penetrating the Tropical Tropopause. *JGR*, 110.

Liu C., Zipser E.J., Cecil D.J., Nesbitt S.W. & Sherwood S.A. (2008) Cloud and Precipitation Feature Database from Nine Years of TRMM Observations. *J Appl Meteorol Climatol*., 47, 2712–2728.

Liu C., Zipser E.J. & Nesbitt S.W. (2007) Global Distribution of Tropical Deep Convection: Different Perspectives from TRMM Infrared and Radar Data. *J. Clim*., 20, 489–503.

Liu N., Liu C., Chen B. & Zipser E. (2020) What Are the Favorable Large-Scale Environments for the Highest-Flash-RateThunderstorms on Earth?.*J Atmos Sci*., 77, 1583–1612.

Matsumoto J. (1997) Seasonal Transition of Summer Rainy Season over Indochina and Adjacent Monsoon Region. *Adv. Atmos. Sci*., 14, 231–245.

Mao J. & Li M. (2020) Interannual variations in spring lightning activity and convective rainfall over South China during the TRMM era. Theor. Appl. Climatol., 142, 483‑495.

McGaughey G.R., Zipser E.J., Spencer R.W. & Hood R.E. (1996) High-Resolution Passive Microwave Observations of Convective Systems over the Tropical Pacific Ocean. *J Appl Meteorol*., 35, 1921–1947.

Medina S., Houze Jr. R.A., Kumar A. & Niyogi D. (2010) Summer Monsoon Convection in the Himalayan region: Terrain and Land Cover Effects. *QJR Meteorol Soc*., 136, 593–616.

Mohr K.I. & Zipser E.J. (1996) Mesoscale Convective Systems Defined by Their 85-GHz Ice Scattering Signature: Size and Intensity Comparison over Tropical Oceans and Continents. *Mon Wea Rev*., 124, 2417–2437.

Nesbitt S.W. & Zipser E.J. (2003) The Diurnal Cycle of Rainfall and Convective Intensity according to Three Years of TRMM Measurements. *J Clim*., 16, 1456-1475.

Nesbitt S.W., Zipser E.J. & Cecil D.J. (2000) A Census of Precipitation Features in the Tropics Using TRMM: Radar, Ice Scattering, and Lightning Observations. *J Clim*., 13, 4087–4106.

Nesbitt S.W., Zipser E.J. & Kummerow C.D. (2004) An Examination of Version-5 Rainfall Estimates from the TRMM Microwave Imager, Precipitation Radar, and Rain Gauges on Global, Regional, and Storm Scales. *J Appl Meteorol*., 43, 1016–1036.

Petersen W.A., Cifelli R.C., Rutledge S.A., Ferrier B.S. & Smull B.F. (1999) Shipborne Dual-Doppler Operations during TOGA COARE: Integrated Observations of Storm Kinematics and Electrification. *Bull Am Meteorol Soc*., 80, 81–96.

Petersen W.A., Nesbitt S.W., Blakeslee R.J., Cifelli R., Hein P. & Rutledge S.A. (2002) TRMM Observations of Intraseasonal Variability in Convective Regimes over the Amazon. *J. Clim*., 15, 1278–1294.

Petersen W.A & Rutledge S.A. (2001) Regional Variability in Tropical Convection: Observations from TRMM. *J Clim*., 14, 3566–3586.

Petersen W.A., Rutledge S.A. & Orville R.E. (1996) Cloud-to-Ground Lightning Observations from TOGA COARE: Selected Results and Lightning Location Algorithms. *Mon Wea Rev*., 124, 602–620.

Qie X., Toumi R. & Yuan T. (2003) Lightning Activities on the Tibetan Plateau as Observed by the Lightning Imaging Sensor. *JGR*., 108, 4551.

Rapp A.D., Peterson A.G., Frauenfeld O.W., Quiring S.M. & Roark E.B. (2014) Climatology of Storm Characteristics in Costa Rica using the TRMM Precipitation Radar. *J. Hydrometeorol*., 15, 2615–2633.

Romatschke U. & Houze Jr. R.A. (2010) Extreme summer convection in South America. *J Clim*., 23, 3761–3791.

Satoh M., Noda A.T., Seiki T., Chen Y.-W., Kodama C., YamadaY., Kuba N. & Sato Y. (2018) Toward reduction of the uncertainties in climate sensitivity due to cloud processes using a global non-hydrostatic atmospheric model. *PEPS*., 5, 67.

Saunders, C.P.R. & Peck, S.L. (1998) Laboratory Studies of the Influence of the Rime Accretion Rate on Charge Transfer during Crystal/Graupel Collisions. *JGR*., 103.

Spencer R.W., Goodman H.G. & Hood R.E. (1989) Precipitation Retrieval over Land and Ocean with the SSM/I: Identification and Characteristics of the Scattering Signal. *J Atmos Ocean Technol*., 6, 254–273.

Szoke E.J. & Zipser E.J. (1986) A Radar Study of Convective Cells in Mesoscale Systems in GATE. Part II: Life Cycles of Convective Cells. *J. Atmos. Sci*., 43, 199–218.

Takahashi H. & Yasunari T. (2006) A Climatological Monsoon Break in Rainfall over Indochina−A Singularity in the Seasonal March of the Asian Summer Monsoon. *J. Climate.,* 19, 1545–1556.

Toracinta E.R., Cecil D.J., Zipser E.J. & Nesbitt S.W. (2002) Radar, Passive Microwave, and Lightning Characteristics of Precipitating Systems in the Tropics. *Mon Wea Rev*., 130(4), 802–824.

Vivekanandan J., Turk J. & Bringi V.N. (1991) Ice Water Path Estimation and Characterization Using Passive Microwave Radiometry. *J Appl Meteorol*.. 30, 1407–1421.

Wang B. & Ho L. (2002) Rainy Season of the Asian–Pacific Summer Monsoon. *J.Climate*., 15, 386–397.

Williams E.R. (1989) The Tripole Nature of Thunderstorms. *JGR*., 94, 13 151–13 167.

Williams E.R., Rutledge S.A., Geotis S.G., Renno N., Rasmussen E. & Rickenbach T. (1992) A Radar and Electrical Study of Tropical "Hot Towers". *J Atmos Sci*., 49, 1386–1395.

Xu W. (2013) Precipitation and Convective Characteristics of Summer Deep Convection over East Asia Observed by TRMM. *Mon Wea Rev*., 141, 1577–1592.

Xu W., Zipser E.J. & Liu C. (2009) Rainfall Characteristics and Convective Properties of Mei-Yu Precipitation Systems over South China, Taiwan, and the South China Sea. Part I: TRMM Observations. *Mon Wea Rev*., 137, 4261–4275.

Xu W., Zipser E.J., Liu C. & Jiang H. (2010) On the Relationships between Lightning Frequency and Thundercloud Parameters of Regional Precipitation Systems. *JGR*., 115, D12203.

Yokoyama C. & Takayabu Y.N. (2008) A Statistical Study on Rain Characteristics of Tropical Cyclones Using TRMM Satellite Data. *Mon Wea Rev*., 136, 3848–3862.

Yuan T. & Qie X. (2008) Study on Lightning Activity and Precipitation Characteristics before and after the Onset of the South China Sea Summer Monsoon. *JGR*., 113, D14101.

Zipser E.J., Cecil D.J., Liu C., Nesbitt S.W. & Yorty D.P. (2006) Where are the most intense thunderstorms on earth? *Bull. Am. Meteorol. Soc*., 87, 1057–1071.

Zipser E.J. & LeMone M.A. (1980) Cumulonimbus Vertical Velocity Events in GATE. Part II: Synthesis and Model Core Structure. *J Atmos Sci*., 37, 2458–2469.

Zipser E.J. & Lutz K.R. (1994) The Vertical Profile of Radar Reflectivity of Convective Cells: A Strong Indicator of Storm Intensity and Lightning Probability? *Mon Wea Rev*., 122, 1751–1759.

AREA-BASED AND DASYMETRIC POINT ALLOCATION INTERPOLATION METHOD FOR SPATIAL MODELLING MICRO-SCALE VOTER TURNOUT IN BUDAPEST

Tamás KOVALCSIK[1*], Balázs SZABÓ[2], György VIDA[1], Lajos BOROS[1]

DOI: 10.21163/GT_2021.161.06

ABSTRACT:
Spatial and temporal distribution of voter turnout can be an appropriate indicator of socio-demographic processes. Since elections are held more frequently than national censuses, their results may refine our picture of the temporal changes of the population. Due to the evolution of statistical applications and queries, gathering data on smaller geographical scales enables researchers to analyze social and political processes on a micro-scale. This kind of research is particularly relevant in the analysis of the transformation of metropolitan areas with significant population concentration are characterized by rapid transformation and high degree of variation. Therefore, the paper aims to develop a method for reaggregating precinct-level electoral results which are spatially inconsistent throughout different elections in the case of Budapest (Hungary). The developed area-based and dasymetric point allocation interpolation can transform the territorially aggregated but inconsistent electoral results into one target subdivision. The changes of voter turnout in different urban areas are related to socio-demographic processes, such as inner suburbanization, gentrification, studentification, or the transformation of former industrial (transitional) areas within the city.

Key-words: *Areal interpolation, Dasymetric mapping, Areal weighting, Budapest, Voter turnout.*

1. INTRODUCTION

One of the most measurable and expressive forms of political participation is voter turnout (Kostadinova, 2003), a good indicator of political activity of a society. Research on the spatiality of voter turnout is important in relation to the political representation of different places, as areas with a stable high level of participation have greater influence on decision-making processes, while areas with lower political activity have a lower influence (Lijphart, 1997). In addition, spatial differences in voter turnout are related to several other spatial social factors, such as disadvantage (Michener, 2017) or the social capital and local cohesion (Putnam, 1995). Furthermore, changes in the level of voter turnout indicate several other social processes as well. For instance, declining turnout is a good indicator of declining trust in political institutions, as disappointed voters stay away from the ballot box (Putnam, 2000). Moreover, elections are held more frequently than population censuses, thus they can serve as additional information of social processes like rapid transformation and high degree of variation in metropolitan areas (Charney & Malkinson, 2015).

Therefore, the examination of both spatial differences and temporal changes of voter turnout in metropolitan areas provides information about the involvement of local society in political issues, the extent of social capital, local cohesion and social exclusion. Therefore, this analysis is investigated the spatial characteristics and temporal variability of voter turnout on the lowest possible scale, in the only metropolitan area of Hungary, Budapest. The country has a mixed electoral system since the change of regime (1990); the mandates come from single-member constituencies and party lists. Until 2010 the elections had two rounds, but after the electoral reforms in 2011 the number of rounds has been decreased to one.

---

[1]Department of Economic and Social Geography, University of Szeged, H-6722 Szeged, Hungary; kovalcsik.tamas@geo.u-szeged.hu; vidagy@geo.u-szeged.hu; borosl@geo.u-szeged.hu.
[2]Geographical Institute, Research Centre for Astronomy and Earth Sciences, Eötvös Loránd Research Network, H-1112 Budapest, Hungary; szabo.balazs@csfk.mta.hu.
** Correspondence: kovalcsik.tamas@geo.u-szeged.hu.*

Even though the capital city appears as a set of constituencies in several studies (Kovács & Vida, 2015; Vida, 2016), our aim is to analyse its complicated inner structure that is not understandable on the level of electoral or administrative districts. Since the change of regime, the area belongs to a polling station (precinct – where the ballots are counted) was redrawn for each election. It represents a typical example for the modifiable area unit problem (MAUP) (Wong, 2004). Thus, in this study an areal interpolation method had to be implemented which can reaggregate the geographically inconsistent precinct-level turnout values to one target subdivision. The method uses an automated algorithm – combining the principles of areal weighting and dasymetric interpolation – to estimate the voter turnout of the target units.

Based on the above, the aim of this research is twofold, on the one hand, the development of a new areal interpolation method for the reaggregation of inconsistent spatial subdivision containing relative indicators specifically for precincts and electoral results. On the other hand, mapping of micro-scale electoral data enable us to analyse detailed socio-demographic transformations within a metropolitan area, through the analysis of the temporal transformation in the spatiality of voter turnout and the identification of the related social processes.

The study is structured as follows, in the literature review we presented the usability and characteristics of areal interpolation and the other methods based on it. In the methodology the difficulties of drawing the geometry of the precincts – due to the lack of geographically defined geometry – were discussed. In the next step, the area-based and dasymetric point allocation interpolation method was developed in order to reaggregate these precinct data into one subdivision. The first part of the results, we checked the accuracy of our reaggregation with RMSE and MAPE indicators, while in the second part, the spatiality and temporal distribution of voter turnout were analysed and visualized. Finally, the wide usage of the method is presented in the conclusions.

2. METHODS OF AREAL INTERPOLATION

Spatial interpolation is a method for estimating values from locations with known values to another spatial formation (Lam, 2009). Contrary to the traditional method – which generates a specific surface from point data – areal interpolation (a special type of spatial interpolation) can estimate the spatial distribution of a variable in a given subdivision using the original aggregated data (Goodchild & Lam, 1980). Thus, it is a spatial data transformation from the original (available) set (source units) to the derived set (target units ‑ in which the necessary analysis can be conducted) of overlapping units (Langford, Maguire & Unwin, 1991). This is a useful method when the different datasets to be compared are in a spatially inconsistent distribution (Walford & Hayles, 2012). Inconsistency in spatial datasets can come from source differences - where different social, economic and demographic data are collected in differing units (i.e., an alternative geography problem (Amos, McDonald & Watkins, 2017)). But same type datasets – from different times, however – can be generated from significantly inconsistent spatial subdivisions (i.e., a temporal mismatch problem – (Pavía & Cantarino, 2017; Walford & Hayles, 2012)). The question is what specific methods should be used in areal interpolation. These methods have already been compared in various studies (Amos, McDonald & Watkins, 2017; Comber & Zeng, 2019; Goodchild, Anselin & Deichmann, 1993; Lam, 1983). Therefore, only those which are relevant to our research methods are detailed below.

Areal weighting is the best known and the most straightforward approach, and one that can be easily implemented (Comber & Zeng, 2019; Kim & Yao, 2010). This method assumes that the population density does not change within the units of the source subdivision (Zoraghein *et al.*, 2016). Therefore, the population of the source zones is distributed area proportionately to spatial units (Goodchild & Lam, 1980; Lam, 1983). Accepting this assumption, the method consists of only one geometric intersection of source and target zones, where the value of each target unit can be calculated as a weighted sum of the data from intersected source zones (Langford, 2006). The weight is the ratio of the area of the intersected source unit to the original area of this unit (Flowerdew & Green, 1992). In several research, areal weighting is the initial and original method of areal interpolation because it has no need for any further (hereinafter referred as ancillary) information to the estimation (Mennis,

2003; Monteiro *et al.*, 2019; Zoraghein *et al.*, 2016). However, its homogeneity assumption – which is rarely true in the real world – is the glaring disadvantage of the method (Comber & Zeng, 2019).

Many studies use ancillary information to alleviate this problem. Without claiming comprehensiveness, this information can even be residential and non-residential zones from imagery (Fisher & Langford, 1996), population density (Eicher & Brewer, 2001), residential or cadastral parcels (Zoraghein *et al.*, 2016), the number of housing units within one census tract (Deng & Wu, 2013) or decennial census data (Liu & Martinez, 2019). According to Mennis (2003), areal interpolation which uses ancillary (additional and related) data can be defined as dasymetric mapping. Wright (Wright, 1936) was one of the first to use population density to refine areal interpolation; the literature considers this work the beginning of dasymetric mapping, even though the method has Russian origins (Mennis, 2009). Dasymetric mapping essentially refines the assumption of homogeneity within the source unit of the areal weighting method so that it can estimate the more appropriate proportion of the population within the target units.

3. DATA AND METHODS

Our investigation is derived from territorially aggregated data (such that unit of analysis is the polling station, where the ballots are counted). Every polling station has a small geographical area within which the associated voters live. Depending on the traditions of various countries, these areas are called: election districts, wards, or most commonly precincts, which is the name we use in this paper (Amos, McDonald & Watkins, 2017). The first task was to geometrically define and draw these areas in physical space, because the (Hungarian) National Electoral Commission has only provides lists of the names of the public spaces belonging to these areas (without any further geographical information). Moreover, these have only been publicly available since the 2002 parliamentary elections. Information for precinct areas in the pre-2002 elections was found only on the website of another research team (o-o-o.hu). It must be noted that the division of the precincts available for the 1990 elections contained so many errors that its results should be considered with due caution. To increase reliability, the precincts' geometries for the post-2002 elections were drawn manually. However, we are working on an automated procedure for future research, which will draw the divisions from the raw precinct descriptive lists. In summary, in the first phase of data preparation the geographical division of Budapest's precincts was prepared for the last eight parliamentary elections (between 1990 and 2018) and connected with their turnout levels.

The next phase of data preparation, namely the precinct-level election results in an inconsistent spatial distribution, was organized into an integrated database, to be able to implement a cross-election analysis. This was achieved using an areal interpolation method, which was developed by the principles of areal weighting and dasymetric mapping. In this new method points represent all eligible voters. In this phase of the methods, these points are evenly distributed within each precinct. Points in each precinct are defined as intersections of square grids. This grid network procedure ensures that the distribution of points is essentially even – thus they are area proportional. One of ArcGIS's plugins, the Geospatial Modelling Environment's 'genregularpntsinpolys' tool, is used to generate points. The tool uses polygons as input data and interprets distance as an input parameter as the side length of the squares that make up the grid. The side lengths of the squares forming the grid of each precinct were calculated using the following equation:

$$x_i = \sqrt{\frac{T_i}{V_i}} \tag{1}$$

where i is the index of each precinct, T_i is the area of the ith precinct and V_i is the number of voters in the ith precinct.

Each point contains the turnout level of its own precinct, in the form of the probability ($0 \leq p \leq 1$) of participation. By accurately placing all the points on the map, the election result of any part of the space can be determined from the sum of the probabilities of the points in that part of the space. In its present state, the result of this method does not differ in any way from an areal interpolation performed via the simple areal weighting method. However, by manipulating the number and placement of points, the interpolation method can be refined more easily and clearly.

The basic principle of dasymetric mapping method holds that the population is not evenly distributed in space, and therefore some ancillary information is needed to achieve a more accurate areal interpolation. As the precincts basically cover a small population (between 500 and 1500 voters), three problems emerged. First, the geometries of precincts do not necessarily cover only residential areas; the municipal governments are responsible for the creation of precincts and, they distribute into polling stations all addresses, regardless of whether they are residential or non-residential. To solve this problem, the areas of those census tracts with residential populations were used, as maintained by the Hungarian Central Statistical Office. These were refined based on the information from freely available orthophotos (geoshop.hu). Thus, only the areas of Budapest where voters live were considered. In this case the areas in any given precinct will not be contiguous, therefore the points belonging to the given precinct must be distributed area proportionally among the individual tracts (area proportional allocation) (**Fig. 1**) according to the following equation:

$$V_{ij} = \frac{T_{ij}}{T_i} * V_i \tag{2}$$

where T_{ij} is the area of the *j*th census tract in the *i*th precinct.

Thus, the distance defined in the first equation is no longer to be determined for each precinct, but instead for each census tract based on the following equation:

$$x_{ij} = \sqrt{\frac{T_{ij}}{V_{ij}}} \tag{3}$$

With this step the method is based on the number of voters in a census tract, which can be further refined with a procedure based on ancillary information.

Fig. 1. A sample of the geographical position of Budapest's precincts, census tracts and generated points.

The second problem is related to large housing estate buildings, because the statistical office's tracts of these areas are much larger than the buildings themselves, due to the large (green or parking) spaces surrounding them buildings (**Fig. 2**). Therefore, two precincts (from two different election years) with the same address list can be correctly defined with completely different boundaries, depending on to which precinct these free spaces are attached. To solve this, the tracts of large housing estates were deleted and instead the geometry of the large housing estate buildings from the 'buildings' layer of the OpenStreetMap database (GeoFabrik) were used. The geometry was cross-checked with ortophotos (obtained from www.fentrol.hu operated by the Lechner Knowledge Center) ensuring its precision and accuracy. The third problem is that there are precincts that include both single-standing family houses and large housing estate buildings. Whereas the population density of the two residential types is completely different, an area proportional allocation would place more points in the tract of family houses than can be occupied (and, in parallel, much fewer in tracts of large housing estates). However, due to the previous work on this issue (Szabó & Bene, 2019), there is a flat number attribute for each building. These were used as a weight to solve this problem. Thus, for these polygons, not their own area, but the number of flats multiplied by the average parcel size (approximately 1000 square meters) was considered in the area proportional allocation. Thus, the assumption is not be perfect, as the parcel of a family house does not have the same area everywhere, and the number of voters living in the large housing estates and the single-standing family house is not the same. Due to the above-mentioned issues this seems to be the best approximation to reality in the absence of further data (**Fig. 2**).

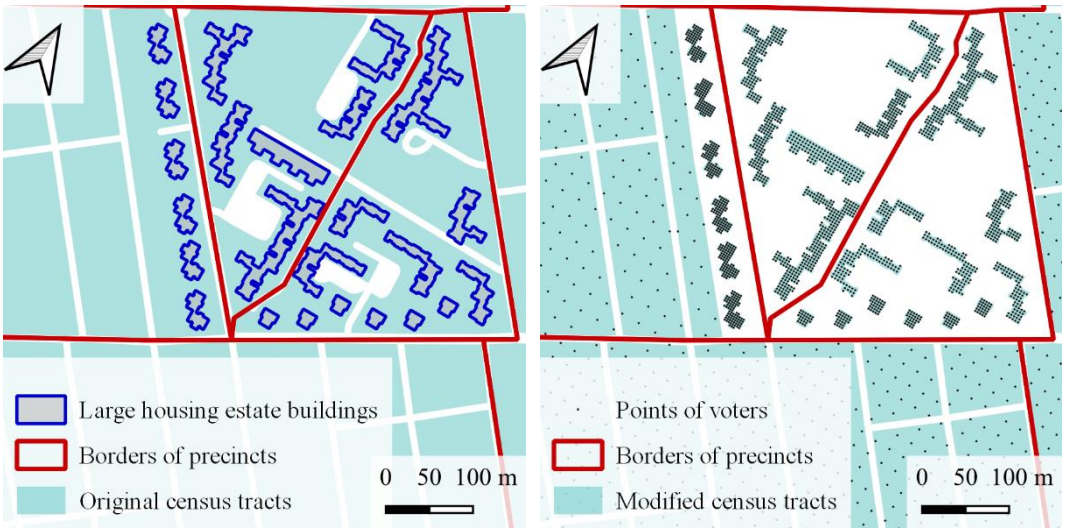

(**a**) (**b**)

Fig. 2. Illustration of the justification for the (a) use and (b) implementation of large housing estate buildings.

The final subdivision into which the precinct results of all parliamentary elections were aggregated was manually formed based on the latest (2018) precinct divisions. The guiding principle was to create consistent units by functional and built-in categories and to keep the variance of voter numbers in units as low as possible. There are 1100 units in the target subdivision, while the numbers for original (source) precincts were between 1410 and 1628. In the further part of the research, this division is used for statistical analysis of spatiality and temporal distribution of voter turnout in Budapest. However, before analyzing databases, estimates were checked. In the previous section, we discussed the limitations of measurement reliability. Taking these limitations into consideration, two different indicators were used. The RMSE is defined in the following equation:

$$RMSE = \sqrt{\frac{1}{n} * \sum_{i=1}^{n} \left(P_i - \hat{V}_i\right)^2} \tag{4}$$

The second indicator is mean absolute percentage error (MAPE), which can eliminate distortions arising from the different sizes of zones (Zhang & Qiu, 2011). The MAPE is defined in the following equation:

$$MAPE = \frac{\sum_{i=1}^{n} \frac{\left|P_i - \hat{V}_i\right|}{P_i}}{n} \tag{5}$$

where i is the index of each target unit, n is the number of target units, P_i is the actual ith target unit total population, and V_i is the estimated ith target unit voters.

After calculating the accuracy of the reaggreation, we examined the spatial structure of Budapest according to the temporal dynamics of voter turnout. On the one hand, the turnout level of the target units in each election year was compared to the average turnout level in Budapest of that year (relative turnout: $\Delta V_{ti} = V_{ti} - \overline{V_{ti}}$, where V is the voter turnout, t is the election year and i is the index of each target unit). This comparison alleviates the effects of the changes in turnout between elections. On the other hand, the target units were classified based on how voter turnout changed in them. For this, four different indicators were calculated for each unit, a standard deviation (σ), an arithmetic mean ($\overline{\Delta V}$), a correlation coefficient (R) and a slope of the regression line (a) (as shown in the **Fig. 3**). The first two do not need further explanation, they are only descriptive statistical indicators of the relative voter turnouts of each unit in different years. However, in the calculation of the latter two indicators, the relative turnouts in each unit were correlated with an increasing linear reference scale (1,2, … ,8 – a larger number means later elections), and the slope of this relationship was used. These indicators show the tendencies within the changes of relative voter turnout; if both the coefficient and the slope are positive and close to 1, the voter turnout within the spatial unit is constantly increasing since 1990.

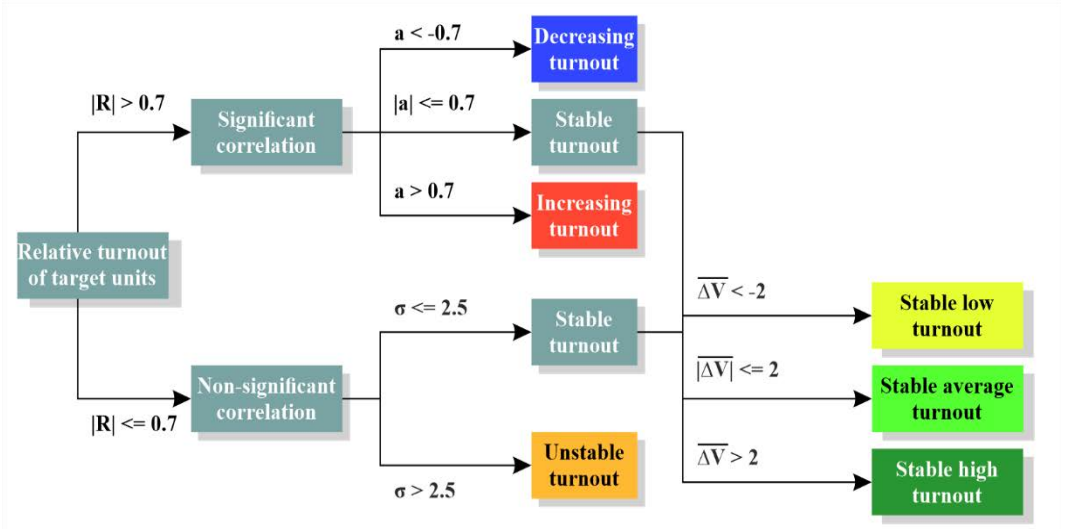

Fig. 3. Classification method of target subdivision by its relative voter turnout.

4. RESULTS

The results are divided into two parts, at first, we evaluated the methodology of database reaggregation, in which we measured the reliability of the developed areal interpolation method. The applied method was called area-based and dasymetric point allocation interpolation method. With the creation of the database, it is possible to analyse the voter turnout of Budapest longitudinally.

4.1. The evaluation of the area-based and dasymetric point allocation interpolation method

The accuracy of the database reaggregation methodology was measured by two metrics, RMSE and MAPE. The RMSE measures absolute error to the related distribution (which in this case is the distribution of the census closest to the election), while MAPE measures relative error. The rate of RMSE errors can be considered average, considering the values in the literature and the usability of the basic data used in the study. In Fisher and Langford's study (1996), 22 percent (mean: 4597), Kim and Yao (2010) have 12 percent (mean: 6156), Langford (2013) has 47 percent (mean: 308), Liu and Martinez (2019) have 11 percent (mean: 4192) the lowest RMSE error. In the latter a much higher error was achieved with lower resolution by the same method, which also shows that the percentage of RMSE error strongly depends on the average size of the target units.

Considering that we did not have a reference population for the census tracts for each election year, and that we calculated the total population and not the population of the voting age, the error can still be considered small (**Table 1**). The high values of 2014 and 2018 do not indicate the inaccuracy of the method, but simply that the election year is moving further and further away from the census and the transformation of the inner spatial structure of the city (e.g. the significant migration to Western countries, inner migration, population change caused by investments etc.) creates more and more discrepancies. However, it is important to highlight that voters with other permanent address (but voting in Budapest) may distort the results of the MAPE or RMSE. The number of these voters during the elections of 2014 and 2018 increased – although it contributes to the growth of the errors, it does not fully explain that.

Table 1.

Errors of area-based and dasymetric point allocation interpolation for each election.

	1990 (to 1990)	**1994 (to 1990)**	**1998 (to 2001)**	**2002 (to 2001)**	**2006 (to 2011)**	**2010 (to 2011)**	**2014 (to 2011)**	**2018 (to 2011)**
RMSE	304 (22.3%)	304 (22.6%)	317 (23.6%)	248 (19.8%)	313 (25.0%)	307 (24.8%)	333 (27.1%)	430 (35.8%)
MAPE	26.7%	24.6%	26.9%	27.6%	29.5%	27.3%	49.9%	76.5%

In the case of the MAPE error, the values are already higher than they appear in the literature, they still do not cross a threshold that would justify the inaccuracy of the method and the reaggregated database. In Deng and Wu's study (2013), 18.49 and 9.98 percent, Zhang and Qiu (2011) have 9.8 percent (mean: 5784) the lowest MAPE error. Although for the latter study, the RMSE error was a multiple of the value what we calculated (1639-2760). Based on these, it can be stated that the method used in the research estimated the proportion of voters in the target units with sufficient accuracy, the difference was not significantly large, and even shows better values in the case of RMSE errors. It is also necessary to validate the distribution of subsequent elections (2014 and 2018) with lower-level data from the 2021 census.

Based on the descriptive statistics of the developed database (**Table 2**), it can be stated that it meets the micro-scale criteria and largely retained the order of precinct-level. On the average, the units contain 1200-1300 voters, and the standard deviation does not exceed 650 in either case. This means that the 50 percent of the units are in the 580 to 2000 range. In addition, the median takes on a lower value than the average, so it is increased by only a few extreme values, so the unit with many voters in the database is not significant. However, units with few voters also skew MAPE values, so this may be the explanation for the higher MAPE values.

Table 2.

Descriptive statistics of the voter numbers of the database in each election results.

	1990	1994	1998	2002	2006	2010	2014	2018
Number of source zones	1504	1628	1626	1612	1598	1605	1483	1410
N	1100	1100	1100	1100	1100	1100	1100	1100
Minimum	0	6	5	87	89	111	71	44
Maximum	4614	4076	4083	4179	4196	4907	5071	5694
Mean	1363.2	1346.1	1345.7	1253.7	1253.6	1237.4	1229.7	1202.8
Median	1197	1181.5	1181.5	1099	1098.5	1066.5	1033	1025
Std.dev.	707.7	643.3	643.4	560.8	560.1	563.3	559.1	611.3

4.2. The spatiality of the voter turnout in Budapest

The spatial characteristics of temporal change of voter turnout in Budapest show a complex structure, which is related to several social processes (**Fig. 4 (b)**). The inner suburbs are characterized by steadily increasing voter turnout since 1990, these low-rise areas surrounded the city (except for the west) have growing population. In contrast, less units have declining voter turnout and they are scattered within the city in the downtown and the transition zone (the large area of former socialist industry between the city center and the inner suburbs mainly in the southern and the southeastern part). The explanation of declining turnout can be connected to the local conflicts such as the gentrification and studentification of sliding-down areas (Fabula *et al.*, 2017) or the rehabilitation of former industrial zones with significant population change. These latter areas are also characterized by unstable and stable low turnout levels, it suggests the mixed population of rapid transforming urban areas are politically less active than the traditional posh districts. The most affluent areas of the city can be characterized with the stable high voter turnout, they are the Buda villa district and similar areas of Pest side in Zugló.

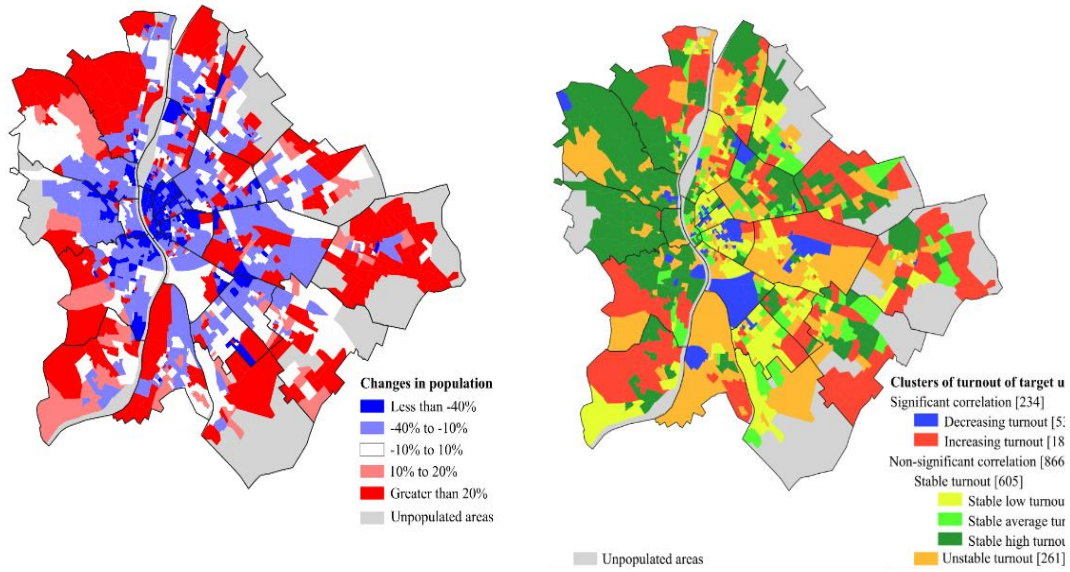

(**a**) (**b**)

Fig. 4. The spatial structure of population change between 1990 and 2018 (a) and voter turnout and its temporality (b) in Budapest.

5. CONCLUSIONS

The research had two interrelated contributions. On the one hand, the development of an areal interpolation method, which can be used to combine databases (for cross-analysis) that contain any kind of spatially aggregated and with a proportion of social subgroups but inconsistent with each other (Comber & Zeng, 2019). The area-based and dasymetric point allocation interpolation uses the principles of simple areal weighting and dasymetric mapping methods (Mennis, 2009), but simplifies them for a simple point allocation problem (Zhang & Qiu, 2011).

Based on this, the points represent the each individual (people in census, voter in elections), which contains the attributes characteristic of the given area unit in the form of the probability. In this way, the attribute data of any area can be deduced from the sum of the variables of the points falling on that part of the space. With this method, any of the above-mentioned databases (social data in a census tract or election data in a precinct, etc.) can be reaggregated using a population-adjusted allocation of points. For this, the polygons of census tracts and large housing estate buildings were used to specify the micro-level eligible voter numbers of the precincts.

On the other hand, micro-scale analysis of election results serves an appropriate indicator of socio-demographic processes of the rapid transformation inside a diverse metropolitan area (Charney & Malkinson, 2015). It has advantage in the inter-census periods, in the 30 years, there were only three censuses (the fourth will be on 2021), but eight parliamentary elections, these latter provides the opportunity for a sophisticated spatio-statistical analysis of a rapidly transforming city. To demonstrate this, the concept of spatiality of voter turnout was used. The spatial and temporal variation of voter turnout is an indicator of other social phenomena, such as local cohesion, trust in institutions (primarily the institution of elections) (Putnam, 1995), or the influence to the decision-making mechanism (Lijphart, 1997).

Our results showed that, there is higher voter turnout in areas with growing population (namely in inner suburbs), suggesting that not necessarily the former local population is more involved in political issues, but rather the new residents (in this case the young middle class). In contrast, the scattered voter turnout in the downtown areas connected to the socio-spatial characteristics of the micro-areas (e.g. local conflicts). In units with high social status, voter turnout is stable high, which (considering the previous statements) reproduces the existing social differences.

Future research could build on precinct-level party election results which can provide information on other aspects of social transformation. Moreover, analysis of social indicators in level of census tracts provides additional statistically significant and so far hidden relationships between social and political processes.

ACKNOWLEDGMENTS

This research was supported by the UNKP-20-3-SZTE-536 New National Excellence Program of the Ministry for Innovation and Technology from the source of the National Research, Development and Innovation Fund and the UNKP 20391-3/2018/FEKUSTRAT project of the Ministry of Human Capacities.

REFERENCES

Amos, B., McDonald, M.P. & Watkins, R. (2017) When Boundaries Collide. *Public Opinion Quarterly*. [Online] 81, 385–400. Available from: doi:10.1093/poq/nfx001.

Charney, I. & Malkinson, D. (2015) Between electoral and urban geography: Voting patterns and socio-spatial dynamics in Tel Aviv. *Applied Geography*. [Online] 58, 1–6. Available from: doi:10.1016/j.apgeog.2015.01.002.

Comber, A. & Zeng, W. (2019) Spatial interpolation using areal features: A review of methods and opportunities using new forms of data with coded illustrations. *Geography Compass*. [Online] 13 (10), e12465. Available from: doi:10.1111/gec3.12465.

Deng, C. & Wu, C. (2013) Improving Small-Area Population Estimation: An Integrated Geographic and Demographic Approach. *Annals of the Association of American Geographers*. [Online] 103 (5), 1123–1141. Available from: doi:10.1080/00045608.2013.770364.

Eicher, C.L. & Brewer, C.A. (2001) Dasymetric mapping and areal interpolation: Implementation and evaluation. *Cartography and Geographic Information Science*. [Online] 28 (2), 125–138. Available from: doi:10.1559/152304001782173727.

Fabula, S., Boros, L., Kovács, Z., Horváth, D., et al. (2017) Studentification, diversity and social cohesion in post-socialist Budapest. *Hungarian Geographical Bulletin*. [Online] 66 (2), 157–173. Available from: doi:10.15201/hungeobull.66.2.5.

Fisher, P.F. & Langford, M. (1996) Modeling sensitivity to accuracy in classified imagery: A study of areal interpolation by dasymetric mapping. *Professional Geographer*. [Online] 48 (3), 299–309. Available from: doi:10.1111/j.0033-0124.1996.00299.x.

Flowerdew, R. & Green, M. (1992) Developments in areal interpolation methods and GIS. *The Annals of Regional Science*. [Online] 26 (1), 67–78. Available from: doi:10.1007/BF01581481.

Goodchild, M.F., Anselin, L. & Deichmann, U. (1993) A framework for the areal interpolation of socioeconomic data. *Environment & Planning A*. [Online] 25 (3), 383–397. Available from: doi:10.1068/a250383.

Goodchild, M.F. & Lam, N.S.-N. (1980) Areal interpolation: a variant of the traditional spatial problem. *Geo-Processing*. 1 (3), 297–312.

Kim, H. & Yao, X. (2010) Pycnophylactic interpolation revisited: Integration with the dasymetric-mapping method. *International Journal of Remote Sensing*. [Online] 31 (21), 5657–5671. Available from: doi:10.1080/01431161.2010.496805.

Kostadinova, T. (2003) Voter turnout dynamics in post-Communist Europe. *European Journal of Political Research*. [Online] 42 (6), 741–759. Available from: doi:10.1111/1475-6765.00102.

Kovács, Z. & Vida, G. (2015) Geography of the new electoral system and changing voting patterns in Hungary. *Acta Geobalcanica*. [Online] 1 (2), 55–64. Available from: doi:10.18509/agb.2015.06.

Lam, N.S.-N. (2009) Spatial Interpolation. In: *International Encyclopedia of Human Geography*. [Online]. Elsevier. pp. 369–376. Available from: doi:10.1016/B978-008044910-4.00530-7.

Lam, N.S.-N. (1983) Spatial interpolation methods: A review. *American Cartographer*. [Online] 10 (2), 129–150. Available from: doi:10.1559/152304083783914958.

Langford, M. (2013) An evaluation of small area population estimation techniques using open access ancillary data. *Geographical Analysis*. [Online] 45 (3), 324–344. Available from: doi:10.1111/gean.12012.

Langford, M. (2006) Obtaining population estimates in non-census reporting zones: An evaluation of the 3-class dasymetric method. *Computers, Environment and Urban Systems*. [Online] 30 (2), 161–180. Available from: doi:10.1016/j.compenvurbsys.2004.07.001.

Langford, M., Maguire, D.J. & Unwin, D.J. (1991) The areal interpolation problem: estimating population using remote sensing in a GIS framework. In: Ian Masser & Michael Blakemore (eds.). *Handling Geographical Information: Methodology and Potential Applications*. London, Longman Pub Group. pp. 55–77.

Lijphart, A. (1997) Unequal Participation: Democracy's Unresolved Dilemma Presidential Address, American Political Science Association, 1996. *American Political Science Review*. [Online] 91 (1), 1–14. Available from: doi:10.2307/2952255.

Liu, X.H. & Martinez, A. (2019) Areal interpolation using parcel and census data in highly developed urban environments. *ISPRS International Journal of Geo-Information*. [Online] 8 (7), 302. Available from: doi:10.3390/ijgi8070302.

Mennis, J. (2009) Dasymetric Mapping for Estimating Population in Small Areas. *Geography Compass*. [Online] 3 (2), 727–745. Available from: doi:10.1111/j.1749-8198.2009.00220.x.

Mennis, J. (2003) Generating Surface Models of Population Using Dasymetric Mapping. *Professional Geographer*. [Online] 55 (1), 31–42. Available from: doi:10.1111/0033-0124.10042.

Michener, J.D. (2017) People, Places, Power: Medicaid Concentration and Local Political Participation. *Journal of Health Politics, Policy and Law*. [Online] 42 (5), 865–900. Available from: doi:10.1215/03616878-3940468.

Monteiro, J., Martins, B., Murrieta-Flores, P. & Moura Pires, J.M. (2019) Spatial Disaggregation of Historical Census Data Leveraging Multiple Sources of Ancillary Information. *ISPRS International Journal of Geo-Information*. [Online] 8 (8), 327. Available from: doi:10.3390/ijgi8080327.

Pavía, J.M. & Cantarino, I. (2017) Dasymetric distribution of votes in a dense city. *Applied Geography*. [Online] 86, 22–31. Available from: doi:10.1016/j.apgeog.2017.06.021.

Putnam, R.D. (1995) Bowling Alone: America's Declining Social Capital. *Journal of Democracy*. [Online] 6 (1), 65–78. Available from: doi:10.1353/jod.1995.0002.

Putnam, R.D. (2000) *Bowling Alone: The Collapse and Revival of American Community*. New York, Simon & Schuster.

Szabó, B. & Bene, M. (2019) Housing estates of Budapest before and after the renovation programmes (Budapesti lakótelepek a panelprogram előtt és után). *Területi Statisztika*. [Online] 59 (5), 526–554. Available from: doi:10.15196/TS590504.

Vida, G. (2016) Possibilities for measuring electoral geographical factors, that create unequal political representation (Az egyenlőtlen politikai reprezentációt létrehozó választási földrajzi hatótényezők mérési lehetőségei). *Területi Statisztika*. [Online] 56 (6), 643–659. Available from: doi:10.15196/TS560603.

Walford, N.S. & Hayles, K.N. (2012) Thirty Years of Geographical (In)consistency in the British Population Census: Steps towards the Harmonisation of Small-Area Census Geography. *Population, Space and Place*. [Online] 18 (3), 295–313. Available from: doi:10.1002/psp.658.

Wong, D.W.S. (2004) The Modifiable Areal Unit Problem (MAUP). In: *WorldMinds: Geographical Perspectives on 100 Problems*. [Online]. Dordrecht, Springer Netherlands. pp. 571–575. Available from: doi:10.1007/978-1-4020-2352-1_93.

Wright, J.K. (1936) A Method of Mapping Densities of Population: with Cape Cod as an Example. *Geographical Review*. 26 (1), 103–110.

Zhang, C. & Qiu, F. (2011) A Point-Based Intelligent approach to Areal interpolation. *The Professional Geographer*. [Online] 63 (2), 262–276. Available from: doi:10.1080/00330124.2010.547792.

Zoraghein, H., Leyk, S., Ruther, M. & Buttenfield, B.P. (2016) Exploiting temporal information in parcel data to refine small area population estimates. *Computers, Environment and Urban Systems*. [Online] 58, 19–28. Available from: doi:10.1016/j.compenvurbsys.2016.03.004.

PREDICTION OF THUNDERSTORM OCCURRENCES IN TROPICAL AREAS USING A NUMERICAL MODEL

***Wayan SUPARTA*[1], *Wahyu Sasongko PUTRO*[2], *T. Ken DARMASTONO*[3]**

DOI: 10.21163/GT_2021.161.07

ABSTRACT:
The prediction of thunderstorm activity is not only significant for weather forecasting but also for the standardization of risk assessment as in the aviation industry or emergency unit purposes. This paper aimed to develop a prediction of thunderstorm occurrences using a nonlinear model. For this work, the data used for a case study is one-year (1 January 2012 to 31 December 2012) located in a tropical area. The Jacobi algorithm has been employed to construct a prediction model with six combinations of input and one output (target). The predicted target is thunderstorm occurrence. The parameter input is surface pressure, air temperature, relative humidity, clouds, precipitable water vapor, and precipitation. The result obtained a better fit prediction model with four optimum parameters and estimation errors of 5.73%. May and October are the highest occurrences of thunderstorms where prediction errors were found high during the intermonsoon season.

***Keywords**: Numerical model development, Meteorological data, Thunderstorm prediction, Tropical areas*

1. INTRODUCTION

Thunderstorm activities in the atmosphere are of subject concern such as to air transportation business as well as security strategies. This phenomenon of thunderstorms can be categorized as the most dangerous natural disaster because it is one of the main causes of spacecraft being constrained in a launch (Kuk et al., 2012). Thunderstorms are an electrical storm where thunder and lightning are generated by cumulonimbus clouds during heavy rain and precipitation. Lightning is also possible at any stage of cumulonimbus development regardless of precipitation. Subsequently, when the cumulonimbus clouds occur and form a cluster, they develop into a thunderstorm ensemble with a high rainfall index of up to about 100 km or more in one last horizontal direction, and then they are defined as convective mesoscale systems (MCS) (Houze, 2018).

The MCS formed to an altitude of 8 ~ 14 km from small to long-lived with an average maximum area of 160×10^3 km^2 and can be active for up to 13 hours (e.g., Maddox, Rodgers, & Howard, 1982) are a major concern in aviation safety. Therefore, the prediction of thunderstorm occurrence over MCS areas is important to commercial space vehicle launch operation and power utilities. Various methods of estimating thunderstorms occurrence have been conducted by several researchers such as Velden et al. (2006) using Dvorak techniques, and Wilson et al. (1998) using mathematics modeling. Maddox (1980) has been identified the MCSs using early infrared satellite imagery. One of the limitations that appeared of this imagery is difficulty in distinguishing cumulonimbus clouds besides equivalently the occurrence of lightning at the same time. However, in recent years, geostationary satellite imagers, for example, Himawari-8 satellite operated by the Japan Meteorological Agency (JMA) has high-resolution to improve thunderstorm monitoring (Lee et al., 2019). On the other hand, a numerical weather prediction (NWP) system is one of the tools that statistically enhance

[1] *Institut Teknologi Nasional Yogyakarta, Department of Electrical Engineering , Jl. Babarsari, Depok, Sleman, Yogyakarta 55281, Indonesia, Corresponding author: wayan@itny.ac.id, drwaynesparta@gmail.com*
[2] *Golden Autotech Corp, Department of Research and Innovation, Sidoarjo 61254, East Java, Indonesia, wahyu@gautotech.com*
[3] *Sekolah Tinggi Teknologi Adisutjipto, Department of Informatics, Bantul, Yogyakarta 55198, Indonesia, tkendarmastono@stta.ac.id*

thunderstorm forecasts (Simon et al., 2018). This also showed a logistic regression (Gijben et al., 2017) or artificial neural networks (Collins and Tissot, 2015) are capable of accommodating nonlinear relationships between latent variables. Thus, Somesan and Makkai (2016), and Ahmed et al. (2019) studied the thunderstorm frequency distribution based on the analysis of convective available potential energy (CAPE) and convective inhibition (CIN) focused in Transylvania and over Pakistan, respectively. Although trends in CAPE do not explain the variability of thunderstorm over the whole study area explicitly, numerical models will be explored in-depth in this recent work for the prediction of thunderstorm occurrence.

The cold surge and its modification such as vortex formation in the equator region especially located over the Borneo region such as in Tawau, Malaysia is important due to the thunderstorm level are dangerous. The transition of the zonal circulation into maritime tropical circulation will generate synoptic processes (Furtuna, Haidu, & Maier, 2018). This is one of the motivations why Tawau located in the Borneo region near the sea waters is one option. Also, with limited funds for purchasing satellite imagery to improve rainfall data, the thunderstorm study in the Tawau area is carried out by numerical analysis. This study focused on exploring numerical modeling to predict thunderstorms. With high accuracy in predicting the occurrence of thunderstorms, this will facilitate future mitigation.

2. METHODS

2.1 Data and Location

For the case study, six input parameters such as Pressure (*P*), Temperature (*T*), Relative Humidity (*H*), Cloud (*C*), precipitation (*Pr*), and precipitable water vapor from Radiosonde (*RSPWV*) for one year period (1 January ~ 31 December 2012) measurement is employed to predict thunderstorm occurrence. *P*, *T*, and *H* are the basic weather parameters that fundamentally affecting daily life and environments, while precipitation and water vapor are the most significant hydrological parameter that controls water cycle variability in the atmosphere. The selection of these six parameters as input was meant to characterize which parameter is most fit for predicting the occurrence of thunderstorms in this area. The first four parameters (*P, T, H,* and *C*) were collected from the Malaysian Meteorological Department (MetMalaysia). RSPWV and Precipitation were taken from the University of Wyoming website (*http://weather.uwyo.edu/upperair/sounding.html*) and the NASA (Tropical Rainfall Measuring Mission, TRMM) website (*http://gdata1.sci.gsfc.nasa.gov*), respectively. Parameters for the input data are made daily because the thunderstorm occurrence based on observations is only available on a daily basis.

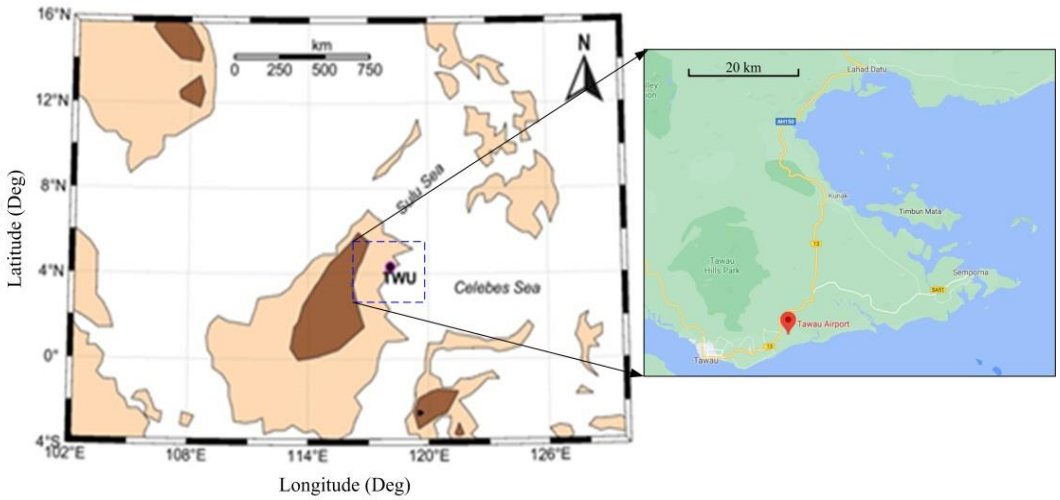

Fig. 1. The location of meteorological data at Tawau.

Figure 1 shows the location of the case study where the weather station is located in the Tawau airport (TWU: 4.32°N, 118.12°E with elevation 17 m) in Borneo Island. The location of the observation station is closed to the Celebes Sea. The climate conditions in this area are similar to other regions in the equatorial where precipitation throughout the year tends to heavy during November, December, and January. This area is probably experienced high precipitation along the Celebes Sea that has been affected by variations of land-ocean distribution and solar activities (Bian et al., 2015).

2.2 Data Processing

The surface meteorological data on a daily basis is processed. To filter and check the quality of the observation data used, the missing data in their time series is replaced by Not a Number (NaN). **Figure 2** shows the flowchart of data processing which applied six parameters for each season. The six combinations parameter is proposed to generate linear equations. Furthermore, the linear equation is transposed to a nonlinear equation using the Jacobi algorithm.

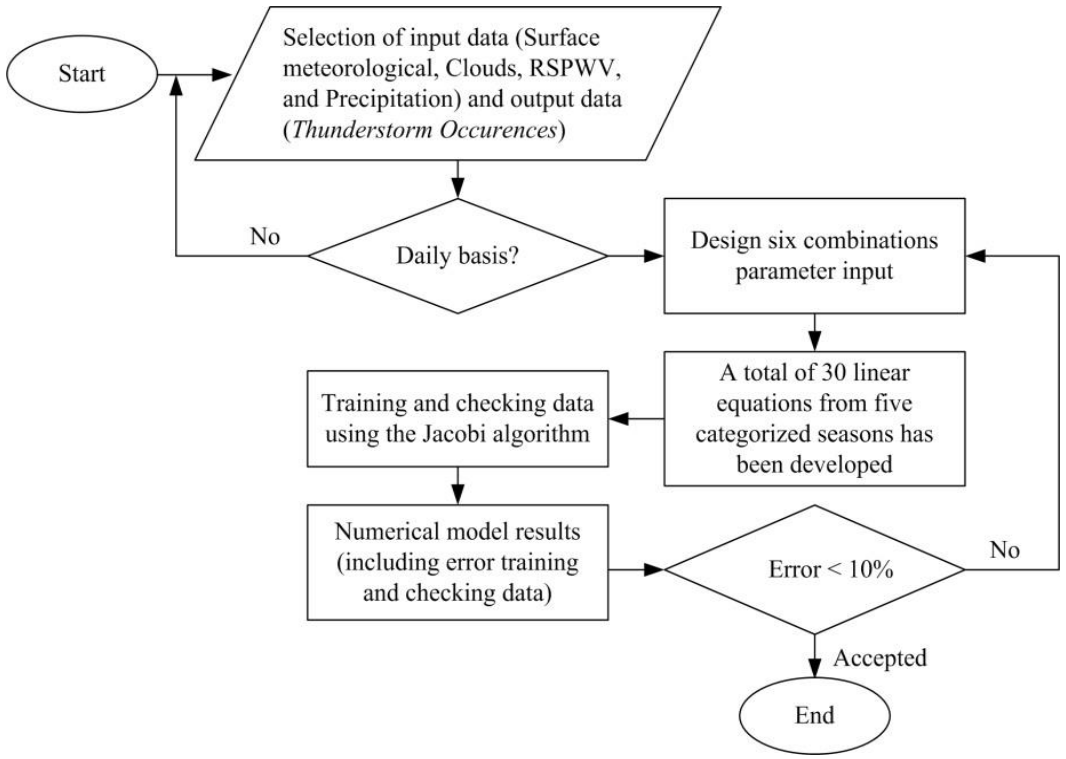

Fig. 2. Flowchart of data processing and identification.

Equatorial region has only two seasons (summer or dry and winter or wet), and another one is called intermonsoon. In this study, five seasons are defined as summer (JJA), winter I (JF), winter II (December), transition I (MAM), and transition II (SON) rather than only three seasons. This categorization is to minimize prediction errors because throughout the year there are incomplete daily data for certain parameters. On the other hand, if only 2 or 3 selected seasons for this case, the criteria defined for the thunderstorm occurrence do not match the data observations. From five categorized seasons and six combination parameters, we have 30 linear equations to be proposed to predict thunderstorms. To achieve a stable numerical model, 1,000 iterations are carried out. Validation is carried out in 20% of the raw data. When the error in the training and checking data is below 10% or very small, the designed model can be used to predict the occurrence of thunderstorms.

2.3 Linear Equations

The linear equation is a first order form and is very useful to model any phenomena based on mathematics method. In the general, linear equations can be written in the form of matrix in $n \times n$ size or $A\boldsymbol{x} = \boldsymbol{b}$ (Collins, 2003; Yang and Mittal, 2014). To solve the first until the n_{th} equations, the multiple linear regression can be formulated in general iteration scheme with the form

$$x_i^{(k)} = \frac{1}{a_{ii}}\left[b_i - \sum_{i \neq j}^{n} \left(a_{ij} x_j^{(k-1)} \right) \right] \tag{1}$$

The equation (1) can be solved by the Gauss-Seidel iteration methods. To improve the iteration rate after the value of x_i is obtained, we can write the iteration scheme as

$$x_i^{(k)} = \frac{1}{a_{ii}}\left[b_i - \sum_{j=1}^{i-1} \left(a_{ij} x_j^{(k)} \right) - \sum_{j=i+1}^{n} \left(a_{ij} x_j^{(k-1)} \right) \right], \qquad for\ i = 1,\ 2, 3, \ldots, n \tag{2}$$

The iteration in equation (2) can produce a faster convergence rate, but there may be problems in the stability of the convergence speed (Collins, 2003). To solve this drawback, the Jacobi iteration method is proposed.

2.4 Jacobi Algorithm

The Jacobi method or Jacobi iterative method can be described as an algorithm for determining solutions of a diagonally dominant system of linear equations (Yang and Mittal, 2014). The method is used for solving systems of multi-dimensional linear equations. If the linear equations in a matrix form split into A, it will obtain as follows.

$$A = \begin{bmatrix} a_{11} & 0 & \ldots & 0 \\ 0 & a_{22} & \ldots & 0 \\ \vdots & \vdots & \vdots & \vdots \\ 0 & 0 & \ldots & a_{nn} \end{bmatrix} - \begin{bmatrix} 0 & \ldots & 0 & 0 \\ -a_{22} & \ldots & 0 & 0 \\ \vdots & \vdots & \vdots & \vdots \\ -a_{n1} & \ldots & -a_{n,n-1} & 0 \end{bmatrix} - \begin{bmatrix} 0 & -a_{12} & \ldots & -a_{1n} \\ 0 & 0 & \ldots & \vdots \\ \vdots & \vdots & \vdots & -a_{n-1,n} \\ 0 & 0 & \ldots & 0 \end{bmatrix} = D - L - U \tag{3}$$

If $\boldsymbol{b} = (D - L - U)\,\boldsymbol{x}$ and D is transposed into D^{-1}, the solution of x from $A\boldsymbol{x} = \boldsymbol{b}$ is given by

$$x = D^{-1}(L + U)\,x + D^{-1} b \tag{4}$$

Equation (4) is a matrix form of Jacobi and in the iterative method, it can be expressed as

$$x^{(k)} = D^{-1}(L + U)\,x^{(k-1)} + D^{-1} b, \qquad for\ k = 1,\ 2, 3, \ldots \tag{5}$$

Assume that $T = D^{-1}(L + U)$ and $\boldsymbol{c} = D^{-1}\,\boldsymbol{b}$, Jacobi iteration method can also be written as

$$x^{(k)} = T\,x^{(k-1)} + c, \qquad k = 1, 2, 3, \ldots, \tag{6}$$

If the initialization initial value $x_n = 0$, the iteration will end if $x_n^{(k-1)} \approx x_n^k$. With n iterations, the predicted value obtained will be very stable, and therefore, this method is similar to the neural network algorithm.

3. RESULT AND DISCUSSION

3.1 Meteorological Variation

Figure 3 showed the variation of surface meteorology (*P, T* and *H*), Cloud (oktas), RSPWV, and precipitation for the period of 1 January 2012 ~ 31 December 2012 for a case study. The value of *P*, *T*, and *H* is reached ≥ 1010 mbar during April, reached ≥ 28°C during June, August and September, and reached ≥ 85% during January, February, and December, respectively. Furthermore, the extreme value of cloud density (oktas), RSPWV, and precipitation are reached ≥ 7 oktas in June and July, reached ≥ 80 mm in February and December, and reached ≥ 55 mm/day in May and October, respectively.

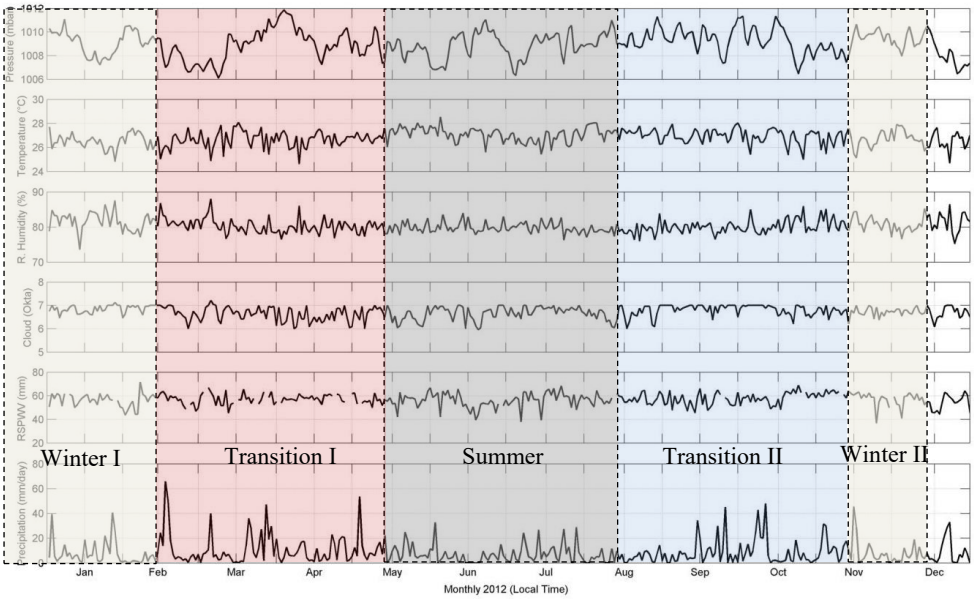

Fig. 3. The variation of meteorological parameters over the Tawau area. The shaded area represented the categorized seasons. The data used is from Suparta and Putro (2017).

As in **Figure 3**, a thunderstorm is probably undetectable if the surface pressure reached ≥ 1000 mbar with a temperature ≥ 27°C, the relative humidity value < 80% and cloud density is less than four oktas, although the RSPWV and precipitation occurred more than 40 mm and ≥ 30 mm/day, respectively. However, the precipitation is a minimum while the temperature is higher as marked by clear days in the summer season (JJA). On the other hand, the rainy days over the winter season occurred in January and February (winter I) and December (winter II), where the temperature has decreased while precipitation has increased.

3.2 Thunderstorm Prediction

Based on the meteorological data depicted in **Figure 3**, a set of linear equation can be generated from six combinations of input: (a) *P*, (b) *P* and *T*, (c) *P, T, H,* and *C*, (d). *P, T, H,* and *C*, (e) *P, T, H, C*, and *Pr,* and (f) *P, T, H, C*, *Pr*, and *RSPWV*. The output target (thunderstorm) is defined as C_7 while $C_1 \sim C_6$ are predictors represented *P, T, H, C*, *Pr*, and *RSPWV*, respectively. The first predictor selected is *P* with the assumption that the atmosphere in low pressure can develop a synoptic or mesoscale system.

Table 1 shows the Jacobi equation in the matrix form and the solution obtained. The first matrix with a single column (left side) is regression constants (intercept) before transformed to the Jacobi equation. The second matrix in the middle is the Jacobi equation where the first row is a linear

equation for configuration (*a*), while the second row is for configuration (*b*). The third row until the sixth row corresponds to the configuration (*c*) until configuration (*f*), respectively. The first to six columns in this matrix are regression coefficients for $x_1 \sim x_6$, respectively. The last a single matrix contained $x_1 \sim x_6$ is predictors. The Jacobi method can also be used to find the best iteration for the six parameter combinations. The maximum iteration for $x_1 \sim x_6$ is presented in five steps with six combinations for each season. To run the iteration, the Python software version 2.7 was used to obtain the prediction model. The best configuration is with a minimum value, both in iterations and the root mean square error (RMSE).

Table 1.

The Jacobi transformation equation for five categorized seasons in 2012

Season in 2012	The Jacobi Equation (in a matrix form)	Solution
Winter I (JF)	$\begin{bmatrix}-149.9\\-130.0\\-128.2\\-101.9\\-117.8\\-105.3\end{bmatrix} = \begin{bmatrix}-0.1484 & 0 & 0 & 0 & 0 & 0\\-0.1234 & -0.199 & 0 & 0 & 0 & 0\\-0.1229 & -0.177 & 0 & 0 & 0 & 0\\-0.0937 & -0.218 & -0.0133 & -0.356 & 0 & 0\\-0.1092 & -0.195 & -0.0119 & -0.450 & -0.0112 & 0\\-0.0969 & -0.163 & -0.0161 & -0.539 & -0.0122 & -0.0052\end{bmatrix} \begin{bmatrix}x_1\\x_2\\x_3\\x_4\\x_5\\x_6\end{bmatrix}$	$x_1 = 1010.11$ $x_2 = 26.86$ $x_3 = 74.05$ $x_4 = 6.69$ $x_5 = 6.57$ $x_6 = -105$ Error: [0 0 0 0 0 0]
Summer (JJA)	$\begin{bmatrix}28.2\\19.6\\9.0\\4.5\\3.7\\22.4\end{bmatrix} = \begin{bmatrix}0.0283 & 0 & 0 & 0 & 0 & 0\\0.0219 & -0.080 & 0 & 0 & 0 & 0\\0.0149 & -0.133 & 0.0342 & 0 & 0 & 0\\0.0109 & -0.013 & -0.120 & 0.0312 & 0 & 0\\0.0103 & -0.120 & 0.0321 & -0.059 & -0.0017 & 0\\0.0280 & -0.106 & -0.0197 & -0.150 & -0.0035 & -0.0140\end{bmatrix} \begin{bmatrix}x_1\\x_2\\x_3\\x_4\\x_5\\x_6\end{bmatrix}$	$x_1 = 996.47$, $x_2 = 28.53$, $x_3 = 76.70$, $x_4 = 7.36$, $x_5 = 139.12$, $x_6 = 44.25$ Error: [0.00000000e+00 0.00000000e+00 0.00000000e+00 0.00000000e+00 - 8.88178420e-16 0.00000000e+00]
Winter II (Dec)	$\begin{bmatrix}43.9\\38.3\\38.3\\39.3\\39.1\\49.7\end{bmatrix} = \begin{bmatrix}0.0438 & 0 & 0 & 0 & 0 & 0\\0.0399 & -0.063 & 0 & 0 & 0 & 0\\0.0369 & 0.011 & 0.0272 & 0 & 0 & 0\\0.0371 & 0.007 & 0.0265 & -0.020 & 0 & 0\\0.0370 & 0.001 & 0.0261 & 0.026 & -0.0030 & 0\\0.0463 & 0.051 & 0.0281 & -0.007 & -0.0050 & 0.0074\end{bmatrix} \begin{bmatrix}x_1\\x_2\\x_3\\x_4\\x_5\\x_6\end{bmatrix}$	$x_1 = 1002.28$ $x_2 = 26.84$ $x_3 = 77.96$ $x_4 = 6.93$ $x_5 = 75.37$ $x_6 = 5886.33$ Error: [0 0 0 0 0 0]
Transition I (MAM)	$\begin{bmatrix}-13.0\\-22.6\\-9.70\\-8.50\\-6.40\\-6.20\end{bmatrix} = \begin{bmatrix}-0.0125 & 0 & 0 & 0 & 0 & 0\\-0206 & -0.0541 & 0 & 0 & 0 & 0\\-0105 & -0.0151 & 0.0218 & 0 & 0 & 0\\-0099 & -0.0050 & 0.0200 & 0.064 & 0 & 0\\-0082 & 0.0050 & 0.0261 & 0.079 & -0.074 & 0\\-0081 & 0.0040 & 0.0271 & 0.084 & -0.0079 & -0.00105\end{bmatrix} \begin{bmatrix}x_1\\x_2\\x_3\\x_4\\x_5\\x_6\end{bmatrix}$	$x_1 = 1040$, $x_2 = 21.74$, $x_3 = 71.02$, $x_4 = 7.57$, $x_5 = 58.39$, $x_6 = -36.27$ Error: [0.00000000e+00 0.00000000e+00 0.00000000e+00 0.00000000e+00 0.00000000e+00 - 8.8817842e-16]
Transition II (SON)	$\begin{bmatrix}34.7\\36.9\\38.3\\39.8\\40.0\\13.0\end{bmatrix} = \begin{bmatrix}0.0438 & 0 & 0 & 0 & 0 & 0\\0.0308 & -0.197 & 0 & 0 & 0 & 0\\0.0310 & -0.216 & -0.0094 & 0 & 0 & 0\\-0.0370 & -0.162 & -0.0094 & 0.0464 & 0 & 0\\-0.0372 & -0.162 & 0.0094 & 0.4640 & -0.0015 & 0\\-0.0115 & -0.100 & -0.0054 & 0.0326 & -0.0034 & 0.0162\end{bmatrix} \begin{bmatrix}x_1\\x_2\\x_3\\x_4\\x_5\\x_6\end{bmatrix}$	$x_1 = 1023.60$, $x_2 = 27.27$, $x_3 = 72.03$, $x_4 = 6.83$, $x_5 = -31.47$, $x_6 = -1694.18$ Error: [0.00000000e+00 0.00000000e+00 7.10542736e-15 0.00000000e+00 0.00000000e+00 0.00000000e+00]

The optimum input value from six configuration equations for each categorized season found that X_5 (RSPWV) or X_6 (precipitation) or both are poor results as marked by gray. It is clear from the table that during Winter (DJF) and Transition (MAM and SON), the RSPWV and/or precipitation values are out-of-range. **Figure 3** can clarify that the minimum and maximum values of RSPWV and precipitation are 38 ~ 82 mm and 0 ~ 76 mm/day, respectively. Furthermore, these two parameters are not used to predict thunderstorms. Therefore, the meteorological parameter to be selected as input for predicting thunderstorm events are $x_1 \sim x_4$. In this model, clouds also play roles in the formation of the MCS, especially on the sea boundary during the late afternoon, where the cloud shield reaches its maximum size in the early morning until the next day.

Figure 4 shows the predicted thunderstorms for each season using the Jacobi method with four input parameters based on the five categorized seasons. The figure shows that the estimation model and the observational data are well corresponded. This can be seen in May and October which are the highest of the occurrence of thunderstorms where this month is categorized as the intermonsoon season. The correlation coefficient (r) obtained is 0.75, which is significant at the 95% confidence level. The RMSE obtained was 5.56% and the average percent error was around 44.94%. This moderate relationship appears to be affected by the low accuracy of predictions over the summer (JJA), and this opens up new options for other input combinations for future work. The estimation error was < 10% indicates that the model is acceptable for the prediction of thunderstorms.

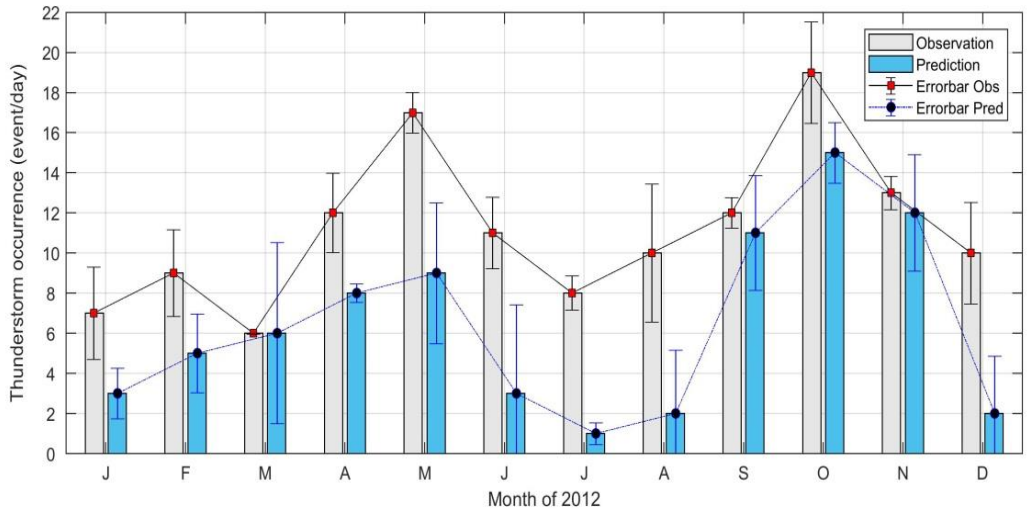

Fig. 4. The prediction of thunderstorm occurrence for each season using the Jacobi method and the standard deviation error. The data used is from Suparta and Putro (2017).

To predict thunderstorm occurrence in **Figure 4**, the rounding number technique was applied. For example, if its output reached ≤ 0.50 would mean that there is no thunderstorm event (rounded value = 0, or No), while the output with > 0.50 indicated that there is a thunderstorm event (rounded value = 1, or Yes). With satisfactory results obtained from configuration *(d)* with 776 iterations, now the performance of thunderstorm occurrence can be determined by using linear regression equation and expressed as

$$y(x) = 22.17 - 0.0197x_1 - 0.00954x_2 + 0.0055x_3 - 0.0099x_4 \quad (7)$$

where $y(x)$ is the prediction of thunderstorm occurrence. For example, if P (x_1) = 995 mbar, T (x_2) = 26°C, H (x_3) = 99%, and Clouds (x_4) = 5 oktas, then the prediction will be 0.6035 ≈ 1, which means that a thunderstorm event is occurred.

5. CONCLUSIONS

The prediction of thunderstorm occurrence was successful by using a numerical model from six parameter inputs such as Pressure, Temperature, Relative Humidity, Cloud, RSPWV, precipitation, and one parameter output of thunderstorm. The model generated using the Jacobi method was completely working in predicting the thunderstorm data.

In the process of predicting the occurrence of thunderstorms, as a case study, a regression equation from 2012 observation data in the Tawau area has been generated. There are five equations for each season, such as winter I, transition I, summer, transition II, and winter II, which are processed to find the best input parameter values for the prediction model. Furthermore, this equation is transformed into a nonlinear equation to find the optimum input parameter value using the Jacobi method. Of the six input parameters, RSPWV and precipitation are found out-of-range. The two peaks from March to May (winter to summer) are referred to as the transition I, and September to November (summer to winter) is called the transition II, which are overabundant thunderstorm events. With validation data of 20% (November and December), the estimation model is obtained with an error of 5.73%.

The numerical model with the Jacobi method is advantageous in constructing the prediction of thunderstorm occurrences. In this region, May and October pronounced the highest month of thunderstorm events. For future studies, the numerical model can be examined again with the combination of other inputs to achieve accurate and cost-effective thunderstorm predictions and employ different years of data for comparison. If too many input parameters are required, the model is high-cost. Estimation models that have been formulated only apply to local climates. Different climates and topography of the region will provide different weather parameters for input in predicting thunderstorms. Thus, examining the same parameters elsewhere is necessary, especially if this model can be compared in performance with other models such as soft computing techniques.

Acknowledgements

The author appreciates the support of previous research from the Ministry of Science, Technology, and Innovation (MOSTI) Malaysia under grant 01-01-02-SF1100. The first author was a former Associate Professor at Universiti Kebangsaan Malaysia. We would like to thank the Malaysian Meteorological Department (MetMalaysia) for providing the surface meteorological data, the NASA website for providing the precipitation data, and also the University of Wyoming for providing the Radiosonde PWV data. We appreciate the reviewer and editors comments that substantially improved the manuscript quality.

REFERENCES

Ahmed, R., Latif, M., Adnan, S., & Abusar, M. K. (2019) Thunderstorm frequency distribution and associated convective mechanisms over Pakistan. *Theor. Appl. Climatol*., 137, 755–773. https://doi.org/10.1007/s00704-018-2619-x.

Bian, Y., Li, J., Jian, Z., Chu, F., Chu, Z., Kuhnt. W., & Ye, L. (2015) Vegetation and climate changes around Celebes Sea during Holocene. *Journal of China University of Geosciences*, 40(5), 870-880, doi: 10.3799/dqkx.2015.071.

Collins, G. W. (2003) Fundamental numerical methods and data analysis. http://ads.harvard.edu/books/1990fnmd.book/ [Accessed 13 November 2020]

Collins, W. & Tissot, P. (2015) An artificial neural network model to predict thunderstorms within 400 km^2 South Texas domains. *Meteor. Appl*., 22, 650–665, doi:10.1002/met.1499.

Furtuna, P., Haidu, I., & Maier, N. (2018) Synoptic processes generating windthrows. a case study in the Apuseni Mountains (Romania). *Geographia Technica*, 13(2), 52-61, doi: 10.21163/GT_2018.132.04.

Gijben, M., Dyson, L. L., & Loots, M. T. (2017) A statistical scheme to forecast the daily lightning threat over southern Africa using the Unified Model. *Atmos. Res*., 194, 78–88, do:10.1016/j.atmosres.2017.04.022.

Houze, R. A. Jr. (2018) 100 years of research on mesoscale convective systems. *Meteor. Monogr*., 59, 17.1–17.54. https://doi.org/10.1175/AMSMONOGRAPHS-D-18-0001.1

Kuk, B., Lim, H., Ha, J., Lee, H., & Lee, G. (2012) A Fuzzy Logic Method for Lightning Prediction Using Thermodynamic and Kinematic Parameters from Radio Sounding Observations in South Korea. *Wea. Forecasting*, 27, 205–217.

Lee, K., Kim, H. S., & Choi, Y. S. (2019) Effects of high-resolution geostationary satellite imagery on the predictability of tropical thunderstorms over Southeast Asia. *Nat. Hazards Earth Syst. Sci*., 19, 2241–2248, 2019, doi://10.5194/nhess-19-2241-2019.

Maddox, R. A. (1980). Mesoscale convective complexes *Bull. Amer. Meteor. Soc*., 61, 1374–1387, doi: 10.1175/1520-0477(1980)061,1374:MCC.2.0.CO;2.

Maddox, R. A., Rodgers, D. M., & Howard, K. M. (1982) Mesoscale convective complexes over the United States in 1981: Annual summary. *Mon. Wea. Rev*., 110, 1501–1514.

Simon, T., Fabsic, P., Mayr, G. J., Umlauf, N., & Zeileis, A. (2018) Probabilistic forecasting of thunderstorms in the Eastern Alps. *Mon. Wea. Rev*., 146, 2999 - 3009, doi: 10.1175/MWR-D-17-0366.1.

Somesan, R. A. & Makkai, G. (2016) Medium and large hail in Transylvania, locality of band, 24th May 2015. *Geographia Technica*, 11(1), 84 – 91, doi: 10.21163/GT_2016.111.09.

Suparta, W. & Putro, W. S. (2017). Using multiple linear regression model to estimate thunderstorm activity. *IOP Conf. Series: Materials Science and Engineering*, 185, 012023, doi:10.1088/1757-899X/185/1/012023.

Velden, C., B. Harper, F. Wells, J. L. Beven II, R. Zehr, T. Olander, M. Mayfield, C. "Chip" Guard, M. Lander, R. Edson, L. Avila, A. Burton, M. Turk, A. Kikuchi, A. Christian, P. Caroff, P. Mccrone., (2006) The dvorak tropical cyclone intensity estimation technique a satellite-based method that has endured for over 30 years. *Am. Meteorol. Soc*., 87, 1195-1210.

Wilson, J. M., Crook, N. A., Mueller, C. K., Sun, J., & Dixon, M. (1998) Nowcasting thunderstorms: A status report. *B. Am. Meteorol. Soc*., 79, 2079–2099.

Yang, X. I. A. & Mittal, R. (2014) Acceleration of the Jacobi iterative method by factors exceeding 100 using scheduled relaxation. *J. Comput. Phys.*, 274, 695–708.

STAKEHOLDERS' SATISFACTION TOWARDS SUSTAINABLE TOURISM DEVELOPMENT IN PUSHKAR REGION OF RAJASTHAN

Shiv Kumar GUPTA[1], Sunil TIWARI[1] , Mihai VODA[2]

DOI: 10.21163/GT_2021.161.08

ABSTRACT:
This article aims at assessing satisfaction of different stakeholders (Hoteliers, Restaurants, Handicrafts Shopkeepers and Transporters) in Pushkar. Their satisfaction level is assessed with core indicators of sustainability. It is a quantitative as well as qualitative assessment based on survey research design in study area. Data was collected through 250 self-administered questionnaires which includes (40 Travel agents, 50 hoteliers, 50 Restaurants, 50 Handicrafts and Souvenir, 30 Foreign exchange agents and 30 transporters) and were analyzed by quantitative methods. Descriptive statistics (Frequencies, Percentages, Means, and Standard Deviations) and inferential statistics (t-test) was performed to assess and analyze stakeholders' satisfaction with reference to 11 core indicators of sustainability such as: Site protection, Stress, Use Intensity, Social Impact, Developing Control, Waste Management, Planning process, Critical ecosystems, Consumer satisfaction, Local Satisfaction, Tourism Contribution to Local Economy. The results of study suggest that stakeholders have different level of satisfaction with different core indicators but on core indicators like Developmental stress, Use intensity, Developing control, Waste Management and critical ecosystem, stakeholders have low level of satisfaction. In order to develop a destination in a responsible and sustainable manner, stakeholders must have very high level of satisfaction on each core indicator of sustainability.

Key-words: *Stakeholders Satisfaction, Sustainable tourism, Responsible tourism, Core Indicators.*

1. INTRODUCTION

Sustainable development is the center of focus since the Brutland report (WCED 1987), followed by the Earth summit in 1991 and United Nations World Tourism Organization set agenda for the 21st century for the sustainable growth and development of Tourism. Most important mile stone in the history of sustainable tourism development was year 2015 when seventeen Sustainable Development Goals (SDGs) were adopted by the United Nations. Now Tourism is an important global socio-economic activity which has an impact on economy, ecology and environment, on societies and culture both positive and negative in many ways. Sustainable tourism is an attempt to develop tourism in such a way that has positive impact on the environment, society, economy, local culture, local people and whatever related to tourism directly or indirectly. Pushkar, bordered by *Nag Pahar* (Snake Mountain), known as *the rose garden* of Rajasthan state of India represent a famous tourist destination for pilgrimage It has a unique cultural heritage which is valorized at the international Pushkar Fair. Tourism and Hospitality industry is very much affected through the perception and satisfaction of the various stakeholders who are directly and indirectly involve in the entire process of tourism at any destination. Stakeholders' perceptions are always considered in relation to expectations and compare with their satisfaction to ensure growth and development of sustainable tourism (Hardy 2005; Alazaizeh et al. 2019).

Sustainability includes all essentials that constitute a complete tourism experience. According to the majority of contributors (Voda et al. 2019; Sharpley 2000; Butler 1991; Vellas and Becherel

[1]*HNBG University, Srinagar Garhwal, Uttarakhand, India, sk_gupta21@yahoo.com, tiwari.sunil10@outlook.com*
[2]*Dimitrie Cantemir University, Targu Mures, Romania, mihaivoda@cantemir.ro*

1999; WCED 1987) 'sustainable tourism development' aims at economic, social and environmental tourism development that concerns to the continuous improvement of tourists' experiences. The tourism industry has great potential to achieve sustainable development goals. The determination of sustainable tourism is to create a balance between environment protection, preserving cultural integrity, creating social justice and promoting economic benefits, meeting the needs of the local community in terms of improved living standards both in the short and long term in both developed and emerging nations (Swarbrooke and Horner 2004; Mitchell and Hall 2005).

Sustainable development has been discussed extensively in tourism sector as it can meet up needs of tourists, service providers, locals and whosoever being associated with this sector (Eagles et al. 2002). Thus, it has become important to develop a destination under core indicators of sustainability (Sebele 2010; Taylor 1995). Various studies have been conducted on different aspects of sustainability such as cultural, social and environmental impacts, perceived economy and perceived benefits (Choi and Murray 2010; Dyer et al. 2007; Ko and Stewart 2002; Nunkoo and Ramkissoon 2011; Oviedo-García et al. 2008; Yoon et al. 2001). Studies have also found that stakeholders' satisfaction level play a significant role in view of sustainable tourism development at any destination (Gursoy et al. 2002; Gursoy and Kendall 2006; Gursoy and Rutherford 2004; Kaltenborn et al. 2008; Nicholas et al. 2009). A wide variety of factors, including social, cultural and economic considerations at each level of the tourism system, affects the implementation of sustainable tourism practices. A few studies on sustainable tourism and ecotourism related to the Garhwal region have been undertaken by Gupta and Bhatt, (2009, 2012); Gupta and Rout (2016, 2017 and 2019). However, a few studies have been conducted on stakeholders' satisfaction towards sustainable tourism development at Pushkar region of Rajasthan India. In order to fill this research gap, this study aims to measure the satisfaction of different stakeholders towards tourism development under core indicators of sustainability.

2. STUDY AREA

Pushkar is located northwesty from Ajmer in central east part of Indian state of Rajasthan on western side of Aravalli Mountains. Bordered by *Nag Pahar* range, it lies between North latitude 26°29'23" and East longitude 74°33'3" and sprawl around 10 kilometers (see **Fig. 1**).

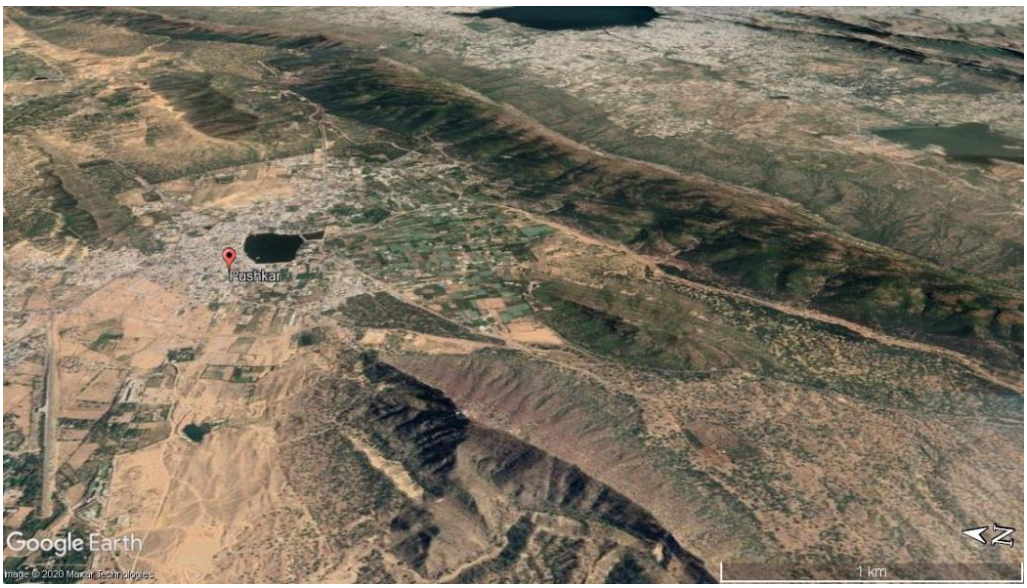

Fig. 1. Location of Pushkar study area of Rajasthan, India.

It is an important Centre of pilgrimage for Hindus. The place has a magnetic appeal with 400 temples that are blue white and a number of Bathing Ghats. The town resounds with chanting of prayers and religious songs, along with drums and gongs. Pushkar is a lively tourist attraction where tourists are flocking from the world over. There is a dash of commercialism but the town retains its mystique and traditional charm. Pushkar is the well-known tourist destination across the India and Globe as it hosting international fair every year. In the year 2019 out of total 1192345 number of tourists, 423234 tourists visited during Pushkar fair only.

3. DATA AND METHODS

In view of assessment and evaluation various stakeholders' satisfaction towards core indicators of sustainability, following research objectives and hypotheses are formulated;

1. To assess and evaluate satisfaction level of stakeholders' towards tourism development in the Pushkar region under all the core indicators of sustainability.
2. To measure the satisfaction level of stakeholders' towards tourism development in the Pushkar region under each core indicator of sustainability.

H01: There is no significant difference between stakeholders' satisfaction and tourism development in the study area under all core indicators of sustainability.

H2: There is significant difference between stakeholders' satisfaction and tourism development in the study area under each core indicator of sustainability.

On the basis of review of literature pertaining to sustainable tourism development, a survey questionnaire was developed on Stakeholders' satisfaction measurement scale (SSMS). Eleven core indicators of sustainability i.e. Site protection, Stress, Use Intensity, Social Impact, Developing Control, Waste Management, Planning process, Critical ecosystems, Consumer satisfaction, Local Satisfaction and Tourism Contribution to Local Economy were included in this questionnaire.

Data was collected from 250 stakeholders which includes (40 Travel agents, 50 hoteliers, 50 Restaurants, 50 Handicrafts and Souvenir, 30 Foreign exchange agents and 30 transporters) self-administered questionnaires by using stratified random sampling technique and five point Likert Scale. Reliability, normality and validity of the data and tool was also checked by examining the Cronbach's alpha, percentage of missing data, mean, standard deviation, item discrimination, skewness and kurtosis. Furthermore, collected data has been analyzed with the help of descriptive statistics; Central tendency (Mean), Z-score, frequency distribution, percentile, Norms, Standard deviation (SD), whereas in Inferential statistics; One sample t-test was computed.

4. RESULTS

To assess and evaluate satisfaction level of stakeholders towards tourism development in the Pushkar region under all the core indicators of sustainability, one sample t- test and Gap analysis was conducted to know the mean difference between stakeholders' overall satisfaction and tourism development in the study area and results are computed in **Table 1.**

Table 1 shows that the sample mean of stakeholders' satisfaction towards tourism development is 34.42, value of hypothesize mean is 55 (test value) and mean difference between them is 20.576, Values of S.D. and t-ratio are 2.144 and 151.711 respectively. Whether mean difference is significant or not with the help of degree of freedom (248) is further confirmed by the p value. Here p value is 0.000 ($p=0.000<0.01$) which is less than 0.01. There is a significant mean difference between sample and hypothesize mean of stakeholder satisfaction towards tourism development, therefore null hypothesis **H01** is **rejected** at 0.01 level of significance and there is significant difference between stakeholders' satisfaction and tourism development in the study area under all core indicators of sustainability.

Further, with the help of graphical presentation it is understood that sample mean of total stakeholders' satisfaction is lying below the level of satisfaction on tourism development under core indicators of sustainability as per the **Table 2**.

Table 1.
Results of One Sample t – test for Satisfaction of all Stakeholders on Tourism Development under Core Indicators of Sustainability

Variable	N	Hypothesize Mean	Mean	S.D	Mean Difference	t-ratio	p-value
Total Stakeholders' Overall Satisfaction	250	55	34.42	2.144	20.576	151.711	0.000**

** Significant at 0.01 level

Source: Primary Data

Table 2.
Level of Satisfaction on Tourism Development under Core Indicators of Sustainability

Mean Scores	Level of Satisfaction on tourism development under core indicators of sustainability
1-11	Very Low
11-22	Low
22-33	Average
33-44	High
44-55	Very High

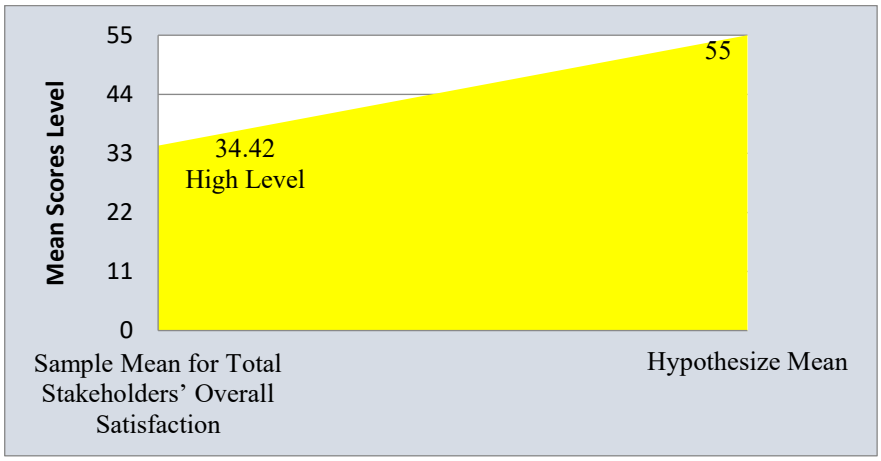

Fig. 2. Area graph of level of total stakeholders' satisfaction on Tourism Development under Core Indicators of Sustainability.

Figure 2 shows that Total stakeholders collectively have high level of satisfaction towards Tourism development under all core indicators of sustainability as sample mean (34.42) falls under high level of satisfaction category (33-44). To measure the satisfaction level of stakeholders towards tourism development in the Pushkar region under each core indicator of sustainability, One sample t- test and Gap analysis was conducted to know the mean difference between stakeholders' satisfaction towards each core indicator of sustainability such as Site protection, Stress, Use Intensity, Social Impact, Developing Control, Waste Management, Planning process, Critical ecosystems, Consumer satisfaction, Local Satisfaction and Tourism Contribution to Local Economy. It is observed that Stakeholders have different level of satisfaction with different core indicators and results are computed in **Table 3**.

Table 3.

Results of One sample t – test for Satisfaction of all stakeholders on Tourism Development under each Core Indicator of Sustainability

Core Indicators of Sustainability	N	Hypothesize Mean	Mean	S.D	Mean Difference	t-ratio	p-value
CI-1	250	5	4.48	0.582	0.520	14.122	0.000**
CI -2	250	5	1.67	0.572	3.332	92.118	0.000**
CI-3	250	5	1.58	0.494	3.416	109.361	0.000**
CI-4	250	5	4.02	0.909	0.976	16.972	0.000**
CI-5	250	5	1.62	0.617	3.380	86.567	0.000**
CI-6	250	5	1.80	0.766	3.200	66.076	0.000**
CI-7	250	5	4.20	0.739	0.800	17.116	0.000**
CI-8	250	5	1.76	0.621	3.244	82.557	0.000**
CI-9	250	5	4.39	0.626	0.608	15.356	0.000**
CI-10	250	5	4.43	0.592	0.568	15.164	0.000**
CI-11	250	5	4.48	0.589	0.524	14.069	0.000**

** Significant at 0.01 level Source: Primary Data

For First Core indicator of Sustainability (CI-1 **Site protection) Table 3** shows the sample mean of total stakeholders' satisfaction is 4.48 and value of hypothesize mean is 5 (test value) and mean difference of 0.520 between them and values of S.D., t-ratio, and p value are 0.582, 14.122 and 0.000 respectively. Hence, p value 0.000 ($p=0.000 < 0.01$) which is less than 0.01 indicates significant mean difference between sample and hypothesize mean of total stakeholders' satisfaction towards first Core indicator of sustainability (CI-1 **Site protection).**

For second Core indicator of Sustainability (**CI-2 Stress) Table 3** shows the sample mean of total stakeholders satisfaction is 1.67 and value of hypothesize mean is 5 (test value) and mean difference of 3.332 between them and values of S.D., t-ratio, and p value are 0.572, 92.118 and 0.000 respectively. Hence, p value 0.000 ($p=0.000 < 0.01$) which is less than 0.01 shows significant mean difference between sample and hypothesize mean of total stakeholders' satisfaction towards 2nd Core indicator of sustainability **(CI-2 Stress).**

For third Core indicator of Sustainability (**CI-3 Use Intensity) Table 3** shows the sample mean of total stakeholders satisfaction is 1.58 and value of hypothesize mean is 5 (test value) and mean difference of 3.416 between them and values of S.D., t-ratio, and p value are 0.494, 109.361 and 0.000 respectively. Hence, p value 0.000 ($p=0.000 < 0.01$) which is less than 0.01 specifies significant mean difference between sample and hypothesize mean of total stakeholders' satisfaction towards 3rd Core indicator of sustainability (**CI-3 Use Intensity.**

For forth Core indicator of Sustainability (**CI-4 Social Impact) Table 3** shows the sample mean of total stakeholders satisfaction is 4.02 and value of hypothesize mean is 5 (test value) and mean difference of 0.976 between them and values of S.D., t-ratio, and p value are 0.909, 16.972 and 0.000 respectively. Hence, p value 0.000 ($p=0.000 < 0.01$) which is less than 0.01 indicates significant mean difference between sample and hypothesize mean of total stakeholders' satisfaction towards 4th Core indicator of sustainability (**CI-4 Social Impact).**

For fifth Core indicator of sustainability (**CI-5 Developing Control) Table 3** shows the sample mean of total stakeholders' satisfaction is 1.62 and value of hypothesize mean is 5 (test value) and mean difference of 3.380 between them and values of S.D., t-ratio, and p value are 0.617, 86.567 and 0.000 respectively. Hence, p value 0.000 ($p=0.000 < 0.01$) which is less than 0.01 shows significant mean difference between sample and hypothesize mean of total stakeholders' satisfaction towards 5th Core indicator of sustainability (**CI-5 Developing Control).**

For sixth Core indicator of sustainability (**CI-6 Waste Management) Table 3** shows the sample mean of total stake holders' satisfaction is 1.80 and value of hypothesize mean is 5 (test value) and

mean difference of 3.200 between them and values of S.D., t-ratio, and p value are 0.766, 66.076 and 0.000 respectively. Hence, p value 0.000 (p=0.000 < 0.01) which is less than 0.01 indicates significant mean difference between sample and hypothesize mean of total stakeholders' satisfaction towards 6th Core indicator of sustainability (**CI-6 Waste Management).**

For seventh Core indicator of tourism development (**CI-7 Planning process) Table 3** shows the sample mean of total stakeholders satisfaction is 4.20 and value of hypothesize mean is 5 (test value) and mean difference of 0.800 between them and values of S.D., t-ratio, and p value are 0.739, 17.116 and 0.000 respectively. Hence, p value 0.000 (p=0.000 < 0.01) which is less than 0.01 shows significant mean difference between sample and hypothesize mean of total stakeholders' satisfaction towards 7th Core indicator of sustainability (**CI-7 Planning process).**

For eighth Core indicator of sustainability (**CI-8 Critical ecosystems) Table 3** shows the sample mean of total stakeholders' satisfaction is 1.76 and value of hypothesize mean is 5 (test value) and mean difference of 3.244 between them and values of S.D., t-ratio, and p value are 0.621, 82.557 and 0.000 respectively. Hence, p value 0.000 (p=0.000 < 0.01) which is less than 0.01 shows a significant mean difference between sample and hypothesize mean of total stakeholders' satisfaction towards 8th Core indicator of sustainability (**CI-8 Critical ecosystems).**

For ninth Core indicator of sustainability (**CI-9 Consumer satisfaction) Table 3** shows the sample mean of total stakeholders' satisfaction is 4.39 and value of hypothesize mean is 5 (test value) and mean difference of 0.608 between them and values of S.D., t-ratio, and p value are 0.626, 15.356 and 0.000 respectively. Hence, p value 0.000 (p=0.000 < 0.01) which is less than 0.01 shows a significant mean difference between sample and hypothesize mean of total stakeholders' satisfaction towards 9th Core indicator of sustainability (**CI-9 Consumer satisfaction).**

For tenth Core indicator of sustainability (**CI-10 Local Satisfaction) Table 3** shows the sample mean of total stakeholders' satisfaction is 4.43 and value of hypothesize mean is 5 (test value) and mean difference of 0.568 between them and values of S.D., t-ratio, and p value are 0.592, 15.164 and 0.000 respectively. Hence, p value 0.000 (p=0.000 < 0.01) which is less than 0.01 shows a significant mean difference between sample and hypothesize mean of total stakeholders' satisfaction towards 10th core indicator of sustainability (**CI-10 Local Satisfaction).**

For eleventh Core indicator of sustainability (**CI-11 Tourism Contribution to Local Economy) Table 3** shows the sample mean of total stakeholders' satisfaction is 4.48 and value of hypothesize mean is 5 (test value) and mean difference of 0.524 between them and values of S.D., t-ratio, and p value are 0.589, 14.069 and 0.000 respectively. Hence, p value 0.000 (p=0.000 < 0.01) which is less than 0.01 shows a significant mean difference between sample and hypothesize mean of total stakeholders' satisfaction towards 11th Core indicator of sustainability (**CI-11 Tourism Contribution to Local Economy).**

5. DISCUSSION

Based on the above findings it is concluded that hypothesis **H2 "**There is significant difference between stakeholders' satisfaction and tourism development in the study area under each core indicator of sustainability has been **Accepted** and its corresponding objective "To measure the satisfaction level of stakeholders' towards tourism development in the Pushkar region under each core indicator of sustainability was **achieved.** Further, with the help of graphical presentation it is understood that sample mean of total stakeholders' satisfaction is lying below the level of satisfaction on tourism development under each core indicator of sustainability as per **Table 4.**

Table 4.

Mean score and Level of Satisfaction under each core indicator of sustainability.

Mean scores	Level of Satisfaction
1 to 2	Low satisfaction
2 to 3	Moderate Satisfaction
3 to 4	High Satisfaction
4 to 5	Very high satisfaction

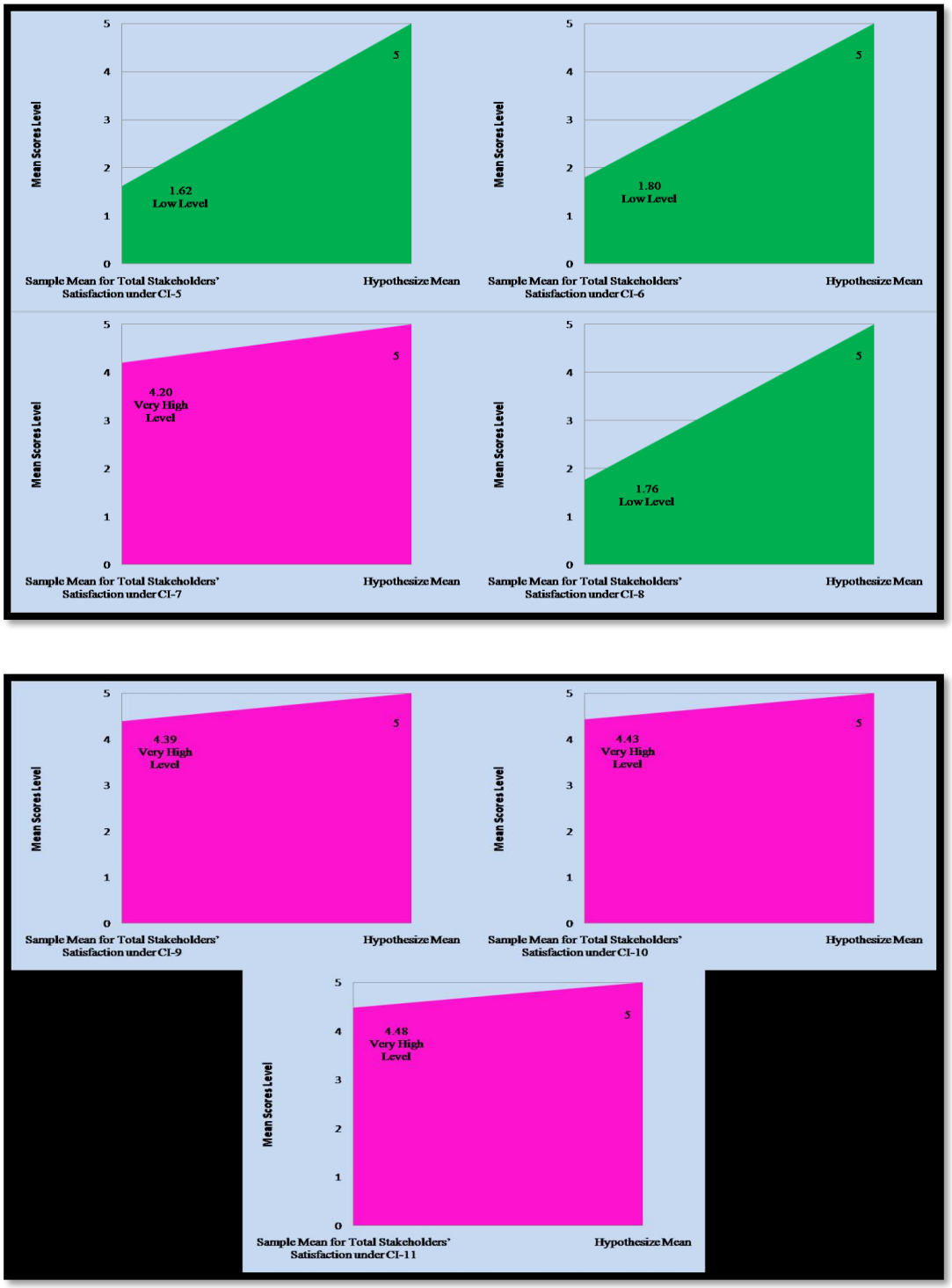

Fig. 3. Area graph of level of total stakeholders' satisfaction category on tourism development under each core indicator of sustainability.

From the **Figure 3** it is clear that stakeholders have very high satisfaction on core indicators.

As hypothesize mean is more than sample mean in reference to satisfaction of total stakeholders towards tourism development in the Pushkar under core indicators of sustainability and mean difference is significant, it is concluded that total stakeholders had high level satisfaction towards tourism development. Total stakeholders altogether have very high level of satisfaction with core indicator 1 (site protection), CI-4 (Social Impacts), CI-7 (Planning process), CI-9 (Consumer satisfaction), CI-10 (Local satisfaction), CI-11(Tourism contribution to local economy) whereas they have low level of satisfaction with CI-2 (Stress), CI-3 (Use intensity), CI-5 (Developing control), CI-6 (Waste management) and CI-8 (critical ecosystem). But transporters have highest level of satisfaction followed by foreign exchange units, hoteliers, handicrafts units, travel agents and Restaurants units towards tourism development in the study area in term of sustainability.

Findings suggest that stakeholders have reasonably satisfied towards tourism development in the Pushkar under core indicators of sustainability. But it is recommended that tourism must be developed in more sustainable way under core indicators of sustainability and should ensure very high level of satisfaction of the stakeholders. Tourism planners and policy makers should focus on minimizing development Stress, maximize the uses of local products and services, ensure carrying capacity, Developmental control, proper waste management and healthy and peaceful ecosystem. On these core indicators stakeholders have low satisfaction. Further efforts should be taken to minimize the leakage and allow equitable distribution of tourism products and resources among the various stakeholders i.e. Foreign exchange agents, Hoteliers, handicrafts units, travel agents, foreign exchange units and Restaurants.

6. CONCLUSIONS

Pushkar is one of the most visited and well-known tourist destinations across India and World, where tourists keep flocking throughout the year. It also hosts International Cattle festival annually which itself attracts lakhs of tourists. Due to sudden outbreak of COVID-19 pandemic the entire tourism business of the region got affected severely. Pushkar has complete shut down since March 2020 and no tourist was allowed inside the city. All the hotels, home stays, restaurants, travel agent units, foreign exchange units, handicraft and souvenir shops, transport units, meditation Centre's and other travel related outlets was closed till July and further restricted movements of Domestic and local tourists were initiated. Lots of Local residents of Pushkar are dependent on the tourism sector. The COVID -19 pandemic has caused massive disruptions in economy, health, developmental activity, employment, sustainability and foreign exchange of the region. This pandemic has some positive impacts on Pushkar as destination such as natural cleaning of Holi Pushkar lake, control of air pollution, better waste management, speedy completion of the construction work of Ghats, sewage treatment, temples and roads, up gradation of environment and ecological balance. Big challenges lie before the local administration, tourism board, different stakeholders, visitors and local communities to organize International Pushkar Fair which is scheduled from 22nd to 30th November 2020. Amidst of COVID-19 pandemic Rajasthan and Pushkar Tourism Boards are working hard and ensuring utmost preparedness towards Sustainable Tourism Development and successfully organization of the Pushkar fair.

For sustainable development the negative impacts of tourism at the study area like demonstration effects, cultural conflicts, spiritual frauds, ethnocentrism, westernization and uncivil practices are to be reduced. Pushkar is well known tourist destination across the world because of its magnificent international camel festival but unfortunately over the years loss of its traditional character and undue commercialization is a great sense of concern .Hence the all organizers like Rajasthan Tourism Board; Ministry of Tourism, Government of India, Pushkar Tourism Board and Various other Local Authorities and Destination Management Organizations have play a pivotal role to maintain the traditional ethnicity of the fair. It is observed that the participation of cattle owners is gradually decreasing year by year. Simultaneously carrying capacity of the destination would also be maintained especially at the time of Pushkar fair.

REFERENCES

Alazaizeh, M.M., Ababneh, A., Jamaliah, M.M. (2019) Preservation vs. use: understanding tourism stakeholders' value perceptions toward Petra Archaeological Park. *Journal of Tourism and Cultural Change,* 1–15. doi:10.1080/14766825.2019.1628243

Butler, J.K. (1991) Toward Understanding and Measuring Conditions of Trust: Evolution of a Conditions of Trust Inventory, *Journal of Management*, *17*(3), 643–663.

Choi, H.C., Murray, I. (2010) Resident attitudes toward sustainable community tourism, *Journal of Sustainable Tourism*, 18(4), 575-594.

Dyer, P., Gursoy, D., Sharma, B., Carter, J. (2007) Structural modeling of resident perceptions of tourism and associated development on the Sunshine Coast, Australia, *Tourism Management*, 28, 409-422.

Eagles, P.F.J., McCool, S.F., Haynes, C.F. (2002*) Sustainable tourism in protected areas: Guidelines for planning and management. Gland, Switzerland: International Union for the Conservation of Nature.*

Gupta, S.K., Rout, C.P. (2016) The Value Chain Approach in Community Based Ecotourism: A Conceptual Framework on Sustainable Mountain Development in The Jaunsar-Bawar Region of Uttarakhand, *Amity Research Journal of Tourism, Aviation and Hospitality*,pp. 24-32, vol. 1, no. 1, January-June 2016.

Gupta, S.K., Rout Prakash Chandra, Tyagi, Pankaj (2019) Community Based Tourism Development amid Complex Mountain Issues: A Strategic Analysis of Chakrata Region of Uttarakhand, *International Journal of Hospitality and Tourism Systems* Pp.47-55, Volume 12.Issue No.1 ,June, 2019, by Publishing India Group, New Delhi.

Gursoy, D., Kendall, K.W. (2006) Hosting mega events - Modeling locals' support, *Annals of Tourism Research*, 33(3), 603-623.

Gursoy, D., Rutherford, D.G. (2004) Host attitudes toward tourism - an improved structural model, *Annals of Tourism Research*, 31(3), 495-516.

Gursoy, D., Jurowski, C., Uysal, M. (2002) Resident Attitudes- a structural modeling approach, *Annals of Tourism Research*, 29(1), 79-105.

Hardy, A. (2005) Using Grounded Theory to Explore Stakeholder Perceptions of Tourism*, Journal of Tourism and Cultural Change,* 3(2), 108–133.

Kaltenborn, B.P., Andersen, O., Nellemann, C., Bjerke, T., Thrane, C. (2008) Resident attitudes towards mountain second-home tourism development in Norway - the effects of environmental attitudes, *Journal of Sustainable Tourism*, 16(6), 664 - 680.

Ko, D.W., Stewart, W.P. (2002) A structural equation model of residents' attitudes for tourism development, *Tourism Management*, 23(5), 521 -530.

Mitchell, M., Hall, D. (2005) Rural tourism as sustain-able business: Key themes and issues. In D. Hall, I. Kirkpatrick, and M. Mitchell (Eds.), *Rural tourism and sustainable business* (pp. 3–16). Tonawanda, NY: Channel View Publications.

Nicholas, L., Thapa, B., Ko, Y. (2009) Residents' perspectives of a world heritage site - the Pitons Management Area, St. Lucia, *Annals of Tourism Research*, 36(3), 390-412.

Nunkoo, R., Ramkissoon, H. (2011) Developing a community support model for tourism, *Annals of Tourism Research*, 38(3), 964-988.

Oviedo-García, M. A., Castellano-Verdugo, M., and Martín-Ruiz, D. (2008) Gaining residents' support for tourism and planning, *International Journal of Tourism Research*, 10(2), 95-109.

Rout Prakash Chandra and Gupta, S.K. (2017) Asset based community development in mountain environs: a strategic application for sustainable community based tourism development in the Jaunsar-Bawar region of Uttarakhand, India, *African Journal of Hospitality, Tourism and Leisure,* Pp.1-11,Volume 6 (3).

Sebele, L.S. (2010) Community-based tourism ventures, benefits and challenges: Khama Rhino Sanctuary Trust, Central District, Botswana, *Tourism Management*, 31, 136-146.

Sharpley, R. (2000) Tourism and sustainable development: Exploring the theoretical divide, *Journal of Sustainable Tourism*, *8*(1), 1–19.

Swarbrooke, J., Horner, S. (2004) *Consumer behavior in tourism*. Burlington, MA: Butterworth- Heinemann.

Taylor, G. (1995) The community approach: does it really work?, *Tourism Management*, 16(7), 487-489.

Vellas, F., Becherel, L. (1999) *The international marketing of travel and tourism: A strategic approach.* London: MacMillan.

Voda, M., Kithia, S., Jackiewicz, E., Du, Q., Sarpe, C.A. (2019) Geosystems 'pathways to the future of Sustainability, *Scientific Reports*, 9, 14446, doi.org/10.1038/s41598-019-50937-z

Wall, G., Mathieson, A. (2006) *Tourism: Change, Impacts and Opportunities*, Harlow: Pearson Education.

WCED (1987) World commission on Environmental development. *Our common future*. Oxford: Oxford University Press.

Yoon, Y., Gursoy, D., Chen, J.S. (2001) Validating a tourism development theory with structural equation modeling, *Tourism Management*, 22(4), 363-372.

DEVELOPMENT OF A DATA-DRIVEN MODEL TO PREDICT LANDSLIDE SENSITIVE AREAS

Seyed Ahmad ESLAMINEZHAD[1], Davoud OMARZADEH[2], Mobin EFTEKHARI[3*], Mohammad AKBARI[4]

DOI: 10.21163/GT_2021.161.09

ABSTRACT:
The occurrence of landslides has always been a problem in spatial planning as one of the environmental threats. The aim of the present study is to estimate the landslide sensitive areas in the Urmia Lake basin based on determining effective criteria and spatial and non-spatial data-driven models. The criteria used in this research include distance to faults, distance to roads, distance to hydrology network, land use, lithology, soil classes, Elevation, slope, aspect and Precipitation. The novelty of this study is to present new combination approaches to determine the effective criteria in landslide sensitive areas (Urmia Lake basin). In this regard, the geographically weighted regression (GWR) with exponential and bi-square kernels and artificial neural network (ANN) combined with a binary particle swarm optimization algorithm (BPSO). The best value of the fitness function (1-R2) for ANN, GWR with the exponential kernel, and GWR with bi-square kernel was obtained 0.2780, 0.07453, and 0.0022, respectively, Which indicates higher compatibility of the bi-square kernel than the other models. It was also found that the criteria used have a significant effect on the landslide sensitive zoning.

Key-words: *Landslide, geographically weighted regression, artificial neural network, binary particle swarm optimization algorithm.*

1. INTRODUCTION

Natural disasters, as man's greatest natural enemy, kill and injure hundreds of people annually and leave millions homeless around the world. Landslides are one of the most devastating natural disasters in sloping areas (Oktorie, 2017). Landslides and soil mass movements are a form of geomorphological processes and are considered as a special type of natural disasters from the perspective of natural hazard management. The occurrence of this type of phenomenon every year in some parts of our country as well as other parts of the world causes significant human, financial and environmental losses (Zhang et al., 2020). Identifying landslide-prone areas by zoning hazard capability with appropriate statistical models is one of the first steps in reducing potential damage and landslide risk management (Ciurleo et al., 2017). Damages caused by natural hazards have always destroyed many human-made structures and facilities, and the identification of high-risk areas should be considered as one of the main programs in land management studies (Jin et al., 2019) .

Environmental issues and forecasting the risks and damages caused by it using spatial modeling is one of the main branches of GIS today, which provides accurate and up-to-date results with very high accuracy compared to reality. In most sources, landslides are considered synonymous with mass movements (Lo et al., 2018). According to this definition and classification of hazards, by collecting data related to these movements, areas with a high probability of occurrence can be identified and the establishment of sensitive facilities and the development of the body of the city in those areas can be

[1]*Department of surveying and Geomatics Engineering, College of Engineering, University of Tehran, Tehran, Iran. Ahmad.eslami73@ut.ac.ir.*
[2]*Geography Information System and Remote Sensing, University of Tabriz, Iran. davoud.omarzadeh@stud.sbg.ac.at.*
[3*] *Young Researchers and Elite Club, Mashhad Branch, Islamic Azad University, Mashhad, Iran. mobineftekhari@yahoo.com.*
[4]*Department of Civil Engineering, University of Birjand, Birjand, Iran. moakbari@birjand.ac.ir.*

prevented. Dozens of landslides occur in different parts of the country every year and threaten many residential areas, roads, and facilities (Amir Yazdadi and Ghanavati, 2016). There are many methods for zoning landslide sensitive areas, but in general, these methods are divided into two categories: data-driven and knowledge-driven models. Data-driven models are highly effective in known areas or areas where the number of known evidence is statistically sufficient (references data). In these models, the purpose is to identify new locations for more detailed work, while in knowledge-driven models, they are effective in less known environments or where there are few targets in the area. Weight estimates and class estimates are based on expert judgment and do not require evidence of an answer (Guevara et al. 2018;Wang and Liu 2019). Numerous studies have been conducted on Landslide zoning maps with approaches based on data-driven and knowledge-driven models, to name a few:

Neaupane and Piantanakulchai (2006) presented an ANP model for assessing landslide risk in a fragile mountainous terrain in the eastern part of Nepal. The results showed that the ANP model can achieve a complex relationship between landslide control factors and minimize the error caused by subjective judgment. Bai et al. (2010) used logistic regression for landslide susceptibility map in the Zhongxian–Shizhu region (China). The results showed that 2.8% of the study area was identified as very sensitive, while very low, low, medium and high areas covered 18.2%, 36.2%, 26.7% and 16.1%, respectively. From the region, the quality of the sensitivity map was confirmed, respectively, and the percentage of correct classification and mean square error values (RMSE) for the validation data were 81.4% and 0.392, respectively. Felicísimo et al. (2013) used four methods of multiple logistic regression (MLR), multivariate adaptive regression splines (MARS), classification and regression trees (CART), and maximum entropy (MAXENT) to landslide susceptibility (Deba Valley, Northern Spain). The results of this study show that the best AUC values were obtained for single models MLR (0.76), MARS (0.76), CART (0.77) and MAXENT (0.78). Xu et al. (2015) conducted a study on landslide sensitivity analysis using a combination of computer science and GIS and artificial neural network methods in the three valleys region. In the mentioned research, geological layers, distance to fault, slope, aspect, precipitation, distance to river, land user, distance to road, water difference index, and normalized differential index of vegetation have been used. According to the results, the accuracy of the model is 88% and the result of comparing the actual recorded data with the product of this research indicates the high accuracy of the model. Rajabi et al. (2016) investigated the possibility of landslides in the Azarshahr Chay catchment using fuzzy logic. In this research, the criteria of distance to road, distance to fault, distance to river, land use, lithology, elevation classes, slope, and aspect have been used. The results of this study show that 24.47, 26.4, 25.92, 17.59, and 5.77% of the area are in very low, low, medium, high, and very high probability occurrence classes, respectively. Ghorbanzadeh et al. (2019) have conducted a study on the application of multi-criteria spatial decision making and location of potential tourism areas in East Azerbaijan province in which the combination of Analytical Network Process (ANP) and Ordered Weighted Averaging (OWA) have been used to achieve potential nature areas. Baharvand et al. (2020) used fuzzy logic and GIS methods for landslide susceptibility zoning in the Sorkhab basin as a part of the Zagros. The results showed that a 0.9 fuzzy gamma operator has high accuracy for the LSZ map in the study area. Also, the accuracy of the landslide susceptibility zoning map showed that there was a strong (R^2) relationship between the sensitivity classes.

Landslide zoning map production is a topic that has received a lot of attention so far, but among the studies conducted, some points have received less attention; first, none of these studies provide an adequate combination of criteria for landslide zoning. Second, proper analysis has not been used to determine the optimal combination of effective criteria and to prepare a landslide zoning map based on the effective criteria. In this study to recognizing the vulnerability of Urmia Lake basin to landslide sensitive, due to the availability of landslide reference map in the region, the combination of spatial and non-spatial data-driven models including artificial neural network (ANN) and geographically weighted regression (GWR) with binary particle swarm optimization (BPSO) were used to prepare Landslide zoning map based on determining the optimal combination of effective criteria.

2. STUDY AREA

The study area in the present study includes the catchment area of Lake Urmia, parts of East Azerbaijan province, and parts of West Azerbaijan province, as well as part of Kurdistan province. This catchment is one of the closed catchments in Iran, which is located in the northwest of the country. The highest heights of this basin include Sabalan with a height of 4811 meters and Sahand with a height of 3707 meters and the lowest point of the basin is Lake Urmia with an average height of 1280 meters. According to the Meteorological Organization, the average rainfall in the basin is 550 mm and its main source is Mediterranean currents. The most important rivers of this basin are Ajichai, Zarrinehrood, and Siminehrood. The geographical position of the study basin includes 44 degrees and 21 minutes east to 47 degrees and 91 minutes east and 35 degrees and 35 minutes north to 38 degrees and 49 minutes north (**Fig. 1**).

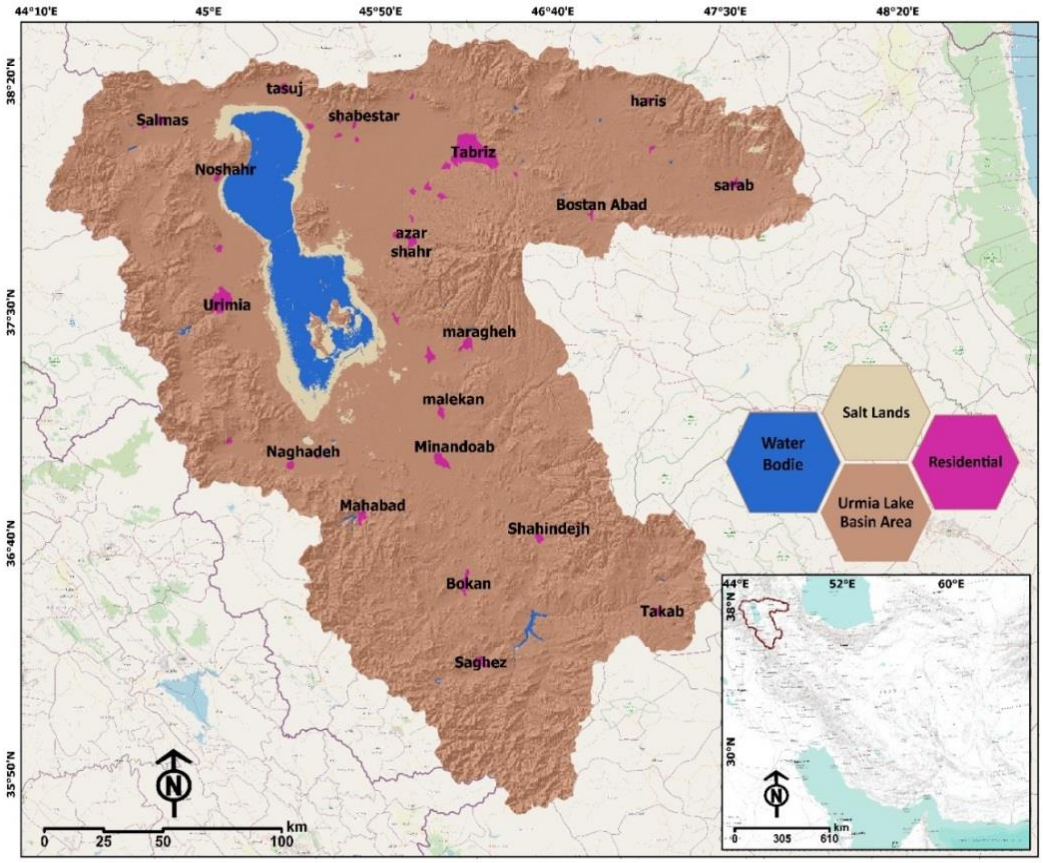

Fig. 1. Geographical location of Lake Urmia catchment in Iran.

3. DATA AND METHODS

3.1. Spatial criteria affecting landslide

According to **Table 1**, in this study, the spatial criteria affecting landslide are considered as independent variables. These criteria, in the order mentioned, form the particle dimension of the BPSO algorithm. Also, the flowchart of the research is also shown in **Fig. 2**.

Table 1.

Independent variables in this study.

Order	Criteria	Order	Criteria
1	Distance to faults	6	Soil classes
2	Distance to roads	7	Elevation
3	Distance to hydrology network	8	Slope
4	Land use	9	Aspect
5	Lithology	10	Precipitation

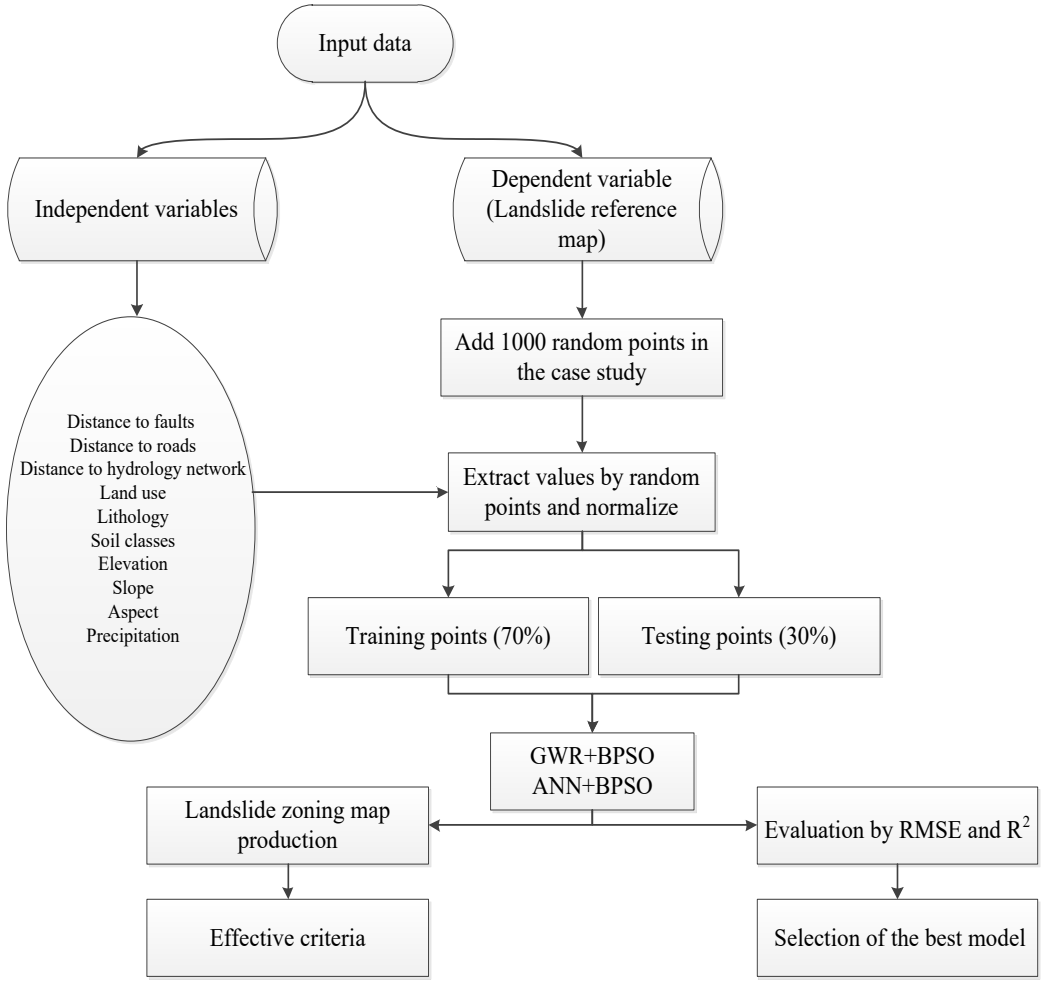

Fig. 2. Flowchart of steps taken in the research.

The spatial criteria affecting landslide was obtained from the Geological Survey and Mineral Exploration of Iran. For implementation, each of the criteria was produced in the form of a raster map with a pixel size of 30 meters. According to **Fig. 3**, the maps of these criteria are shown in a normalized way.

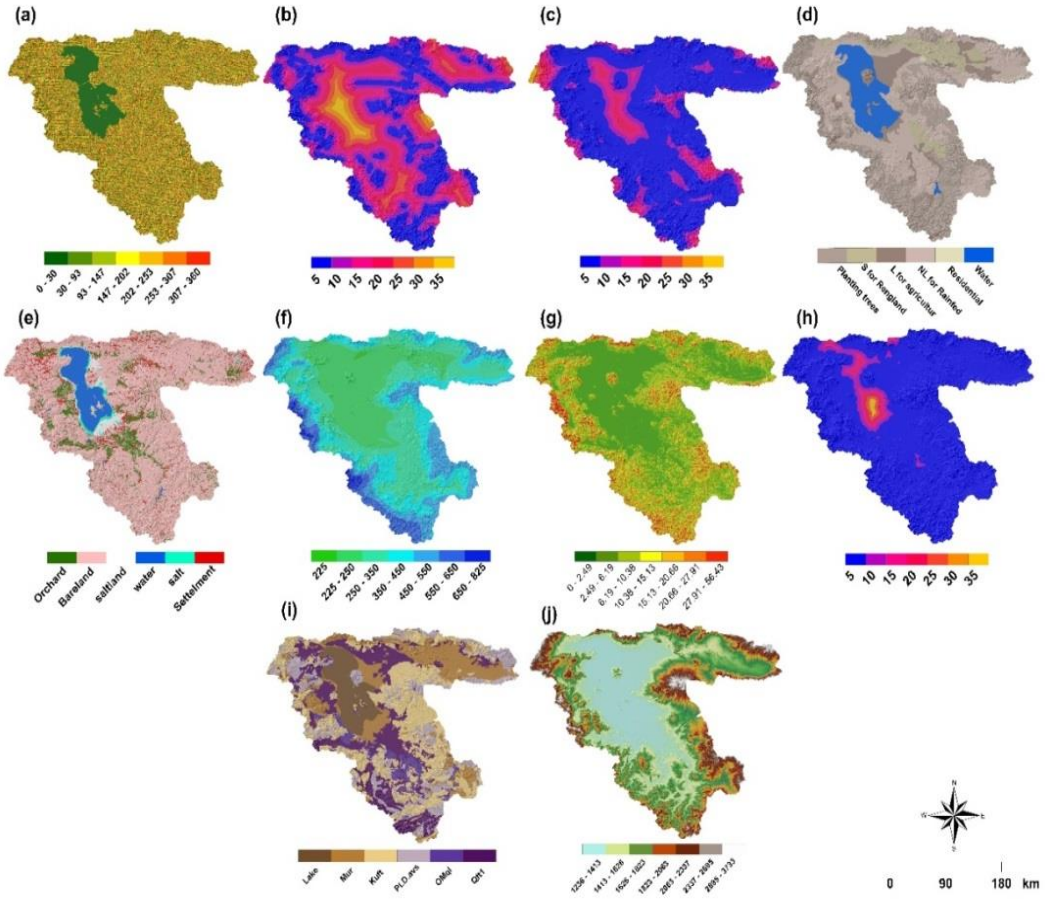

Fig. 3. Map of criteria used in landslide zoning (a) Aspect (b) Distance to fault (c) Distance to road (d) Soil type (e) Land use (f) Precipitation (g) Slope (h) Distance to hydrology network (i) Lithology (j) Elevation.

3.2. Proposed methods

3.2.1. Artificial neural network

Artificial neural networks are one of the computational methods inspired by the neural system of the human brain. One of the remarkable characteristics of this type of network is their ability to learn and the ability to generalize this learning, because of this feature, they make it possible to learn to understand patterns (El_Jerjawi and Abu-Naser, 2018). The most important advantage of artificial neural networks over regression methods for modeling a pattern is that there is no need for an initial model in linking input and output data (Lee et al., 2018). Based on the intrinsic relationships between data, a linear or nonlinear model is established between independent and dependent variables.

In this study, a multilayer perceptron neural network has been used to model landslide sensitive. This type of neural network consists of a set of neurons arranged in different layers in a row. The law of multilayer perceptron learning is called the error propagation rule, which is used to estimate unknown network parameters. The multilayer perceptron works in such a way that a pattern is supplied to the network and its output is calculated. Actual output values and desired output cause the network coefficients to change; in such a way that a more accurate output is obtained in later stages. To succeed in network training, its output must be gradually brought closer to the desired output and the error rate must be reduced. The design ANN used in this study is illustrated in **Fig. 4**.

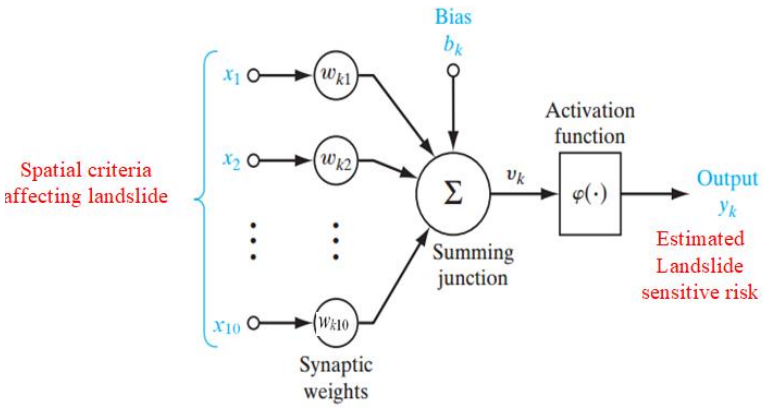

Fig. 4. ANN architecture applied in this study (Lee et al., 2018).

3.2.2. Geographically weighted regression

According to spatial autocorrelation and spatial non-stationarity properties for spatial data, it is less possible to use basic global regressions such as Ordinary Least square (Murray et al., 2020). In this model, the spatial dependencies between the events are considered as weight matrices, and due to the heterogeneity of the environmental factors and the existence of local variation, regression coefficients of the GWR model for observation are measured locally (Wu, 2020). The equation of the GWR model is calculated as Eq. 1 (Fotheringham and Oshan, 2016):

$$y_i = \sum_{j=0}^{n} \beta_j(u_i, v_i) x_j + \varepsilon_i \quad (1)$$

where:

y_i	- the dependent variable (Landslide sensitive rate);
x_j	- the independent variables (Spatial criteria affecting landslide);
n	- the total random points;
εi	- the residual GWR model;
(u_i,v_i)	- the coordinates of the ith point in space;
$\beta_j(u_i,v_i)$	- the regression coefficient;

To calculate the spatial weight matrix, it is necessary to specify the desired kernel function. According to previous research, this study used two kernels including exponential and bi-square these two kernels which are calculated as Eq. 2 and Eq. 3, respectively (Oshan et al., 2019; Fotheringham and Oshan, 2016):

$$W(u_i, v_i) = \exp(-(\frac{|d_{ij}|}{b})) \quad (2)$$

$$W(u_i, v_i) = \begin{cases} (1-(\frac{d_{ij}}{b})^2)^2 & |d_{ij}| < b \\ 0 \quad otherwise \end{cases} \quad (3)$$

where:

d_{ij}	- the euclidean distance value between two observations i and j;
b	- the bandwidth value;

The regression coefficients are different for each location, so in the GWR model, local variation of the regression coefficients can be obtained by the standard deviation function according to Eq. 4 (Wu, 2020):

$$SE = \sqrt{\sum_{i=1}^{n} \frac{(\beta_{ij} - \beta_j)^2}{n}} \tag{4}$$

where:

β_{ij} - the regression coefficient for the factor j in the observation i;

β_j - the mean regression coefficient of factor *j;*

n - the total random points;

To evaluate the ANN and GWR models output the Coefficient of Determination (R^2) is usually used to measur`e the goodness of fit and the RMSE value measure the residuals distribution of the observation, which are obtained based on Eq. 5 and Eq. 6 (Fotheringham and Oshan, 2016):

$$R^2 = 1 - \frac{\sum_{i=1}^{n} (y_i - \hat{y}_i)^2}{\sum_{i=1}^{n} (y_i - \bar{y})^2} \tag{5}$$

$$RMSE = \sqrt{\frac{\sum_{i=1}^{n} (y_i - \hat{y}_i)^2}{n}} \tag{6}$$

where:

y_i - the value for observation;

y_i - the estimated value for observation *i;*

n - the total random points;

$\bar{y}_i$ - the mean value for total observations;

3.2.3. Binary particle swarm optimization

The PSO algorithm is an optimization algorithm that makes it less likely to be captured at a local minimum and can search uncertain and complex areas based on probabilistic rules (Aghbashlo et al., 2019). Also in this algorithm, the solution of the proposed path is not dependent on the initial population and starting from each point in the search space, the solution converges to the optimal solution (Abed and Ahmad, 2020). After a while, Kennedy and Eberhart (1997) introduced the Binary PSO algorithm, which, unlike the continuous version of it, is limited to having zero and one (binary) variables and the velocity value can change a particle from zero to one. According to the purpose of this study, The BPSO algorithm has been used. In this algorithm, Eq. 7 and Eq. 8 are used to update the velocity and position of each particle (Kennedy and Eberhart, 1997):

$$V_i(t+1) = w \times V_i(t) + c_1 \times r_1 \times (pbest - X_i(t)) + c_2 \times r_2 \times (gbest - X_i(t)) \tag{7}$$

$$X_i(t+1) = \begin{cases} 1 & \rho \le sig(v_i^{t+1}) \\ 0 & Otherwise \end{cases} \tag{8}$$

where:

$V_i(t)$ - the velocity of the particle *i*;

$X_i(t)$ - the position of the particle *i*;

$V_i(t+1)$ - velocity of the particle *i* in the next position;

$X_i(t+1)$ - the position of the particle *i* in the next position;

pbest - the best position of the experience for the particle *i*;

gbest - the best position experienced in all particles;

c_1 - the personal learning coefficient;

c_2 - the collective learning coefficient;

w - the inertia weight;

r_1, r *and* ρ - the random numbers in the range [0.1];

In this study the steps of the BPSO algorithm (In combination with the ANN and GWR models) are as follows which showed in **Fig. 5**:

1. Give the initial value to a population of particles with random positions and velocities.
2. Training ANN and GWR models and calculating the fitness function (R^2) of each particle in this population.
3. Stop the BPSO algorithm (reach 100 iterations), otherwise go to step 4. If the algorithm reaches the condition of stopping, then the selected criteria are the same effective parameters in estimating landslide risk.
4. Determine the pbest and gbest for particles.
5. Calculate the velocity of each particle and move to the next position based on the relations (Go to step 2).

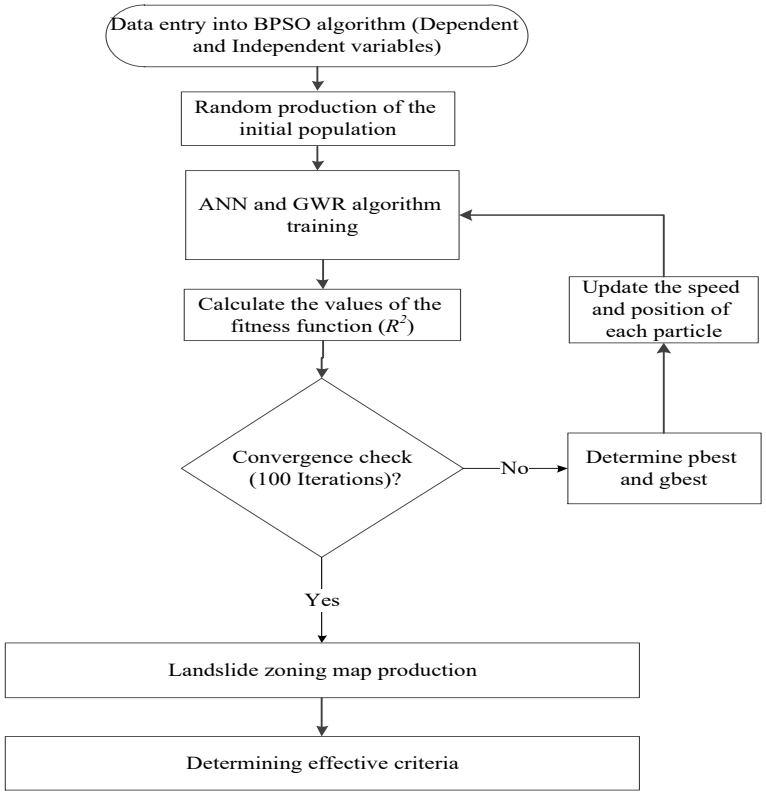

Fig. 5. Calculation steps of the recommended models.

4. RESULTS AND DISCUSSIONS

4.1. Data preparation

In order to implement the proposed models, it is necessary to produce random points in the desired area. The Landslide is the result of the reference map related to June 2017 (**Fig. 6a**), which has been obtained from Geological Survey & Mineral Explorations of Iran. Then, according to **Fig. 6b**, 1000 points were generated randomly and uniformly in the study area (Elfil and Negida, 2019). Then the values of all available information criteria for these points were calculated (In a normalized way). Of these, 70% for training and 30% for testing were randomly selected and used equally for all models. Based on previous research and trial and error method, a ratio of 70:30 was selected (Paulino et al., 2019). In article this ratio gives the best performance results.

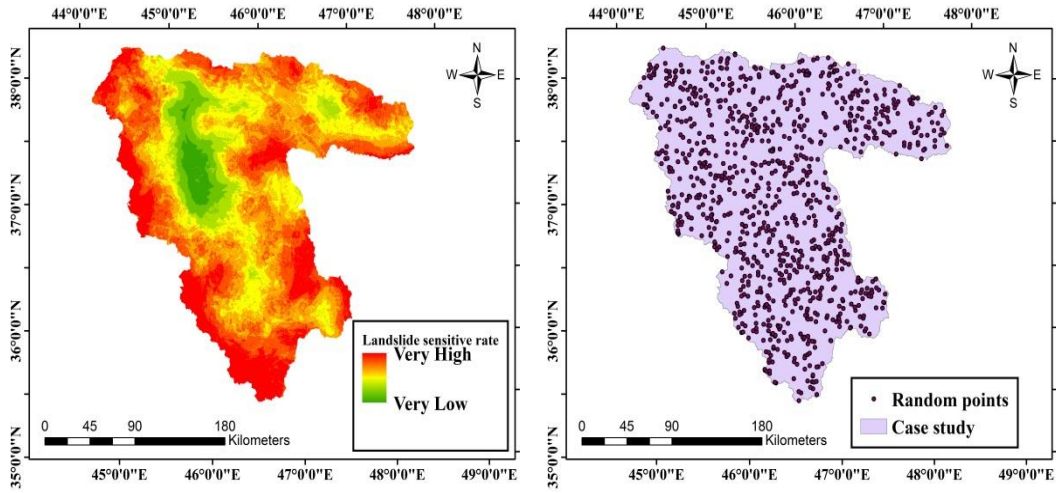

(a) (b)

Fig. 6. (a) The landslide reference map (b) The random point created in the case study.

The correlation between the criteria from Eq. 9 was examined (Aad et al., 2014):

$$r = \frac{\sum_{i=1}^{n}(x_i - \bar{x})(y_i - \bar{y})}{n.\sigma_x.\sigma_y} \quad (9)$$

where:

$\bar{x}$ and $\bar{y}$ - the mean of data x and y;

n - the total data;

σ_x and σ_y - the deviation of data x and y;

As shown in **Fig. 7**, the correlation between the criteria is near 0. Therefore, all criteria entered the algorithms.

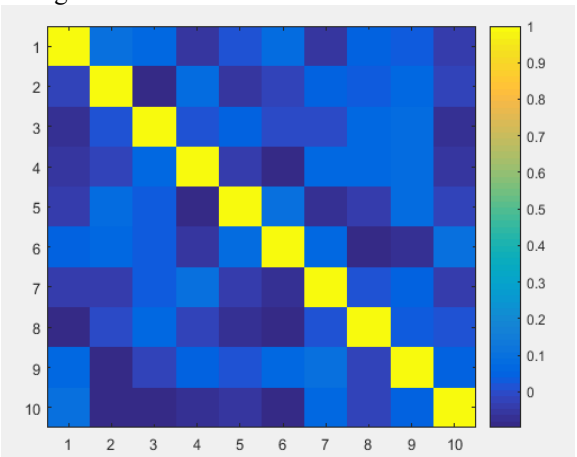

Order	Criteria
1	Distance to faults
2	Distance to roads
3	Distance to hydrology network
4	Land use
5	Lithology
6	Soil classes
7	Elevation
8	Slope
9	Aspect
10	Precipitation

Fig. 7. Correlation matrix between criteria

4.2. Implement data-driven models

For the implementation of the ANN and GWR models, 70% of the total data was used for training and 30% of the total data was used for testing, and all data were normalized before entering the algorithms (Paulino et al., 2019). Due to the fact that one of the most important parameters for evaluating data-driven models (Model compatibility with data) is the Coefficient of Determination

parameter (R^2), therefore, the BPSO algorithm fitness function has been selected to minimize the value of 1-R^2 (Fotheringham and Oshan, 2016). The optimal values of the initial parameters of the BPSO algorithm were selected based on the experiments obtained from different iterations and through trial and error according to **Table 2**. The condition for stopping to simplify the implementation process is the number of specific executions.

Table 2.

Set Parameters in the BPSO algorithm.

Parameters	Value	Parameters	Value
Swarm size	30	C_2	2
Total iterations	100	W	1
C_1	2	Minimum and maximum velocity	[-4,4]

Fig. 8 shows the swarm structure of the BPSO algorithm in this study, which the criteria mentioned in Table 1 form the particle dimension of the BPSO algorithm.

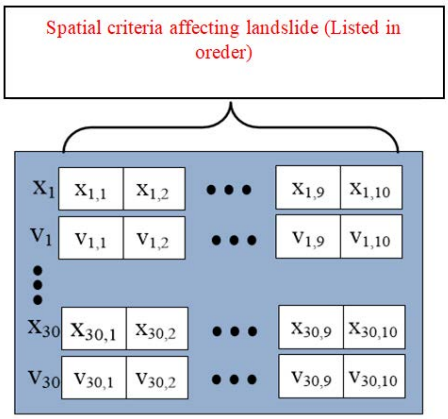

Fig. 8. Swarm structure of the BPSO algorithm.

Due to the random nature of the BPSO algorithm and based on previous research, this algorithm with the desired number of iterations was repeated 10 executions and the Best of these 10 executions was considered as the final output (Saeidian et al., 2018). According to **Fig. 9a**, by performing the combination of the ANN model and the BPSO algorithm, the best value of fitness function (1-R^2) was obtained 0.2780 (the best of 10 executions). Also, According to **Fig. 9b** for the ANN model, four criteria of distance to faults, distance to roads, distance to hydrology network and aspect were determined as effective criteria in predicting landslide risk. In fact, **Fig. 9b** shows the best particle in terms of fitness function (R^2) among all particles (30 particles) in the 100th iteration of the BPSO algorithm.

Then, the GWR model with two exponential and bi-square kernels and BPSO algorithm was combined to determine the effective criteria in predicting landslide risk. To implement the GWR model, the random points' coordinates were used as inputs in the weight matrix. According to **Fig. 10**, the best value of fitness function (1-R^2) for combination the GWR model with two exponential and bi-square kernels and the BPSO algorithm, was obtained 0.07453 and 0.0022 (the best of 10 executions), respectively. Also, According to **Fig. 11** for the GWR model with the exponential kernel, nine criteria of Distance to roads, Distance to hydrology network, Land use, Lithology, Soil classes, Elevation, Slope, Aspect, and Precipitation and for the bi-square kernel, eight criteria of Distance to roads, Land use, Lithology, Soil classes, Elevation, Slope, Aspect, and Precipitation were determined as effective criteria in predicting landslide risk.

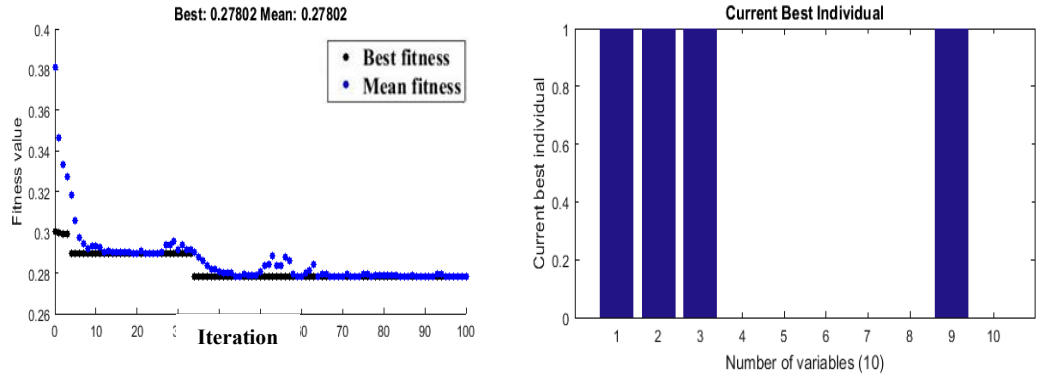

(a) (b)

Fig. 9. (a) The best value of fitness function by combining of ANN model and BPSO algorithm (b) Effective criteria in predicting landslide risk by combining of ANN model and BPSO algorithm

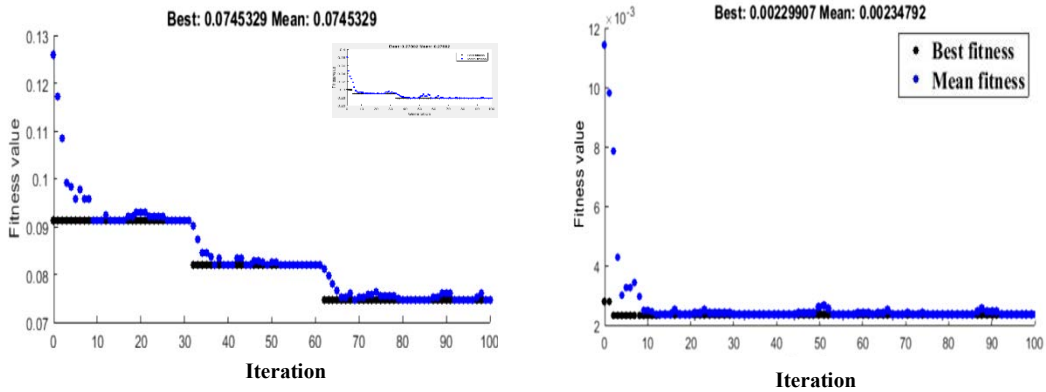

Fig. 10. The best value of fitness function by combining of GWR model and BPSO algorithm (a) Exponential kernel (b) Bi-square kernel

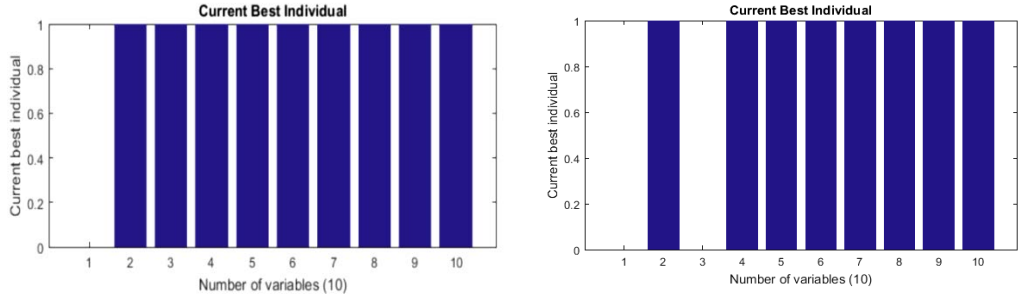

(a) (b)

Fig. 11. Effective criteria in predicting landslide risk by combining of GWR model and BPSO algorithm (a) Exponential kernel (b) Bi-square kernel

In **Fig. 12**, the values of R^2 and RMSE for the ANN and GWR models are shown. Accordingly, the bi-square kernel has higher accuracy in predicting landslide risk based on effective criteria.

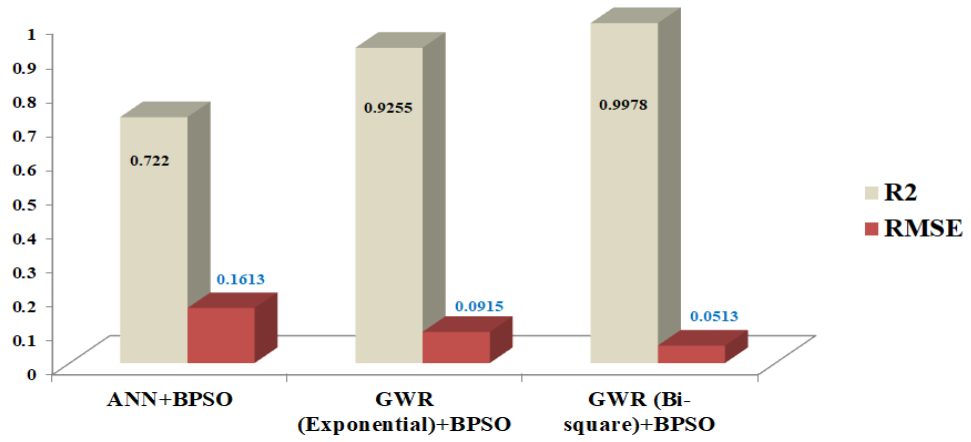

Fig. 12. Comparison of ANN and GWR models in terms of R^2 and RMSE

According to **Fig. 13**, the maps of predicted landslide risk (based on effective criteria) by combining ANN and GWR models and BPSO algorithm showed in the range [0,1]. The estimated landslide risk is classified into five output classes according to the Equal Interval classification method. According to the results obtained from R^2 value (goodness of fit) and the RMSE value (Residuals distribution of the observation and accuracy of model), the combination of GWR model with Bi-square kernel and BPSO algorithm has a higher ability to predict landslide risk, which showed in **Fig. 13c**.

As mentioned, since the regression coefficients are different for each location in the GWR model, local variation and spatial non-stationarity of the regression coefficients can be obtained by the standard deviation function. **Fig. 14** shows the standard deviation of regression coefficients GWR model (with two exponential and bi-square kernels) for calculating the rate of local variation and spatial non-stationarity.

According to **Fig. 14**, for the GWR model with the exponential kernel, the relationship between soil classes and landslide risk with displacement has the most variation and the relationship between Precipitation and landslide risk has the least variation. Also, in the GWR model with the bi-square kernel, the relationship between aspect and landslide risk with displacement has the most variation and the relationship between Precipitation and landslide risk has the least variation. Finally, global Moran's index was used to determine the spatial autocorrelation of GWR model residuals, which is calculated from Eq. 10 (Zemestani and Soori, 2019):

$$I = \frac{n\sum_{i=1}^{n}\sum_{j=1}^{n} W_{ij}(x_i - \overline{X})(x_j - \overline{X})}{S_0 \sum_{i=1}^{n}(x_i - \overline{X})^2} \tag{10}$$

where:

x_i and x_j - estimated lanslide risk for random points i and j;
W_{ij} - the spatial weight matrix between random points i and j;
S_0 - the total of all weights;
$\overline{X}$ - the mean estimated landslide risk for random points;
n - the total random points;

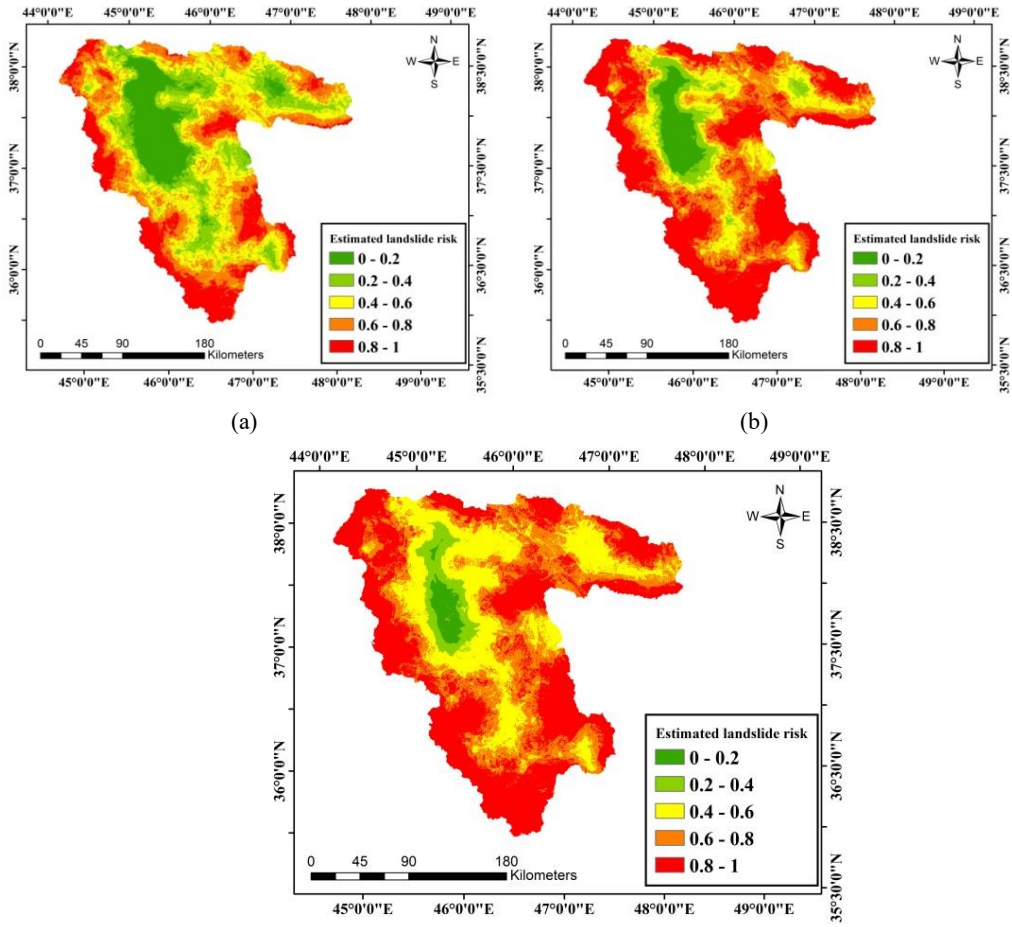

Fig. 13. The map of estimated landslide risk (a) ANN + BPSO (b) GWR (Exponential) + BPSO (c) GWR (Bi-square) + BPSO

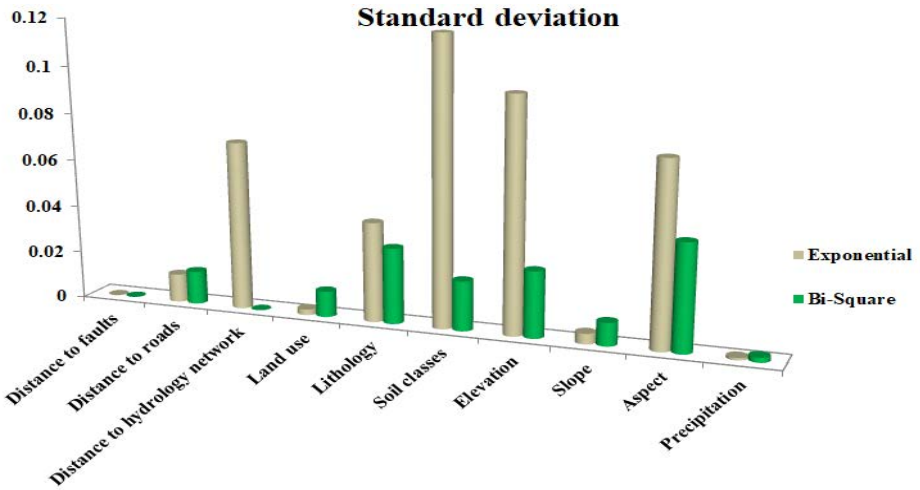

Fig. 14. The standard deviation of regression coefficients GWR model with exponential and bi-square kernels.

Table 3, shows the values of global Moran's index for GWR model residuals with two exponential and bi-square kernels. According to **Table 3** for the GWR model with the bi-square kernel, the Moran's index has a closer value to the expected index than the exponential kernel, which indicates the high ability of the bi-square kernel in modeling the spatial correlation of observations.

Table 2.
The values of Moran's index for GWR model residuals with two exponential and bi-square kernels.

Parameters	Kernel type	
	Exponential	Bi-square
Moran's index	0.153	0.112
Expected index	0.000632	0.000632
Z-Score	11.72	12.03
P-value	0.000	0.000

5. CONCLUSIONS

Due to the increase in landslide, especially in cities and the emergence of human, financial and environmental risks, the identification of criteria affecting the occurrence of landslide is of great importance. Therefore, by identifying these criteria, we can prevent this phenomenon as much as possible by using public education to the people, enacting effective management laws and policies, and more oversight in order to deal with the stimulus criteria for increasing landslide rates. Therefore, in this study, we tried to analyze the role of spatial criteria affecting in predicting landslide sensitive risk, which has been neglected in many previous studies.

The models used in previous research were not very suitable for spatial data and in most cases the spatial correlation and non-stationarity of the data were ignored. To achieve the main purpose of this study, the spatial and non-spatial data-driven models including GWR and ANN model were used to predict landslide sensitive risk based on the effective criteria. The results showed that the GWR model used, taking into account the characteristics of spatial autocorrelation and spatial non-stationarity, has higher accuracy in predicting landslide sensitive risk based on the effective criteria. In this study, an attempt was also made to determine the effective criteria in predicting landslide sensitive risk in the form of another study purpose. Therefore, the binary particle swarm optimization algorithm was used in combination with the ANN and GWR models, which showed that the criteria have a significant effect in predicting landslide sensitive risk (study area). The important point is that the mentioned method is not limited to this case study and can be used to predict the landslide sensitive risk in various types of regions.

Due to the success of the spatial data-driven model used in this research, it is suggested for future research other spatial data-driven models such as Generalized Method of Moments Estimation for Spatial Autoregressive (GMM-SAR), Matrix Exponential Spatial Specification (MESS) and combination of GWR with neural networks were used.

REFERENCES

Aad G, Abbott B, Abdallah J, Abdel Khalek S, et al. (2014) Measurements of spin correlation in top-antitop quark events from proton-proton collisions at √s =7 TeV using the ATLAS detector. Physical Review D - Particles, Fields, Gravitation and Cosmology 90: . https://doi.org/10.1103/PhysRevD.90.112016

Abed KA, Ahmad AA (2020) The best parameters selection using pso algorithm to solving for ito system by new iterative technique. Indonesian Journal of Electrical Engineering and Computer Science 18: . https://doi.org/10.11591/ijeecs.v18.i3.pp1638-1645

Aghbashlo M, Tabatabaei M, Nadian MH, Davoodnia V, Soltanian S (2019) Prognostication of lignocellulosic biomass pyrolysis behavior using ANFIS model tuned by PSO algorithm. Fuel 253: . https://doi.org/10.1016/j.fuel.2019.04.169

Amir Yazdadi E, Ghanavati E (2016) Landslide Hazard Zonation by using AHP (Analytical Hierarchy Process) model in GIS (Geographic Information System) Environment (Case study: Kordan Watershed)

Baharvand S, Rahnamarad J, Soori S, Saadatkhah N (2020) Landslide susceptibility zoning in a catchment of Zagros Mountains using fuzzy logic and GIS. Environmental Earth Sciences 79:204 . https://doi.org/10.1007/s12665-020-08957-w

Bai SB, Wang J, Lü GN, Zhou PG, Hou SS, Xu SN (2010) GIS-based logistic regression for landslide susceptibility mapping of the Zhongxian segment in the Three Gorges area, China. Geomorphology 115:23–31 . https://doi.org/10.1016/j.geomorph.2009.09.025

Ciurleo M, Cascini L, Calvello M (2017) A comparison of statistical and deterministic methods for shallow landslide susceptibility zoning in clayey soils. Engineering Geology 223:71–81 . https://doi.org/10.1016/j.enggeo.2017.04.023

El_Jerjawi NS, Abu-Naser SS (2018) Diabetes Prediction Using Artificial Neural Network. International Journal of Advanced Science and Technology 121:55–64 . https://doi.org/10.14257/ijast.2018.121.05

Elfil M, Negida A (2019) Sampling methods in clinical research; an educational review. Archives of Academic Emergency Medicine 7:52 . https://doi.org/10.22037/emergency.v5i1.15215

Felicísimo ÁM, Cuartero A, Remondo J, Quirós E (2013) Mapping landslide susceptibility with logistic regression, multiple adaptive regression splines, classification and regression trees, and maximum entropy methods: A comparative study. Landslides 10:175–189 . https://doi.org/10.1007/s10346-012-0320-1

Fotheringham AS, Oshan TM (2016) Geographically weighted regression and multicollinearity: dispelling the myth. Journal of Geographical Systems 18: . https://doi.org/10.1007/s10109-016-0239-5

Ghorbanzadeh O, Pourmoradian S, Blaschke T, Feizizadeh B (2019) Mapping potential nature-based tourism areas by applying GIS-decision making systems in East Azerbaijan Province, Iran. Journal of Ecotourism 18:261–283 . https://doi.org/10.1080/14724049.2019.1597876

Guevara J, Zadrozny B, Buoro A, Lu L, Tolle J, Limbeck J, Wu M, Hohl D (2018) A hybrid data-driven and knowledge-driven methodology for estimating the effect of completion parameters on the cumulative production of horizontal wells. In: Proceedings - SPE Annual Technical Conference and Exhibition. Society of Petroleum Engineers (SPE)

Jin KP, Yao LK, Cheng QG, Xing AG (2019) Seismic landslides hazard zoning based on the modified Newmark model: a case study from the Lushan earthquake, China. Natural Hazards 99:493–509 . https://doi.org/10.1007/s11069-019-03754-6

Kennedy J, Eberhart RC (1997) Discrete binary version of the particle swarm algorithm. In: Proceedings of the IEEE International Conference on Systems, Man and Cybernetics

Lee S, Hong SM, Jung HS (2018) GIS-based groundwater potential mapping using artificial neural network and support vector machine models: the case of Boryeong city in Korea. Geocarto International 33:847–861 . https://doi.org/10.1080/10106049.2017.1303091

Lo C-M, Feng Z-Y, Chang K-T (2018) Landslide hazard zoning based on numerical simulation and hazard assessment. Geomatics, Natural Hazards and Risk 9:368–388 . https://doi.org/10.1080/19475705.2018.1445662

Murray AT, Xu J, Baik J, Burtner S, Cho S, Noi E, Pludow BA, Zhou E (2020) Overview of Contributions in Geographical Analysis: Waldo Tobler. In: Geographical Analysis

Neaupane KM, Piantanakulchai M (2006) Analytic network process model for landslide hazard zonation. Engineering Geology 85:281–294 . https://doi.org/10.1016/j.enggeo.2006.02.003

Oktorie O (2017) A Study of Landslide Areas Mitigation and Adaptation in Palupuah Subdistrict, Agam Regency, West Sumatra Province, Indonesia. Sumatra Journal of Disaster, Geography and Geography Education 1:43 . https://doi.org/10.24036/sjdgge.v1i1.34

Oshan TM, Li Z, Kang W, Wolf LJ, Stewart Fotheringham A (2019) MGWR: A python implementation of multiscale geographically weighted regression for investigating process spatial heterogeneity and scale. ISPRS International Journal of Geo-Information 8: . https://doi.org/10.3390/ijgi8060269

Paulino Â de C, Guimarães LNF, Shiguemori EH (2019) Hybrid adaptive computational intelligence-based multisensor data fusion applied to real-time UAV autonomous navigation. Inteligencia Artificial 22:162–195 . https://doi.org/10.4114/intartif.vol22iss63pp162-195

Rajabi M, Vlizadeh Kamran K, Abedi Gheshlaghi H (2016) Evaluation and zoning landslide hazard by using the analysis network process and artificial neural network (case study Azarshahr Chay basin). 5:60–74

Saeidian B, Mesgari MS, Pradhan B, Ghodousi M (2018) Optimized location-allocation of earthquake relief centers using PSO and ACO, complemented by GIS, clustering, and TOPSIS. ISPRS International Journal of Geo-Information 7: . https://doi.org/10.3390/ijgi7080292

Wang X, Liu H (2019) A Knowledge-and Data-Driven Soft Sensor Based on Deep Learning for Predicting the Deformation of an Air Preheater Rotor. IEEE Access 7:159651–159660 . https://doi.org/10.1109/ACCESS.2019.2950661

Wu D (2020) Spatially and temporally varying relationships between ecological footprint and influencing factors in China's provinces Using Geographically Weighted Regression (GWR). Journal of Cleaner Production 261: . https://doi.org/10.1016/j.jclepro.2020.121089

Xu K, Guo Q, Li Z, Xiao J, Qin Y, Chen D, Kong C (2015) Landslide susceptibility evaluation based on BPNN and GIS: a case of Guojiaba in the Three Gorges Reservoir Area. International Journal of Geographical Information Science 29:1111–1124 . https://doi.org/10.1080/13658816.2014.992436

Zemestani A, Soori H (2019) Relationship between fatal road traffic injury rates and Human Development Index in Iran. Journal of Injury and Violence Research 11:

Zhang Y, Wu W, Qin Y, Lin Z, Zhang G, Chen R, Song Y, Lang T, Zhou X, Huangfu W, Ou P, Xie L, Huang X, Peng S, Shao C (2020) Mapping Landslide Hazard Risk Using Random Forest Algorithm in Guixi, Jiangxi, China. ISPRS International Journal of Geo-Information 9:695 . https://doi.org/10.3390/ijgi9110695

INTERLINKAGES BETWEEN STRATEGIC, FINANCIAL AND REGIONAL FRAMEWORKS OF BROWNFIELD REGENERATIONS: THE CASE OF THE CZECH REPUBLIC

***Michal TVRDOŇ*[1], *Petra CHMIELOVÁ*[1]**

DOI : 10.21163/GT_2021.161.10

ABSTRACT:
Brownfield regeneration is one of the key measures for sustainable development and it combines three pillars – economic, environmental and social. The aim of this paper is to identify interlinkages between strategic, financial and regional frameworks of brownfield regeneration in the Czech Republic. The first part of the paper consists of literature review associated with brownfield regeneration. The second part of paper focuses on practical aspects of brownfield regeneration in the Czech Republic during the period 2000 to 2020. This empirical part is based on analysis of strategic documents, financial instruments and regional disparities. In this paper, national level and regional level data were applied (7 NUTS II regions excluding the region of the capital city Prague). Data summarizing the drawn funds or allocated financial amount to support the regeneration of brownfields from EU funds were obtained from secondary sources mainly (national strategies, websites of individual operational programs or national programs). The results show certain time delay in solving this issue in this post-socialistic country in comparison with Western European countries. Data also indicate noticeable differences between regions, both in terms of the number of brownfields and their regeneration, especially in terms of a number of projects or financial resources. Another finding is that the Czech Republic significantly improved the strategic planning of brownfield regeneration and as this problem is cross-sectional more institutions are involved both in strategic and financial dimension.

Key-words: *Brownfields regeneration, Czech Republic, EU funds, Regional disparities, Spatial analysis.*

1. INTRODUCTION

The structure of the economy transforms over time. This process has a number of consequences, both positive and negative. One of the negative impacts is the formation of brownfields that can be characterized as sites (land or premises) completely or partially abandoned. We can find relatively many definitions of brownfield. Moreover, these definitions differ among countries. For example, in the US, a brownfield is considered (according to United States Environmental Protection Agency – cited in Ahmad et al. (2018) *"abandoned, idled, or under-used industrial and commercial facility where expansion or redevelopment is complicated by real or perceived environmental contamination*". According to Franz et al. (2006) the EU defines brownfield as (through Concerted Action on Brownfield and Economic Regeneration Network – CABERNET): *"(i) sites that have been affected by the former uses of the site and surrounding land; (ii) re derelict and underused; (iii) may have real or perceived contamination problems; (iv) are mainly in developed urban areas; and (v) require intervention to bring them back to beneficial use".* As this paper deals with brownfields regeneration in the Czech Republic it is necessary to mention definition of brownfield in this country. We can find it in the National strategy of brownfields regeneration 2019-2024, which is the joint document of Ministry of Industry and Trade, CzechInvest, Ministry of Regional Development, Ministry of Agriculture and Ministry of the Environment: *"brownfield is a property (territory, complex, land, or building) that is unused, neglected and can be contaminated. It arises as a remnant*

[1]*Silesian University in Opava, School of Business Administration in Karviná, 73340 Karviná, Czech Republic, tvrdon@opf.slu.cz; chmielova@opf.slu.cz.*

of industrial, agricultural, residential, military or other activities. Brownfield cannot be used appropriately and effectively without a regeneration process".

If we look at the process of brownfield formation, we realise that they arise due to structural changes in the economy mainly – according to Kunc et al. (2014) they are perceived as scars on the faces of cities, as commitments reducing the value of the surrounding land, and as obstacles to local development, which municipalities or other self-governing units are often unable to revitalize from their own resources. In other words, brownfields are most often localities which were originally used for agricultural, industrial or military purposes; however, due to changes in the structure of the economy, they have lost this original use. Moreover, the existence of brownfields means a serious problem in many ways – political, social and economic.

According to Alberini et al. (2005) the problems associated with the existence of brownfields began to appear in the countries of Western Europe and the USA in the early 1970s as a result of two concurrent factors: the numerous plant closings and downsizing as these regions experienced a structural change of their economies away from manufacturing, and the passage of environmental legislation holding specified parties liable for the cost of cleanup at contaminated sites. As these processes took place in these regions for a long time their impact has not been as strong as in post-socialist countries, where these processes began to appear with a certain time delay (approximately 20 years), but with much greater intensity due to the complexity of the transition process focused on restructuring of traditional industries and following globalization trends (Osman et al. 2015). In addition, Matlovič et al. (2001) also mentions that apart from standard agricultural or industrial brownfields, many military brownfields occurred in the Czech Republic after the withdrawal the Soviet Army and military sector restructuring. The number of these types of brownfields has decreased over time and Navrátil et al. (2019) find out that some of these brownfields had been utilised for non-agricultural purposes. According to Garb and Jackson (2010) there was estimated that economic transition left close to 10,000 brownfields in the Czech Republic alone with over 2,000 of these in the larger size category, some in prominent urban positions (Klusáček, 2005; Wirth & Lintz, 2006; Filip & Cocean, 2012). Moreover, Tureckova et al. (2019) mentioned that this generally used number is underestimated. Klusáček et al. (2018) find out that structural changes affected regions of the Czech Republic in different way – most affected regions were Moravia-Silesia Region and Ústecký Region which had to cope with intense deindustrialization. According to Gwosdz, Domański & Bilska-Wodecka (2020) some Polish regions have had a similar experience accompanied by rising unemployment. Although there is great development potential in the regeneration of these properties, however, this is often not possible without the initiative and support of the state and the public sector. Moreover, public intervention is all the more necessary if it is an area with social and environmental problems associated with the transition process. Unfortunately, post-socialist governments and markets were unable to 'metabolise' these unused properties in the first decade of transition. Recognition of the importance of the existence of brownfields as a societal problem and the subsequent implementation of pilot projects occurs only after the year 2000. This was followed by the relatively dynamic development of the legislative, institutional and financial framework for tackling this problem in the first two decades of the 21st century. According to Garb and Jackson (2010) the brownfield issue is now strongly (though often only formally) embedded in EU, national, regional and local policies and strategies.

According to National Strategy of Brownfields Regeneration 2019 – 2024 brownfields regeneration is defined as the process that results in the possibility of reusing the property or entire locality. The extent of remediation and construction work depends on the degree of damage to surfaces, buildings and equipment and on the need for modifications for new use. Brownfield regeneration projects may include the removal or reconstruction of original buildings, their completion and extensions. The following activities may be part of regeneration and revitalization projects: (i) restoration = return of natural functions to the territory; (ii) remediation = elimination of defects (technical, soil and water contamination); (iii) reconstruction = restoration of the original state, from the point of view of technical condition the objects will be as new; and (iv) modernization =

achieving a new technical standard, including achieving a higher standard of technical and transport infrastructure.

Bartke et al. (2016) mentioned that each brownfield represents specific challenges for the environment and adjacent community as it has been affected by former uses. As shown in Loures & Vaze (2018) the presence or absence of contamination is a crucial aspect of brownfield regeneration - if no significant contamination is detected, the value of the area increases, allowing for relatively rapid public or private remediation. Conversely, when pollution is detected, there is a significant reduction in the value of this place, depending on its extent and severity (see **Figure 1**).

According to Kadeřábková & Piecha (2009) brownfield regeneration depends on many factors. These factors include location, environmental burden, property relations, the existence of infrastructure, the relationship between the municipality and citizens, and last but not least, financial resources. According to Turečková et al. (2018) it is even more complicated to ensure that particular brownfield regeneration will be successful.

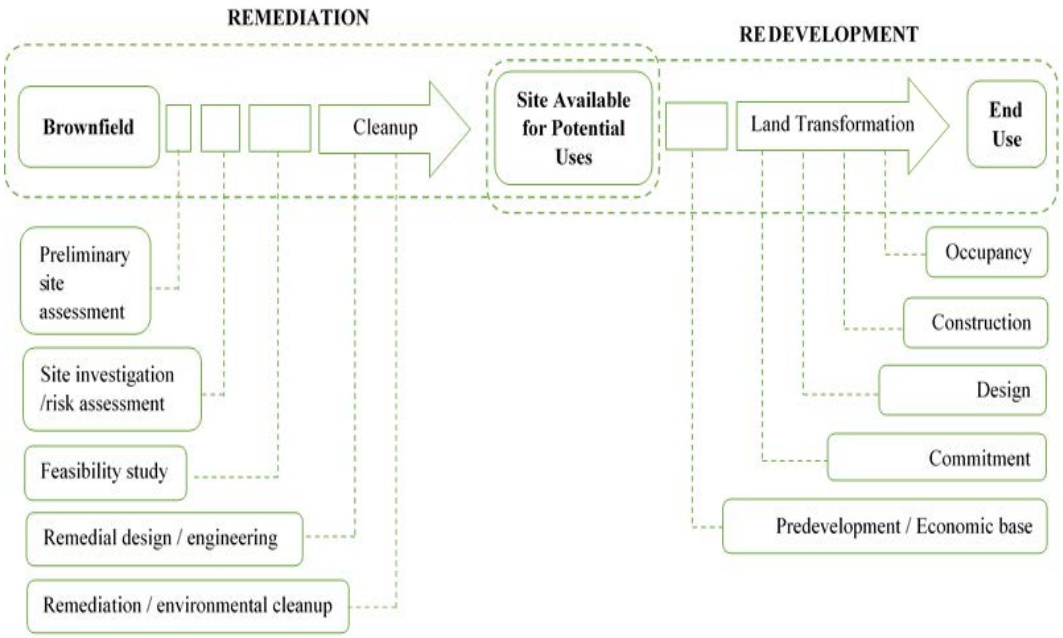

Fig. 1. Stages of brownfield redevelopment processes considering both contaminated and non-contaminated sites. (Source: Loures & Vaz 2018)

Last but not least brownfields have been associated with foreign direct investment as a potential location of investment in last decades - at the local planning level, where there is pressure to attract new developers with the aim of generating tax revenues and creating jobs, greenfields are often perceived as being more attractive to investors and are therefore willingly earmarked for development (Bartke & Schwarze, 2015). Investors usually prefer greenfield projects due to lower costs associated with construction, better localization outside the municipalities´centres or agglomeration aspects. On other hand brownfields regeneration has some advantages compared with greenfields: (i) they are often well located; (ii) infrastructure is available in these premises; (iii) originally degraded areas come back to live after regeneration and (iv) revitalised areas could bring people back to originally abandoned areas. The discussion is usually directed towards whether it would not be appropriate to make more use of existing industrial areas instead creation of new industrial zones. However, the disadvantage of brownfields is the fact that regeneration is a complex and costly process that also requires financial and administrative support from the public sector. In addition, brownfield

development in some countries have been set at the national level, with the twin objectives of furthering urban regeneration and reducing greenfield development (Ganser & Williams, 2007). On the other hand, this complexity requires considerable efforts to successfully initiate and complete brownfield revitalisation processes, including a proper strategy for the involvement of a considerable number of stakeholders with potentially divergent interests (Rizzo et al. 2015). In addition, brownfield regeneration could be a part of economic policy at both national and regional levels and some of them can be used by public sector (Schädler et al., 2011). As we known that brownfield regeneration is a challenge for regional and national authorities, the research question of this paper is whether there is a functioning strategic, financial and institutional framework in the Czech Republic to support brownfield regeneration.

In the present paper we analyse strategic, financial and regional links of brownfields regeneration in the Czech Republic. The authors´ motivation is to summarize the need to support the regeneration of brownfields as a significant measure of socio-economic development which is much more environmentally friendly than greenfields. Another motivating aspect is to provide the summary of the contribution of European financial resources. The paper is organised in these parts: (i) the introductory part is based on literature review which contains the theoretical background associated with brownfields and their regeneration in the Czech Republic; (ii) the second part focused on empirical results – it consists of strategic, financial and regional aspects of brownfields regeneration in the Czech Republic; (iii) and the last part recapitulates findings.

2. DATA

Empirical part of this paper is based on data obtained from national databases like National Brownfield Database which is coordinated by the CzechInvest (a state contributory organization subordinate to the Ministry of Industry and Trade of the Czech Republic). We focus on NUTS II regions which are the relevant regions for EU financial support within the main objectives of the EU cohesion policy. The region of the capital city Prague is excluded mainly due to statistical bias - as mentioned in Skrabal (2020) there is only one abandoned building registered in this database and it does not reflect the reality and problematics of the brownfield incidence in the capital city. The figure below (**Figure 2**) shows the number of brownfields and their area (in hectares). As seen from table we can see higher number of brownfields in North-West (123) and North-East (117). On the contrary, the lowest number of brownfields is in the Central Moravia and Central Bohemia regions.

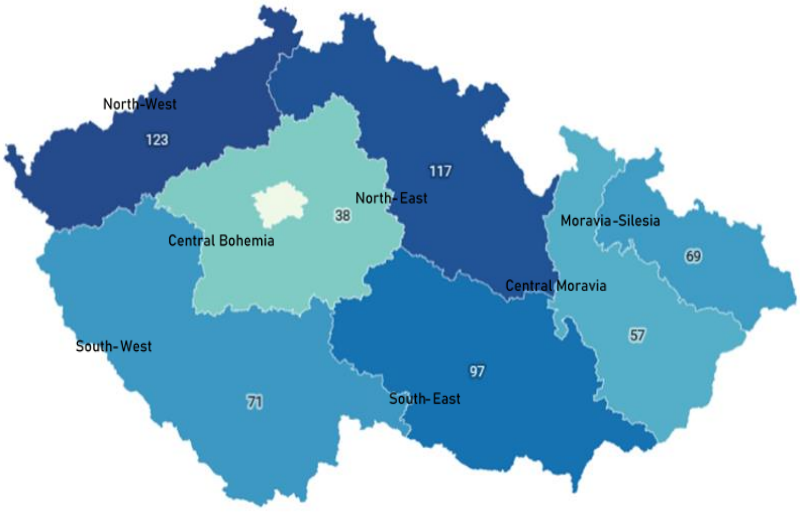

Fig. 2. The number of brownfields in NUTS 2 level (year 2020, excluding Prague region) *(Source of data: CzechInvest).*

Figure below (**Figure 3**) shows previous use of current brownfields – data are in hectares and the second number express the share of each category. It can be seen from the figure below that the three main categories of previous use dominate – industrial premises with the share of 42 %, military areas with share of 30 % and agriculture areas with the share of 14 %. Remaining uses of these abandoned areas represent a marginal percentage.

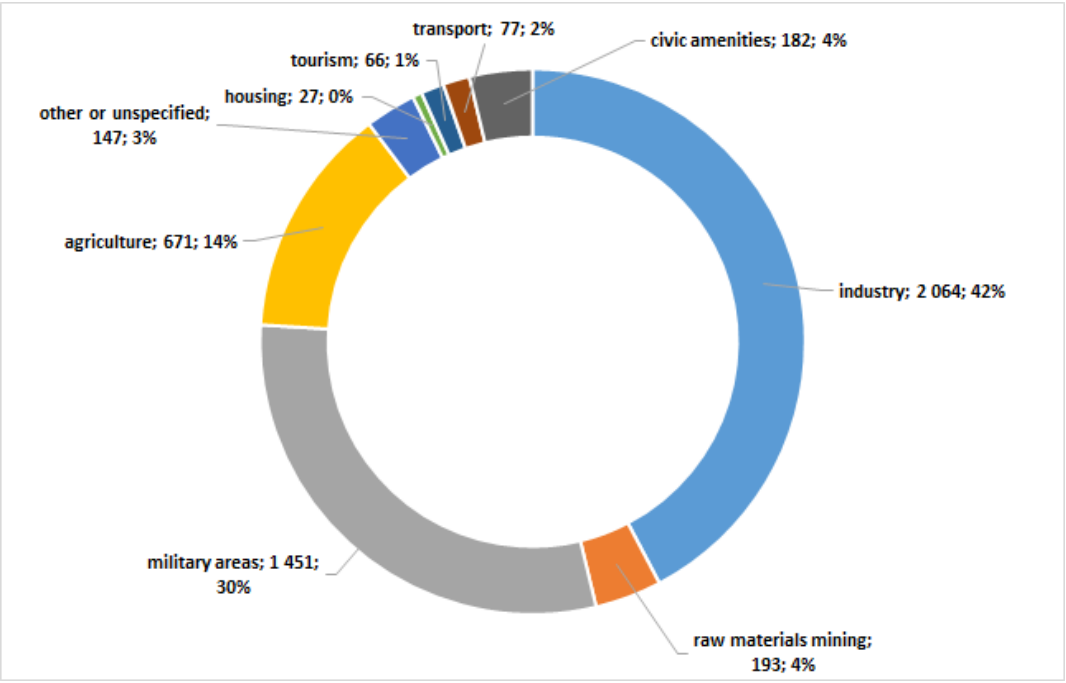

Fig. 3. Previous use of current brownfields *(Source of data: CzechInvest; Ekonom).*

3. STRATEGIC, FINANCIAL AND REGIONAL ASPECTS OF BROWNFIELDS REGENERATION

This part of the paper deals with strategic, financial and regional aspects of brownfields regeneration during the period 2000 to 2020. This part of the paper is based on publicly available strategic documents defining the development of the Czech Republic's strategy regarding brownfield regeneration. Data summarizing the drawn funds or allocated financial amount to support the regeneration of brownfields from EU funds are obtained mainly from secondary sources (national strategies, websites of individual operational programs or national programs).

3.1. Strategic documents and institutional framework

The brownfield regeneration strategy in the Czech Republic is derived from the National Brownfield Regeneration Strategy, which was first developed in 2004 and the last update took place in 2019 with a view to 2024. The pilot strategy was created as part of PHARE pre-accession assistance and the UK's experience with brownfield regeneration served as an example of a good practice. Moreover, another goal was to identify key characteristics and sizes of brownfields in the Czech Republic. According to Grulich and Gargoš (2009) development of this strategy was problematic, as it turned out that the British experience is not fully transferable to the Czech environment, mainly due to the different functioning of local governments. Therefore, the government commissioned the Ministry of Trade and Industry and CzechInvest (business and investment development agency) to

develop a strategy that reflects the specifics of the Czech legal environment. CzechInvest began preparing an Exploratory Study for the Localization of Brownfields, which was also to serve as supporting material for the upcoming programming period 2007-2013, in which the Czech Republic could already fully draw on EU funds.

The first conceptual strategy was adopted in 2008. The basic goal of the Strategy was to create a suitable environment for fast and efficient implementation of regeneration projects and prevention of new brownfields. In addition to the main goal, three medium-term goals were defined, the fulfillment of which was expected by the end of 2013: (i) maximum involvement of available EU resources for brownfield regeneration in the programming period 2007-2013; (ii) taking into account the possibility of regeneration of brownfields for non-industrial use (e.g. mixed urban function, civic amenities, agriculture, housing) and (iii) development of an education system in the field of brownfield regeneration and ensuring the professionalization of public administration in this area. The following long-term goals were set: (i) reduction of the number of brownfields and occupation of agricultural land for new construction in accordance with the principles of sustainable development; (ii) prevention of brownfields; (iii) improving the quality of the urban environment and socio-economic development of the affected regions; (iv) improving the quality of the environment and removing old environmental burdens in brownfield sites (this goal has both a medium and long-term dimension); (v) targeted and effective use of public funds to support the regeneration of brownfields, where public intervention is necessary and justified; (vi) introduction and ensuring the application of best practice in the implementation of brownfield regeneration projects, support for professionally managed implementation of regeneration.

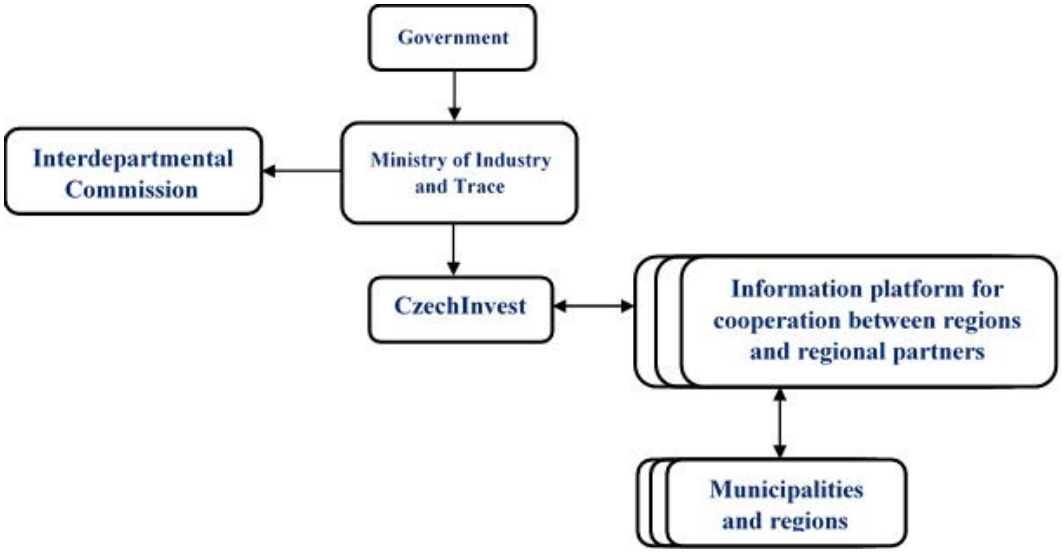

Fig. 4. Initial institutional framework *(Source of data: National Brownfield Regeneration Strategy, 2008).*

This strategy is followed by another, which is for the period from 2019 to 2024 (National Strategy of Brownfields Regeneration). The vision of this strategy is to make brownfields competitive areas for new uses and development. The main goal is developing a coordinated approach to brownfield regeneration through state policies, financial programs and appropriate conditions that will enable brownfields to find new economic or public benefits. The reuse of brownfields will contribute to the economical use of the built-up area and the development of towns and villages. The strategy emphasizes the involvement and coordination of all stakeholders (Ministry of Industry and Trade, CzechInvest, Ministry of Agriculture, Ministry of Regional Development, Ministry of Environment) both horizontally and vertically (see **Figure 4**). Other priorities are Financial Support, Territorial

Measures and Education, Research and Awareness. All these areas proved to be key for setting up support for brownfield regeneration in the Czech Republic.

Moreover, as brownfields regeneration is cross-sectional problem it is mentioned in several national documents that overlap in both programming periods: (i) Regional Development Strategy of the Czech Republic 2014-2020; (ii) Strategies to support the use of the potential of cultural heritage, 2014; (iii) Territorial development policy, 2014; (iv) Program for the support of business real estate and infrastructure, version 2015; (v) Strategic Framework for Sustainable Development of the Czech Republic, 2010; (vi) State Environmental Policy of the Czech Republic 2012-2020; (vii) Principles of Urban Policy, 2010. Current institutional framework is shown in **Figure 3** below.

The one of NSBR measure is the "National Brownfields Database", which registers selected localities corresponding to the definition of brownfields. It is divided into a public part of the database serving as an offer of sites for investors. The non-public part is used for statistical purposes on the monitored phenomena and creates overviews on the support of brownfield regeneration.

3.2. Financial sources

If look at financial sources that could be used for brownfield regeneration in the initial phase (years from 2000 to 2006) there existed few EU sources. As mentioned in Garb and Jackson (2010) study Czech Republic as the candidate country (till April 2004) and the member state (from May 2004) could draw funds for the regeneration of brownfields from these funds which are listed in a **Table 1**.

Table 1.

EU programme titles and priorities available for brownfield regeneration during the period 2000‑2006

Programme name	Priority
PHARE 2001	Border regions assistance - best practices
ISPA	Reuse of agricultural brownfield property
Cohesion fund	Remediation of environmental damage
OP Industry	Industrial premises
OP Infrastructure	Removing environmental damage
OP SROP	Urban regeneration
OP Development of Human Resources	Regionally based education (included support for training and promotional activities on brownfields)
JPD2 Prague	Measure 1.2: Regeneration of damaged and unsuitably used areas

(Source: Garb and Jackson (2020).

As the Czech Republic is the EU Member State from 2004, in addition to national financial resources, it could also fully draw funds from European structural and investing funds for the regeneration of brownfields. No specific program was designed to support brownfields regeneration during 2007-2013 programming period. However, it was possible to draw subsidies within several operational programs. Brownfield regeneration requires a relatively large number of financial resources and as written in 2008 Strategy; maximum use of EU funds was expected. In addition, national resources are used to regenerate brownfields. First, we will focus our attention on funds obtained from EU funds. If we look at the programming period 2007 to 2013, we will find that a specific program designed directly for the regeneration of brownfields has not been develop. Thus, funding for brownfield regeneration took place across programs. Brownfield regeneration was financed from Operational Programme Environment (OPE), Operational Programme Enterprise and Innovation (OPEI), Regional Operational Programmes (ROPS) and Rural Development Programme (RDP). As written in National Strategy of Brownfield regeneration 2019 – 2023, the accuracy of the statistics seems to be a problematic aspect in the evaluation of the used financial resources from EU

projects - in addition to the mentioned OPs that has been used for brownfield regeneration, brownfield regeneration in other areas and programs was supported at the same time as reconstruction projects. In some OPs, it was not possible to separate the reconstruction of buildings from the regeneration / reconstruction of brownfields.

In general, projects of public entities (especially municipalities and regions) using European subsidies most often concerned the re-use of brownfields for public facilities. As can be seen from **Table 2** subsidies for this type of project were provided from seven Regional Operational Programs. In total, there were 211 projects with a subsidy of over EUR 214 million. **Table 2** below shows that 531 brownfields regeneration projects in the amount of EUR 259 million were supported from the OPEI. Another important program for the regeneration of rural brownfields was the RDP, which supported projects of regeneration and reconstruction of real estate serving agricultural business, civic amenities and business in rural communities (total of 3,330 reconstruction projects of used and abandoned properties were revitalized with subsidies in the amount of EUR 266 million). Subsidies in the amount of EUR 111 million were allocated to projects related to the removal of old environmental burdens from the OPE.

Table 2.

Support from EU funds for projects of reconstruction, revitalization, regeneration and removal of old environmental burdens (years 2007-2013)

Programme	Reconstruction – number of projects	Number of brownfields	Subsidies for brownfields (in millions EUR)
OP Environment	156	33	111.24
OP Enterprise and Innovation	975	531	259.22
Rural Development Programme	3 330		267.16
Regional Operational Programmes		211	214.61
Total			**852.23**

(Source of data: National Brownfield Regeneration Strategy 2019-2024).

If we look at these specific OPs more deeply, we can see that the vast majority of brownfields revitalization projects focused on removing old environmental burden (see **Table 3**). In the case of the OPE brownfield revitalization was financed through the area of support called Properties mainly. In this context, it is important to mention the significant regional impact of this support, which is shown in **figure 5** below. It shows that the most projects were financed within NUTS II regions in the east of the Czech Republic (Moravia-Silesia, Central Moravia, South – East or North – East), where there are a large number of agricultural brownfields that have just been the subject of regeneration projects.

Table 3.

Allocation from Operational Programme Environment (years 2007 – 2013)

Area of support	Total allocation (in mil. EUR)	Number of brownfield projects	Allocation for brownfield projects (in mil. EUR)
4.2 Removing old environmental burden	248.23	32	111.22
6.5 Regeneration of urban landscape	0.050	1	n.a.
Total	**248.28**	**33**	**111.22**

(Source of data: National Brownfield Regeneration Strategy 2019-2024).

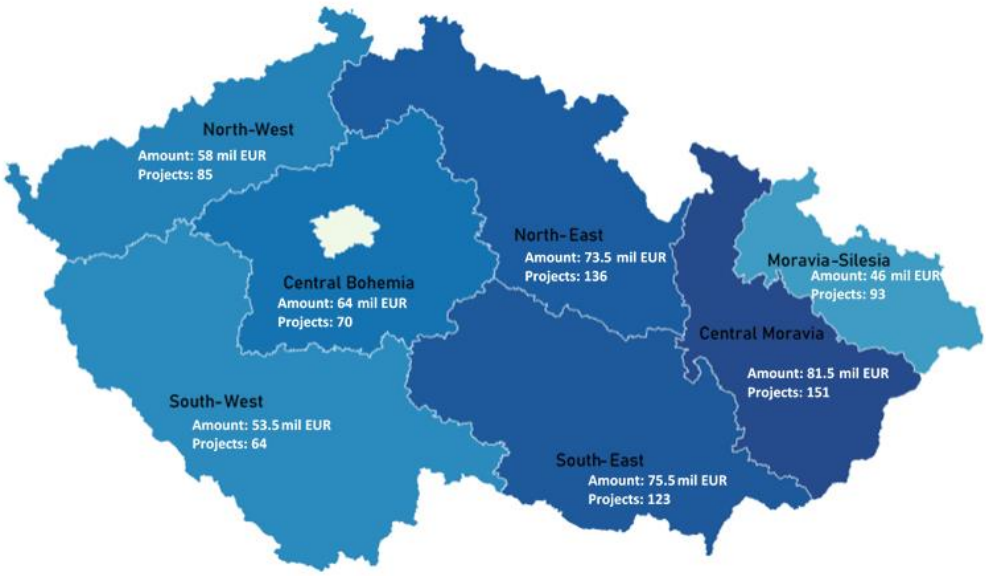

Fig. 5. Brownfield projects support in cohesion regions from OP Enterprise and Innovation (years 2007 – 2013). (Source of data: National Brownfield Regeneration Strategy 2019-2024).

Within the RDP, it was possible to use several areas and sub-areas of support for the regeneration of brownfields, which is illustrated in **Table 4**. It is evident that the largest number of brownfield revitalizations was financed under axis 1.1 Modernization of agricultural holdings. The second largest number of projects falls under Axis 3 Diversification of the rural economy.

Table 4.

Brownfield regeneration from the Rural development programme (years 2007 – 2013)

Area of support/programme	Total allocation for sub-area (mil. EUR)	Number of brownfield projects	Allocation for reconstruction (mil. EUR)
I.1 Modernization, vč. I.3.2.	386.88	2 613	169.15
III.1 Business diversification	284.43	535	60.99
III.2 Rural areas	196.45	182	51.06
Celkem	**867.76**	**3 330**	**281.20**

(Source of data: National Brownfield Regeneration Strategy 2019-2024).

If we look at the support of brownfield regeneration from regional operational programs, we see that the largest number of supported projects was in the NUTS II Moravia - Silesia and Nort-East regions, but the largest support was provided by brownfield regeneration in North-West and Central Bohemia (see **Figure 6**).

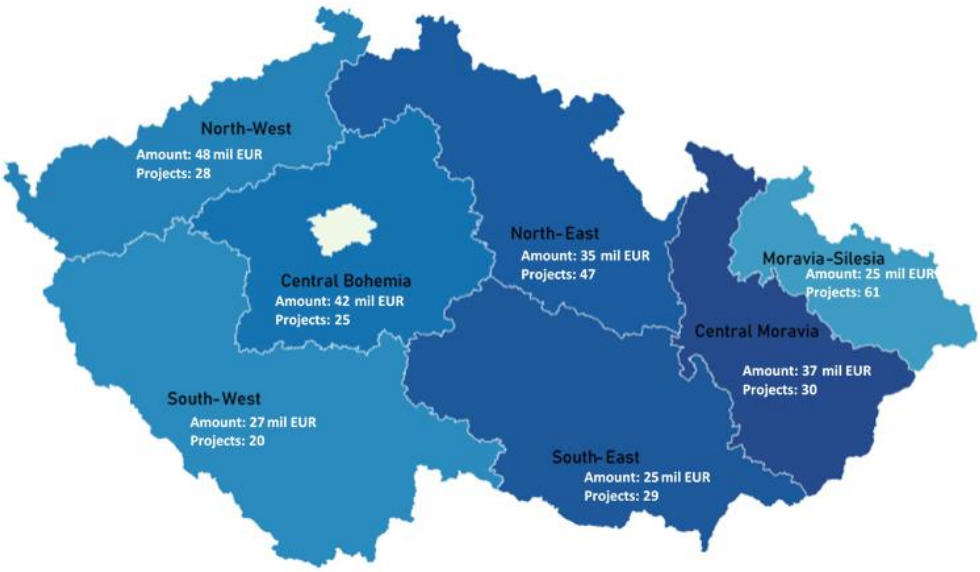

Fig. 6. Brownfield regeneration subsidies from ROPS (years 2007 – 2013) *(Source of data: National Brownfield Regeneration Strategy 2019-2024).*

3.3. Financial sources 2014 to 2020

Similar to the previous period it is possible to draw subsidies within several operational programs. Although the setting of OPs is similar, the financial amount that can be drawn for the regeneration of brownfields has been reduced. Due to the fact that this period is still running, this section only contains estimates based on publicly available information as of end 2019. **Figure 7** below shows institutional and financial framework of this programming period 2014 – 2020.

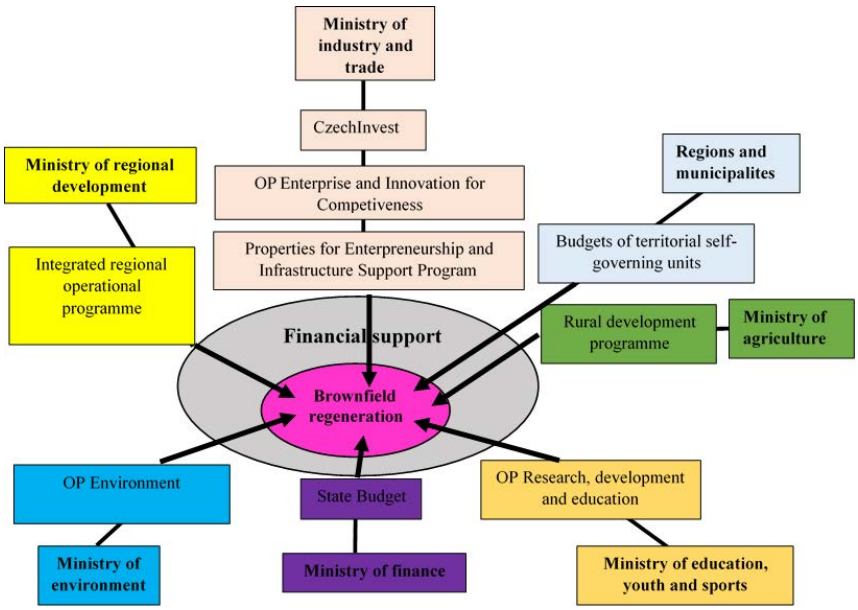

Fig. 7. Current institutional and financial framework *(Source of data: National Brownfield Regeneration Strategy 2019-2024).*

The OPEI was replaced by the Operational Programme Enterprise and Innovation for Competiveness (OPEIC) – Program Properties. The aim of the program is to facilitate the modernization of obsolete, spatially and technically unsatisfactory buildings for small and medium-sized businesses, for the implementation of supported economic activities or their replacement by new buildings for business in all regions except the region of the capitol city Prague, thus enabling the maintenance and increase of employment in the region or contributing to the improvement of the environment or working conditions of employees. An important circumstance is that this program only supports comprehensive reconstructions (not partial interventions and repairs) and also previously supported "greenfield" constructions were excluded. Within this program five calls were announce till mid 2020: (i) call 1 to 3 which had general setting focusing on brownfield regeneration; (ii) call 4 named Tourism which aims exclusively at the modernization of obsolete, spatially and technically unsuitable facilities, buildings and premises, which will be used for the development of business activities and services of SMEs in tourism; and (iii) call 5 named Coal Regions that which aims to facilitate SMEs in the modernization of obsolete and technically unsuitable buildings for the implementation of supported economic activities, or their replacement by new business buildings. The sum of current calls represents 5.8 billion CZK, which is almost 83 % of the total allocated amount for this program (EUR 200 million). If we focus on individual calls, the financially largest calls were 1, 3 and 5. **Table** 5 also shows a relatively different maximum allocation per project – it varies from EUR 36,000 to 7,272,00.

Table 5.

Operational Programme Enterprise and Innovation for Competiveness – Program Properties (years 2014 – 2020)

Call	Total allocation possible for brownfields regeneration (in mil. EUR)	Minimum and maximum amount for one application (in thousands EUR)
1	54.5	Between 36 and 7 272
2	34.5	Between 36 and 1 818
3	51.0	Between 36 and 1 090
4	29.0	Between 36 and 3 636
5	51.0	Between 36 and 3 636
Total	220.0	

(Source of data: Operational Programme Enterprise and Innovation for Competiveness).

Available statistical data relate to calls 1 and 2 only (details on calls 3 to 5 were not known at the time of writing) - 270 projects were supported under this program with a current allocated subsidy of EUR 91 million.

Another operational program that can be used for the needs of brownfields regeneration in this programming period is the Operational Program Environment (OPE 2014-2020), which follows on from a similar program in the previous period (OPE 2007-2013). The OPE 2014-2020 is involved in the remediation of severely contaminated sites for which there is evidence of risk to human health and ecosystems. The program is divided into five priority axes, of which in the case of brownfield regeneration, priority axis 3 can be used: Waste and material flows, environmental burdens and risks (Specific Objective 4: To complete the inventory of and remove environmental burdens). In relation to commercial real estate, support can be obtained under Priority Axis 5: Energy savings (Specific Objective 1: To reduce the energy intensity of public buildings and increase the use of renewable energy sources and Specific Objective 3: To reduce the energy intensity and increase the use of renewable energy sources in buildings of central government institutions). The total number of calls and total available allocation for brownfields regeneration is shown in **Table 6**.

Table 6.

Operational Programme Environment (years 2014 – 2020)

Call	Specific objective	Total allocation available for brownfields regeneration (in mil. EUR)
6	3.4 To complete the inventory and remove environmental burdens	11.0
7	3.4 To complete the inventory and remove environmental burdens	20.4
19	5.1 To reduce the energy intensity of public buildings and increase the use of renewable energy sources	109.1
36	3.4 To complete the inventory and remove environmental burdens	21.8
39	5.1 To reduce the energy intensity of public buildings and increase the use of renewable energy sources	109.1
44	3.4 To complete the inventory and remove environmental burdens	18.2
65	3.4 To complete the inventory and remove environmental burdens	14.5
70	5.1 To reduce the energy intensity of public buildings and increase the use of renewable energy sources	109.1
75	3.4 To complete the inventory and remove environmental burdens	14.5
77	3.4 To complete the inventory and remove environmental burdens	5.5
86	3.4 To complete the inventory and remove environmental burdens	7.3
99	3.4 To complete the inventory and remove environmental burdens	7.3
100	5.1 To reduce the energy intensity of public buildings and increase the use of renewable energy sources	109.1
121	5.1 To reduce the energy intensity of public buildings and increase the use of renewable energy sources	91.0
135	5.3 To reduce the energy intensity and increase the use of renewable energy sources in buildings of central government institutions	72.7
146	5.1 To reduce the energy intensity of public buildings and increase the use of renewable energy sources	72.7
152	5.3 To reduce the energy intensity and increase the use of renewable energy sources in buildings of central government institutions	18.2

Other operational program that allows financial support for the regeneration of brownfields is the Rural Development Program for the period 2014 to 2020 (RDP 2014-2020), which builds on the previous RDP program 2007-2013. The supported areas of the Program are divided into six priorities. Real estate concerns in particular priority axis 2: Increasing the viability of agricultural holdings and the competitiveness of all types of agricultural activity in all regions and promoting innovative agricultural technologies and sustainable forest management. Within this priority axis these activities are supported: (i) - investment in agricultural holdings; (ii) forestry infrastructure; (iii) start-up of young farmers; (iv) investments to support energy from renewable sources; and (v) investments in non-agricultural activities.

5. CONCLUSIONS

The paper dealt with the issue of brownfields regeneration in the Czech Republic during the year 2000 to 2020. In comparison with Western Europe countries, the problem of brownfields began to be solved with a delay of approximately twenty years, which resulted from the existence of a centrally planned economy.

After 1989, the main activities focused on the process of transition to a market economy and the problem of abandoned areas seemed to be marginal at that time so no strategy was developed. Opening of economy, the loss of traditional consumer markets, low competitiveness vis-à-vis foreign producers have led to traditional sectors such as industry and agriculture starting to clear their positions in many sub-sectors, which has led to the emergence of abandoned sites defined as brownfields. The government began to address this serious phenomenon only after the years 2000, when there was a huge expansion of greenfield projects and the centers began to deepen problems with abandoned industrial areas, in the case of rural areas it were agricultural areas.

The first analysis and strategies had been developed in the first decade of this century. As the Czech Republic joined the European Union, it was clear that financial support was possible not only from national sources. Firstly, the Czech Republic use pre-accession funds (PHARE, ISPA). Afterward it was possible to prepare measures to solve the problem of brownfields regeneration within specific operational programs. It can be stated that brownfields regeneration is the cross-sectional task so there are more subjects responsible for this process especially the Ministry of Industry and Trade, Ministry of Agricultural, Ministry of Environment and also the Ministry of Regional Development.

If we look at regional differences (on the example of cohesion regions (NUTS II regions) other than the region of the capital city of Prague) in the existence of brownfields or the number of projects implemented for their regeneration, certain differences can be seen – e.g. most projects were implemented within the brownfield projects support in cohesion regions from OP Enterprise and Innovation in South-east region, North-East region and Central-Moravia. In addition, if look at the total number of implemented projects within individual Regional operational programs we can see that the most successful regions were Moravia-Silesia and North-East regions. In comparison in the case of total spent money we can see that leaders were North-West and Central Bohemia regions.

Moreover, within the brownfields regeneration, a relevant regional distribution appears to be key factor of the national approach to this problem, with an emphasis on addressing this issue in structurally lagging-behind regions or rural regions where there is an insufficient supply of private capital that prevents the natural regeneration of these abandoned sites. The important task is to evaluate the number of implemented projects and the total amount of funds intended for the brownfields regeneration in this ending programming period. Another challenge is to effectively combine national and EU financial resources in the next programming period 2021 to 2027.

ACKNOWLEDGMENT

This paper was supported by the project SGS/20/2019 "Brownfields in urban and rural space: geographic, economic, business and public administrative contexts and their importance for regional development (BURAN 2)"

REFERENCES

Ahmad, N., Zhu, Y., Ibrahim, M., Wagas, M. & Waheed, A. (2018) Development of a Standard Brownfield Definiton, Guidelines, and Evaluation Index System for Brownfield Redevelopment in Developing Countries: the Case of Pakistan. Sustainability, 10 (12), 1 -22.

Alberini, A., Longo A., Tonin, S., Trombetta, F. & Turvani M. (2005) The role of liability, regulation and economic incentives in brownfield remediation and redevelopment: evidence from surveys of developers. *Regional Science and Urban Economics*, 35 (4), 327-351.

Bartke, S., Stanislav, M., Klusacek, P., Pizzol L., Alexandrescu, F., Frantal B., Critto, A. & Zabeo, A. (2015) Targeted selection of brownfields from portfolios for sustainable regeneration: User experiences from five cases testing the Timbre Brownfield Prioritization Tool. *Journal of Environmental Mana*gement, 184 (1), 94–107.

Bartke, S. & Schwarze, R. (2015) No perfect tools: Trade-offs of sustainability principles and user requirements in designing support tools for land-use decisions between greenfields and brownfields. *Journal of Environmental Management*, 153. 11–24

Filip, S. & Cocean, P. (2012) Urban Industrial Brownfields: Constraints and Opportunities in Romania. *Carpathian Journal of Earth and Environmental Sciences*, 7 (4), 155-164.

Franz, M., Pahlen, G., Nathanail, P., Okuniek, N. & Koj, A. (2006) Sustainable development and brownfield regeneration. What defines the quality of derelict land recycling? *Environmental Sciences*, 3 (2), 135-151.

Ganser,R. & Williams, K. (2007) Brownfield development: Are we using the right targets? Evidence from England and Germany. *European Planning Studies*, 15 (5), 603–622.

Garb, Y., & Jackson, J. (2010) Brownfields in the Czech Republic1989–2009: The long path to integrated land management. *Journal of Urban Regeneration and Renewal*, 3 (3), 263-276.

Grulich,T. & Gargoš, I. (2009) Brownfieldy v České republice: Koncepční podpora regenerace agenturou Czechinvest. *Urbanismus a územní rozvoj,* 12 (6), 6-8.

Gwosdz, K., Domaňski, B. & Bilska-Wodecka, E. (2020) Localised capabilities as an intermediating factor in the transition from an old to a new development path: The case of post-socialist industrial towns. *Moravian Geographical Reports*, 28 (2), 124-135.

Kadeřábková, B. & Piecha, M. (2009) *Brownfields. Jak vznikají a co s nimi*. Praha: C.H. Beck.

Klusáček, P. et al. (2018) Good governance as a strategic choice in brownfield regeneration: Regional dynamics from the Czech Republic. *Land Use Policy*, 73, 29-39.

Klusáček, P. (2005) Downsizing of Bituminous Coal Mining and the Restructuring of Steel Works and Heavy Machine Engineering in the Ostrava Region. *Moravian Geographical Reports*, 13 (2), 3-12.

Kunc, J., Martinát, S., Tonev, P. & Frantál, B. (2014) Destiny of urban brownfields: spatial patterns and perceived consequences of post-socialistic deindustrialization. *Transylvanian Review of Administrative Sciences*, 10 (41E), 109-128.

Loures, L. & Vaz, E. (2018) Exploring expert perception towards brownfield redevelopment benefits according to their typology. *Habitat International*, 72 (February), 66-76.

Matlovič, R., Ira, V., Sýkora, L., Szczyrba, Z., (2001) Procesy transformacyjne struktury przestrzennej miast postkomunistycznych (na przykładzie Pragi, Bratysławy, Ołomun´ ca oraz Preszowa). In: Jaz˙ dzewska, I. (Ed.), *Miasto postsocjalistyczne – organizacja przestrzeni miejskiej i jej przemiany(*II), XIV Konwersatorium Wiedzy o Mie´scie. Uniwersytet Łódzki, Łód´ z, pp. 9–21.

MPO (2020) Narodní strategie regenerací brownfieldů 2019-2024. Available from: https://www.mpo.cz/cz/podnikani/dotace-a-podpora-podnikani/podpora-brownfieldu/narodni-strategie-regeneraci-brownfieldu-2019-2024--248322/ [Accessed October 2020].

Navrátil, P. et al. (2019) The Fate or Socialist Agricultural Premises: to Agricultural ´Brownfields´and Back Again? *Moravian Geographical Reports*, 27 (4), 207-216.

Osman, R., Frantál, B., Klusáček P., Kunc, J. & Martinát, S. (2015) Factors affecting brownfield regeneration in post-socialist space: The case of the Czech Republic. *Land Use Policy*, 48 (2015), 309-316.

Rizzo, E., Pesce, M., Pizzol, L., Alexandrescu, F. M., Giubilato, E., Critto, A., Marcomini, A. & Stephan. B. (2015) Brownfield regeneration in Europe: identifying stakeholder perceptions, concerns, attitudes and information needs. *Land Use Policy*, 48, 437–453.

Schädler, S. et al. (2011) Designing sustainable and economically attractive brownfield revitalization options using an integrated assessment model. *Journal of Environmental Management*, 92 (3), 827-837.

Skrabal, J. (2020) What Can We Learn from Brownfield Databases? Exploring specifics of the location of brownfields in the Czech Republic. *Geographia Technica*, 15 (2), 191-201.

Turečková, K., Nevima, J., Škrabal, J. & Tuleja, P (2019) Categorization of Impact of the Selected Variables for Potential Brownfield Regeneration in the Czech Republic by Means of Correspondence Analysis. *Geographia Technica*, 14 (2), 120-130.

Turečková, K., Nevima, J., Škrabal, J. & Martinát, S. (2018) Uncovering patterns of location of brownfields to facilitate their regeneration: Some remarks from the Czech Republic. *Sustainability*, 10 (6), 224-234.

Wirth, P. & Lintz, G. (2006) Rehabilitation and Development of Mining Regions in Eastern Germany – Strategies and Outcomes. *Moravian Geographical Reports*, 14 (2), 69-82.

ANALYSIS OF CROSS-BORDER COMMUTERS' SPATIAL MOBILITY BETWEEN WESTERN REGIONS OF HUNGARY AND SLOVAKIA

Péter KARÁCSONY[1], Mikhail V. VINICHENKO[2], Imrich ANTALÍK[3], Lóránt Dénes DÁVID[4*] and László VASA[5]

DOI: 10.21163/GT_2021.161.11

ABSTRACT:
Commuting, defined as daily traveling for employment purposes, has gradually grown in importance in the past decades in Eastern European countries. According to Eurostat, although the freedom of movement may have encouraged cross-border commuting in the EU, it accounted just for 0.9 % of the EU-28 workforce. Between the highest number of cross-border commuters, we can find Slovakian (147 thousand), and Hungarian (111 thousand) workers. We chose this topic because there has been a significant increase in the willingness to commute for economic reasons in recent years, and we want to explore the reasons of this. In the case of both examined countries, the inhabitants of the western regions are characterized by high willingness for cross-border commuting. Due to this reason, in own research, we conducted a questionnaire survey in the western regions of Hungary and Slovakia. The results indicate that there are similarities between Hungarian and Slovakian commuters. The regression analysis clearly showed that commuter satisfaction is most affected by the variety of jobs offered and the level of wages.

Key-words: *Cross-border, Mobility, region, Regional differences, Spatial analysis*

1. INTRODUCTION

Since 1990, there have been a number of important changes in the Hungarian and Slovak society, such as the transition from a centrally planned economy to a market economy, the introduction of parliamentary democracy, and integration into the European Union.

The transition has typically been characterized by a collapse of state-owned firms, which was only partially offset by an increase in private sector (Kolodko, 1994; Filep et al., 2013). While before the change of regime, local state bodies had the task of providing employment, they lost this role with the change of regime (Durán, 2001). One of the worst effects of regime change on people was the loss of their jobs (Sokol, 2001; Magda, 2013). According to Fialová and Schneider (2009) over the last three decades, employee habits have changed significantly, with many workers being forced to leave their homes and work in another region or even another country. For these reasons the commuting from eastern European countries to western Europe has become widespread (De Simone and Manchin, 2012). First time mostly in an illegal way, but after the European Union integration, in a

[1]*Eötvös Loránd University, Institute of Research on Adult Education and Knowledge Management, Budapest, Hungary, karacsony.peter@ppk.elte.hu*
[2]*Russian State Social University, Department of Personnel Management and Personnel Policy, Moscow, Russia, mih-vas2006@yandex.ru*
[3]*Janos Selye University, Faculty of Economics and Informatics, Department of Economics, Komarno, Slovakia, antaliki@ujs.sk*
[4*]*Szent István University, Faculty of Economics and Social Sciences, Gödöllő, Hungary, david.lorant.denes@szie.hu (corresponding author)*
[5]*Széchenyi István University, Győr, Hungary, laszlo.vasa@ifat.hu*

legal way too (Fassmann and Münz, 2002). Commuting is an economically, socially, culturally, and environmentally important process for both the individual and society.

We choose this research topic for two main reasons. First of all, because cross-border commuting is popular and an important topic in scientific research nowadays. Secondly, these scientific literatures are mostly dealing with commuting between two western European countries (De Gijsel and Janssen, 2000; Medeiros, 2019; Buch et al., 2009) or the western and eastern European countries (Bujdosó et al 2011; Bujdosó et al. 2015; Bagdi, 2018; Cavallaro and Dianin, 2020) and there is lack of examining the cross-border commuting between two eastern European countries. Although data and estimates indicate that the magnitude of this is significantly higher than the expectation.

The main objective of this study to analyse the characteristics of the labour force commuting along Slovakian-Hungarian cross-borders. The main purpose was to study commuters' behavior and identify the main reasons for spatial mobility in the western region of examined countries.

2. LITERATURE REVIEW

In the 1980s, unusual labour trends had emerged in the European labour market. These changes were followed by individual globalization processes, and with various changes in the world economy, labour began to move freely (Lipták, 2013).

The functioning of any market is based on the pursuit of balance between supply and demand, which is regulated by price. In the labour market, this relationship is between demand by the employer and supply by the employee (Lipták, 2019). In case of the labour market, the price is the wage that is created through a bargain between the employer and the employee (Kwiatkowski, 2011).

Work, which plays a key role in a person's life is present in our daily lives for a variety of reasons, because we need money to meet our needs, or because we love to do it, but it also helps to deepen our social relationships. According to the literature, most people work for financial reasons (Grund and Sliwka, 2007).

Commuting is one of the basic elements of modern society. With the improvement of transport, it has become possible for workplace and residence to be spatially separated (Rouwendal, 1998). With the strengthening of the spatial concentration of jobs, commuting became more and more important, the main direction of which has developed between the countryside and the city. Most studies in the scientific literature are related to commuting between rural areas and city centers (Green and Meyer, 1997; Green et al., 2019; Lavesson, 2016). The motivations of classical commuting are mainly the workplace as a commuting goal, so the commuter would not be able to get a job in his own place of residence, or only at the cost of great compromises. Thus, it is necessary to go to a geographically another settlement every day to work (Sharma, 2019). Commuting is shaped by economic, social, and geopolitical factors and this renders it a multivariate phenomenon.

The meeting of different economic systems can generate spatial movement and commuting processes, which can be fundamentally different from "traditional" commuting movements within a country (Bochkarev, 2019). The meeting of different economic systems is manifested first and foremost in the difference in prices and wages, which have the strongest impact on labour mobility (Paril et al., 2015; Dauth and Haller, 2020). However, the direction of spatial mobility is also affected by other differences, for example working conditions, social benefits differences, or shortage in professional qualifications of the labour force in the border area. In spite of differences in taxes, legal systems can also strengthen cross-border commuting (Jin, 2019).

The state border modifies the geographical features that affect the direction and distance of commuting. This modification may vary in magnitude and quality depending on the functions of the boundary. Strong spatial structural relations between the areas on both sides of the border reduce the distorting effects of the state border. At the same time, geographical features, like the meeting of peripheral areas, the difficult interoperability of the border, and few transit routes can prevent the development of cross-border commuting (Van der Veen and Evers, 1983). From 2004, when joining the European Union, this last barrier has also disappeared and the citizens of both examined countries were given the opportunity of free movement and to work freely. The principle of a common market in the European Union is the free movement of production factors. This means not only the free

movement of goods, services, and capital but also the free movement of labour. The Treaty of Rome, which established the European Economic Community, already provides the establishment of a common labour market. The main goal of the integration, which was based on economic interests, was to increase competitiveness in the regions with a coordinated labour market. According to European Union law, the free movement of workers means that nationals of any member state of the European Union can take up employment in another member state with the same conditions as the nationals of that particular member state. In particular, no discrimination based on nationality is allowed. There are several definitions of the term "cross-border commuter". According to ETUC (2015) terminology, cross-border commuters are workers (including self-employed workers) who pursue their profession in one Member State and geographically reside in another (neighbouring) Member State. The second criterion is that cross-border commuters return to their place of residence abroad at least once a week.

The drivers of cross-border workers can be several. The social benefits may be one of the main reasons for commuting. According to the EC Regulation 883/2004, an individual is subject to the legislation of the country where he actually works as an employed or a self-employed person, independently of where he lives, so the country of work is responsible for his social benefits.

Summarizing the essence of the literature, it can be stated that employees who, for quantitative or structural reasons, are unable or unwilling to find a workplace in their place of residence decide for commuting. Commuting to workplaces in other settlements typically takes place within the border, but with the accession of eastern European countries to the European Union, the borders were opened for eastern workers. With the removal of geographical barriers to the free movement of labour, commuting has become available primarily to people living along the border. In our publication, we examine the characteristics of these commuters.

3. DATA AND METHODS

In the first part of own research, we compared the development of the western regions of both countries and their labour market characteristics based on secondary data. In our primary research, we conducted a quantitative (questionnaire) survey. In 2020, a total of 724 questionnaires were sent out using the snowball method, of which 342 evaluable responses were returned by October 2020, of which 205 were Slovak respondents and 137 were Hungarian. The selection of commuters was assisted by regional employment offices, our former university students, and the university partner contacts. When handing out the questionnaire, we asked everyone that if they had an acquaintance who they knew was a commuter, then give our questionnaire to them.

Fig. 1. Research area (own editing by using ArcGIS software).

The criteria for selecting the respondents were that the commuter must work in the Hungarian or Slovak labour market. The questionnaire consists of 3 main parts: 1) demographic information; 2) travel information, travel time, distance; 3) reasons for commuting, satisfaction, factors affecting commuting, etc.

The official classification of research area were the European Union NUTS 2 level regions: from Slovakia Bratislavsky Kraj, Západné Slovensko, and from Hungary Közép-Dunántúl, Nyugat-Dunántúl regions (see **Fig. 1**). These geographic regions are located along the Slovak-Hungarian-Austrian-Czech border. These regions have been the focus of research because they are characterized by a high degree of development and a high level of foreign capital investment. These geographic regions attract many workers from the whole country, many of whom take part in cross-border commuting.

The data obtained during the questionnaire survey were analysed using regression analysis by SPSS.21. In the following, the main results of our own research are presented, first, we introduce secondary comparative research, after the results of our questionnaire survey.

4. RESULTS AND DISCUSSION

In the first part of own studies, we analyse the main macro-economic and labour market characteristics of the studied regions, from the accession to the European Union until 2020.

After the 2004 EU integration commuting abroad has changed significantly in case of the examined regions. While initially, it was mainly characteristic for the inhabitants of the Západné Slovensko region, by 2019 this ratio had almost equalized between the Nyugat-Dunántúli and Západné Slovensko regions. In 2019, 36 600 people commuted from the Západné Slovensko region, compared to 38 400 people in the Western Transdanubia region. Based on the data, it can be stated that commuter activity is significant in the western region of both examined countries (see **Fig. 2**).

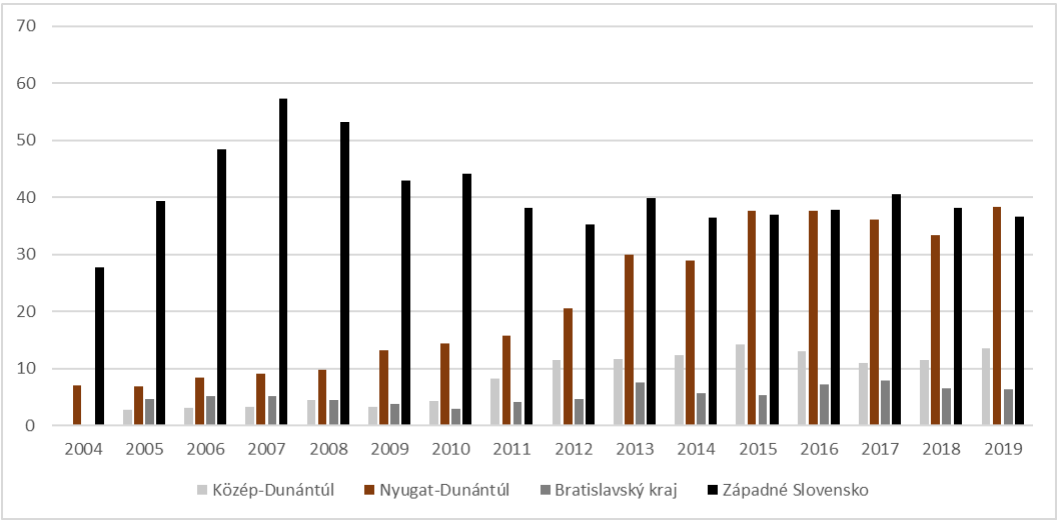

Fig. 2. International commuting in examined regions, NUTS 2, thousand people (own compilation based on Eurostat data).

European Union statistics did not detail which member states are the main destinations for commuters in these regions, but it can be concluded from international researches (Michniak, 2016) that Slovak commuters commute mainly to Austria and the Czech Republic, while Hungarian commuters commute to Austria (Hardi and Uszkai, 2017).

In the following part of the research, we will present the most important results of the questionnaire survey. In case of the research, we tried to get a more accurate picture of the

characteristics of commuters. We searched for statistical correlations between the answers received, and we tried to prove our hypothesis:

There is a positive relationship between the level of wages and cross-border commuting.

The following **Table 1** shows the main demographic data of the respondents, males having the highest proportion of respondents in both countries, with 135 males responding in Slovakia and only 70 responses from females. Out of the Hungarian respondents, 98 were males and 39 were females. In terms of age composition, more than half of the respondents were under the age of 50 in both countries, the difference is that there were more commuters over the age of 60 among Slovak respondents. In terms of education, the proportion of people with secondary education was highest in both countries, in case of the Slovak respondents, it was 49.8 percent, while in case of the Hungarian respondents it was 57.7 percent.

It can be observed from the differences that the proportion of Hungarian commuters with a primary school education is 6 percent higher than of Slovak commuters. In both countries, the proportion of university graduates was below 10 percent, meaning that workers with university degree are less likely to take part in cross-border commuting, as they are more likely to find a suitable job for them in their region of residence.

Table 1.

Main demographic characteristics of respondents.

	Slovakia		**Hungary**	
	Frequency	Percent	Frequency	Percent
Gender				
Male	135	65,9	98	71,5
Female	70	34,1	39	28,5
Age				
18-25	32	15,6	29	21,2
26-35	76	37,1	48	35,0
36-45	44	21,5	35	25,5
46-60	31	15,1	16	11,7
60+	22	10,7	9	6,6
Educational level				
Primary school	84	41,0	47	34,3
Secondary school	102	49,8	79	57,7
University	19	9,3	11	8,0
How many years commuting				
0-2 year	44	21,5	35	25,5
2-5 year	73	35,6	46	33,6
6-10 year	61	29,8	39	28,5
more than 10 years	27	13,2	17	12,4

Table 2 shows the average one-way commuting distance between workplace geographic locations at different distances and the residence place. Based on the answers received, it can be stated that the interviewed commuters are willing to commute for a geographically longer distance for better working conditions and benefits. 44.9 percent of Slovak cross-border commuters commute 36-50 kilometers per day between their place of residence and their Hungarian workplace, while 44.5

percent of Hungarian commuters commute 36-50 kilometers between their place of residence and their Slovakian workplace. 31.7 percent of Slovak commuters commute beyond 50 kilometers daily, while in the case of Hungarian respondents this proportion is 28.5 percent. The received results show similar results to international studies (Carlsson et al., 2018; Gunko and Nefedova, 2017; Ahlfeldt and Wendland, 2016), meaning that cross-border commuters are willing to commute for more than 50 kilometers per day for better job conditions.

Table 2.

The distance of commuting, km.

	Slovakia		**Hungary**	
	Frequency	**Percent**	**Frequency**	**Percent**
0-20 km	18	8,8	13	9,5
21-35	30	14,6	24	17,5
36-50	92	44,9	61	44,5
50+	65	31,7	39	28,5
Total	**205**	**100**	**137**	**100**

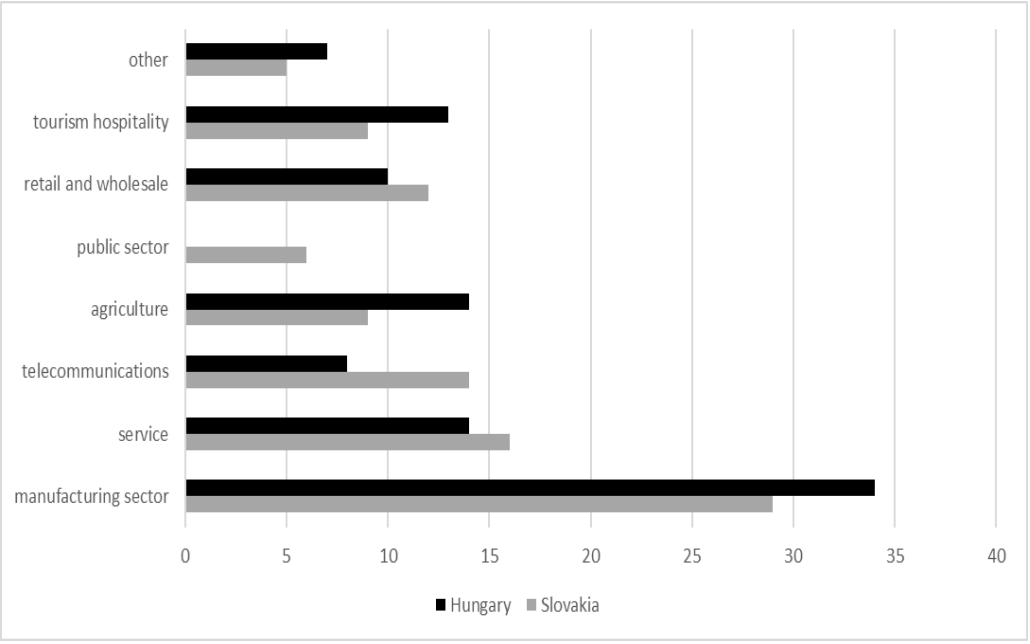

Fig. 3. Type of examined commuters' workplace, percent

Based on the data in **Fig. 3**, it can be stated that commuters work mostly in the manufacturing sector. 29 percent of Slovak respondents and 34 percent of Hungarian respondents work in the manufacturing sector. In most cases, manufacturing jobs are related to the automotive industry, the two most important multinational companies in the examined regions are Volkswagen in Bratislava and Audi in Győr. Both companies have a significant number of commuter workers.

The manufacturing sector is followed by service (17 percent) in case of the Slovak respondents, while service and agriculture were in the same proportion (14 percent) in case of the Hungarian commuters. It can be stated that commuters in the studied regions are most attracted by large, foreign-owned companies. These companies appeared in large numbers in the examined area after the

European Union integration of Hungary and Slovakia. These large foreign companies clearly have a positive impact on employment in these regions.

The difference in the figure is that in the public sector only Slovak commuters work in Hungary, while vice versa this is not typical, it probably has language barriers, because in the southern part of Slovakia many people speak the Hungarian language for historical reason. The public sector is typically the sector where one needs to know the official language of the country on a high level.

The same difference between the responses can be said for the agricultural sector. While 14% of Hungarian respondents work in the Slovak agricultural sector, on the Slovak side this proportion is only 9%. The reason for the discrepancy can be found in the fact that the regions of southern Slovakia were already regions engaged in agricultural production even before the 2000s. Many of the Hungarian employees who went to work in Slovakia even before joining the European Union, still work in agriculture, while those who went from the mid-2000s are working mostly in the manufacturing industry.

Question regarding commuting satisfaction was answered by all the respondents independently from their travel distance (see **Fig. 4**). Commuters were simply asked if they were satisfied with their daily work commute. The possible choices were on Likert-scale: very unsatisfied, unsatisfied, satisfied, and very satisfied. Concerning the commuting satisfaction, among the Slovakian respondents, only 7.8 percent were very unsatisfied, 13,7% were unsatisfied, 53.7 percent were satisfied and finally, 24.9 percent were very satisfied. In case of the Hungarian respondents this satisfaction level was above average too. Among the Hungarian respondents only 12.4 percent were very unsatisfied, 16.1 percent were unsatisfied, 52.6 percent were satisfied and finally, 19 percent were very satisfied. Summarizing the responses, it can be said that the commuter workers interviewed are satisfied with the commuting employment.

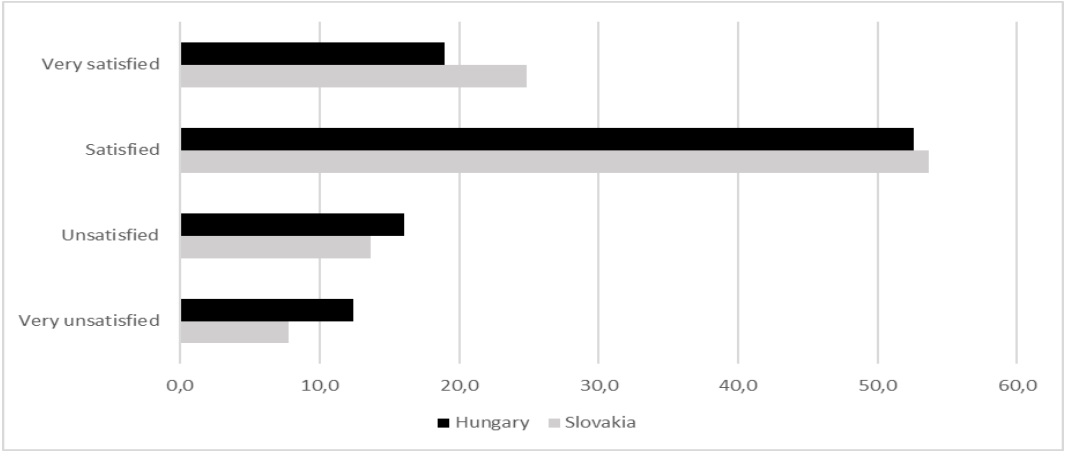

Fig. 4. The satisfaction level of examined commuters, percent

We analysed in the research which factors have the greatest impact on commuter satisfaction. Based on scientific literature and personal interviews, we examined 9 factors (**Fig. 5**) that we believe may have an impact on commuting *(higher wages, old-age pension, medical treatment, family benefits, sickness, maternity and paternity benefits, unemployment benefits and labour market reintegration, taxes, the variety of jobs offered, knowledge of the language spoken in the country)* These factors were taken as independent variables, while dependent variables were commuters' satisfaction.

One of the main objectives of the research was to identify the affecting factors of commuting. A Multiple regression analysis was conducted to identify the best predictors of the dependent variable and to show the proportion of variance in the dependent variable explained by the independent variables. The commuters from the two countries were evaluated separately.

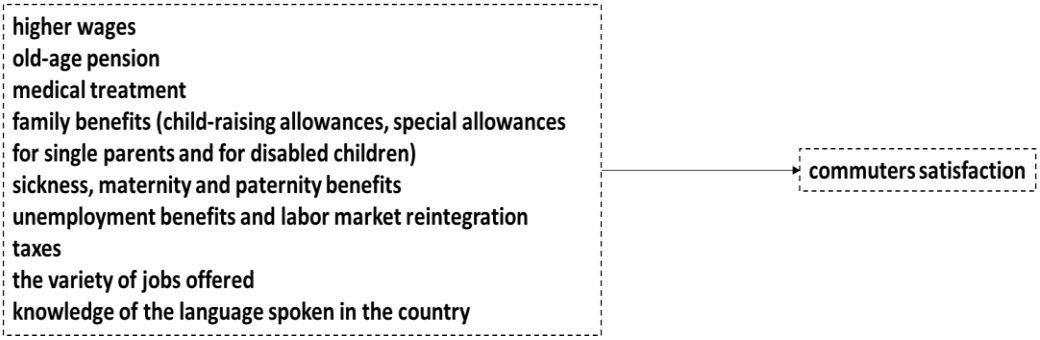

Fig. 5. The conceptual framework of the factors affecting commuting.

Table 3.

Model summary of regression analysis, Hungary.

Model	R	R Square	Adjusted R Square	Std. Error of the Estimate	Change Statistics					Durbin-Watson
					R Square Change	F Change	df1	df2	Sig. F Change	
1	,666[a]	,443	,404	,693	,443	11,241	9	127	,000	1,829

a. Predictors: (Constant), languageknowledge, medicaltreatment, wages, unemploymentbenefits, oldagepension, taxes, familybenefits, sickmatpatbenefits, varietyofjobs

b. Dependent Variable: satisfaction

Table 3, shows that R-squared of 0.443 which implied that nine predictor variables explained about 44.3 percent of the variance on cross-border commuting of Hungarian workers. The ANOVA results show that F-statistics (11.241) and the p-value was highly significant (.000) at the .05 level of significance.

Table 4, shows the standardized regression coefficients (Beta). Beta gives an indication of the contribution of each independent variable in predicting the dependent variable. This table showed that the largest beta coefficient is 0.323 ($p < .05$) which was for a variety of offered jobs. It means that such variables made the strongest contribution in explaining the dependent variable (commuter's satisfaction). Similarly, wages (0.301), old-age pension benefits (0.226), unemployment benefits (0.189) and family benefits (0.156) were among the significant predictors of commuting. The beta value for sickness, maternity and paternity benefits, medical treatment, taxes, and knowledge of the language spoken in the country did not contribute significantly.

The obtained results show that Hungarian commuters are most attracted to Slovak job opportunities. In Slovakia, after the accession to the European Union, the number of foreign direct investment increased significantly, these were mostly large automotive companies located in the western regions, e.g., a Volkswagen, Citroen, Land Rover. Thus, a number of attractive jobs have been created that have also attracted the attention of foreign commuters. In addition, wages and several social benefits, e.g., the old-age pension make the Slovak labour market attractive for Hungarian commuters.

In the following part of empirical research, we examine which factors affect the satisfaction of Slovakian cross-border commuters. **Table 5** shows that R-squared of 0.256 which implied that nine predictor variables explained about 25.6 percent of the variance on cross-border commuting of Slovakian workers. The ANOVA results show that F-statistics (7.440) and the p-value was highly significant (.000) at the .05 level of significance.

Table 4.

The coefficient selected factors affecting of Hungarian commuter's satisfaction.

Model		Unstandardized Coefficients		Standardized Coefficients		
		B	Std. Error	Beta	t	Sig.
1	(Constant)	1,175	,546		2,152	,033
	varietyofjobs	,324	,076	,323	4,285	,000
	unemploymentbenefits	,177	,074	,189	2,382	,019
	oldagepension	,214	,071	,226	3,003	,003
	sickmatpatbenefits	,066	,052	,087	1,269	,207
	familybenefits	,125	,058	,156	2,157	,033
	languageknowledge	,086	,056	,109	1,547	,124
	taxes	,017	,063	,021	,274	,785
	wages	-,224	,055	,301	4,049	,000
	medicaltreatment	-,278	,066	-,334	-4,221	,459

a. Dependent Variable: satisfaction

Table 5.

Model summary of regression analysis, Slovakia.

Model	R	R Square	Adjusted R Square	Std. Error of the Estimate	Change Statistics					Durbin-Watson
					R Square Change	F Change	df1	df2	Sig. F Change	
1	,506[a]	,256	,221	,738	,256	7,440	9	195	,000	2,034

a. Predictors: (Constant), languageknowledge, medicaltreatment, wages, unemploymentbenefits, oldagepension, taxes, familybenefits, sickmatpatbenefits, varietyofjobs

b. Dependent Variable: satisfaction

Table 6 showed that the largest beta coefficient is 0.285 ($p < .05$) which was for wages and a variety of jobs (0.186, $p < .05$). It means that such variables made the strongest contribution in explaining the dependent variable (commuter's satisfaction). The beta value of other examined variables did not contribute significantly to the dependent variable.

Slovak commuters are clearly attracted to the Hungarian labour market because of higher salaries and a variety of job opportunities.

Comparing the responses of the Hungarian and Slovak commuter workers, we get similar opinions, thus the job opportunities and the level of salary are the most attractive in commuting for both parties. Based on this, it can be said that high wages and variety of job opportunities offered in the western region of the studied countries are the reasons for commuting. The results of own research are in line with the results of other similar scientific research (Wiesböck, 2016; Mayerhofer, 2004; Moritz, 2011; Novotná et al., 2013) according to which the main drives for cross-border commuting are higher salaries and other financial benefits.

The last question in the empirical research was, that what was the most negative experience of respondents during commuting. Most of the negative experiences met by Slovak commuters during their cross-border commuting were workplace conditions (22 percent), followed by fatigue (resulting from the combination of daily commuting and work, 18 percent), foreign culture (15 percent), and bureaucracy (13 percent). The bureaucracy received a relatively high percentage, which is due to the fact, that official administration in Hungary is very complicated and long. Hungarian commuters most often encountered discrimination (24 percent) in connection with their commuting work in Slovakia, followed by working conditions (18 percent) and working in a foreign culture (18 percent) as a negative factor.

Table 6.

The coefficient selected factors affecting of Slovakian commuter's satisfaction.

Model	Unstandardized Coefficients		Standardized Coefficients	t	Sig.
	B	Std. Error	Beta		
1 (Constant)	1,254	,515		2,435	,016
oldagepension	-,035	,050	-,046	-,693	,489
sickmatpatbenefits	,088	,070	,090	1,267	,207
medicaltreatment	-,047	,048	-,063	-,965	,336
wages	,278	,069	,285	4,017	,000
unemploymentbenefits	-,024	,047	-,033	-,510	,611
varietyofjobs	,189	,079	,186	2,383	,018
familybenefits	-,063	,059	-,082	-1,078	,283
taxes	,054	,068	,057	,794	,428
languageknowledge	,072	,053	,098	1,360	,175

a. Dependent Variable: satisfaction

5. CONCLUSIONS

Geographic labour mobility covers both migrations as well as cross-border commuting. Our analysis provides some new information in terms of research into cross-border commuting, focusing on labour spatial mobility between Hungary and Slovakia.

One of the biggest advantages of the European Union is the free movement. After the integration of the Eastern European countries into the EU, it has become possible for the citizens of these countries to participate freely in the EU labour markets. Initial commuting to western countries has now changed and commuting has also become a significant factor among neighbouring Eastern European countries. Labour market trends over the past decade have influenced commuting trends. Our research has shown that commuting plays an important role in the western region of Slovakia and Hungary, and both countries have a number of advantages that make them attractive.

Based on the answers to the satisfaction question the Hungarian and Slovak commuters are also satisfied with their current workplace.

Based on the results of our research, it can be said that while Slovakia is attractive to Hungarian commuters in terms of variety of offered job positions, wages, and other social benefits (e.g. old-age pension, family benefits, etc.), Slovak commuters come to Hungary because of the higher wages and variety of offered job positions. In both countries, the inflow of foreign direct investment has made it possible to create quality jobs with high salary level, and these, especially in industrial jobs, are the most attractive for the inhabitants of both examined regions. The results presented here support the economic motivation of commuters, as shown in previous literature (van Ommeren et al., 2000; Clark, et al. 2003; Filep et al., 2010).

In terms of sectoral participation, we found significant differences in the public sector and agriculture, which are justified by the historical past of both countries. On one hand, there are many Hungarian-speaking Slovak citizens in southern Slovakia, who can easily find a job in the Hungarian public sector. While working in the agriculture sector is more dominant among Hungarian commuters who have been working on farms in southern Slovakia for a long time, as the south-western part of Slovakia is historically a region for agricultural production.

In the course of our research, it was also proved that commuting has not only positive but also negative effects, most negative effects mentioned discrimination, fatigue, and the bureaucracy of the country.

Our view is that free movement and commuting can help reduce labour market imbalances, so commuting will play an increasing role in the future.

Similarly, to most research, we also encountered obstacles during our own research. The first such obstacle was that research participants were from the western region of both countries, which means that no relevant conclusions can be drawn for all Hungarian-Slovakian cross-border commuting. The other limiting factor was that we had difficulties in finding a reliable respondent. This was partly due to the fact, that many people refused to respond because of the coronavirus, and partly because we were researching a very specialized segment of employees, which also made it difficult to find them. Thus, in many cases, we relied on our university contacts to find respondents.

The crisis caused by the coronavirus has rearranged the world of labour market, it has also had a major impact on cross-border commuting, as restrictive measures have been introduced due to the coronavirus, which has suspended the geographically free movement through the borders, risking the daily commuting. In the second wave of the coronavirus, we have found that border controls are becoming more stringent, and the previous lighter measures are being replaced by increasingly stringent controls that do not avoid commuter workers either. While in the past commuters were subject to milder requirements, nowadays they also have to meet several strict requirements (e.g. they have to be tested continuously, they cannot enter another country without a valid negative test), which make daily commuting difficult for them. In our opinion, it would be worthwhile to investigate later how the coronavirus affected commuter employment and whether it caused a decline in the number of commuters in the two regions.

Our results can primarily be used as the foundation of other studies. The results may serve as a guideline for other researchers, helping them determine the direction of their research when examining cross-border commuting in case of other countries.

Acknowledgements

This publication was funded by the Pallas Athéné Foundations.

REFERENCES

Ahlfeldt, G. M. & Wendland, N. (2016) The spatial decay in commuting probabilities: Employment potential vs. commuting gravity. *Economics Letters*, 143, 125–129.

Bagdi, R. (2018) Destination development along the Austrian-Hungarian border. *Modernity, Frontiers and Revolutions*, 14, 453–458. doi: 10.14254/2071-789X.2020/13-1/13

Bite, P., Konczosné, M. & Vasa, L. (2020) The Concept of Labour Migration from the Perspective of Central and Eastern Europe. *Economics and Sociology* 13 (1) pp. 197-216.

Bochkarev, A. N. (2019) Methodological Aspects of Studying Labor Commuting. *Regional Research of Russia*, 9(2), 173–180.

Buch, T., Schmidt, T. D. & Niebuhr, A. (2009) Cross-border commuting in the Danish-German border region - integration, institutions and cross-border interaction. *Journal of Borderlands Studies*, 24(2), 38–54.

Bujdosó, Z., Dávid, L., Remenyik, B. & Tóth, G. (2011) Connection between tourism and regional development on the Hungarian-Croatian border. *Central European Regional Policy and Human Geography*, 1(2) pp. 27-40.

Bujdosó, Z., Dávid, L., Varga, D., Pénzes, J., Gyurkó, Á. & Zhapukov, A. (2015) Tourism Development and Cross-Border Cooperation in The Hungarian-Romanian Border Region. *Geojournal Of Tourism and Geosites*, 16(2), pp. 153-163.

Carlsson, M., Reshid, A. A. & Rooth, D.-O. (2018) Neighborhood signaling effects, commuting time, and employment. *International Journal of Manpower*, 39(4), 534–549.

Cavallaro, F., & Dianin, A. (2020) Efficiency of public transport for cross-border commuting: An accessibility-based analysis in Central Europe. *Journal of Transport Geography*, 89, 102-118.

Clark, W., Huang, Y. & Withers, S. (2003) Does commuting distance matter? Commuting tolerance and residential change. *Regional Science and Urban Economics*, 33, 199–221.

Dauth, W. & Haller, P. (2020) Is There Loss Aversion in the Trade-Off Between Wages and Commuting Distances? *Regional Science and Urban Economics*, 83, 103-127.

De Gijsel, P., & Janssen, M. (2000) Understanding the Dutch-German cross-border labour market: are highly educated workers unwilling to move? *Tijdschrift voor economische en sociale geografie*, 91, 61–77.

De Simone, G. & Manchin, M. (2012) Outward Migration and Inward FDI: Factor Mobility between Eastern and Western Europe. *Review of International Economics*, 20(3), 600–615.

Durán, R. (2001) Regime Change, State Capacity and Mass Behaviour: Southern, Central and Eastern Europe in Comparative Perspective. *South European Society and Politics*, 6(2), 1–26.

ETUC's recommendations to the national governments and to the European Union on how to overcome obstacles to the mobility of frontier workers in Europe. ETUC Executive Committee at its meeting on 10-11 March 2015. Online available at: https://www.etuc.org/en/document/etucs-recommendations-how-overcome-obstacles-mobility-frontier-workers-europe

EU Regulation 883/2004. Online available at: https://eur-lex.europa.eu/eli/reg/2004/883/2014-01-01

Fassmann, H. & Münz, R. (2002) EU Enlargement and Future East-West Migration. In New Challenges for Migration Policy in Central and Eastern Europe. Asser Press, Berlin/Heidelberg, Germany, 1-276.

Fialová, K. & Schneider, O. (2009) Labor Market Institutions and Their Effect on Labor Market Performance in the New EU Member Countries. *Eastern European Economics*, 47(3), 57–83.

Filep, B., Kovács, Zs., Kara, Á. & Tömböly, T. (2013). "City – University – Company" coordinated strategic development: Industry Zone in Győr focused on the vehicle industry. In: Dermol, V., Trunk Širca, N. & Đaković, G. (eds) Active Citizenship by Knowledge Management & Innovation: Proceedings of the Management, Knowledge and Learning. ToKnowPress, pp. 797-808. ,

Filep, B., Földesi, P. & Csík, Á. (2010). Competitiveness of cities, searching for a model to optimize cities. *Acta Technica Jaurinensis* 3 (3), pp. 383-393.

Green, D. A., Morissette, R., Sand, B. M. & Snoddy, I. (2019) Economy-Wide Spillovers from Booms: Long-Distance Commuting and the Spread of Wage Effects. *Journal of Labor Economics*, 37(2), 643–687.

Green, M. B. & Meyer, S. P. (1997). An overview of commuting in Canada: With special emphasis on rural commuting and employment. *Journal of Rural Studies*, 13(2), 163–175.

Grund, Ch. & Sliwka, D. (2007) Reference-Dependent Preferences and the Impact of Wage Increases on Job Satisfaction: Theory and Evidence. *Journal of Institutional and Theoretical Economics*, 163(2), 307-313.

Gunko, M. & Nefedova, T. (2017) Coping with employment issues through commuting: Evidence from Central Russia. *Moravian Geographical Reports*, 25(2), 118–128.

Hardi, T., & Uszkai, A. (2017) Theoretical Models of Cross-border Integration. *Sociální Studia*, 14(1), 9–30.

Jin, J. (2019) The effects of labor market spatial structure and the built environment on commuting behavior: Considering spatial effects and self-selection. *Cities*, 95, 102392.

Kolodko, G. W. (1994) Recession and Growth during Transition to a Market Economy in Eastern Europe. *Eastern European Development and Public Policy*, 39–48.

Kwiatkowski, E. (2011) Recent Labour Market Trends in the Visegrad Group Countries. *Comparative Economic Research. Central and Eastern Europe,* 14(2), 25–40.

Lavesson, N. (2016) When and how does commuting to cities influence rural employment growth? *Journal of Regional Science*, 57(4), 631–654.

Lipták, K. (2013) The Labour Market Situation in the Central-Eastern European Region – Towards a New Labour Paradigm. *Journal of Geography and Geology*, 5(3), 88-100.

Lipták, K. (2019): The importance of social innovations in rural areas. DETUROPE – The Central European *Journal of regional development and tourism*, 11(3), 160-174.

Magda, R. (2013): Structural problems of the rural employment in Hungary. *Regional Development Bulletin* 34 (1-2), pp. 20-25.

Mayerhofer, P. (2004) Austrian Border Regions and Eastern Integration. *Review of Regional Research*, 24(1), 73–104.

Medeiros, E. (2019) Cross-border transports and cross-border mobility in EU border regions. *Case Studies on Transport Policy*, 7(1), 1-12.

Michniak, D. (2016). Main trends in commuting in Slovakia. *European Journal of Geography*, 7(2), 6 – 20.

Moritz, M. (2011) The Impact of Czech Commuters on the German Labor Market. *Prague Economic Papers,* 20(1), 40–58.

Novotná, M., Preis, J., Kopp, J. & Bartoš, M. (2013) Changes in Migration to Rural Regions in The Czech Republic: Position and Perspectives. *Moravian Geographical Reports*, 21(3), 37–54.

Paril, V., Kunc, J., Sasinka, P, Tonev, P. & Viturka, M. (2015) Agglomeration effects of the Brno city (Czech Republic) as exemplified by the population labour mobility. *Geographia Technica*, 10(1), 66-76.

Rouwendal, J. (1998) Search Theory, Spatial Labor Markets, and Commuting. *Journal of Urban Economics,* 43(1), 1–22.

Sharma, A. (2019) Commuting between Rural and Urban Areas: Evidence from India. *Built Environment,* 45(4), 493–506.

Sokol, M. (2001) Central and Eastern Europe a Decade After the Fall of State-socialism: Regional Dimensions of Transition Processes, *Regional Studies*, 35(7), 645–655.

Van der Veen, A. & Evers, G. (1983) A simultaneous model for regional labor supply, incorporating labor force participation, commuting and migration. *Socio-Economic Planning Sciences*, 17(5-6), 239–250.

van Ommeren, J., van den Berg, G. J. & Gorter, C. (2000) Estimating the marginal willingness to pay for commuting, *Journal of Regional Science*, 40, 541–63.

Wiesböck, L. (2016) A preferred workforce? Employment practices of East–West cross-border labour commuters in the Central European Region. *Österreichische Zeitschrift Für Soziologie*, 41(4), 391–407.

FLOOD PRONE RISK AREA ANALYSIS DURING 2005 - 2019 IN LAM SE BOK WATERSHED, UBON RATCHATHANI PROVINCE, THAILAND

***Katawut WAIYASUSRI*[1*], *Nayot KULPANICH*[1], *Morakot WORACHAIRUNGREUNG*[1], *Pornperm SAE-NGOW*[1], *Pornsmith CHAYSMITHIKUL*[1]**

DOI: 10.21163/GT_2021.161.12

ABSTRACT:
This research investigates the application of logistic regression analysis for flood prone risk mapping in the Lam Se Bok watershed area. The study found that floods have occurred as many as 15 times since 2005. In 2019, flooding covered 200.01 km^2 of the watershed (5.51% of the total watershed). Among the areas that flood every year, 15 floods occurred in the lower part of the LSBW basin in Na Udom village, Khok Sawang and Fa Huan village, Rai Khi sub-district, which are in the south of Lue Amnat District, Amnat Charoen Province, as well as in parts of Dum Yai sub-district, Muang Sam Sip district, Ubon Ratchathani. Logistic regression analysis was used to determine the influence of certain variables on this flooding. The variables showing positive β values were mean annual precipitation and distance to a road. The variables showing negative β values included elevation, terrain, slope, soil drainage, distance to stream, land-use, and distance to village, respectively. All of these variables can be analyzed for their Flood Prone Risk area in GIS. The study found that flood-prone areas at the very high-level flood prone risk areas, with a total area of 638.59 km^2 (17.59%), high level flood prone risk areas cover an area of 1,848.10 km2 (50.92%). Medium flood prone risk areas cover 794.95 km2 (21.90%). Low flood prone risk areas cover 310.86 km2 (8.56%), the least vulnerable to flooding encompassed 46.35 km2 (1.27%)., and occurred in areas with low elevation and areas with high annual average rainfall when the variable was located in the middle and downstream parts of the LSBW river basin.

Key-words: *Flood prone, Flood Risk Analysis, Lam Se Bok Watershed, Ubon Ratchathani.*

1. INTRODUCTION

Floods are a frequent problem and occur annually in watershed areas. Factors affecting flooding often include heavy rains over a long time period, since the monsoon troughs run across this watershed area (Papaioannou et al., 2015; Şarpe & Haidu, 2017; Cabrera & Lee, 2020). Terrain with inefficient drainage is also one of the top factors affecting flooding, such as a river with a large amount of sediment, a curved river with few branches, etc. Besides the physical factors, socio-economic factors are also contributing factors that accelerate more frequent flooding (Geist & Lambin 2002; Luo et al., 2010; Lambin & Meyfroidt 2010). These factors inevitably cause changes in land use patterns, which is why it is important to study the context of such factors through flood prone risk area analysis (Waiyasusri & Chotpantarat, 2020).

[1]*Geography and Geo-Informatics Program, Faculty of Humanities and Social Sciences, Suan Suandha Rajabhat University, Thailand, katawut.wa@ssru.ac.th* [*], *nayot.ku@ssru.ac.th, morakot.wo@ssru.ac.th, pornperm.sa@ssru.ac.th, pornsmith.ch@ssru.ac.th*

Thailand has flooded areas of 78,400 km^2, accounting for 15 % of the country. Lam Se Bok watershed (LSBW) is a sub-watershed of the Mun River Basin. The watershed area is in Amnat Charoen and Ubon Ratchathani province with a total basin area of 3,629 km^2, and annual floods are common when the monsoon season is reached (July - October of every year), causing a lot of agricultural land damage. The topography of Phu Sing-Phu Pha Phung Forest Park in Amnat Charoen Province is only that of a low hill with non-steep elevation gain, thus the ability to hold water is relatively low, although there are many tributaries in this basin, which also flood every year. The flood prone risk area analysis approach that has been used over the past decade analyzes flood prone area data at the watershed level, providing a very important dataset for watershed management (Kongmuang et al., 2020; Prasanchum et al., 2020). The information should be obtained from an accurate and efficient source in order to be used as a spatial database for Geo-informatics. The Radarsat-2, a Canadian natural resource satellite, is one of the top flood databases frequently used in flood disasters. It is effective in recording data with a Synthetic Aperture Radar (SAR) system in the C band spectrum, and can record flood data both by day and night (Singhroy, 1995; Baiocchi et al., 2014). This makes it possible for flood monitoring that efficiently monitors unusual high-water levels.

Different methods have been employed to describe flood prone risk areas using various stochastic methods with GIS and remote sensing. Nandi et al. (2016) studied cases of flooding in Jamaica during heavy rainfall from tropical storms and Atlantic hurricanes, revealing the related variables of local geology, geomorphology, hydrology and land-use. Tehrany et al. (2017) applied the principles of logistic regression to the analysis of flood susceptibility mapping in China. Their results revealed that the slope variable had a relatively high influence on flooding, making the slope variable one of the top priorities in the analysis of flood-prone areas. Lim and Li (2018) produced a study entitled “Flood Mapping Using Multi-Source Remotely Sensed Data and Logistic Regression in the Heterogeneous Mountainous Regions in North Korea”, it found that the DEM data for terrain analysis should be of high resolution. Chen et al. (2019) used a machine learning technique for flood mapping in the Yangtze River Delta, China, determining that the rainfall variable is important for model analysis and can also be a catalyst for flooding. On the other hand, Ma et al. (2019) also used Machine Learning Techniques in the Yunnan Province, China, but found that the Curve number (CN), surface runoff and interflow, which are related to the Soil drainage variable, were the primary variables. Variable data for the analysis of those factors requires important tools like GIS and remote sensing to be used for efficient spatial analysis, as with the Hossian and Meng (2020) integrated GIS and cartographic approach, which analyzed variables affecting flooding to determine the flood prone risk areas of Birmingham.

In this research, logistic regression analysis was applied in the analysis of flood prone risk areas using a spatial database that allowed for the construction of a flood prone risk area map in the LSBW. The study took into account the most important variables referred to by other studies to come up with a digital elevation model (DEM), which is widely used in terrain analysis (Barreca et al., 2020). DEM data can effectively generate the terrain and slope data of the watershed (Ahmad, 2018; Banerjee et al., 2017; Goulden et al., 2016). In addition, the main physical variables considered to be the highlights of flood risk analysis included the mean annual precipitation and soil drainage variables. Socio-economic factors that were relevant and provided information on flooding considered to be important variables that were used in these flood applications included: Land-use, Distance to stream, Distance to village, and Distance to road (Rama, 2014; Sujatha et al., 2015; Chandniha & Kansal, 2014). The use of these variables to quantify flood-associated attributes is a significant contribution to the current work. This study aims to find and predict the variables that have the greatest impact on flooding.

The key to solving spatial issues in watershed management to solve the problem of areas susceptible to flooding, guidelines for the flood maps on various planning structures should be established for protecting cultural landscape against flood risks, such as A Framework for Boosting Cultural and Natural Heritage Conservation in Central Italy (Dastgerdi et al., 2020). Sustainable solutions to flooding should be based on integrated community cooperation between researchers, local

authorities and local communities, to gain a true local understanding of understanding of climate – weather – flood linkages. It is a bottom-up, vulnerability-based decision analysis frameworks, such as case studies in Tompkins County, New York, USA, and in various European areas as Flanders (Belgium), Niedersachsen (Germany) and Calabria (Italy) (Schelfaut et al., 2011; Knighton, et al., 2018).

The objective of this research was to analyze the recurrent flood prone risk areas in the LSBW, Amnat Charoen and Ubon Ratchathani Provinces during the period 2005-2019, and analyze the factors affecting such flooding in order to forecast them. By using logistic regression analysis as a guideline for planning and surveillance in the event of future floods, we prepared the data of the aforementioned study in a spatial database format for sustainable flood prone risk area management that may occur in the future.

2. STUDY AREA

LSBW is geographically located at latitude 15° 16' 26" N to 15° 57' 7" N and longitude 104° 30' 21" N to 105° 13 '44" N, with a total basin area of 3,629 km^2. The topography of the basin is in a dendritic drainage pattern (Strahler, 1964). The upstream area is in the north and northeast of the basin. This is a low hill with an altitude of 200-300 meters above sea level (msl) in Phu Sing-Phu Pha Phung Forest Park. The drainage system has the direction of water flow going from the northwest to the southeast. The major streams are the Huai Se Bok, Chan Lan, Phra Lao, Ta Thiao, Khulu, Saphue, and Wang Hai-Phang Ho-Yang, all of which flow into Lam Se Bok and into the Mun River at Tan Sum District, Ubon Ratchathani province (**Fig. 1**).

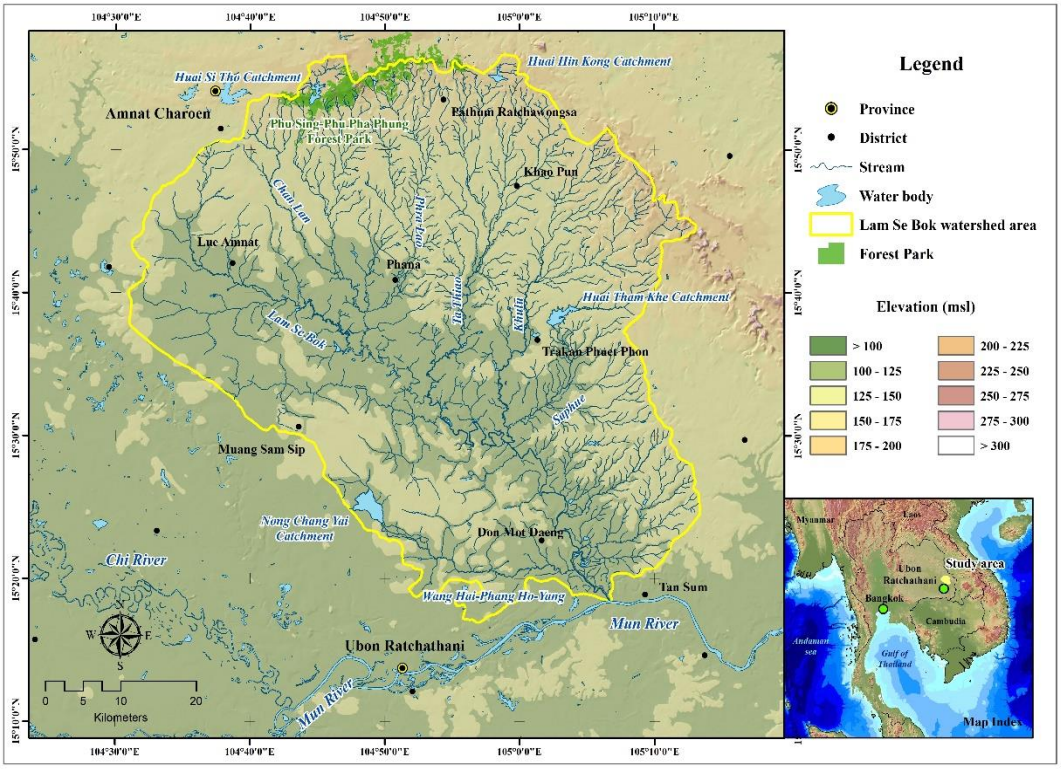

Fig. 1. Geographic map of the Lam Se Bok watershed area.

3. DATA AND METHODS

The methods for conducting this research consisted of analyzing recurring flood prone areas in LSBW, Amnat Charoen and Ubon Ratchathani Provinces, from 2005 to 2019, and analyzing the factors affecting flooding to forecast flood prone risk areas using a Logistic Regression analysis method. Data preparation is shown in **Table 1** and the research process is shown in **Fig. 2,** as follows.

Table 1.

Spatial data layers used in study.

Main themes	Year	Data preparation methodology
Actual flood area	2005-2019	Geo-Informatics and Space Technology Development Agency (public organization) (GISTDA)
Digital Elevation Model (DEM)	2014	Land Development Department
Terrain data	2014	Derived from the DEM
Slope	2014	Derived from the DEM
Soil drainage	2013	Land Development Department (LDD)
Mean annual precipitation	2005-2019	Interpolated from existing rainfall information from the observation stations of the Thai Meteorological Department (TMD)
Distance to stream	2013	Interpolated grid theme contains a Euclidean distance from the drainage system on spatial analysis. Derived from Department of Water Resource, Thailand
Distance to village	2013	Interpolated grid theme contains a Euclidean distance from the village. Derived from Royal Thai Survey Department (RTSD)
Distance to road	2013	Interpolated grid theme contains a Euclidean distance from the highway and road. Derived from Department of Public Works and Town & Country Planning.
Land use	2018	Land Development Department (LDD)

3.1. Flood Prone Area Analysis

The flood prone area was generated from actual flooded areas from 2005 to 2019 using overlay analysis tools in GIS, resulting in repeated flooding area data over the past 15 years. Then, the flood prone areas were analyzed in LSBW areas and those flood prone areas were analyzed for the next statistical logistic regression.

3.2 Affecting the Flood Risk Area using Logistic Regression Analysis

From the flood prone area analysis, it was necessary to search for the factors affecting the flooding to determine the flooding context in Lam Se Bok watershed. The factors analyzed included 9 variables: Elevation, Terrain, Slope, Mean annual precipitation, Soil drainage, Distance to stream, Distance to village, Distance to road, and Land use (**Fig. 3**). These variables were analyzed in conjunction with flood prone area data using logistic regression analysis.

Logistic Regression is a technique for discovering the empirical relationships between a binary dependent and several independent categorical and continuous variables) Nandi et al., 2016; Tehrany et al., 2017) .Logistic regression analysis is calculated using the following, Eq. (1):

$$Log\left(\frac{P_i}{1-P_i}\right) = \beta_0 + \beta_1 x_{1,i} + \beta_2 x_{2,i} + \ldots + \beta_n x_{n,i} \quad (1)$$

where P is the flood prone area, x_i are independent variables and β is the coefficient value.

This statistical method was used to provide and analyze the variables that influenced the flooding of the area. It will show the effect of the variable in the value of β, showing how much that factor affects the flooding in that area. The aforementioned statistical principle considers the preliminary and the variables for every grid cell in the LSBW area.

In conclusion, the spatial data obtained from Logistic Regression can be used to forecast flood risk areas in the LSBW area using a classification method utilizing 5 classes: very high, high, moderate, low, and very low. A flood prone risk area map is thus shown in order to obtain results highlighting the areas that should be urged to promptly resolve potential flooding disasters for sustainable spatial development in the future.

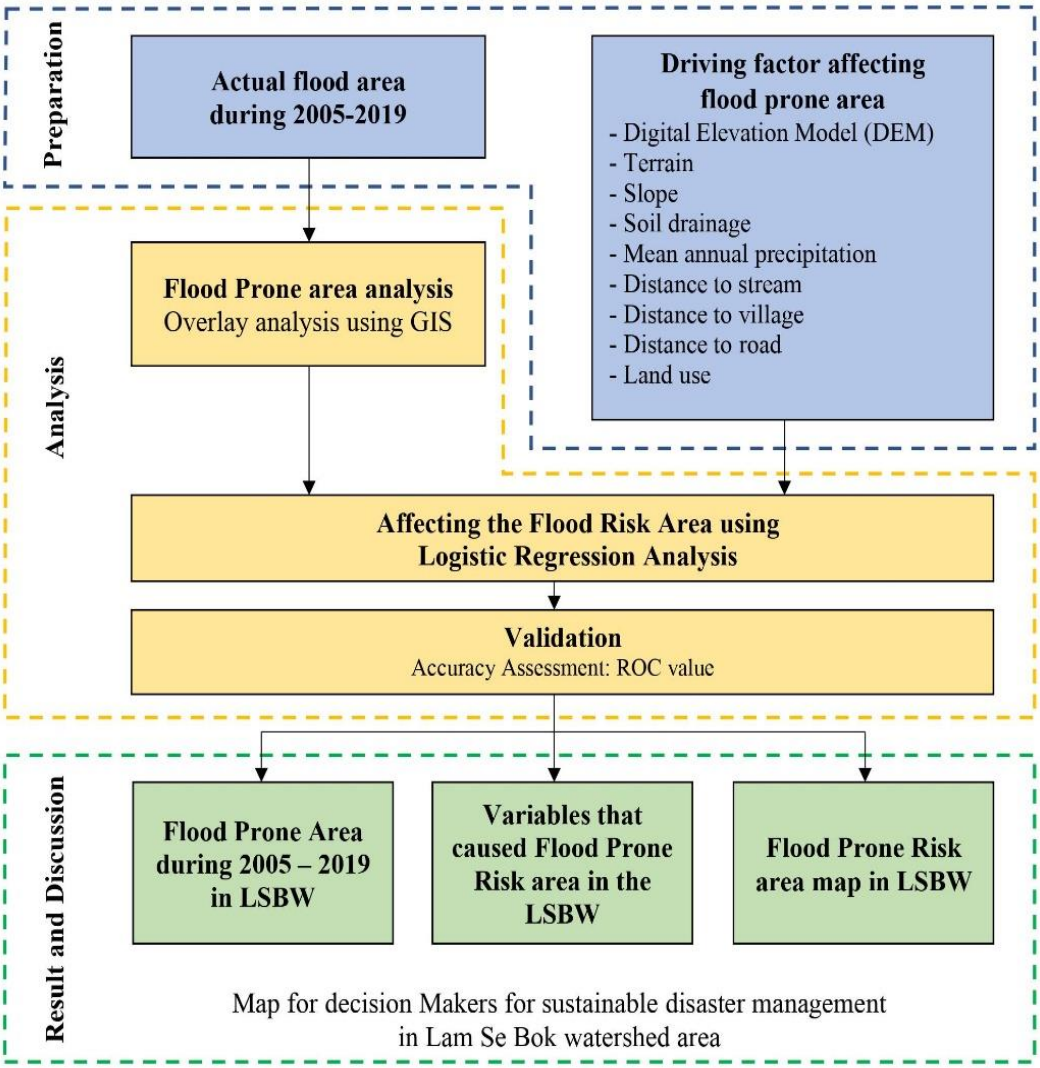

Fig. 2. Flowchart of the Research Process.

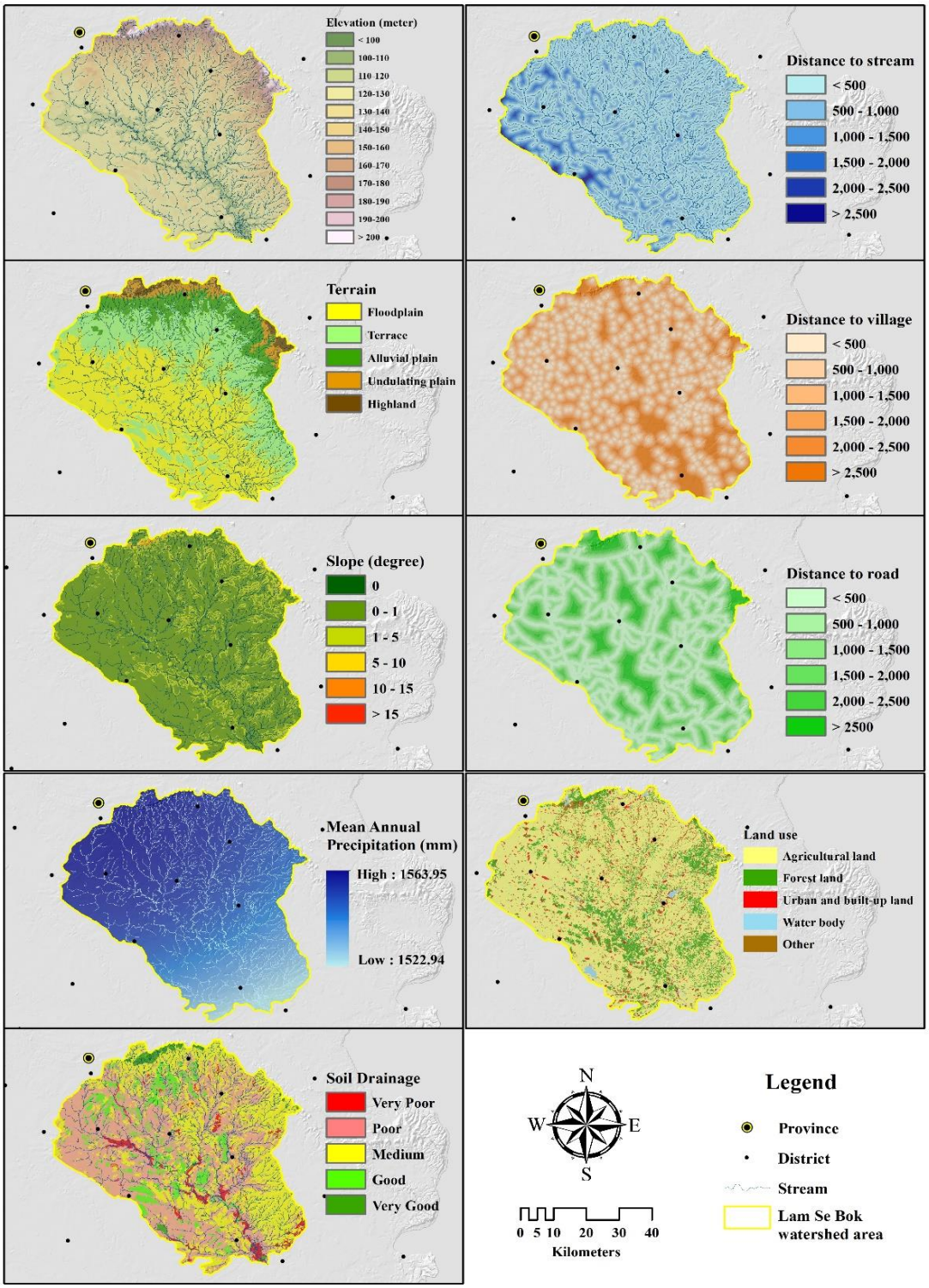

Fig. 3. Nine variables for the analysis of factors affecting flooding.

4. RESULTS AND DISCUSSION

4.1 Flood Prone Areas from 2005 - 2019 in LSBW

LSBW is a tributary of the Mekong River Basin originating in Phu Sing-Phu Pha Pha Phung Forest Park. The flow pattern of the watershed is in a dendritic drainage pattern, creating a cumulative flow area from the middle to the downstream parts of the watershed. Results from the Flood Prone Area study during the 2005 - 2019 period in LSBW found that there have been as many as 15 frequent floods since 2005. In 2019, floods covered 200.01 km^2 of watershed area (5.51% of the total watershed); in 2017, floods covered 179.59 km^2 (4.95% of the total watershed) and the year with the least flooding was 2016 with only 1.24 km^2 (representing 0.03% of the total watershed). **Table 2** shows the proportion of flooded areas**.**

Table 2.

Lam Se Bok watershed flooded area from 2005-2019.

Year		2005	2006	2007	2008	2009	2010	2011	2012
Area	km^2	5.49	27.27	36.8	8.67	17.36	83.91	113.02	7.87
	%	0.15	0.75	1.01	0.24	0.48	2.31	3.11	0.22
Year		2013	2014	2015	2016	2017	2018	2019	
Area	km^2	106.35	109.41	18.12	1.24	179.59	35.86	200.01	
	%	2.93	3.01	0.50	0.03	4.95	0.99	5.51	

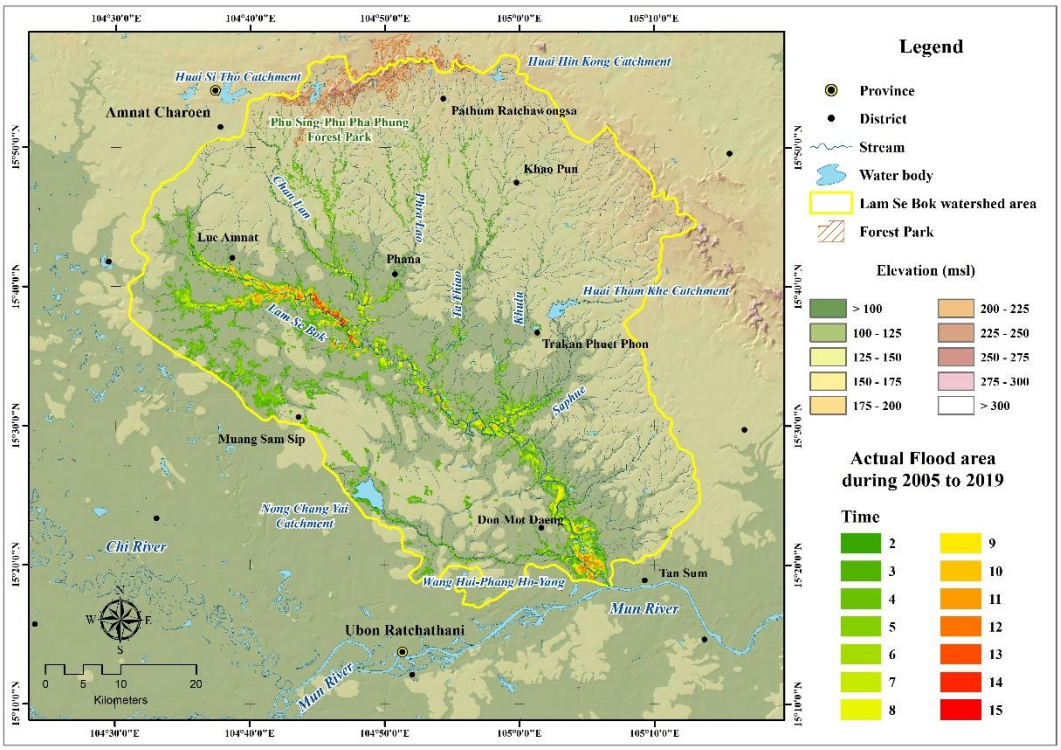

Fig. 4. Recurring flooding areas over a period of 15 years (2005-2019) in LSBW area from GIS analysis.

Flood Prone area analysis by GIS resulted in a very important study: the repeating flood prone areas that appear frequently in LSBW. The results of the study showed that the repeated flooding areas that flood every year have occurred up to 15 times since 2005 in the lower area of LSBW in Na Udom village, Khok Sawang and Fa Huan village, Rai Khi sub-district, located on the south side of Lue Amnat District, Amnat Charoen Province, and in some areas of Dum Yai sub-district, Muang Sam. Sip. district, Ubon Ratchathani (**Fig. 4** and **Fig. 5**).

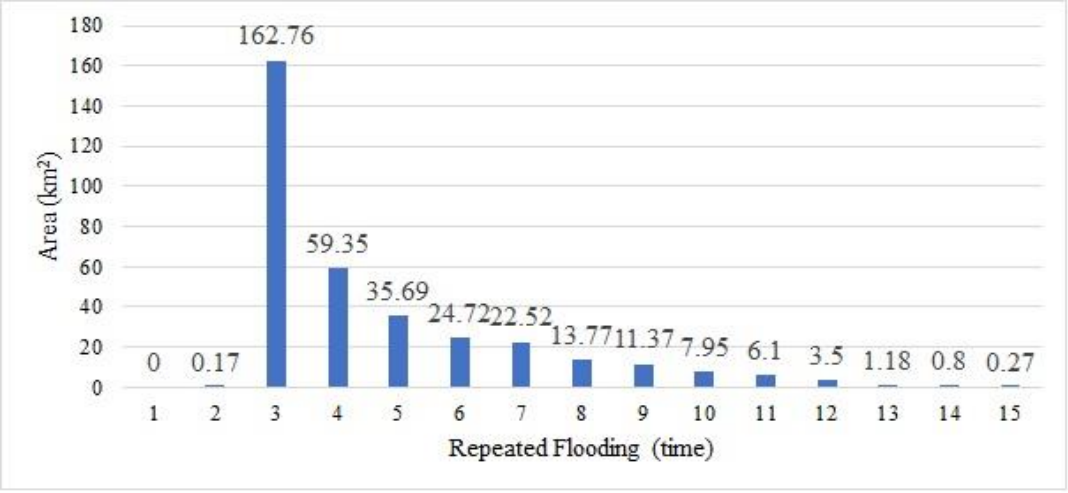

Fig. 5. Frequency data of recurring floods over a period of 15 years (2005-2019) in LSBW area.

4.2 Variables that Cause Flood Prone Areas in the LSBW

Variables that cause flood prone areas in the LSBW were obtained from Logistic Regression analysis, as shown in **Table 3**. The study results are shown using statistical value β, which variables are positive means that the higher the variable, the more susceptible to flooding. However, if the **β** value of the variable is negative means that the lower the variable, the more susceptible to flooding. (Lim & Lee, 2018).

Table 3.

Logistic regression analysis of flood prone areas and affecting factors.

Variable	β value	Exp β	Standard Error	Sig.
Elevation	-1.578	0.206	0.015	0.00
Terrain	-0.695	0.499	0.018	0.00
Slope	-0.487	0.614	0.014	0.00
Mean annual precipitation	0.100	1.106	0.004	0.00
Soil drainage	-0.469	0.626	0.009	0.00
Distance to stream	-0.079	0.924	0.009	0.00
Distance to village	-0.015	0.985	0.005	0.00
Distance to road	0.089	1.093	0.005	0.00
Land use	-0.026	0.975	0.005	0.00
Constant	4.840			
The relative operating characteristic (ROC)	0.850			

The relative operating characteristic (ROC) shows how the regression equation can be used to predict flood prone risk areas based on probability (Nandi et al., 2016; Lim & Lee, 2018; Waiyasusri & Wetchayont, 2020). The ROC values obtained for the probability of flood prone risk area was 0.85 (**Fig. 6**), which indicates a high value, since approaching 1.00 is an indication that all 9 variables are effective in analyzing flood prone areas.

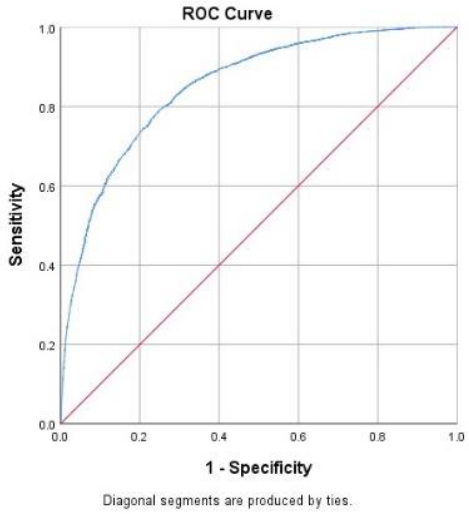

Fig. 6. The relative operating characteristic (ROC) value.

The study found that the Mean annual precipitation and Distance to road factors were the 2 variables showing positive β values. Mean annual precipitation, showing the highest value, was the most influencing factor for flooding. The average annual rainfall value with the highest average rainfall appears in the southernmost area of LSBW, which greatly affects the flooding in that area. Distance to road is also a variable that shows a positive β value. The areas that are farther from a road are indeed areas more susceptible to flooding, since the road area is engineered to elevate the road's height from its base area. The LSBW areas adjacent to roads are therefore less affected by flooding than those further away from a road.

Results showing negative β values were varied, from the highest negative to the lowest negative comprising Elevation, Terrain, Slope, Soil drainage, Distance to stream, Land use, and Distance to village, respectively. It can be seen that the top variables affecting the flood prone area in the LSBW are physical factors, especially the Elevation, Terrain, Slope, and Soil drainage variables. The lower the variable, the more susceptible to flooding, such as Elevation, Terrain and Slope, where low-lying terrain with a floodplain landform and 0-5 degrees of slope is easy to become a flood prone area. For Soil drainage, the low value represents soil types that are very poor and with a poor priority drainage system, causing the water mass to be immersed in the area. As the area is covered with hygroscopic clay and clay loam, the above physical factors are hallmarks of this LSBW area.

With the Distance to stream, Land use, and Distance to village variables, the study found that the lower the three variables, the more susceptible to flooding. The results showed that when the Distance to stream variable was closer to a water source, the more susceptible it was to flooding. Distance to stream and Distance to village variables affecting the susceptibility to flood prone areas in LSBW, both are at a level not exceeding 500 m. Regarding the Land use variable, the low value represents land use conditions for cultivating and farming, as the LSBW is mainly engaged in paddy cultivation planted on low slopes and floodplain. With the Distance to village variable, the results showed that the closer to the village area, the easier it was to create a flood prone area. Since these areas do not have an efficient drainage system, it often floods in the villages.

The results of all the variables that are indicators of flood prone areas were analyzed for a Flood Prone Risk area map in LSBW. With this we can create a spatial database for effective management of flood prone areas.

4.3 Flood Prone Risk Area Map in LSBW

The study results of flood prone risk areas in LSBW by logistic regression statistical analysis, β value as a database and spatial analysis using GIS, were used to create maps for watershed disaster management (**Fig. 7**), as Eq. (2).

$$Y = 4.840 + (-1.578 * \text{"Elevation"}) + (-0.487 * \text{"Slope"}) + (-0.695 * \text{"Terrain"}) + (-0.469 * \text{"Soil drainage"}) + (-0.026 * \text{"Landuse"}) + (0.100 * \text{" Mean\_annual\_precipitation"}) + (-0.079 * \text{" Distance\_to\_stream"}) + (0.089 * \text{" Distanc\_ to\_road"}) + (-0.015 * \text{" Distance\_to\_village"}) \quad (2)$$

Flood Prone Risk area map in LSBW has classified risk levels according to criteria, which can be described into the following categories: Very low (0 - 0.20), Low (0.21 - 0.40), Medium (0.41 - 0.60), High (0.61 -. 0.80) and Very high (0.81 - 1.00) (Ma et al., 2019). The β value results of the variables led to the highlight of this research; also, the risk level could be expressed as spatial data, as follows. The very high level flood prone risk areas, with a total area of 638.59 km^2 (17.59%), are mostly low-elevation areas and areas with high annual average rainfall, which appear around the middle and end of the LSBW near Lue Amnat and Phana District, Amnat Charoen Province; and Trakan Phuet Phon, Tan Sum, Don Mot Daeng, and Muang Sam Sip, Ubon Ratchathani Province. The high-risk area covers a wide area in the middle of the LSBW, as it is a floodplain terrain and has an elevation of only 100-200 m, so it is susceptible to flooding.

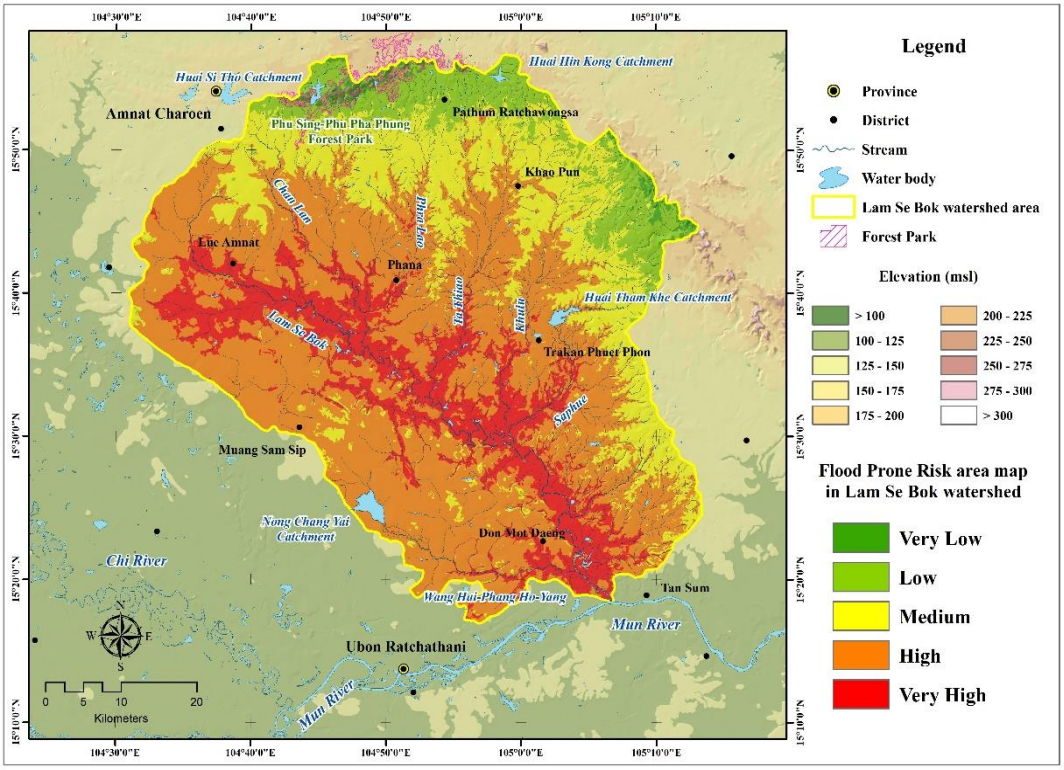

Fig. 7. Flood Prone Risk area map in LSBW.

High level flood prone risk areas cover an area of 1,848.10 km^2 (50.92%). Medium flood prone risk areas cover 794.95 km^2 (21.90%). Low flood prone risk areas cover 310.86 km^2 (8.56%), the least vulnerable to flooding encompassed 46.35 km^2 (1.27%). The least vulnerable to flooding in LSBW is located in Phu Sing-Phu Pha Phung Forest Park, the northern and northeastern slopes of LSBW.

This study developed the feasibility and credibility by applying results from the logistic regression model and validating the actual flood area. Actual flood area data is a collection of information from flood related agencies at local, central level and community policy participation in order to know how to manage the flood by creating flood-vulnerable maps (Dastgerdi et al., 2019; Seebauer & Babcicky, 2017). The validation results between the actual flood area data and the Flood Prone Risk area map from the logistic regression model were as shown in **Table 4**, where the results showed that during the 15 years of repeated flooding. Flood cover area of up to 228.26 km^2, representing 65.19 %. Relation level of the two datasets had a good level of reliability.

Table 4.

The validation results between the actual flood area data and the Flood Prone Risk area map.

Repeated flooding	Flood Prone Risk area (km^2)					Actual Flood area (km^2)
	Very Low	Low	Medium	High	Very High	
1	0.00	0.00	0.00	0.00	0.00	0.00
2	0.00	0.00	0.00	0.17	0.00	0.17
3	0.00	0.50	7.53	71.66	83.12	162.81
4	0.00	0.03	1.10	21.81	36.39	59.33
5	0.00	0.00	0.21	11.15	24.26	35.62
6	0.00	0.00	0.03	3.75	20.93	24.71
7	0.00	0.00	0.00	1.29	21.18	22.47
8	0.00	0.00	0.00	0.88	12.97	13.85
9	0.00	0.00	0.00	0.79	10.58	11.37
10	0.00	0.00	0.00	0.37	7.57	7.94
11	0.00	0.00	0.00	0.27	5.82	6.09
12	0.00	0.00	0.00	0.29	3.23	3.52
13	0.00	0.00	0.00	0.02	1.16	1.18
14	0.00	0.00	0.00	0.01	0.79	0.80
15	0.00	0.00	0.00	0.00	0.27	0.27
Sum	0.00	0.53	8.87	112.46	228.27	350.13
%	0.00	0.15	2.53	32.12	65.20	

5. CONCLUSIONS

Floods are disasters that occur almost every year during the monsoon season in Thailand, especially in the watershed areas of Northeast Thailand which are often affected by such disasters. This research aims to solve this problem by analyzing individual factors to find solutions to the causes of floods by using logistic regression analysis in conjunction with GIS to create a Flood Prone Risk area map in LSBW.

One of the objectives of this paper is to find the most influential variables of flood prone occurrence. Based on our results of logistic regression analysis, the order of flood conditioning factors

for negative β values were the Elevation, Terrain, Slope, Soil drainage, Distance to stream, Land-use, and Distance to village variables, respectively. The positive β values were Mean annual precipitation and Distance to road, respectively. It was found that the very high-level flood prone risk areas, with a total area of 638.59 km2 (17.59%), high level flood prone risk areas cover an area of 1,848.10 km2 (50.92%). Medium flood prone risk areas cover 794.95 km2 (21.90%). Low flood prone risk areas cover 310.86 km2 (8.56%), the least vulnerable to flooding encompassed 46.35 km2 (1.27%). The important variables are low-elevation areas and areas with high annual average rainfall which are mostly located at the middle and southern end of the LSBW.

This research shows that the utilization of a flood prone risk map is a useful basis for taking preventive actions to mitigate floods and expedite relevant agencies to assist those areas at highest risk for flood mitigation and land use planning. Although this risk map is suitable for watershed terrain, the context of flooding and other relevant factors affecting flooding should be investigated for effective logistic regression analysis if used in other areas.

REFERENCES

Ahmad, I. (2018) Digital elevation model (DEM) coupled with geographic information system (GIS): an approach towards erosion modeling of Gumara watershed, Ethiopia. *Environmental Monitoring and Assessment*, 190, 568. https://doi.org/10.1007/s10661-018-6888-8

Baiocchi, V., Brigante, R., Dominici, D., Milone, M.V., Mormile, M. & Radicioni, F. (2014) Automatic three-dimensional features extraction: The case study of L'Aquila for collapse identification after April 06, 2009 earthquake, *European Journal of Remote Sensing*, 47(1), 413-435.

Banerjee, A., Singh, P. & Pratap, K. (2017) Morphometric evaluation of Swarnrekha watershed, Madhya Pradesh, India: an integrated GIS-based approach. *Applied Water Science*, 7, 1807‑1815. https://doi.org/10.1007/s13201-015-0354-3

Barreca, G., Bruno, V., Dardanelli, G., Guglielmino, F., Brutto, M.L., Mattia, M., Pipitone, C. & Rossi, M. (2020) An integrated geodetic and InSAR technique for the monitoring and detection of active faulting in southwestern Sicily. *Annals of Geophysics*, 63, EP03, DOI: 10.4401/ag-8327

Cabrera, J.S. & Lee, H.S. (2020) Flood-Prone Area Assessment Using GIS-Based Multi-Criteria Analysis: A Case Study in Davao Oriental, Philippines. *Water*, 11, 2203.

Chandniha, S.K. & Kansal, M.L. (2014) Prioritization of sub-watersheds based on morphometric analysis using geospatial technique in Piperiya watershed, India. *Applied Water Science*, 7, 329‑338.

Chen, J., Li, Q., Wang, H., & Deng, M. (2019) A Machine Learning Ensemble Approach Based on Random Forest and Radial Basis Function Neural Network for Risk Evaluation of Regional Flood Disaster: A Case Study of the Yangtze River Delta, China. *International Journal of Environmental Research and Public Health*. 17, 49.

Dastgerdi, S.A., Sargolini, M., Broussard, A.S., Chatrchyan, A. & De Luca, G. Climate Change and Sustaining Heritage Resources: A Framework for Boosting Cultural and Natural Heritage Conservation in Central Italy. *Climate*, 2020, 8(2), 26. https://doi.org/10.3390/cli8020026

Dastgerdi, A.S., Sargolini, M., & Pierantoni, I. (2019) Climate Change Challenges to Existing Cultural Heritage Policy. *Sustainability*. 2019, 11(19), 5227. https://doi.org/10.3390/su11195227

Geist, H.J. & Lambin, E.F. (2002). Proximate causes and underlying driving forces of tropical deforestation. Bioscience, 52, 8.

Goulden, T., Hopkinson, C., Jamieson, R. & Sterling, S. (2016) Sensitivity of DEM, slope, aspect and watershed attributes to LiDAR measurement uncertainty. *Remote Sensing of Environment*, 179, 23-35. https://doi.org/10.1016/j.rse.2016.03.005.

Hossian, M.K. & Meng, Q. (2020) A fine-scale spatial analytics of the assessment and mapping of buildings and population at different risk levels of urban flood. *Land Use Policy*, 99, 104829.

Knighton, J.O., Tsuda, O., Elliott, R., & Walter, M. T. (2018) Challenges to implementing bottom-up flood risk decision analysis frameworks: how strong are social networks of flooding professionals? *Hydrology and Earth System Sciences*, 22(11), 5657‑5673, https://doi.org/10.5194/hess-22-5657-2018.

Kongmuang, C., Tantanee, S. & Seejata, K. (2020) Urban flood hazard map using GIS of Muang Sukhothai district, Thailand. *Geographia Technica*, 15(1), 143‑152. DOI: 10.21163/GT_2020.151.13.

Lambin, E.F. & Meyfroidt, P. (2010). Land use transitions: socio-ecological feedback versus socio-economic change. Land Use Policy, 27, 11, DOI: 10.1016/j.landusepol.2009.09.003.

Lim, J & Lee, K. (2018) Flood Mapping Using Multi-Source Remotely Sensed Data and Logistic Regression in the Heterogeneous Mountainous Regions in North Korea. *Remote Sensing*, 10, 1036.

Luo, G., Yin, C., Chen, X., Xu, W. & Lu L. (2010). Combining system dynamic model and CLUE-S model to improve land use scenario analyses at regional scale: A case study of Sangong watershed in Xinjiang, China. Ecological Complexity, 7, 10, DOI: 10.1016/j.ecocom.2010.02.001.

Ma, M., Liu, C., Zhao, G., Xie, H., Jia, P., Wang, D., Wang, H., & Hong, Y. (2019) Flash Flood Risk Analysis Based on Machine Learning Techniques in the Yunnan Province, China. *Remote Sensing*, 11,170.

Nandi, A., Mandal, A., Wilson, M. & Smith, D. (2016) Flood hazard mapping in Jamaica using principal component analysis and logistic regression. *Environmental Earth Sciences*, 75, 465.

Papaioannou, G., Vasiliades, L. & Loukas, A. (2015) Multi-Criteria Analysis Framework for Potential Flood Prone Areas Mapping. *Water Resources Management*, 29, 399‑418.

Prasanchum, H., Sirisook, P., & Lohpaisankrit, W. (2020) Flood risk areas simulation using swat and gumbel distribution method in yang catchment, Northeast Thailand. *Geographia Technica*, 15(2), 29‑39. DOI: 10.21163/GT_2020.152.04

Rama, V.A. (2014) Drainage basin analysis for characterization of 3rd order watersheds using Geographic Information System (GIS) and ASTER data. *Journal of Geomatics*, 8, 200‑210.

Şarpe, C.A. & Haidu, I. (2017) Temporal sampling conditions in numerical integration of hydrological systems time series. *Geographia Technica*, 12(1), 82‑94. DOI: 10.21163/GT_2017.121.09.

Schelfaut, K., Pannemans, B., Van der Craats, I., Krywkow, J., Mysiak, J. & Cools, J. (2011). Bringing flood resilience into practice: the FREEMAN project, *Environmental Science & Policy*, 14(7), 825-833. https://doi.org/10.1016/j.envsci.2011.02.009.

Seebauer, S. & Babcicky, P. (2017) Trust and the communication of flood risks: comparing the roles of local governments, volunteers in emergency services, and neighbours. *Journal of Flood Risk Management*. 11, 305-316. https://doi.org/10.1111/jfr3.12313.

Singhroy, V. (1995) SAR integrated techniques for geohazard assessment. *Advances Space Research*, 15, 67-78.

Strahler, A.N. (1964) Quantitative geomorphology of drainage basin and channel networks. In Handbook of Applied Hydrology; Chow, V.T., Ed.; McGraw Hill: New York, NY, USA, 4‑76.

Sujatha, E.R., Selvakumar, R., Rajasimman, U.A.B. & Victor, R.G. (2015) Morphometric analysis of sub-watershed in parts of Western Ghats, South India using ASTER DEM. *Geomatics, Natural Hazards and Risk*, 6, 326‑341.

Tehrany, M.S., Shabani, F., Jebur, M.N., Hong, H., Chen, W. & Xie, X. (2017) GIS-based spatial prediction of flood prone areas using standalone frequency ratio, logistic regression, weight of evidence and their ensemble techniques. *Geomatics, Natural Hazards and Risk*, 8(2), 1538-1561.

Waiyasusri, K. & Chotpantarat, S. (2020). Watershed Prioritization of Kaeng Lawa Sub-Watershed, Khon Kaen Province Using the Morphometric and Land-Use Analysis: A Case Study of Heavy Flooding Caused by Tropical Storm Podul. *Water*, 12(6), 1570, DOI: 10.3390/w12061570.

Waiyasusri, K. & Wetchayont, P. (2020) Assessing Long-Term Deforestation In Nam San Watershed, Loei Province, Thailand Using A Dyna-Clue Model. *GEOGRAPHY, ENVIRONMENT, SUSTAINABILITY*, 13(4), 81-97. https://doi.org/10.24057/2071-9388-2020-14

Aims and Scope

Geographia Technica is a journal devoted to the publication of all papers on all aspects of the use of technical and quantitative methods in geographical research. It aims at presenting its readers with the latest developments in G.I.S technology, mathematical methods applicable to any field of geography, territorial micro-scalar and laboratory experiments, and the latest developments induced by the measurement techniques to the geographical research.

Geographia Technica is dedicated to all those who understand that nowadays every field of geography can only be described by specific numerical values, variables both oftime and space which require the sort of numerical analysis only possible with the aid of technical and quantitative methods offered by powerful computers and dedicated software.

Our understanding of *Geographia Technica* expands the concept of technical methods applied to geography to its broadest sense and for that, papers of different interests such as: G.I.S, Spatial Analysis, Remote Sensing, Cartography or Geostatistics as well as papers which, by promoting the above mentioned directions bring a technical approach in the fields of hydrology, climatology, geomorphology, human geography territorial planning are more than welcomed provided they are of sufficient wide interest and relevance.

Targeted readers:

The publication intends to serve workers in academia, industry and government.
Students, teachers, researchers and practitioners should benefit from the ideas in the journal.

Guide for Authors

Submission

Articles and proposals for articles are accepted for consideration on the understanding that they are not being submitted elsewhere.

The publication proposals that satisfy the conditions for originality, relevance for the new technical geography domain and editorial requirements, will be sent by email to the address editorial-secretary@technicalgeography.org.

This page can be accessed to see the requirements for editing an article, and also the articles from the journal archive found on www.technicalgeography.org can be used as a guide.

Content

In addition to full-length research contributions, the journal also publishes Short Notes, Book reviews, Software Reviews, Letters of the Editor. However the editors wish to point out that the views expressed in the book reviews are the personal opinion of the reviewer and do not necessarily reflect the views of the publishers.

Each year two volumes are scheduled for publication. Papers in English or French are accepted. The articles are printed in full color. A part of the articles are available as full text on the www.technicalgeography.org website. The link between the author and reviewers is mediated by the Editor.

Peer Review Process

The papers submitted for publication to the Editor undergo an anonymous peer review process, necessary for assessing the quality of scientific information, the relevance to the technical geography field and the publishing requirements of our journal.

The contents are reviewed by two members of the Editorial Board or other reviewers on a simple blind review system. The reviewer's comments for the improvement of the paper will be sent to the corresponding author by the editor. After the author changes the paper according to the comments, the article is published in the next number of the journal.

Eventual paper rejections will have solid arguments, but sending the paper only to receive the comments of the reviewers is discouraged. Authors are notified by e-mail about the status of the submitted articles and the whole process takes about 3-4 months from the date of the article submission.

Indexed by: **CLARIVATE ANALYTICS**
SCOPUS
GEOBASE
EBSCO
SJR
CABELL

ISSN: 1842 - 5135 (Print)
ISSN: 2065 - 4421 (Online)